

EXPERIMENTAL AERODYNAMICS
OF A
TWO-DIMENSIONAL SAIL

Thesis by
Bain Dayman, Jr.

In Partial Fulfillment of the Requirements
For the Degree of
Aeronautical Engineer

California Institute of Technology
Pasadena, California

1953

ACKNOWLEDGEMENTS

The author wishes to express his thanks and appreciation to Dr. Clark B. Millikan under whose direction these investigations were conducted and to the other members of the committee, Dr. Homer J. Stewart and Dr. Vito A. Vanoni, for their helpful criticism, and to Mr. Edwin Pounder for his technical advice.

The author also wishes to thank the following members of the GALTIT Ten-Foot Wind Tunnel staff for their valuable assistance, without which this work would have been impossible: Lewis Balthasar, Wilfred McNay, Robert Kimberly, Lloyd Eagan, and Ben Williams for the construction of the models and testing equipment and for the running of the tests; Nell Kindig, Georgette Pauwels, Dorothy Nicholson, and Ruth Thomas for the computing and the plotting of the data; and Alyce Blessing for the typing of this thesis.

ABSTRACT

Some basic low-speed aerodynamic characteristics of a two-dimensional sail located between endplates were obtained during these investigations for two sail sizes. The effects of the amount of camber (resulting from variation of the slack in the sail) upon the lift, drag, and pitching moment of a sail constituted the major portion of these investigations. A limited study on the advantages of a sail with a jib was made for one particular jib location and camber.

Ideally, the results should be independent of sail size. The results of these investigations, although not quite identical, are consistent for the two sail sizes. As the camber (measured in percent of length of the sail perpendicular to the leading edge) increased from zero to 10%, the maximum lift increased from 0.92 to a maximum of 1.7 and remained fairly constant as the camber increased to 23%, then it decreased to 1.5 as the camber further increased to 27%. The maximum ratio of lift to drag at maximum lift occurred at 7% camber. The addition of the jib did not affect the maximum lift relationship with the camber, but it did increase the lift to drag ratio at maximum lift.

TABLE OF CONTENTS

<u>PART</u>	<u>TITLE</u>	<u>PAGE</u>
I.	Introduction	1
II.	Test Set-Up and Procedure.	4
III.	Methods of Reduction and Presentation of Data.	7
IV.	Nomenclature	10
V.	Definition of Configuration Symbols.	14
VI.	Dimensional Data	
	A. Basic Model Dimensions.	16
	B. Slack and Camber Measurements	17
VII.	Index of Runs.	19
VIII.	Index of Figures	24
IX.	Index of Model Photos.	27
X.	Discussion	28
XI.	Conclusions.	41
XII.	Bibliography	43
XIII.	Calculated and Experimental Lift and Drag at $\alpha_g = 90^\circ$	44
XIV.	Figures (1 - 43).	45
XV.	Model Photos (1 - 6).	158

I. INTRODUCTION

Although sails have been used for thousands of years very little research work, experimental or theoretical, has been conducted on them. The little experimental work which has been done, most of it during this century, has centered upon specific sail configurations which are applicable to racing yachts rather than upon sail configurations which are very general and basic in nature. A basic approach is necessary in order to determine the effects of each individual sail parameter. Virtually no theoretical work has been attempted owing to the obvious complications caused by non-rigidity, large camber, and by the fact that in actual practice sails are used in and beyond the region of stall. Therefore it is well that an experimental approach to the problem be the method used.

A sail, as most commonly used, is a non-rigid airfoil constructed of fabric. Its leading edge is usually rigidly supported, and generally at least one other edge is supported in a like manner. The sail may be provided with a jib which is similar in location and in purpose to a slat for a conventional rigid airfoil.

The most basic sail configurations would naturally be of the two-dimensional group; that is, the leading and trailing edges would be rigidly supported, and the chordwise section would be constant across the span. As virtually no data are available for the two-dimensional set-up, the various specific sail variables that could profitably be investigated are too numerous to permit thorough study in this thesis. Some of these possible two-dimensional sail variables are: camber, leading-edge support shape and location, porosity, location and relative size of the jib, and Reynolds number.

INTRODUCTION (Cont'd)

In this study the two-dimensional effect was achieved by the use of circular endplates located about four feet apart. With this endplate system the basic aerodynamic characteristics of the following four-foot span models were investigated: 6-inch and 12-inch chord flat plates ($\frac{1}{8}$ inch thick); 6-inch and 12-inch (length of model surface perpendicular to the leading edge) non-porous cloth sails; and 6-inch cloth sail with 3-inch cloth jib.

The major portion of these investigations was concentrated upon the effects of camber as this appeared to be the most basic and effective of the two-dimensional sail variables. Both the 6-inch and the 12-inch cloth sails were used for the variation-of-camber studies. The 12-inch sail was used in order to obtain as accurate data as possible up to the maximum lift region ($\alpha_g \doteq 24^\circ$). Beyond this region the flow over the 12-inch sail was no longer two-dimensional. As the two-dimensional flow over a 6-inch sail did not break down until a higher angle of attack ($\alpha_g \doteq 64^\circ$), the 6-inch sail was used to obtain data beyond the accurate region of the 12-inch sail. Basically the data of the 6-inch sail are not as accurate as those of the 12-inch sail as the small measured forces are halved and the large tares due to the aerodynamic effects on the endplate system are doubled.

In order to obtain some idea of the effects of a jib on a sail a very limited study was made of the effects of camber of the 6-inch sail with a single jib configuration. Unfortunately, owing to the short period of tunnel time available for these investigations, a more complete study

INTRODUCTION (Cont'd)

of the effects due to other jib configurations was not possible.

For several reasons the most basic "sail" configuration, a flat plate, was studied. The reasons were: to obtain a configuration from which data could be compared with known results in order to ascertain the validity of the test set-up and procedure used; to provide data to use as a standard such that future investigations on two-dimensional sails using other test set-ups and procedures would have a basis for comparison; and to have a "sail" configuration which had zero camber. Investigations were conducted on both a 6-inch and a 12-inch flat plate.

The nature of the test and the models limited the experiments to a tunnel dynamic pressure of 5 psf. The flat plate models began to vibrate excessively for tunnel dynamic pressures greater than 7 psf. As it was necessary to enter the tunnel during runs to measure the camber of the cloth sail models, it was "convenient" to limit the tunnel dynamic pressure to about 5 psf (about 45 mph).

A good many runs were preliminary in nature as it was necessary to determine the model construction and the testing procedure. Very few details about such runs will be mentioned in this thesis. The other pertinent experimental data obtained during these investigations are presented here in their entirety along with a general discussion of the results. These investigations were conducted intermittently during the period of December 10, 1952 through February 25, 1953 as GALCIT Report 606.

II. TEST SET-UP AND PROCEDURE

The investigations conducted on the models were carried out in the closed throat three-dimensional working section of the GALCIT (Guggenheim Aeronautical Laboratory, California Institute of Technology) Ten-Foot Wind Tunnel. The working section is 10 feet in diameter and 10 feet in length with the trunnion axis $4\frac{3}{4}$ feet downstream from the leading edge of the working section. The contraction ratio is 4 to 1 (see Figure 1). The velocities in the working section were obtained by setting a static pressure difference between the tunnel piezometer (velocity calibration) rings.

Endplates suspended from the normal GALCIT three strut support system were used in order to approximate two-dimensional flow over the models tested. The angle of attack was controlled by a tail cross-piece connecting the pitch arms which were attached to the endplates. In order to obtain the necessary pitch variation it was necessary to move the pitch arms with respect to the endplates. Two such positions were used, P_1 permitting angles of attack from 0° to 45° and P_2 for angles of attack from 45° to 90° . To minimize the variations in, and the magnitudes of, the aerodynamic tares due to the presence of the endplate system in the windstream, the tail cross-piece and trunnion, and the main strut brace and trunnions were shielded (see Figure 2 and Model Photos 1, 2, and 3).

Before any tests were made on the models it was necessary to conduct two preliminary investigations, one to determine if a constant angle of attack could be obtained across the span of a cloth sail model, and the other to determine the magnitude of the aerodynamic tares due to the presence of the endplate system in the windstream.

TEST SET-UP AND PROCEDURE (Cont'd)

A 12-inch paper sail with $\frac{1}{8}$ inch rod leading and trailing edges (threaded at the ends for attaching to the endplates) was used to observe whether the leading and trailing edges of the model would bow the same amount. Equal bow was necessary to obtain a constant angle of attack across the model span. Photographs were made of the paper sail at a tunnel dynamic pressure of about 5 psf. The photographs showed that it was possible to adjust the tension in the leading and trailing edges of the models in such a way that they would have an equal amount of bow (see Model Photo 2). Another paper sail was tested having a $\frac{1}{16}$ inch wire for the trailing edge. As the wire trailing edge decreased the drag considerably, this trailing edge configuration was used for the cloth sails. Four non-adjustable ribs equally spaced across the span were used to keep the distance constant between the leading and trailing edges.

The following procedure was used to determine the aerodynamic tares. A 12-inch chord plywood model $\frac{1}{4}$ inch thick was used to generate a wake in order to obtain as realistic a set of aerodynamic tares as possible. The plywood model was suspended between the endplates, without coming into contact with them, by guy wires attached to the tunnel walls (see Model Photo 3). Aerodynamic tares were obtained by varying the angle of attack of the endplates independently of the plywood model. As it was a lengthy process to alter the angle of attack of the plywood model, only a limited number of widely spaced angles were used.

The flat plate models were attached to the endplates by threaded $\frac{1}{8}$ inch rods at the leading and trailing edges of each model. The leading edges were rounded and the trailing edges were beveled from the trailing

TEST SET-UP AND PROCEDURE (Cont'd)

edge of the lower surface to one inch forward on the upper surface in order to minimize the flow from the lower surface over the trailing edge to the upper surface. It was found that this beveling did not alter the flow from that obtained with the rounded trailing edge. Pictures of tufts attached to the upper surface of both flat plate models were taken in order to indicate the surface flow conditions.

The cloth sails all had $\frac{1}{16}$ inch wire for the trailing edges and $\frac{1}{16}$ inch wire, $\frac{3}{32}$ inch rod, and $\frac{1}{8}$ inch rod for the leading edges of the 3-inch, 6-inch, and 12-inch models, respectively. All the cloth sail models had five equally spaced ribs between the leading and trailing edges. These ribs were adjustable in order that the slack could be varied. The gaps between the edges of all the models tested (with the exception of the plywood wake-generator model) and the endplates were sealed with the approximate airfoil shape that occurred in the center of the model span. No tufts were attached to the upper surface of the cloth sail models but probing was done with a tufted rod to observe the flow conditions in the vicinity and on the upper surface of the models. In order to measure the camber of the cloth sail models it was necessary for an observer to remain in the working section while the tunnel was being run at a dynamic pressure of 5 psf.

III. METHODS OF REDUCTION AND PRESENTATION OF DATA

A. Reduction of Data

The data obtained during the course of these investigations are: lift, drag, pitching moment, maximum camber, and position of maximum camber. These data are all reduced to dimensionless coefficient form. In addition, from the force and moment data, the resultant force, its position, and its direction were determined and are included in the plots. The force and moment data are corrected for the aerodynamic tares due to the presence of the endplate system in the windstream. It was not necessary to correct for the flow inclination at zero lift as the lift curves for the flat plate models (see Figures 15 and 28) indicate that the geometric angle of attack is very nearly the aerodynamic angle of attack. No attempt was made to correct for the effects of wind-tunnel wall interference, solid and wake blockage of the models, and variation of tunnel velocity in the vicinity of the models. As the investigations are relative in nature, the above effects do not affect the relationships of the various models to an appreciable degree. The variation of the tunnel velocity in the vicinity of the models is quite small (about $\frac{1}{2}\%$ from the value at the tunnel centerline) when the endplate system is not installed. Its presence should make very little difference on the velocity distribution between the endplates.

As these investigations are concerned with the comparison of the data of a sail having varying slack, the lift, drag, and pitching moment coefficients are based upon the total area of the models (when the 3-inch jib is used its area is included in the total area). Since the pitching

METHODS OF REDUCTION AND PRESENTATION OF DATA (Cont'd)

moment coefficient data as presented in this thesis are about the leading edge of either the 6-inch or the 12-inch models, the characteristic length used in the reduction of these data is the length of model surface perpendicular to the leading edge (the length of the 3-inch jib is not included). The location of the resultant force is expressed as a ratio of the chord, i.e., the actual distance between the leading and trailing edges of the 6-inch or 12-inch models.

B. Presentation of Data

The data are presented in the form of plotted points connected by faired curves. All plotted points represent experimental observations. The data appear in the following groups of figures:

1. Aerodynamic tares
2. Cross plots and comparison plots
3. Idealized force plots for a flat plate model
4. Data of the various models tested
5. Pictures of tufts on the flat plate models

The following convention of symbols indicating experimental data is used:

1. Aerodynamic Tares

$\circ \sim$ Lower α_g range; $q = 10$ psf	}	With 12-inch wake generator
$\Delta \sim$ Lower α_g range; $q = 5$ psf		
$\oslash \sim$ Upper α_g range; $q = 10$ psf		
$\triangleleft \sim$ Upper α_g range; $q = 5$ psf		

METHODS OF REDUCTION AND PRESENTATION OF DATA (Cont'd)

$++ \sim 10^\circ$ too much wake*

$+ \sim 5^\circ$ too much wake

$- \sim 5^\circ$ too little wake

$-- \sim 10^\circ$ too little wake

$\times \sim$ No wake generator used

2. Cross Plots

$\circ \sim$ 12-inch model

$\Delta \sim$ 6-inch model

$\square \sim$ 6-inch model with 3-inch jib

$\nabla \sim$ 3-inch jib

$\diamond \sim$ For parabolic airfoil shape

3. Data of the Various Models Tested

$\circ \sim$ Lower α_g range } Data obtained with
 $\Delta \sim$ Upper α_g range } increasing α_g

Tagged symbols (σ, Δ) \sim Check points

Crossed tagged symbols (σ^x, Δ^x) \sim Hysteresis effects; Data
obtained with decreasing α_g

*Wake generator set at an angle of attack 10° greater than the effective angle of attack of the endplate system

IV. NOMENCLATURE

Definition of Tests

- P_1 = Polar test; angle of attack variation for which pitching moment static tares due to weight of model and endplate system are determined at $q = 0$
- P = Polar test; angle of attack variation for which lift, drag, and pitching moment data are obtained
- TVC = Tunnel velocity calibration; relation of tunnel dynamic pressure at intersection of tunnel centerline with trunnion axis with respect to static pressure difference of piezometer rings
- TFC = Tunnel static pressure calibration; relation of static pressure at intersection of tunnel centerline with trunnion axis with respect to tunnel dynamic pressure
- M = Measurements of maximum camber of sail and its distance aft of the sail leading edge are obtained
- M_1 = Measurements of maximum camber of sail are obtained
- Pict. = Pictures of model W_p^{12} are obtained which show the relative upward bow of the leading and trailing edges of the sail. It is shown that the leading and trailing edges bowed approximately the same amount, hence the angle of attack across the model span is constant
- Tuft Pict. = Pictures of tufts on upper surface of flat plate models are taken to indicate the flow
- Probe = Probing with a tufted rod in the vicinity of the model in order to determine the flow conditions

NOMENCLATURE (Cont'd)

Definition of Angular and Linear Measurements

- α_g = Angle of attack of model reference chord with respect to tunnel horizontal plane of symmetry. Reference chord is defined as the line connecting the midpoints of the leading and trailing edges. Positive angular displacement is defined when the leading edge is raised relative to the trailing edge (as a tunnel observer would see it). When two values $(-/x)$ appear in the Index of Runs the dash indicates that the α_g of the endplates is varied while the x indicates the α_g of the model. Otherwise the α_g is the same for the endplates and the model. When the 3-inch jib is present, α_g refers to the 6-inch sail
- ψ = Angle of yaw of model vertical plane of symmetry with respect to tunnel vertical plane of symmetry = 0°
- θ = Direction of resultant force on model with respect to tunnel axis. Measured positive in an upward direction; equal to zero degrees for resultant force in direction of windstream
- ℓ = Length of model surface perpendicular to the leading edge
- c = Chord of model; distance between leading and trailing edges
- Δ = Slack of model; distance trailing edge moved toward leading edge from maximum chord ($c = \ell - \Delta$). When two values of slack appear in the Index of Runs, the first refers to the 3-inch jib and the second refers to the 6-inch sail
- x = Distance of center of pressure (resultant force) from leading edge of model. When 3-inch jib is used, x refers to leading edge of 6-inch sail
- x_c = Distance of maximum camber position from leading edge of model
- y = Maximum camber of model
- d = Distance model leading edge forward of trunnion axis
- e = Distance model trailing edge above trunnion axis at $\alpha_g = 0^\circ$

NOMENCLATURE (Cont'd)

()_x = Refers to model with $\ell = x$

See Figures 4 and 5 for pictorial definitions of above angular and linear measurements

Definition of Coefficients

- C_L = Lift coefficient = $\frac{\text{lift}}{qS}$ (C_L is positive when it tends to lift the model)
- $C_{L\tau}$ = Tare lift coefficient = $\frac{\text{tare lift}}{qS}$
- C_D = Drag coefficient = $\frac{\text{drag}}{qS}$ (C_D is positive when it acts in the direction of the relative wind)
- $C_{D\tau}$ = Tare drag coefficient = $\frac{\text{tare drag}}{qS}$
- C_m = Pitching moment coefficient = $\frac{\text{pitching moment}}{qS\ell}$ (C_m is positive when it tends to raise the leading edge)
- $C_{m\tau}$ = Tare pitching moment coefficient = $\frac{\text{tare pitching moment}}{qS\ell}$
- $C_{m_{LE}}$ = C_m referred to leading edge of 6-inch or 12-inch model
- C_R = Resultant force; vector sum of C_L and C_D
- R = Reynolds Number = $\frac{\rho \ell V}{\mu}$

The following symbols are used for the foregoing coefficients

- S = Surface area of model (one side only; not wetted area).
 $S = b(\ell_6 + \ell_3)$ when the 3-inch jib is used
- b = Model span
- ℓ = Length of model surface perpendicular to leading edge. When 3-inch jib is used, ℓ is for 6-inch sail only
- q = Tunnel dynamic pressure at intersection of tunnel centerline and trunnion axis ($\frac{\rho V^2}{2}$, psf)
- V = Windstream velocity = $\sqrt{\frac{2q}{\rho}}$
- ρ = Mass density of air (Note: A correction is applied in the

NOMENCLATURE (Cont'd)

tunnel airspeed calibration so that in the above formulae ρ is to be taken as the free air density unaffected by compressibility.)

μ = Absolute viscosity of air = $3.726 \times 10^{-7} \frac{\text{lbwt. sec}}{\text{ft}^2}$
(for $T = 15^\circ\text{C}$, $h = 760 \text{ mm Hg}$)

V. DEFINITION OF CONFIGURATION SYMBOLS

<u>Notation</u>		<u>Figure No.</u>	<u>Photo No.</u>
P_1	= Endplate system positioned for α_g range of -5° to 50°	2	1
P_2	= Same as P_1 except positioned for α_g range of 40° to 95°	2	4
W_w^{12}	= 12-inch model made of $\frac{1}{4}$ inch plywood used to generate wake for the determination of aerodynamic tares. It was suspended between endplates in position of other 12-inch models by guy wires attached to the tunnel walls, but did not come into contact with the endplates	3	3
$W_{p'}^{12}$	= 12-inch pilot test model constructed of tissue paper on a framework. The leading and trailing edges of the framework were $\frac{1}{8}$ inch rods separated by four equally spaced non-adjustable ribs	3	2
W_p^{12}	= Same as $W_{p'}^{12}$ except $\frac{1}{16}$ inch wire used for trailing edge	3	
W_s^{12}	= 12-inch standard model constructed of $\frac{1}{32}$ inch sheet steel. Because of excessive flutter no tests were performed on this model	3	
$W_{a'}^{12}$	= 12-inch standard (flat plate) model constructed of $\frac{1}{8}$ inch aluminum sheet. Leading and trailing edges were rounded	3,42	
W_a^{12}	= Same as $W_{a'}^{12}$ except with a sharp trailing edge	3	
W_a^6	= Same as W_a^{12} except 6-inch model	3,43	
W_c^{12}	= 12-inch sail model constructed of 30 mesh nylon material attached to framework. Material was impregnated with a latex compound in order to make it non-porous. Framework consisted of a $\frac{1}{8}$ inch rod leading edge and a $\frac{1}{16}$ inch wire trail-	3	

DEFINITION OF CONFIGURATION SYMBOLS (Cont'd)

<u>Notation</u>	<u>Figure No.</u>	<u>Photo No.</u>
ing edge separated by five equally spaced adjustable ribs		
W_c^6 = 6-inch sail model constructed of 100 mesh nylon material made non-porous attached to framework. Framework consisted of a $\frac{3}{32}$ inch rod leading edge and a $\frac{1}{16}$ inch wire trailing edge separated by five equally spaced adjustable ribs	3	5,6
W_c^3 = 3-inch sail model used as a jib for W_c^6 . Similar in construction to W_c^6 except $\frac{1}{16}$ inch wire for leading edge	3	6

Model dimensions (3-inch, 6-inch, 12-inch) refer to length of model surface perpendicular to leading edge. These dimensions are nominal. See table on page 16 for exact dimensions

VIA. BASIC MODEL DIMENSIONS

	Model						
	W_{p}^{12}	W_{w}^{12}	W_{a}^{12}	W_{a}^6	W_{c}^{12}	W_{c}^6	W_{c}^3
Span, Inches	$48\frac{1}{4}$	$47\frac{3}{4}$	$48\frac{1}{4}$	$48\frac{1}{4}$	$48\frac{1}{4}$	$48\frac{1}{4}$	$48\frac{1}{4}$
Length, Inches	12	12	12	6	$11\frac{7}{8}$	$5\frac{7}{8}$	$3\frac{1}{16}$
Surface Area, Ft ²	4.021	3.979	4.021	2.010	3.979	1.968	1.026

Endplates

Diameter	3 Feet
Thickness	$1\frac{1}{4}$ Inches
Bevel Angle	30°
Span	$48\frac{1}{4}$ Inches
Main Trunnion Spacing	55.70 Inches
Tail Length	37.72 Inches

Approximate Reynolds Numbers, $R \times 10^{-5}$

q, psf	Model		
	W^{12}	W^6	$W^6 + W^3$
5	3.82	1.91	2.86
10	5.40	---	---

VIB. SLACK AND CAMBER MEASUREMENTS

Run	ℓ , Inches	Δ , Inches	c, Inches	y, Inches	Δ/ℓ	y/ℓ
3	12	0	12	0	0	0
12	$11\frac{7}{8}$	"	$11\frac{7}{8}$	$\frac{11}{16}$	"	.058
15	"	$\frac{1}{8}$	$11\frac{3}{4}$	$\frac{15}{16}$.011	.079
14	"	$\frac{1}{4}$	$11\frac{5}{8}$	$1\frac{3}{16}$.021	.100
18	"	$\frac{3}{8}$	$11\frac{1}{2}$	$1\frac{7}{16}$.032	.121
13	"	$\frac{1}{2}$	$11\frac{3}{8}$	$1\frac{9}{16}$.042	.132
17	"	$\frac{5}{8}$	$11\frac{1}{4}$	$1\frac{11}{16}$.053	.142
16	"	$\frac{7}{8}$	11	$2\frac{1}{16}$.074	.174
8	"	1	$10\frac{7}{8}$	*	.084	*
10	"	$1\frac{1}{4}$	$10\frac{5}{8}$	$2\frac{5}{16}$.105	.195
21	"	$1\frac{5}{8}$	$10\frac{1}{4}$	$2\frac{9}{16}$.137	.216
19	"	2	$9\frac{7}{8}$	$2\frac{11}{16}$.168	.226
20	"	3	$8\frac{7}{8}$	$3\frac{3}{16}$.253	.268
5	6	0	6	0	0	0
23	$5\frac{7}{8}$	"	$5\frac{7}{8}$	$\frac{1}{4}$	"	.043
24	"	$\frac{1}{8}$	$5\frac{3}{4}$	$\frac{5}{8}$.021	.106
25	"	$\frac{3}{16}$	$5\frac{11}{16}$	$\frac{11}{16}$.032	.117
26	"	$\frac{1}{4}$	$5\frac{5}{8}$	$\frac{3}{4}$.043	.128
27	"	$\frac{3}{8}$	$5\frac{1}{2}$	$\frac{7}{8}$.064	.149
28	"	$\frac{1}{2}$	$5\frac{3}{8}$	$1\frac{1}{8}$.085	.192
36	"	"	"	"	"	"
37	"	"	"	"	"	"
29	"	$\frac{5}{8}$	$5\frac{1}{4}$	$1\frac{3}{16}$.106	.202

* No camber measurements taken (q = 10 psf)

SLACK AND CAMBER MEASUREMENTS (Cont'd)

Run	ℓ , Inches	Δ , Inches	c , Inches	y , Inches	Δ/ℓ	y/ℓ
34	$5\frac{7}{8}$	$\frac{5}{8}$	$5\frac{1}{4}$	$1\frac{1}{4}$.106	.213
31	"	$\frac{7}{8}$	5	$1\frac{7}{16}$.149	.245
35	"	"	"	"	"	"
32	"	$1\frac{1}{4}$	$4\frac{5}{8}$	$1\frac{9}{16}$.213	.266
34	$3\frac{1}{16}$	$\frac{5}{16}$	$2\frac{3}{4}$	$\frac{5}{8}$.102	.225
35	"	"	"	"	"	"
36	"	"	"	"	"	"

VII. INDEX OF RUNS

Run	Configuration	Test	$q, \frac{lb}{ft^2}$	$\alpha, ^\circ$	Remarks
P1	$P_1 W_p^{12}$	Pict.	5.07	-	Check bowing of L.E. and T.E.
P2	"	P	10.08	-	Pilot run
P3	P_1	"	"	-	Aero Tares
P4	$P_1 W_w^{12}$	"	-	12	" "
P5	"	"	-	8	" "
P6	"	"	-	4	" "
P7	"	"	-	-/16	" "
P8	"	"	-	-/20	" "
P9	"	"	-	-/35	" "
P10	"	"	-	-/45	" "
P11	"	"	-	-/60	N.G. (W_w^{12} incorrectly positioned)
P12	"	"	-	-/75	N.G. (W_w^{12} incorrectly positioned)
P12A	"	"	-	-/75	Aero Tares
P13	"	"	-	-/90	N.G. (Interference)
P13A	"	"	-	-/90	Aero Tares
P11A	"	"	-	-/60	" "
P14	"	"	-	-/25	" "
P15	"	"	-	-/30	" "
P16	P_1	"	10.08	-	" "
P17	"	P_1	0	-	Static Tares

INDEX OF RUNS (Cont'd)

Run	Configuration	Test	$q, \frac{lb}{ft^2}$	α_g°	Remarks
P18	P_1	TVC	-	-	Velocity Calibration
P19	"	TPC	-	-	Static Pressure Calibration
P20	" + W_s^{12}	P_1	0	-	Static Tares
P21	" + W_a^{12}	"	"	-	" "
P22	" + "	P	5	-	Pilot Run
P21A	P_2 + "	P_1	0	-	" "
P22A	" + "	P	5	-	" "
P23	P_1 + W_p^{12}	"	10	-	" "
1	" + W_a^{12}	"	5	-	
2	" + " + Tufts	Tuft Pict.	"	-	
2A	P_2 + " + "	Tuft Pict.	"	-	
1A	" + "	P	"	-	
3	P_1 + W_a^{12}	P + Probe	"	-	
3A	P_2 + "	P + Probe	"	-	
4	P_1 + W_a^6	P_1	0	-	
5	" + "	P	5	-	
6	" + " + Tufts	Tuft Pict.	"	-	
6A	P_2 + " + "	Tuft Pict.	"	-	
7	" + "	P_1	0	-	
5A	" + "	P	5	-	

INDEX OF RUNS (Cont'd)

Run	Configuration	Test	$q, \frac{lb}{ft^2}$	α_g^o	Slack (Inches)
8	$P_1 + W_c^{12}$	P	10	-	1
9	" + "	P_1	0	-	"
10	" + "	MP + Probe	5	-	$1\frac{3}{4}$
11	$P_2 + "$	P_1	0	-	"
10A	" + "	P + Probe	5	-	"
12	$P_1 + "$	MP	"	-	0
12A	$P_2 + "$	P	"	-	"
13	$P_1 + "$	MP	"	-	$\frac{1}{2}$
13A	$P_2 + "$	P	"	-	"
14	$P_1 + "$	MP	"	-	$\frac{1}{4}$
14A	$P_2 + "$	P	"	-	"
15	$P_1 + "$	MP	"	-	$\frac{1}{8}$
15A	$P_2 + "$	P	"	-	"
16	$P_1 + "$	MP	"	-	$\frac{7}{8}$
16A	$P_2 + "$	P	"	-	"
17	$P_1 + "$	MP	"	-	$\frac{5}{8}$
17A	$P_2 + "$	P	"	-	"
18	$P_1 + "$	MP	"	-	$\frac{3}{8}$
18A	$P_2 + "$	P	"	-	"
19	$P_1 + "$	MP	"	-	2

INDEX OF RUNS (Cont'd)

Run	Configuration	Test	$q, \frac{lb}{ft^2}$	α° g	Slack (Inches)
19A	$P_2 + W_c^{12}$	P	5	-	2
20	$P_1 + "$	MP	"	-	3
20A	$P_2 + "$	P	"	-	"
21	$P_1 + "$	MP	"	-	$1\frac{5}{8}$
21A	$P_2 + "$	P	"	-	"
22	$P_1 + W_c^6$	P_1	0	-	0
22A	$P_2 + "$	"	"	-	"
23	$P_1 + "$	$M_1P +$ Probe	5	-	"
23A	$P_2 + "$	P + Probe	"	-	"
24	$P_1 + "$	M_1P	"	-	$\frac{1}{8}$
24A	$P_2 + "$	P	"	-	"
25	$P_1 + "$	M_1P	"	-	$\frac{3}{16}$
25A	$P_2 + "$	P	"	-	"
26	$P_1 + "$	M_1P	"	-	$\frac{1}{4}$
26A	$P_2 + "$	P	"	-	"
27	$P_1 + "$	M_1P	"	-	$\frac{3}{8}$
27A	$P_2 + "$	P	"	-	"
28	$P_1 + "$	M_1P	"	-	$\frac{1}{2}$
28A	$P_2 + "$	P	"	-	"
29	$P_1 + "$	M_1P	"	-	$\frac{5}{8}$

INDEX OF RUNS (Cont'd)

Run	Configuration	Test	$q, \frac{lb}{ft^2}$	$\alpha, \frac{^\circ}{g}$	Slack (Inches)
29A	$P_2 + W_c^6$	P	5	-	$\frac{5}{8}$
30	$P_1 + "$	P_1	0	-	"
31	" + "	M_1P	5	-	$\frac{7}{8}$
31A	$P_2 + "$	P	"	-	"
32	$P_1 + "$	MP	"	-	$1\frac{1}{4}$
32A	$P_2 + "$	P	"	-	"
33	$P_1 + " + W_c^3$	P_1	0	-	$\frac{5}{16}$ $\frac{5}{8}$
33A	$P_2 + " + "$	"	"	-	" "
34	$P_1 + " + "$	M_1P	5	-	" "
35	" + " + "	P	"	-	" $\frac{7}{8}$
36	" + " + "	M_1P	"	-	" $1\frac{1}{2}$
36A	$P_2 + " + "$	P	"	-	" "
37	" + "	M_1P	"	-	$\frac{1}{2}$

VIII. INDEX OF FIGURES

I. Sketches

	<u>Page</u>
1. Sketch Showing Vertical Section Through Tunnel	45
2. Sketch Showing Two-View of Endplate System	46
3. Sketch Showing Various Models.	47
4. Sketch Showing Model Nomenclature.	48
5. Sketch Showing Location of Models.	49

II. Experimental Data

A. Aerodynamic Tares

6. C_{D_t} , C_{L_t} , C_{m_t} vs. α_g	50
---	----

B. Cross Plots

7. Effects of Camber— $C_{L_{max}}$, α_g (at $C_{L_{max}}$) vs. y/l	53
8. Effects of Camber— C_L , C_D , C_L/C_D , θ vs. y/l at $C_{L_{max}}$	54
9. Effects of Camber— C_L , C_D , C_L/C_D , θ vs. y/l at θ_{max}	55
10. Effects of Slack on Camber— y/l vs. Δ/l	56

C. Comparison Plots

11. Effects of Chord, $y/l = .1$ — C_D , C_L , C_m , C_R , x/c , θ vs. α_g ; C_D vs. C_L	57
12. Effects of Jib, $y/l = .192$ — C_D , C_L , C_m , C_R , x/c , θ vs. α_g ; C_D vs. C_L	61

D. Idealized Flat Plate Curves

13. C_{D_5}/C_{D_3} , C_{L_5}/C_{L_3} , C_{m_5}/C_{m_3} vs. α_g	65
14. C_D , C_L , C_m , C_R , x/c , θ vs. α_g ; C_D vs. C_L	66

E. 12-Inch Models

15. $y/l = 0$ — C_D , C_L , C_m , C_R , x/c , θ vs. α_g ; C_D vs. C_L	70
16. $y/l = .058$ — C_D , C_L , C_m , C_R , x/c , θ vs. α_g ; C_D vs. C_L	73
17. $y/l = .079$ — C_D , C_L , C_m , C_R , x/c , θ vs. α_g ; C_D vs. C_L	76

INDEX OF FIGURES (Cont'd)

	<u>Page</u>
18. $y/l = .100$ — C_D , C_L , C_m , C_R , x/c , θ vs. α_g ; C_D vs. C_L	79
19. $y/l = .121$ — C_D , C_L , C_m , C_R , x/c , θ vs. α_g ; C_D vs. C_L	82
20. $y/l = .132$ — C_D , C_L , C_m , C_R , x/c , θ vs. α_g ; C_D vs. C_L	85
21. $y/l = .142$ — C_D , C_L , C_m , C_R , x/c , θ vs. α_g ; C_D vs. C_L	88
22. $y/l = .174$ — C_D , C_L , C_m , C_R , x/c , θ vs. α_g ; C_D vs. C_L	91
23. $y/l = .195$ — C_D , C_L , C_m , C_R , x/c , θ vs. α_g ; C_D vs. C_L	94
24. $y/l = .216$ — C_D , C_L , C_m , C_R , x/c , θ vs. α_g ; C_D vs. C_L	97
25. $y/l = .226$ — C_D , C_L , C_m , C_R , x/c , θ vs. α_g ; C_D vs. C_L	100
26. $y/l = .268$ — C_D , C_L , C_m , C_R , x/c , θ vs. α_g ; C_D vs. C_L	103
27. $y/l =$ not measured, $\Delta/l = .084$ — C_D , C_L , C_m vs. α_g	106

F. 6-Inch Models

28. $y/l = 0$ — C_D , C_L , C_m , C_R , x/c , θ vs. α_g ; C_D vs. C_L	108
29. $y/l = .043$ — C_D , C_L , C_m , C_R , x/c , θ vs. α_g ; C_D vs. C_L	112
30. $y/l = .106$ — C_D , C_L , C_m , C_R , x/c , θ vs. α_g ; C_D vs. C_L	115
31. $y/l = .117$ — C_D , C_L , C_m , C_R , x/c , θ vs. α_g ; C_D vs. C_L	118
32. $y/l = .128$ — C_D , C_L , C_m , C_R , x/c , θ vs. α_g ; C_D vs. C_L	122
33. $y/l = .149$ — C_D , C_L , C_m , C_R , x/c , θ vs. α_g ; C_D vs. C_L	126
34. $y/l = .192$ — C_D , C_L , C_m , C_R , x/c , θ vs. α_g ; C_D vs. C_L	130
35. $y/l = .192$ — C_D , C_L , C_m vs. α_g ; C_D vs. C_L	134
36. $y/l = .202$ — C_D , C_L , C_m , C_R , x/c , θ vs. α_g ; C_D vs. C_L	137
37. $y/l = .245$ — C_D , C_L , C_m , C_R , x/c , θ vs. α_g ; C_D vs. C_L	140
38. $y/l = .266$ — C_D , C_L , C_m , C_R , x/c , θ vs. α_g ; C_D vs. C_L	143

G. 6-Inch Sail with 3-Inch Jib

39. $(y/l)_6 = .192$, $(y/l)_3 = .225$ — C_D , C_L , C_m , C_R , x/c , θ vs. α_g ; C_D vs. C_L	147
40. $(y/l)_6 = .213$, $(y/l)_3 = .225$ — C_D , C_L , C_m , C_R , x/c , θ vs. α_g ;	

INDEX OF FIGURES (Cont'd)

	<u>Page</u>
C_D vs. C_L150
41. $(y/l)_6 = .245$, $(y/l)_3 = .225$ — C_D , C_L , C_m , C_R , x/c , θ vs. α_g ; C_D vs. C_L153
<u>H. Tuft Pictures—Upper Surface</u>	
42. 12-Inch Flat Plate156
43. 6-Inch Flat Plate157

IX. INDEX OF MODEL PHOTOS

Photo
No.

1. Side view of P_1
2. Rear view of $P_1 + W_{p1}^{12}$, $q \doteq 5 \text{ lb/ft}^2$, $\alpha_g = 18^\circ$ (Run P1)
3. Front view of $P_1 + W_w^{12}$
4. Front view of $P_2 + W_a^{12}$
5. Front view of $P_1 + W_c^6$
6. Rear view of $P_2 + W_c^6 + W_c^3$

X. DISCUSSION

As the scope of the investigations covered by this thesis is quite extensive, it would be prohibitive to discuss in detail each of the many aspects, however important they may be. Since this thesis is mainly concerned with some basic aerodynamics of two-dimensional sails, only the effects of camber in a sail and the effects of a particular jib on a sail will be discussed in any detail while other items will be only briefly mentioned. For the convenience of those who might be interested in details of the other phenomena observed during these investigations, the data are included in order to facilitate such further study, but they may not be extensive enough to permit a full understanding of the phenomena.

A. Tares

The aerodynamic tares due to the presence of the endplate system in the windstream were determined with a 12-inch chord wake generator and also for no wake generator present. Because the process of obtaining tares was excessively time consuming, tares were determined only for the wake generator set at angles of attack of 4° , 8° , 12° , 16° , 20° , 25° , 30° , 35° , and 45° in the lower α_g range and for 45° , 60° , 75° , and 90° in the upper α_g range. The endplate system angle of attack intervals were 4° up to $\alpha_g = 20^\circ$ and then 5° up to $\alpha_g = 90^\circ$. Therefore situations occurred when the angle of attack of the wake generator was not equivalent to that of the endplate system. This resulted in either too much or too little wake being generated for certain angles of attack of the endplate system. This was taken into consideration in the fairing of the tare curves (see Figure 6).

DISCUSSION (Cont'd)

The following table gives the expected accuracies of the tare data for a 12-inch flat plate model:

C_D	$0^\circ < \alpha_g < 20^\circ$	$\pm .005$
	$20^\circ < \alpha_g < 90^\circ$	$\pm .010$
C_L	$0^\circ < \alpha_g < 90^\circ$	$\pm .015$
C_m	$0^\circ < \alpha_g < 90^\circ$	$\pm .010$

In estimating tares for the 6-inch models, an average of the tares determined for no wake generator present and for the 12-inch wake generator present was used. This is not the ideal method and no estimate of the accuracy can be specifically determined. As the data of the 6-inch and the 12-inch flat plate models are not quite identical before either has a breakdown in the two-dimensional flow, it can be seen that tares for each model size should be determined using the proper size of wake generator.

Tares for the 12-inch sail models having slack of 2 and 3 inches were estimated in proportion to the resulting chord length in a manner similar to that used for the 6-inch model. Also, the tares estimated for the 12-inch model with 3-inch slack were used for the 6-inch model with the 3-inch jib (corrected for the proper sail area).

It is necessary to exercise much more care in the determination of tares for the smaller chord models owing to the increased magnitude of the tares.

DISCUSSION (Cont'd)

B. Flat Plate Models

In spite of the use of estimated tares for the 6-inch models, the data for the 6-inch flat plate model compare quite favorably with those for the 12-inch flat plate model. Also, the data common to both angle of attack ranges are almost coincident. The main point is that the comparison does indicate the validity of the method of estimating tares for the 6-inch flat plate model.

At first only one size of model, the 12-inch, was to be tested during these investigations. But, as the two-dimensional flow over the 12-inch flat plate broke down at $\alpha_g = 32^\circ$, a 6-inch model was tested. Then the two-dimensional flow continued until $\alpha_g = 64^\circ$ before breaking down. The tuft pictures in Figures 42 and 43 indicate that for both the 6-inch and the 12-inch flat plate models the two-dimensional flow changes into sidewise flow outward from the center of the models at the critical angles of attack. This phenomenon is probably a function of the relationships of the model span and chord and the endplate diameter and model chord. It is possible that the Reynolds Number may have some effect, but Run 8 ($q = 10$ psf) does not indicate this possibility. More rigorous investigations of this phenomenon should be undertaken.

A very interesting relationship between the data for the 6-inch and the 12-inch flat plate models for $32^\circ < \alpha_g < 64^\circ$ is indicated in Figure 13. The ratios of the 6-inch data to the 12-inch data are nearly the same for the drag and lift (about 1.5) and just slightly higher for the pitching moment (about 1.65). By applying this relationship to the data of the

DISCUSSION (Cont'd)

12-inch model it is possible to estimate what the data for the 12-inch flat plate would have been had the flow remained two-dimensional throughout the entire angle of attack range. This was done with several refinements. According to Reference (1) the drag coefficient of a two-dimensional flat plate at $\alpha_g = 90^\circ$ is 1.98. In order to obtain this coefficient the factor of 1.45 was applied to the drag data rather than the factor of 1.5. The factor of 1.5 was applied to the lift data. As the factor for the pitching moment data was greater than the factors for the other data, it was decided to use 1.5 as the factor since the inaccuracy in the pitching moment tares for the 6-inch model could easily be responsible for this larger factor. This choice is further justified by the fact that the drop in the pitching moment data for the 12-inch model at $\alpha_g = 32^\circ$ is of the order of 1.5. It was necessary to alter the lift data so that the curve would go through zero at $\alpha_g = 90^\circ$ and the pitching moment data so the moment coefficient would be half the value of the drag coefficient at $\alpha_g = 90^\circ$. Figure 14 presents the two-dimensional flat plate coefficients (C_D , C_L , C_m , C_R , x/c , θ vs. α_g and C_D vs. C_L) estimated in this way.

C. 12-inch Sail

The effects of camber, $y/l = .058$ to $y/l = .268$ (obtained by varying the slack from $\Delta/l = 0$ to $\Delta/l = .168$) on the aerodynamic characteristics of a 12-inch, two-dimensional sail were investigated. One must use caution when analyzing the data for the 12-inch sail since the two-dimensional flow broke down at $\alpha_g = 32^\circ$ for the 12-inch flat plate. Except for $y/l = .058$ no readily apparent break occurs in the data. For $y/l = .058$ the break occurs at $\alpha_g = 27^\circ$, considerably sooner than for the flat plate.

DISCUSSION (Cont'd)

The reason for the general absence of this break is that the flow does not change abruptly from two-dimensional to cross flow. It changes in a very gradual manner. Investigations made by probing with a tufted rod indicated a very gradual change in the flow, so gradual that it could hardly be observed. It is likely that this gradual breakdown in the two-dimensional flow did not begin until after maximum lift. This is substantiated by the fact that the magnitudes of the maximum lifts of the 6-inch and the 12-inch models are nearly the same for each y/l value (see Figure 7).

In general, check points taken at maximum lift indicated that the data were repeatable. Apparently the hysteresis effects of angle of attack are small as the data are consistent regardless of the direction in which the angle of attack was changed (see Figure 17). The data common to both α_g regions are fairly consistent for all components and for all y/l values.

It is interesting to note the change in the shapes of the lift curves with increasing camber. The peak at maximum lift becomes broader for increasing camber until $y/l = .174$. Then the peak begins to form into two peaks. As this same effect occurs for the 6-inch sail, it may be considered not a result of the gradual breakdown of the two-dimensional flow, although the change in flow may influence the detailed shape and rate of change of shape.

It was possible to obtain positive lift for all camber values up to $y/l = .195$ at zero angle of attack. At $y/l = .195$ and $y/l = .226$, the minimum α_g required for positive lift was 5° . For $y/l = .268$ the minimum α_g

DISCUSSION (Cont'd)

for positive lift was 16° . When negative lift was first obtained (as α_g was decreased) the sail fluttered violently against its ribs. Otherwise no serious flutter occurred in the sails. At maximum lift the sails "buzzed", but this was limited to a very small α_g region of about 2° on either side of α_g for maximum lift.

D. 6-inch Sail

The effects of camber, $y/l = .043$ to $y/l = .266$ (obtained by varying the slack from $\Delta/l = 0$ to $\Delta/l = .213$) on the aerodynamic characteristics of a 6-inch, two-dimensional sail were investigated. Here one need not consider the breakdown in the two-dimensional flow when analyzing the data in the lower α_g region. The break occurs at about $\alpha_g = 64^\circ$ for $y/l = .043$ and increases to $\alpha_g = 68^\circ$ for $y/l = .245$. No break in the data occurs for the sail with $y/l = .266$. Apparently the flow remained almost two-dimensional up to $\alpha_g = 90^\circ$ as the drag value is about what would be expected for such flow.

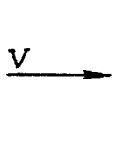
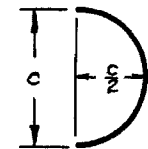
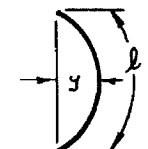
The drag data common to the two α_g ranges are fairly consistent, the lift data are not quite so consistent (a discrepancy of perhaps .05 to .10), and there is no correlation whatsoever in this region for the pitching moment data. In general, the pitching moment data show no well defined sequence of points during the entire α_g range. This is probably caused by the inherent inaccuracies of the balance readings. A token fairing is attempted for the pitching moment data, but it really has little significance.

The shapes of the lift curve peaks change in a manner similar to that described for the 12-inch sail. Also, beginning with $y/l = .149$ it

DISCUSSION (Cont'd)

was not possible to obtain positive lift at $\alpha_g = 0^\circ$. At maximum camber the minimum α_g for positive lift was only 5° . No reason is known for the difference in minimum α_g for positive lift at maximum camber between the 6-inch and the 12-inch sails. The same "buzzing" occurred in the region of maximum lift.

Included in a table on page 44 are experimental values of C_L and C_D at $\alpha_g = 90^\circ$ along with expected or computed values of these coefficients. Naturally, the expected C_L is zero (except for the 6-inch sail with a jib), but the estimated value for C_D was computed by the following method:

		
$C_{D_c} = 1.98$ (Reference 1)	$C_{D_c} = 2.30$	$C_{D_c} = 1.98 + \frac{2y}{c}(2.30 - 1.98)$ (Estimated for this thesis)

Then $C_D = \frac{c}{l} C_{D_c}$ where C_{D_c} is the drag coefficient based on the chord rather than on the arc length.

Inspection of this table reveals the following information: (a) Except for one case, the ratio of experimental to calculated drag coefficient lies between .672 and .721, a spread of only .049. This is quite remarkable as it shows that the type of flow at $\alpha_g = 90^\circ$ is virtually the same for all the model sizes. (b) The one case, $y/l = .266$ for the 6-inch sail, has a ratio of .940. This indicates that the flow probably is still nearly two-dimensional at $\alpha_g = 90^\circ$. A look at Figure 38 shows that no break in the data occurs. The reason why the flow over this particular configuration did

DISCUSSION (Cont'd)

not break down in the usual manner is not known. (c) The magnitude of the lift coefficient is greater at $\alpha_g = 90^\circ$ for the 12-inch case than for the 6-inch case. As the tares for the 6-inch case are doubtful, nothing definite can be stated. But a possible explanation for this is that the 12-inch models changed the effective flow direction several degrees while the 6-inch models had very little effect on the flow direction.

E. 6-inch Sail with 3-inch Jib

Because of the extremely limited testing period available for the investigation of the effects of a 3-inch jib on a 6-inch sail, only one jib camber, $y/l = .255$, and one jib location were used for three cambers of the 6-inch sail. Only data for $y/l = .192$ for the 6-inch sail were obtained for $\alpha_g = 46^\circ$. Nevertheless, as is indicated in the 6-inch and the 12-inch sail data, the data in the upper α_g region should not be materially different for such small changes in camber.

The shape of the lift curve peak is changed by the addition of the jib. It is more peaked for the same amount of camber in the 6-inch sail, but the maximum lift is virtually unchanged. The breakdown in the two-dimensional flow occurs at $\alpha_g = 53^\circ$. This seems reasonable as this α_g value lies between that for the 6-inch sail and that for the 12-inch flat plate (with a jib the 6-inch sail is essentially a 9-inch sail).

As the jib was at approximately negative 10° angle of attack relative to the 6-inch sail, no data below $\alpha_g = 10^\circ$ were obtained since it was necessary that the jib itself develop positive lift, i.e., that the cloth be free of the ribs.

DISCUSSION (Cont'd)

Here again the pitching moment tares appear to be unsatisfactory as there is no correlation in the data common to both α_g ranges. The lift and drag data compare favorably in the common region, but not as satisfactorily as for the 12-inch sail models. Apparently the procedure used to estimate the tares is not quite valid for this sail configuration.

F. Effects of Camber

Maximum C_L increases from about .92 for zero camber to about 1.7 for 10% camber and remains fairly constant until 23% camber before decreasing to 1.5 at 27% camber. Meanwhile α_g at $C_{L_{max}}$ steadily increases from 12° at zero camber to about 25° at 27% camber (see Figure 7). This variation and magnitude of maximum C_L is the same for the 12-inch models, 6-inch models, and the 6-inch sail with the 3-inch jib. Hence the conclusion can be drawn, pending more camber variation investigations on the 6-inch sail with a jib, that this jib configuration does not affect the maximum C_L for a particular camber of the sail. It is to be expected that the 12-inch and the 6-inch models show similar if not identical results as the only difference is a model scale factor. Although for both model sizes the α_g at $C_{L_{max}}$ increases steadily as the camber increases, the $C_{L_{max}}$ for the 12-inch sail occurs at a higher α_g (about 4°) than for the 6-inch sail. This is surprising as the α_g for $C_{L_{max}}$ is virtually the same for the flat plate models. Not enough data were taken during these investigations to indicate the reason for this discrepancy. The value of α_g at $C_{L_{max}}$ for $y/l = .268$ of the 12-inch sail is low compared to the rest of the data. It is possible that the two-dimensional flow broke down sooner than it usually did, hence causing this lower $C_{L_{max}}$.

DISCUSSION (Cont'd)

At $C_{L_{\max}}$ the ratio of C_L/C_D for the 6-inch and the 12-inch models increases from 4.5 at zero camber to its maximum of 8 at 7% camber and then gradually decreases to 2.4 at 27% camber (see Figure 8). As the camber effects of the 6-inch sail with a jib were investigated for only 19% to 25% camber, no definite conclusion can be drawn from the data. However, it appears that the jib, in the camber region investigated, increases the C_L/C_D ratio at $C_{L_{\max}}$ by about 2.5. This means that for the same camber the addition of a jib does decrease the drag at $C_{L_{\max}}$ although it does not affect the magnitude of $C_{L_{\max}}$.

The maximum ratio of C_L/C_D obtained as a function of camber increases from 14.3 at zero camber, reaches a maximum of 15 at 5% camber, and then steadily decreases to 3 at 27% camber (see Figure 9). In this case the maximum ratio of C_L/C_D is independent of the sail size and of the presence of the jib. Hence it can be concluded that the major effect of the jib is to increase the C_L/C_D ratio at $C_{L_{\max}}$ but not to increase the maximum C_L/C_D ratio.

In order to check the camber measurements, the camber function (y/l) is plotted against the slack function (Δ/l) in Figure 10. These curves for both the 6-inch and the 12-inch sails are similar to within the accuracy of measurement. For comparison a calculated curve, the ratio of y/l vs. Δ/l for a parabola, is superimposed. Except at small values of slack, it is consistent with those for the 6-inch and the 12-inch sails.

In order to compare in a direct manner the data obtained from a 6-inch sail and a 12-inch sail having the same camber ratio, the curves of

DISCUSSION (Cont'd)

Figure 30 ($y/l = .106$ for the 6-inch sail) and those of Figure 18 ($y/l = .100$ for the 12-inch sail) are both plotted in Figure 11. Except for the 5° shift in the α_g at maximum lift between the 6-inch and the 12-inch sails, the data are quite consistent when consideration is given to the fact that the flow over both models is different during the central α_g region ($25^\circ < \alpha_g < 65^\circ$). Superimposed upon this plot is a lightly dashed curve which is an estimation as to what the data should be for an ideal two-dimensional sail with a camber of 10%.

A qualitative comparison of the effects of a jib on the 6-inch sail with $y/l = .192$ can be obtained from Figure 12 where the curves from Figure 34 ($y/l = .192$ for the 6-inch sail) and from Figure 39 ($y/l = .192$ for the 6-inch sail with a jib) are plotted. The effects of the jib are to sharpen the lift curve peak, but not to change the maximum lift, and to decrease the drag at the maximum lift. Naturally the moment about the leading edge of the 6-inch sail and the location of the resultant force will be affected by the addition of the jib. But the direction of the resultant force is not materially affected by the addition of the jib. Here again a lightly dashed curve gives an estimation as to the expected data for a two-dimensional sail with a jib under two-dimensional flow conditions.

Also included in Figure 12 is a check run for the 6-inch sail at $y/l = .192$. This run was performed during a separate model installation, hence it should indicate not only the repeatability of the data, but also the repeatability of the test set-up. Unfortunately, as a result of the

DISCUSSION (Cont'd)

rush involved in the test set-up, apparently the angle of attack indicator was not zeroed when the model was leveled. Hence the indicated α_g is apparently 2° greater than the actual α_g . No correction has been made for this α_g discrepancy as it is not certain that this is the correct explanation for the 2° shift in all of the data. As the C_D vs. C_L curves are almost coincident up to $\alpha_g = 40^\circ$ and the shapes of the other curves are similar, this check run indicates that the data obtained from two entirely separate test set-ups are consistent if consideration is given to the 2° α_g shift.

G. Accuracy of Measurements

Owing to the fact that the measurements of the camber, slack, and sail length in the vicinity of the ribs differed from those measurements taken between the ribs, errors in these quantities resulted as all measurements were taken in the vicinity of the ribs. The following table indicates the probable maximum variation of these quantities across the span:

	W_c^{12}		W_c^6	
	inches	% l	inches	% l
l	$\frac{1}{16}$	0.5	$\frac{1}{16}$	1.0
s	$\frac{1}{8}$	1.0	$\frac{1}{16}$	1.0
x_c	$\frac{1}{4}$	2.1	$\frac{1}{16}$	1.0
y	$\frac{1}{8}$	1.0	$\frac{1}{16}$	1.0

Also, the accuracies of the individual measurements made are not expected to be better than the deviations of the measurements across the span.

DISCUSSION (Cont'd)

As the balance readings were unsteady, the raw data, when reduced to the usual dimensionless coefficient form, are reliable to no more than to the amounts indicated in the following table ($q = 5$ psf):

	W^{12}	W^6	$W^6 + W^3$
C_D	.0090	.0040	.0060
C_L	.012	.024	.018
C_m	.0072	.0288	.0172

XI. CONCLUSIONS

In spite of the many problems encountered and the estimates used, the data obtained can be interpreted to give consistent relative results and probably even absolute results to within a few percent. The effects that camber has upon the maximum lift and upon the ratio of lift to drag for the 12-inch and the 6-inch models are about the same. The only discrepancy, other than that in the pitching moment curves (and this discrepancy can easily be explained by the excessively large pitching moment tares which were estimated for the 6-inch models), occurs in the α_g for the maximum lift. For some not apparent reason the lift curve slopes of the 12-inch sails are less than those of the 6-inch sails for the same camber ratio although the maximum lifts are about the same (see Figure 7). This results in the maximum lift occurring for the 12-inch sails some 4° later than for the 6-inch sails. This phenomenon becomes even more baffling when it is realized that the α_g at maximum lift is the same for both the 12-inch and the 6-inch flat plate models.

It is felt that a good share of the discrepancies between the data of the 12-inch and the 6-inch models could be eliminated by a much more thorough procedure of obtaining the aerodynamic tares. More wake generators should be used in order to match the chord and airfoil shapes of the models to be tested. The usefulness of this elaborate procedure is limited by the fact that the flow over the wake generator would tend not to be quite two-dimensional as there are gaps between it and the endplates. Tufting of the surface would indicate to what degree the flow is two-dimensional. Also, more angles of attack of the wake generator should be used. A better approach to the refinement of the tare procedure would

CONCLUSIONS (Cont'd)

be to minimize the magnitudes of the tares. This could be accomplished by a more thorough shielding of the endplate system. The ultimate in this respect would be to use a two-dimensional tunnel for these investigations.

The results of these studies invite additional investigations on the following:

1. Effects of jib
 - a. Use more jib positions, sizes, and cambers
 - b. Use more cambers for the main sail with a jib
2. Side flow phenomenon
 - a. Use flat plates of varying chord and span
 - b. Use different endplate diameters
 - c. Tuft upper surface of sail models
 - d. Vary tunnel dynamic pressure over models
3. Determine reason for upward shift in α_g at maximum lift with increase in sail length perpendicular to leading edge

Possible investigations on additional two-dimensional parameters are as follows:

1. Effects of porosity
2. Effects of Reynolds number as obtained by a change in q . This presents the problem that the camber will be different for different values of q although the slack will be the same
3. Effects of size, shape, and location of leading edge and methods of attaching sail to it
4. Effects of controlling sail profile by using battens

XII. BIBLIOGRAPHY

1. Hoerner, Sighard F., "Aerodynamic Drag", Self-Published, 1951
2. Description of the GAIT Ten-Foot Wind Tunnel, The Model Suspension System, General Facilities and Model Specifications, Revised September 10, 1942 (Unpublished)
3. Everett, H. A., "Wind Tunnel Experiments with Yacht Sails", C. H. Peabody paper (MIT), 1915
4. Warner, E. P. and Ober, Shatswell, "The Aerodynamics of Sails" Proceedings of the Soc. of Naval Arch. and Marine Eng., Vol. 33, 1925
5. Davidson, K. S. M., "Some Experimental Studies of the Sailing Yacht" Soc. of Naval Arch. and Marine Eng. Transactions, Vol. 44, 1936

XIII. CALCULATED AND EXPERIMENTAL LIFT AND DRAG

AT $\alpha_g = 90^\circ$

Run	Model	y/l	C_L		C_D		
			Expected	Experimental	Calculated ⁺	Experimental	Ratio
3	W^{12}	0	0	.032	1.980	1.372	.693
12	"	.058	"	.070	2.017	1.454	.721
15	"	.079	"	.048	2.010	1.425	.709
14	"	.100	"	.031	2.002	1.384	.691
18	"	.121	"	.028	1.995	1.421	.712
13	"	.132	"	.052	1.981	1.373	.693
17	"	.142	"	.084	1.967	1.365	.694
16	"	.174	"	.083	1.945	1.343	.691
10	"	.195	"	.072	1.897	1.349	.712
21	"	.216	"	.082	1.847	1.298	.703
19	"	.226	"	.076	1.791	1.234	.689
20	"	.268	"	.072	1.652	1.113	.674
5	W^6	0	"	.010	1.980	1.330	.672
23	"	.043	"	.064	2.007	1.358	.677
24	"	.106	"	.018	2.005	1.364	.680
25	"	.117	"	-.008	1.992	1.360	.683
26	"	.128	"	-.002	1.977	1.339	.677
27	"	.149	"	.010	1.949	1.350	.693
28	"	.192	"	.010	1.934	1.330	.688
29	"	.202	"	-.023	1.920	1.337	.696
31	"	.245	"	-.008	1.842	1.277	.693
32	"	.266	"	-.027	1.729	1.625	.940
36	$W^6 + W^3$.192*	-	.170	1.893	1.349	.713

⁺ See page 34 in discussion for procedure used

* For 6-inch sail

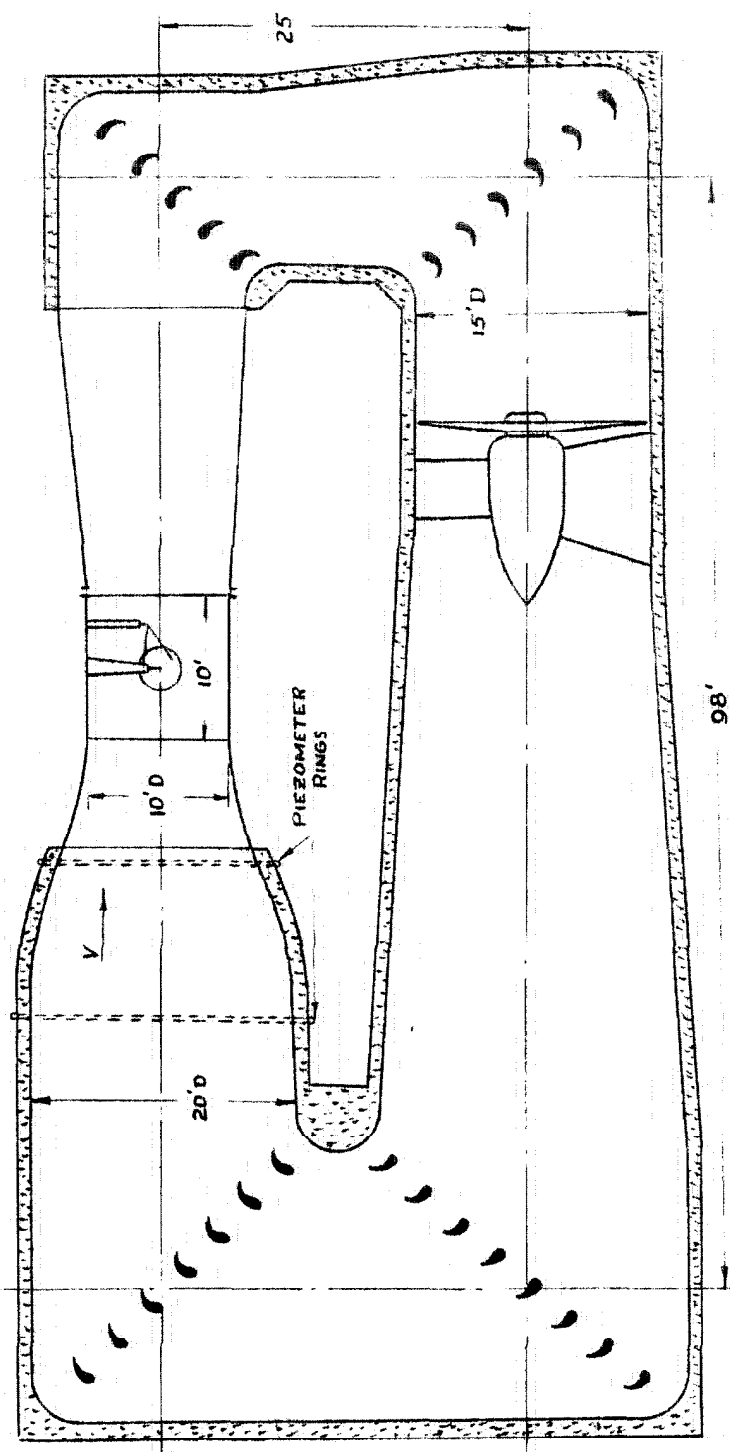
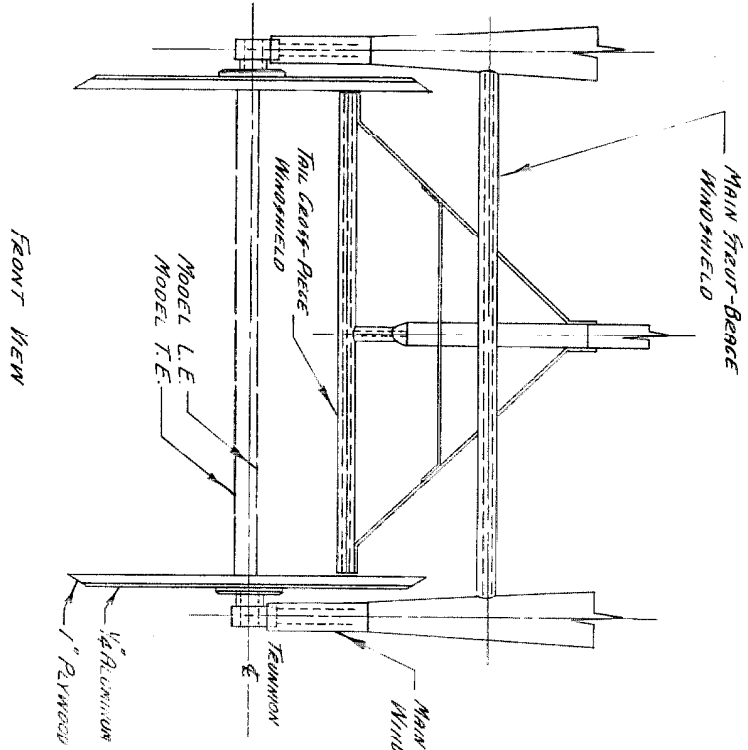
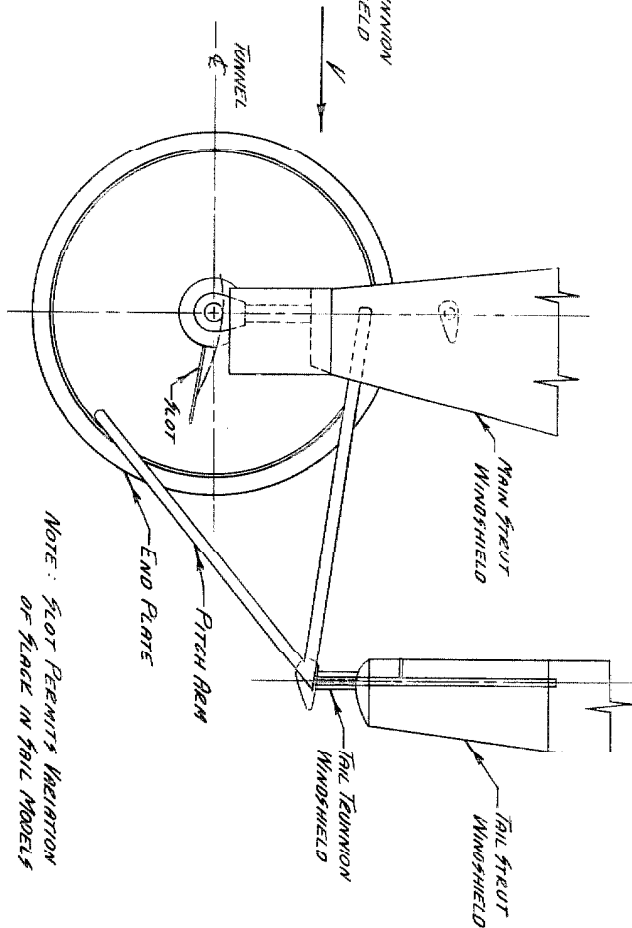


FIGURE 1

SKETCH SHOWING VERTICAL SECTION THROUGH TUNNEL



FRONT VIEW



SIDE VIEW

NOTE: SLOT PERMITS VARIATION
OF PLACE IN TAIL MODELS

SCALE: 1"=12"

FIGURE 2

SKETCH SHOWING
TWO-VIEW OF ENDPLATE SYSTEM

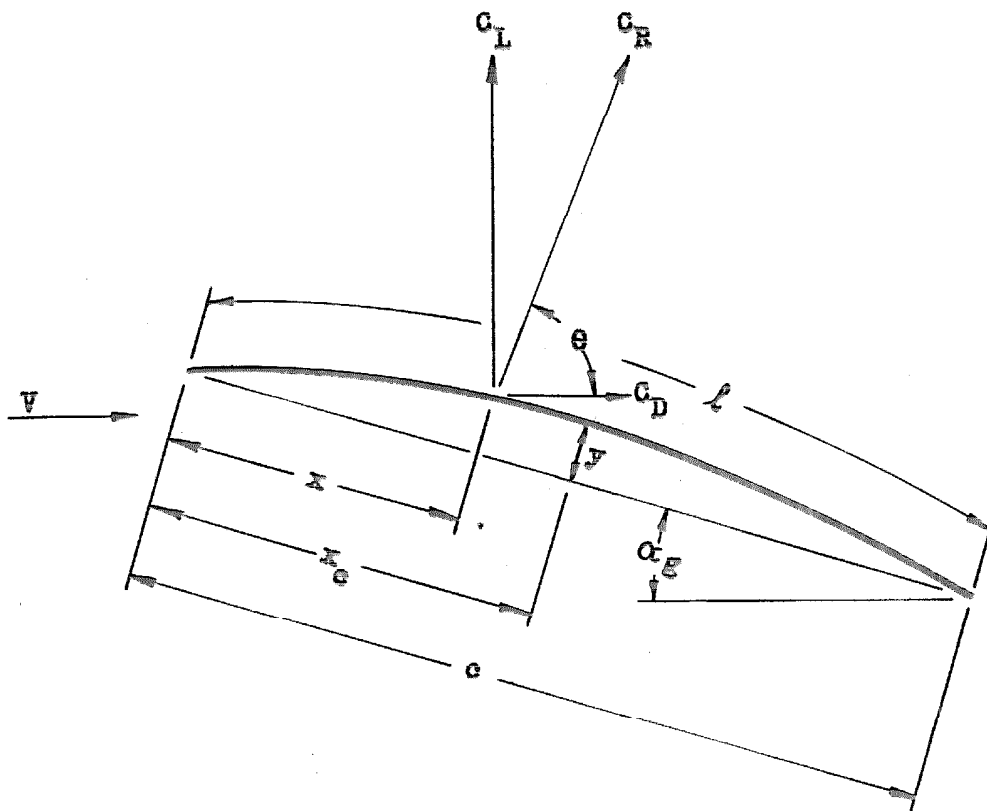
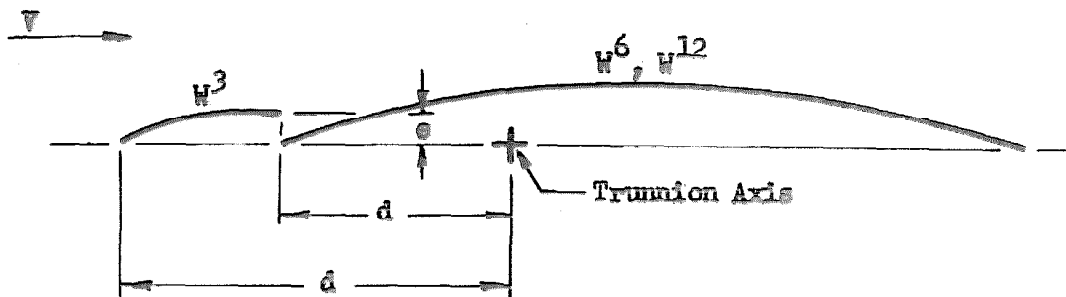


FIGURE 4
SKETCH SHOWING
MODEL NOMENCLATURE



Model	d	•
W_v^{12}	3.75	0
W_p^{12}	"	"
W_s^{12}	"	"
W_a^{12}	"	"
W_a^6	1.95	"
W_c^{12}	3.75	"
W_c^6	1.92	"
W_g^3	4.69	0.50

Dimensions Are in Inches

FIGURE 5
SKETCH SHOWING
LOCATION OF MODELS

$$\frac{0.01 \text{ CO}}{\Delta \cdot \Delta \text{ CO}} = \frac{11.6 \text{ LB/FT}^2}{\Delta \cdot \Delta \text{ CO}}$$

$$q = 4 \text{ CO/FT}^2$$

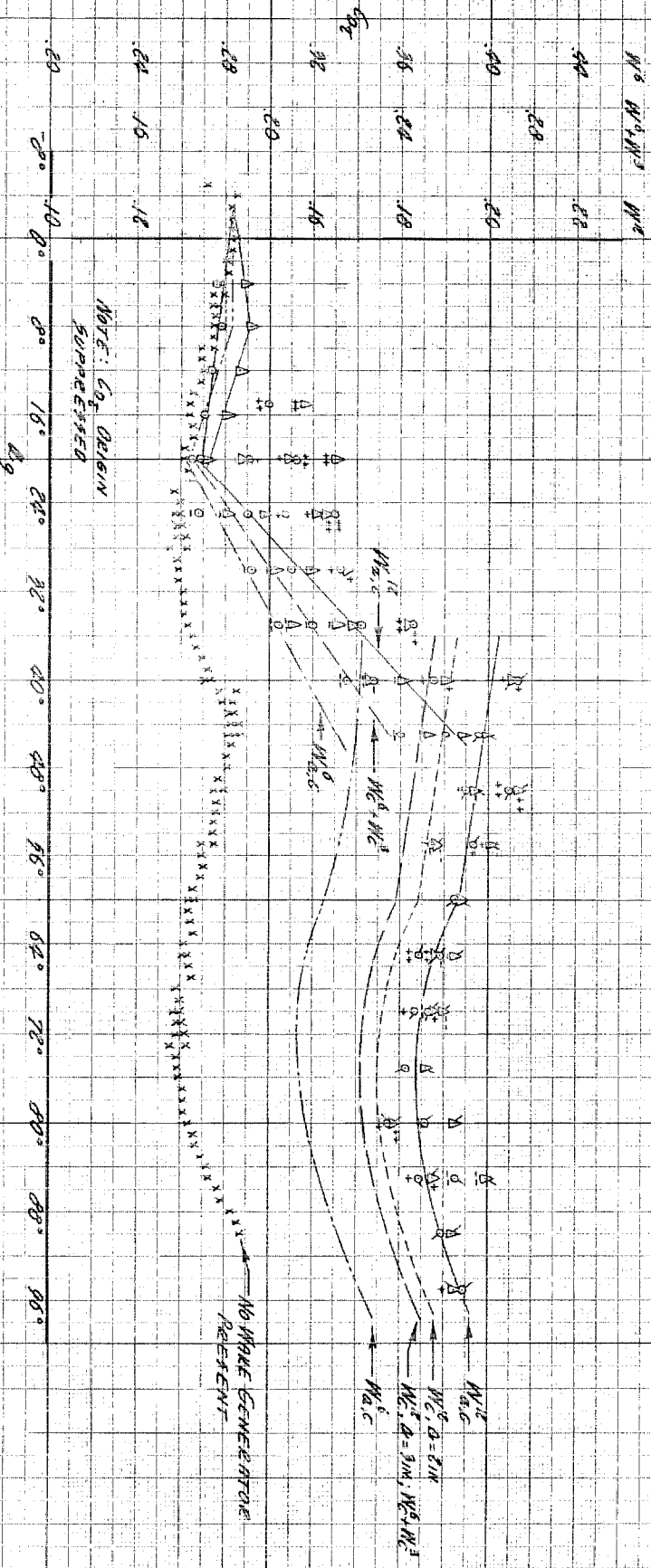
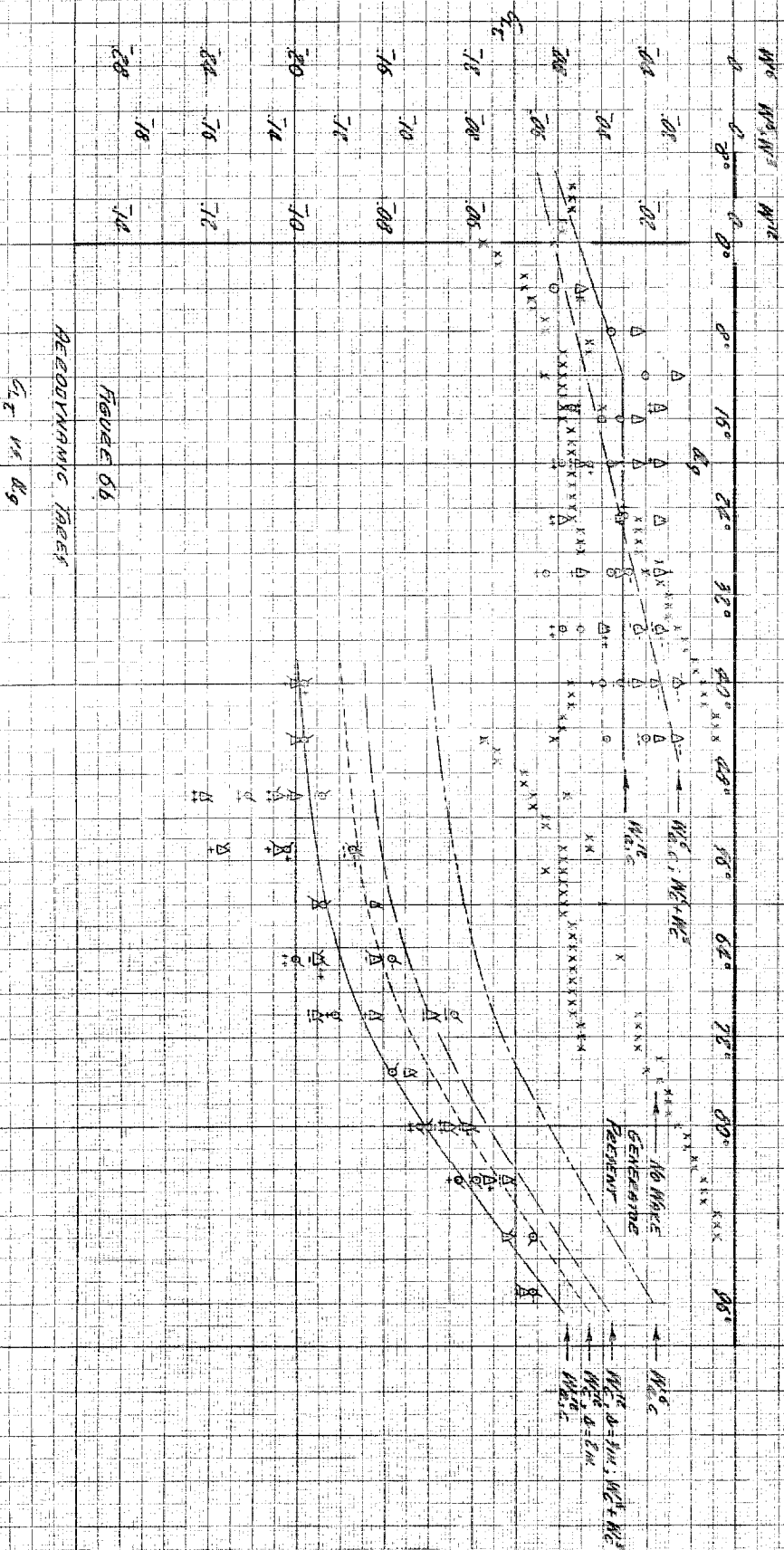


FIGURE 5A
DYNAMIC TREES
CO₂ VS. t

$$0.01 \text{ sec } \rho = 10.0 \text{ ft/sec}^2$$

$$\Delta X \text{ sec } \rho = 1.0 \text{ ft/sec}^2$$



HYDRODYNAMIC FORCES

CLT 14 Rg

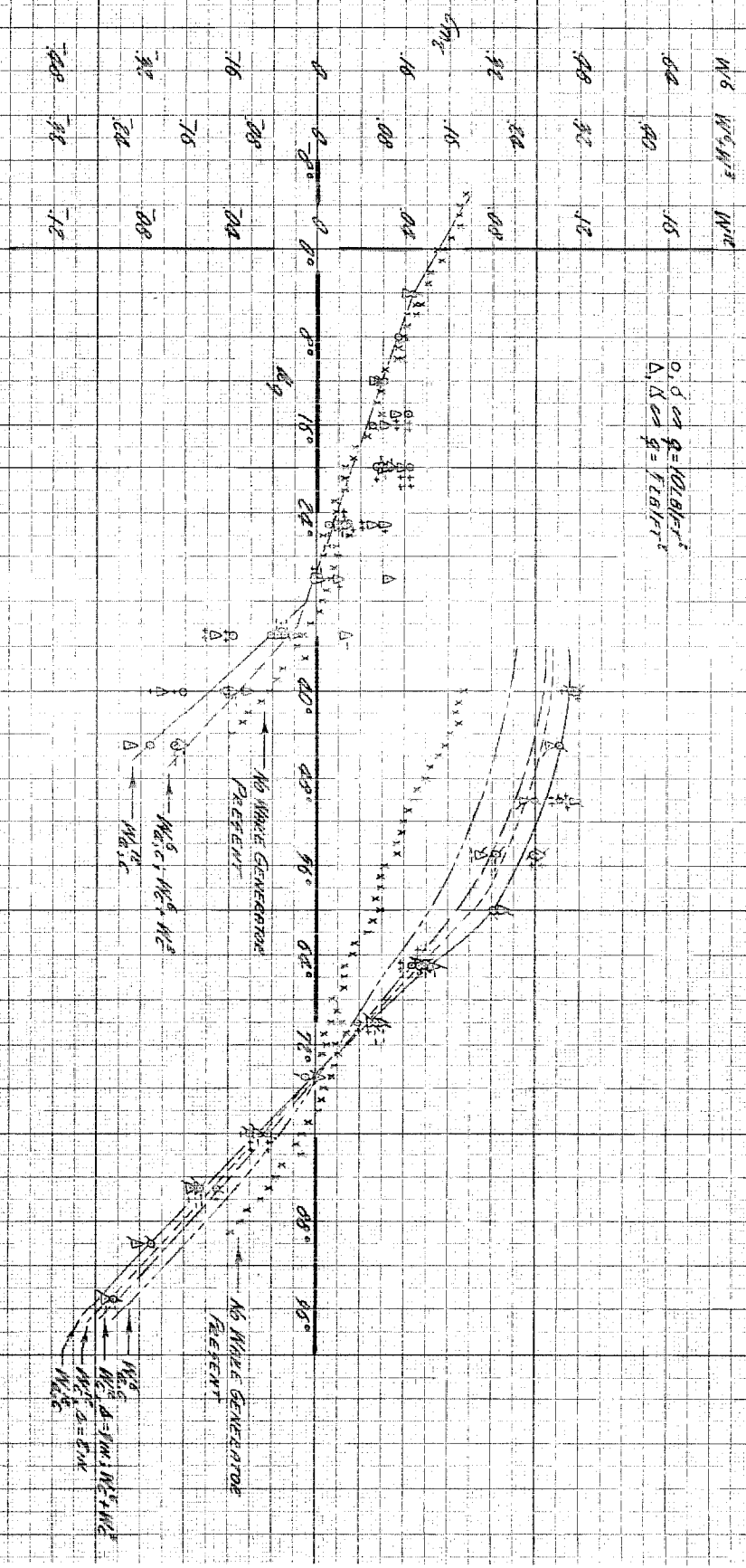


FIGURE 6C

HYDRODYNAMIC PRESSURE

Cont. of 6B

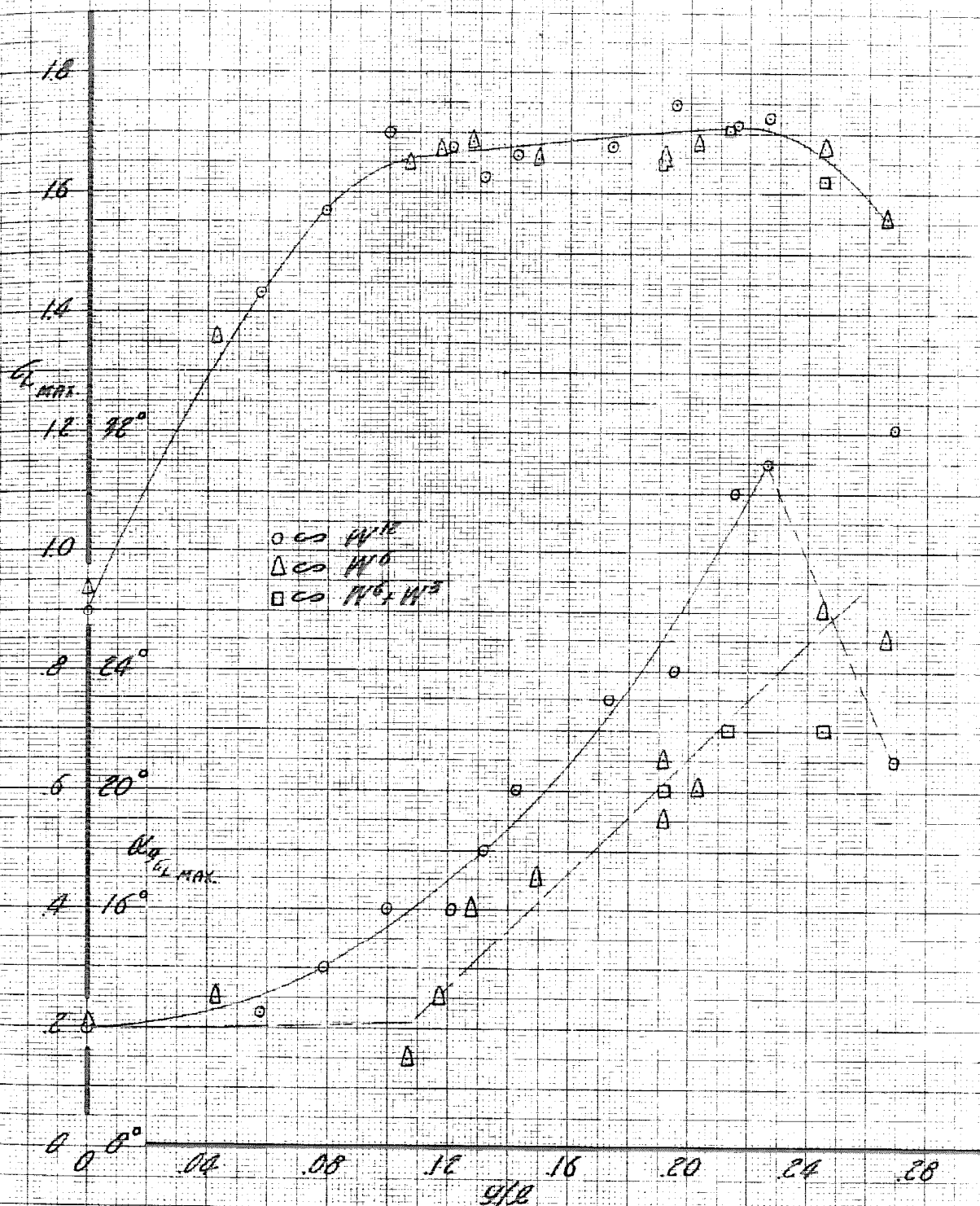


FIGURE 7

EFFECTS OF CAMBER

$G_{max}, G_d(AT G_{max})$ vs. y/R

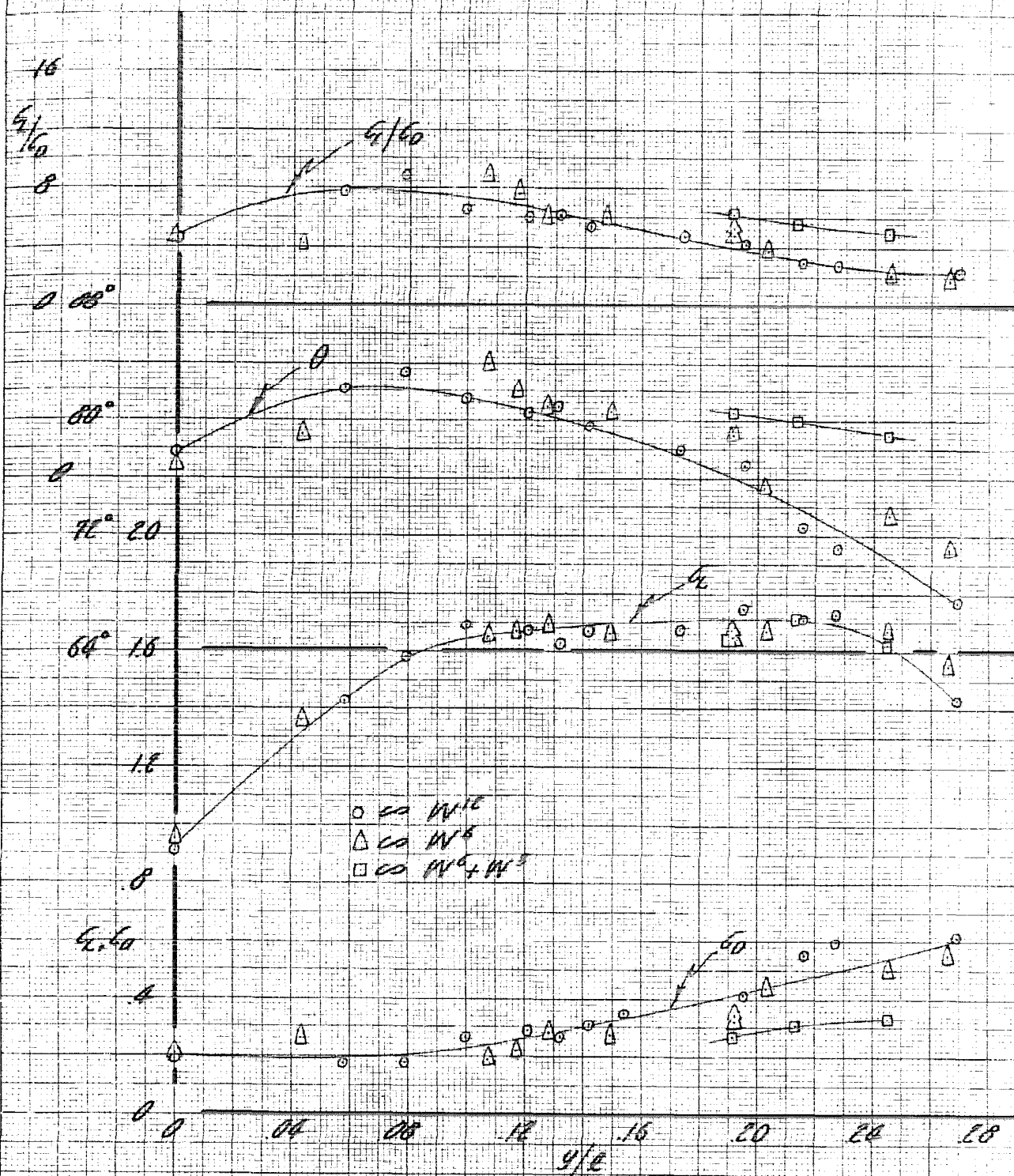


FIGURE 8
EFFECTS OF CAMBER

$G/L, G/D, G/L/GD, \theta$ VS. y/l AT $G_1 \text{ MAX}$

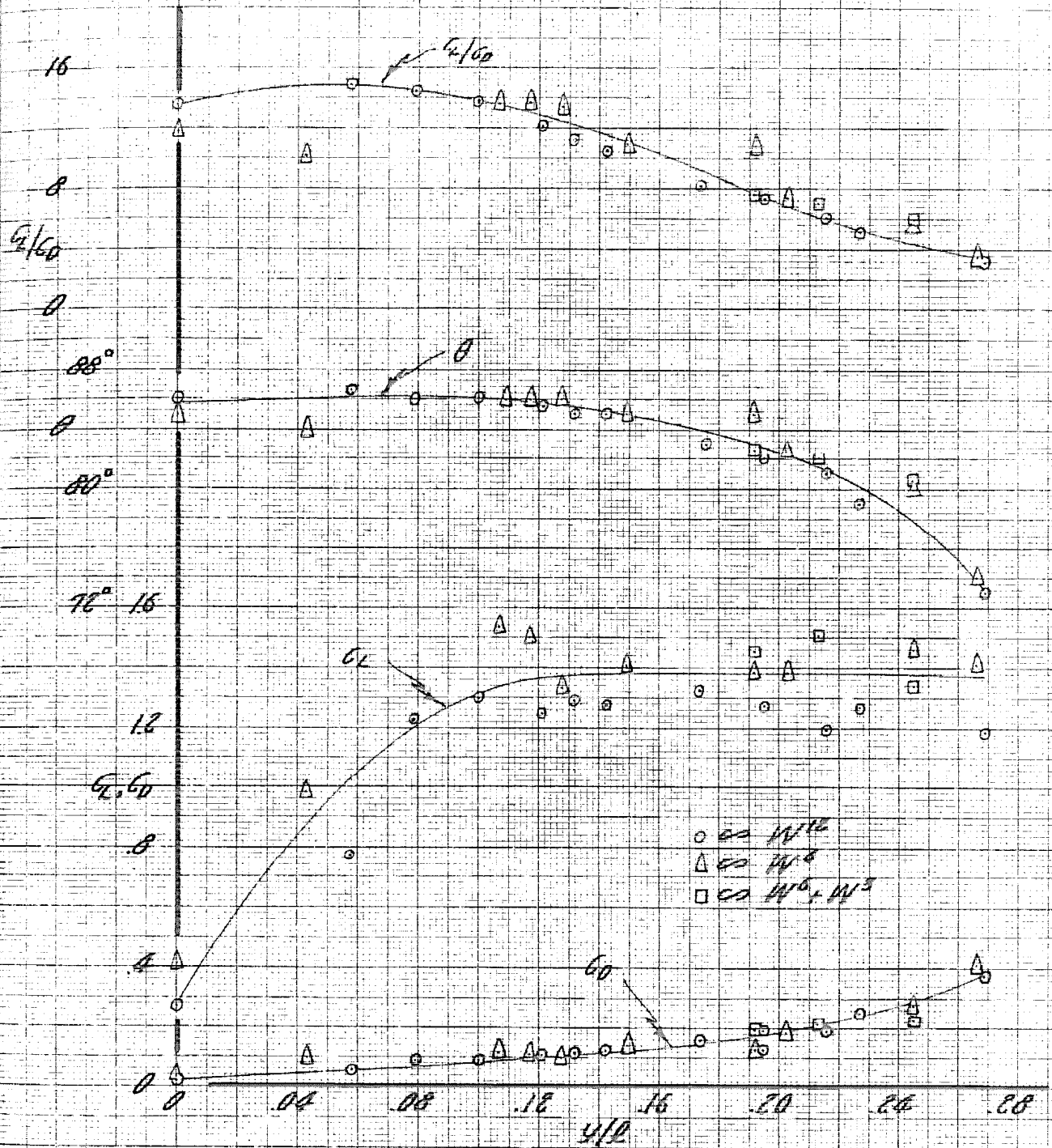


FIGURE 9

EFFECTS OF GAMBER

$GL, GD, GL/GD, \theta$ vs. y/B
AT θ_{max}

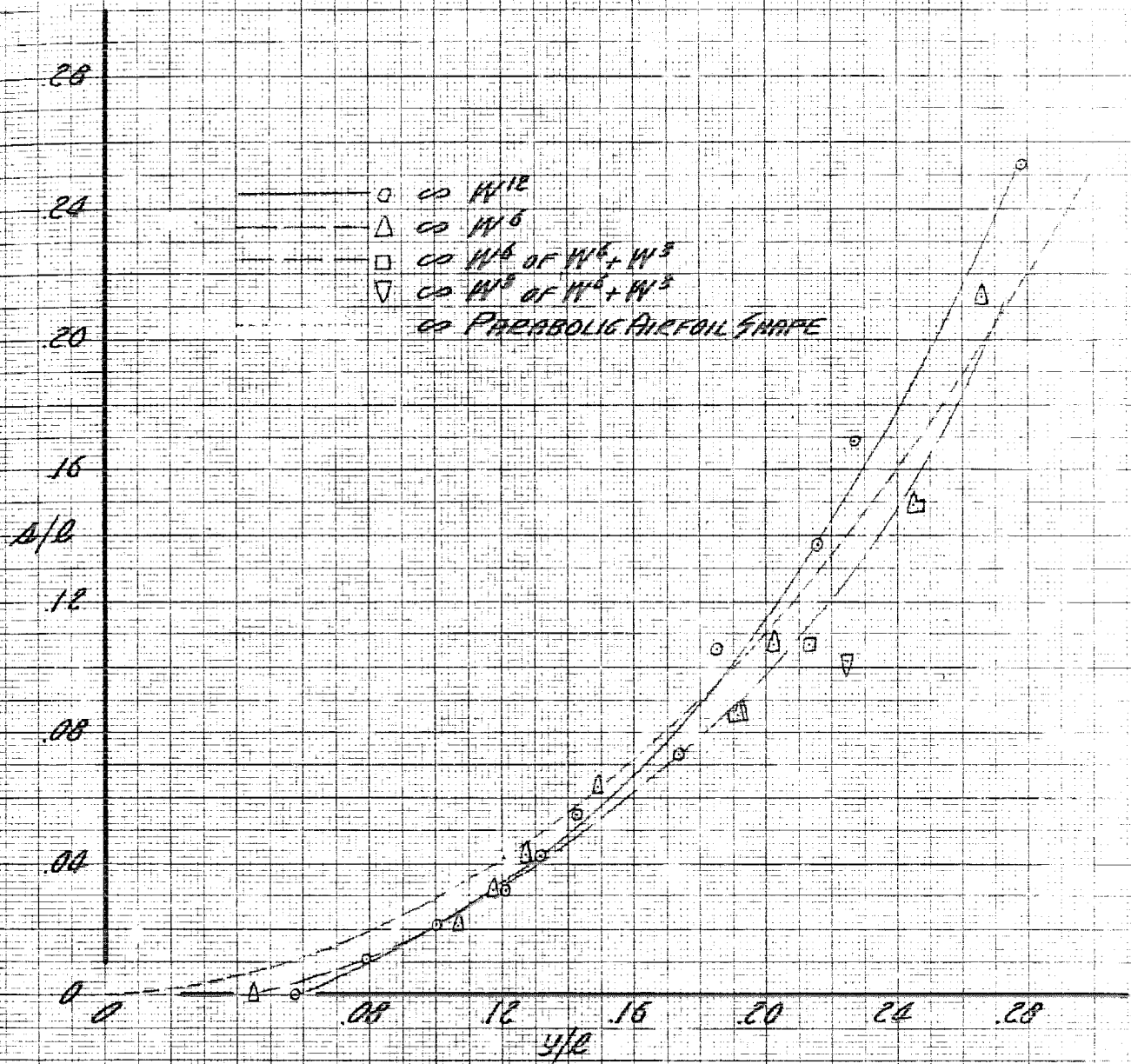
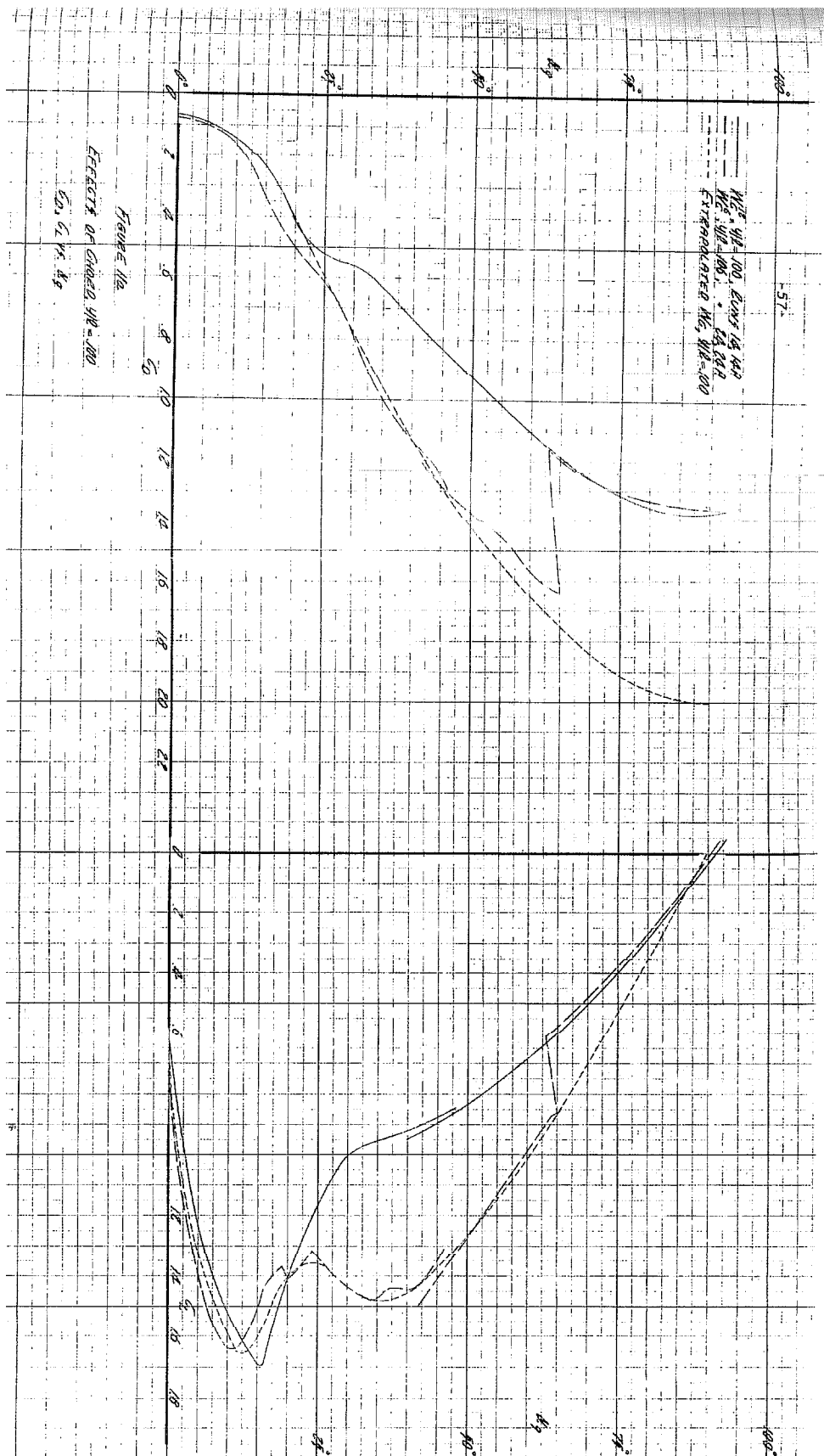


FIGURE 10
EFFECTS OF FLACK ON CAMBER
 y/b vs. d/b

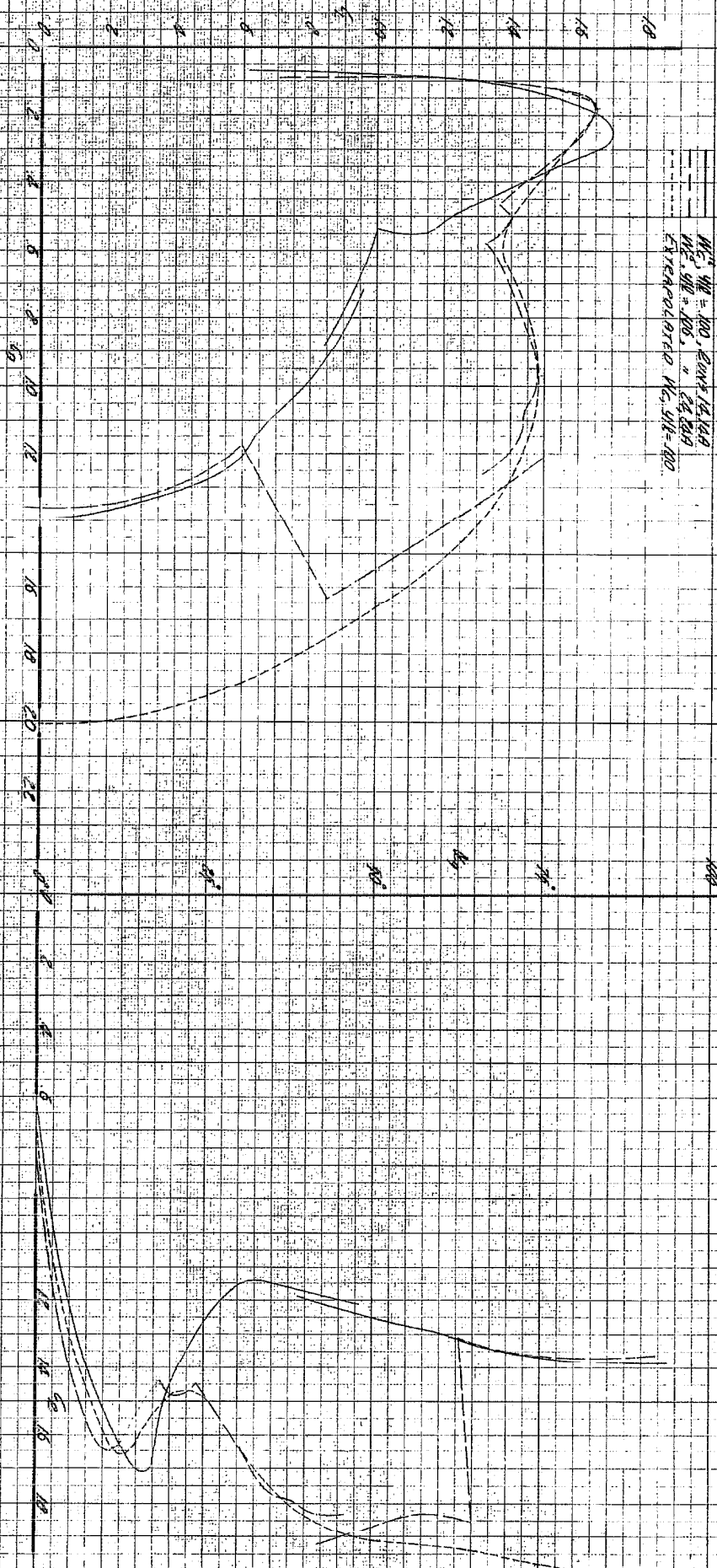


— $M_E^2, y_E = 100, \text{ RUNS } 14, 14.9$
- - - $M_E^2, y_E = 105, \text{ " } 14, 14.9$
- · - · - EXTRAPOLATED $M_E, y_E = 100$

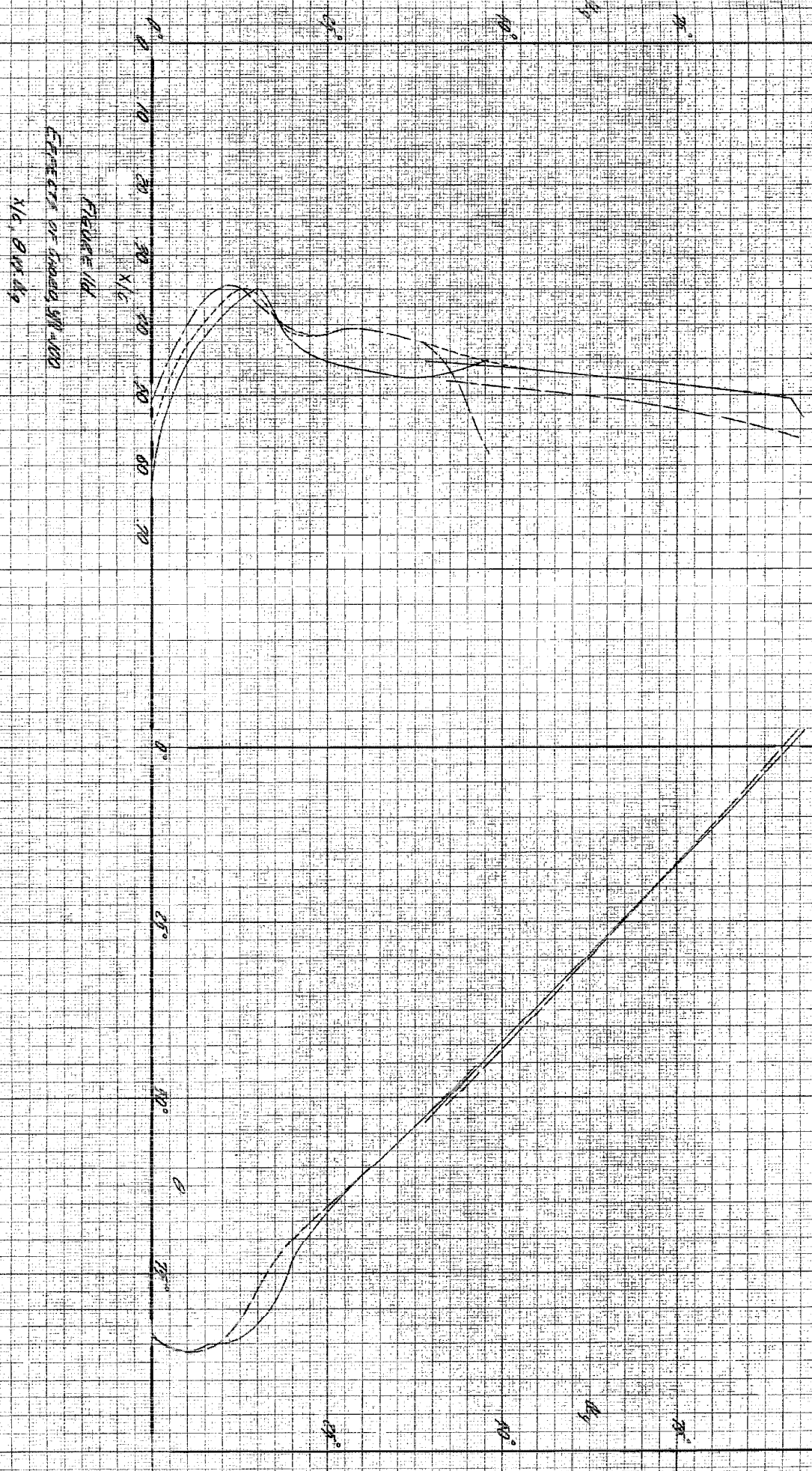


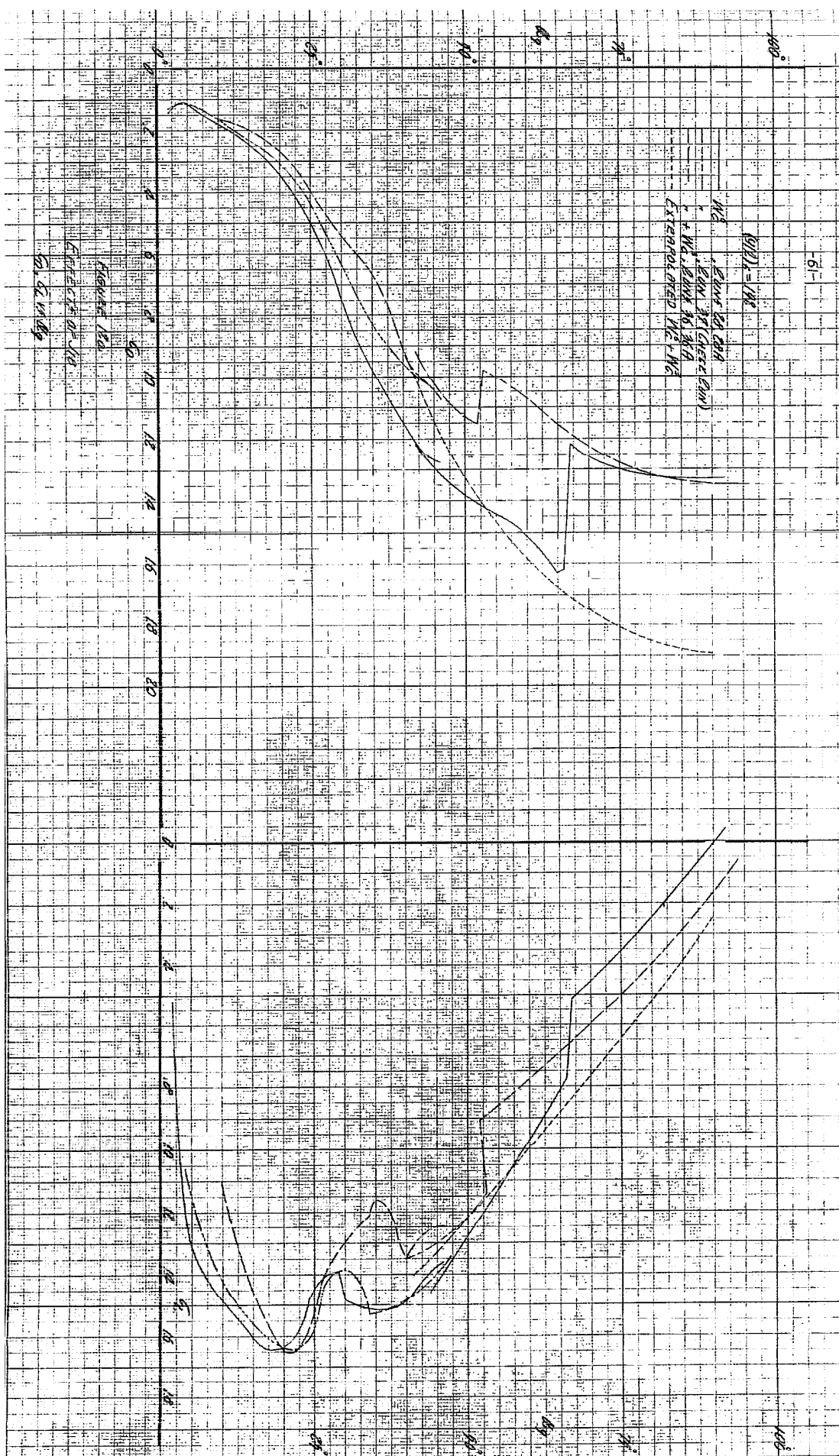
$W_c, W_H = 100, \text{ ELEV } 12, 14.4$
 $W_c, W_H = 100, \text{ " } 24, 24.4$
 EXTRACTED $W_c, W_H = 100$

FIVE-11C
 EFFECTIVE A-GROUND, $W_H = 100$
 ON W.C. CENTER



$W_0 = 100$, $W_1 = 100$, $W_2 = 100$, $W_3 = 100$
 $W_4 = 100$, $W_5 = 100$, $W_6 = 100$, $W_7 = 100$
 EXTENDED $W_8 = 100$




$$(912)5 = 1988$$

W.C. Evans 28, 28A
2000 301 Quaker Drive

n	EAN 37	EAN
n	+ WC; EANT 86	WC 36A
n		

EXTENDED W_0 & W_0

MILLMETER GROSS SECTION
CHARLES BRINING COMPANY

MILLIMETER CROSS SECTION

[illegible]

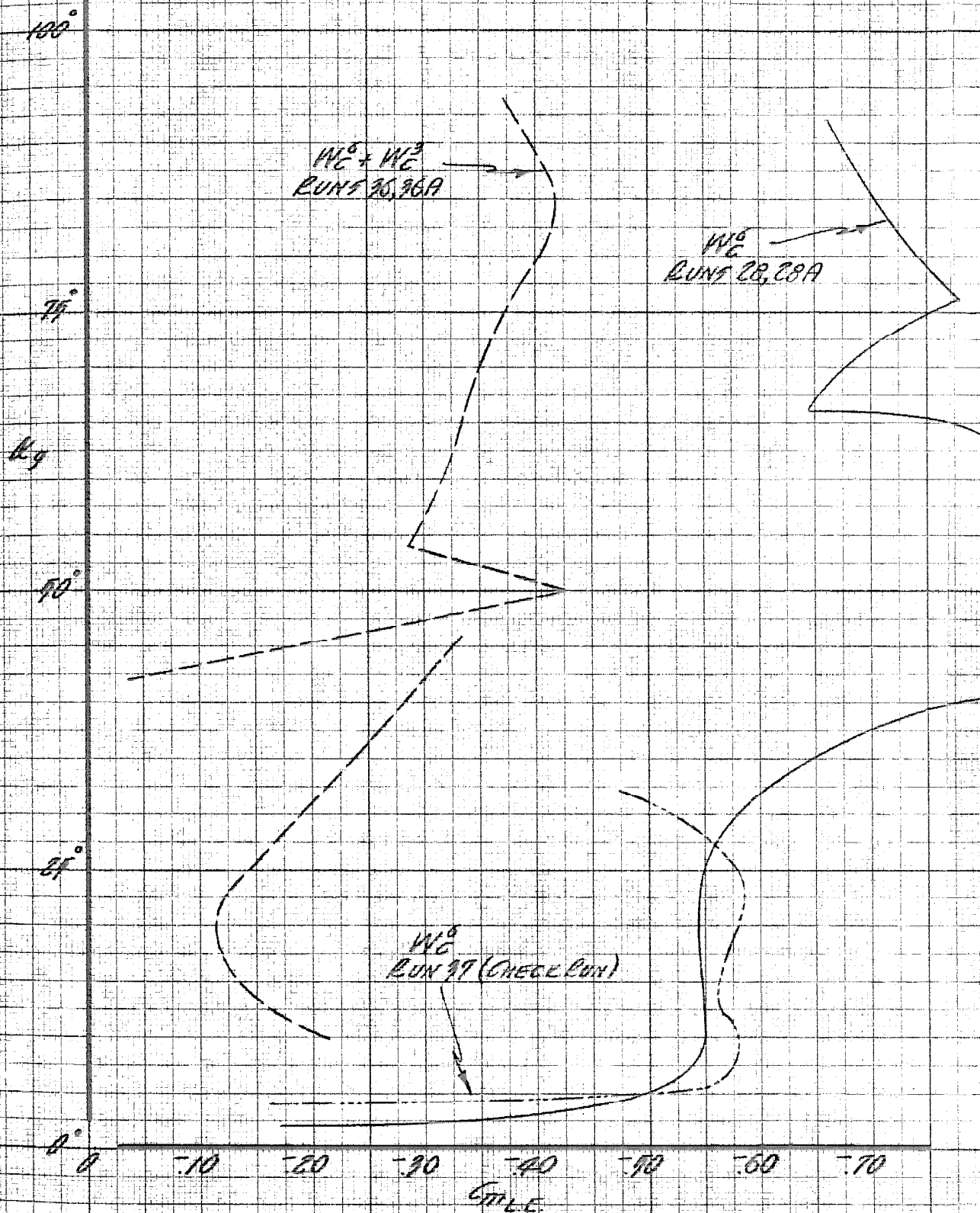
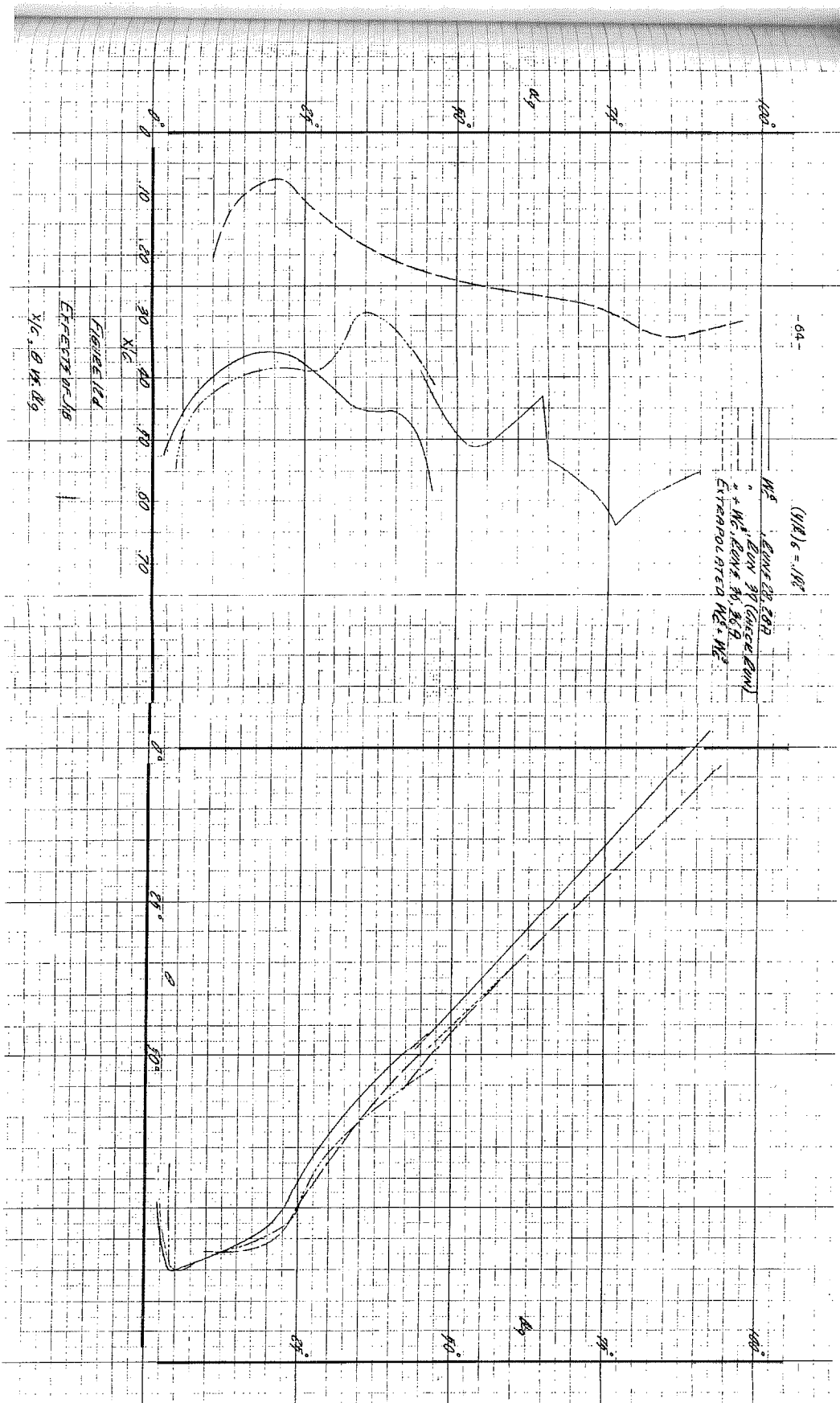


FIGURE 186

EFFECTS OF JIB

CM vs. W_g



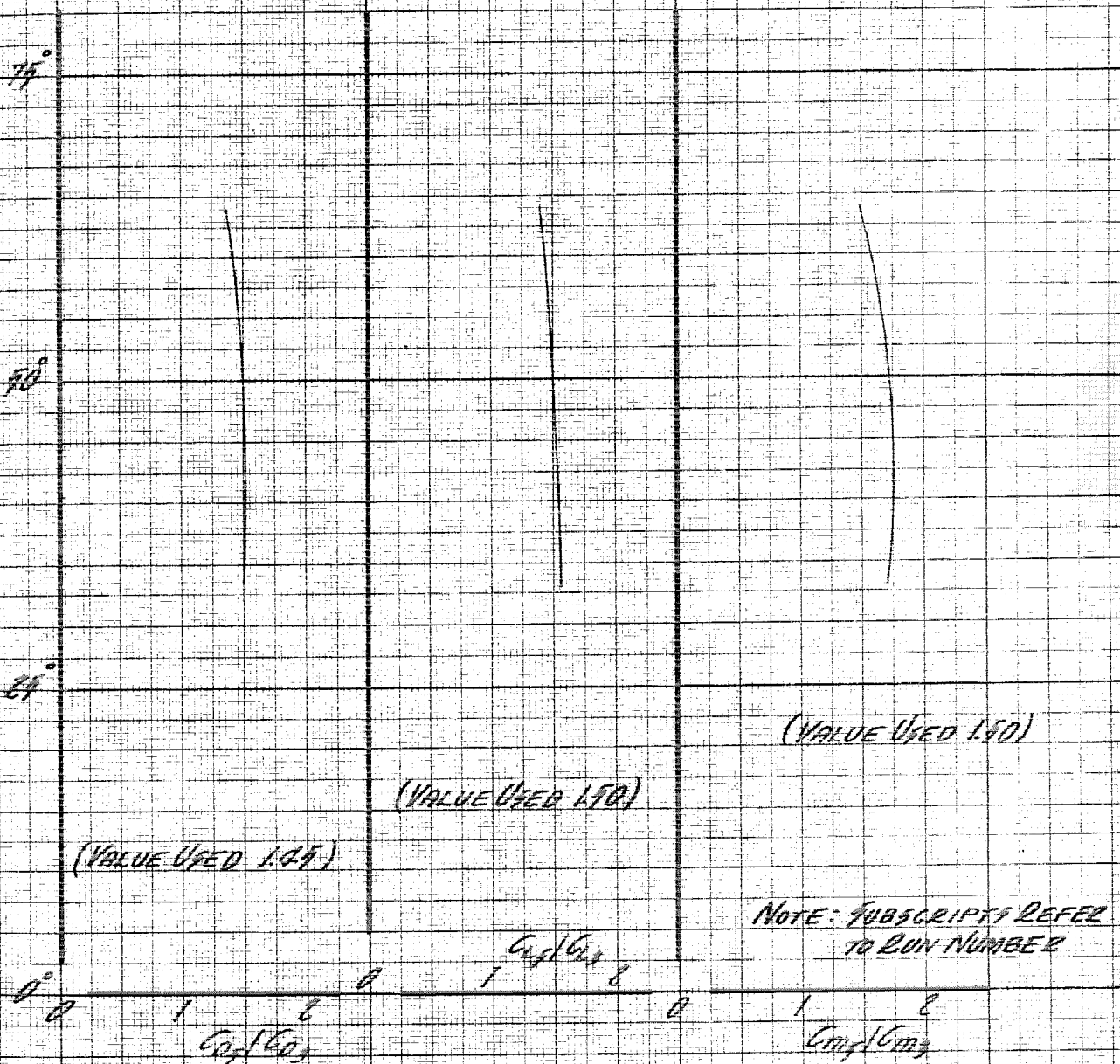
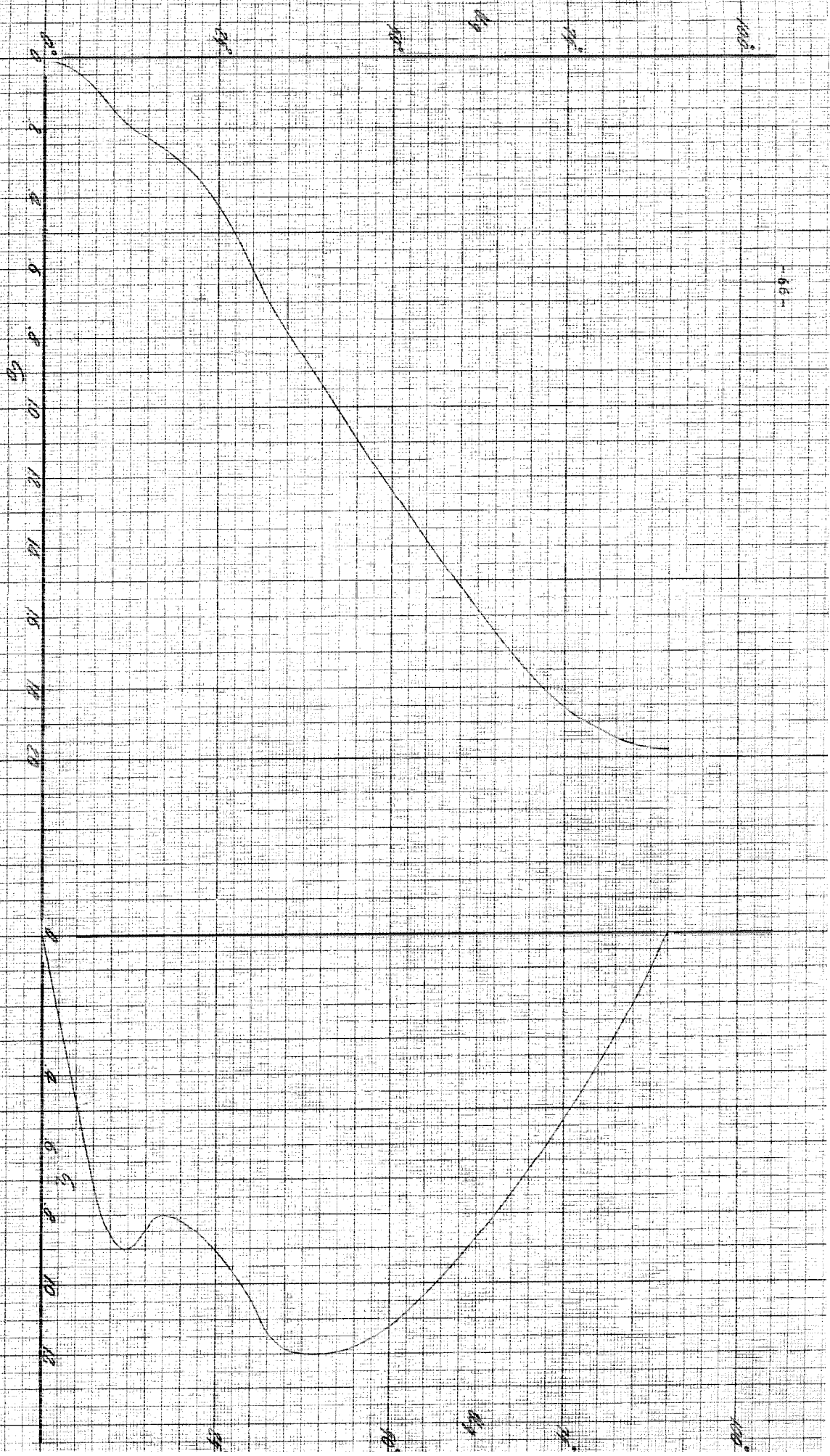


FIGURE 19

IDEALIZED FLAT PLATE CURVES

Co_2/Co_1 , Cl_2/Cl_1 , Cm_2/Clm_1 vs. α

FIGURE 10a
 IDENTIFIED COAT THICKNESS CURVES
 CO. C. W. 49



-67-

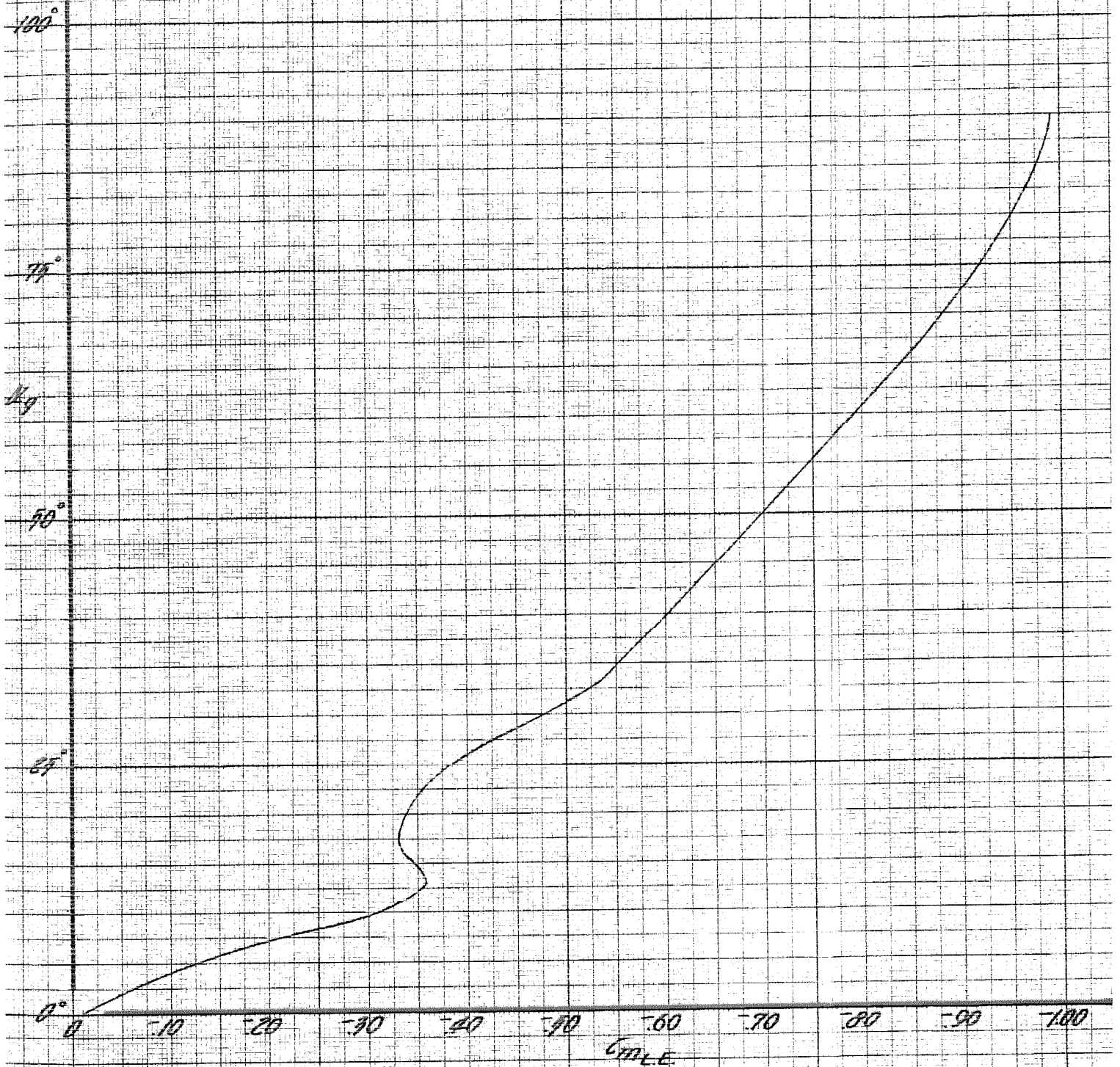


FIGURE 106

IDEALIZED FLAT PLATE CURVES

C_m vs. α

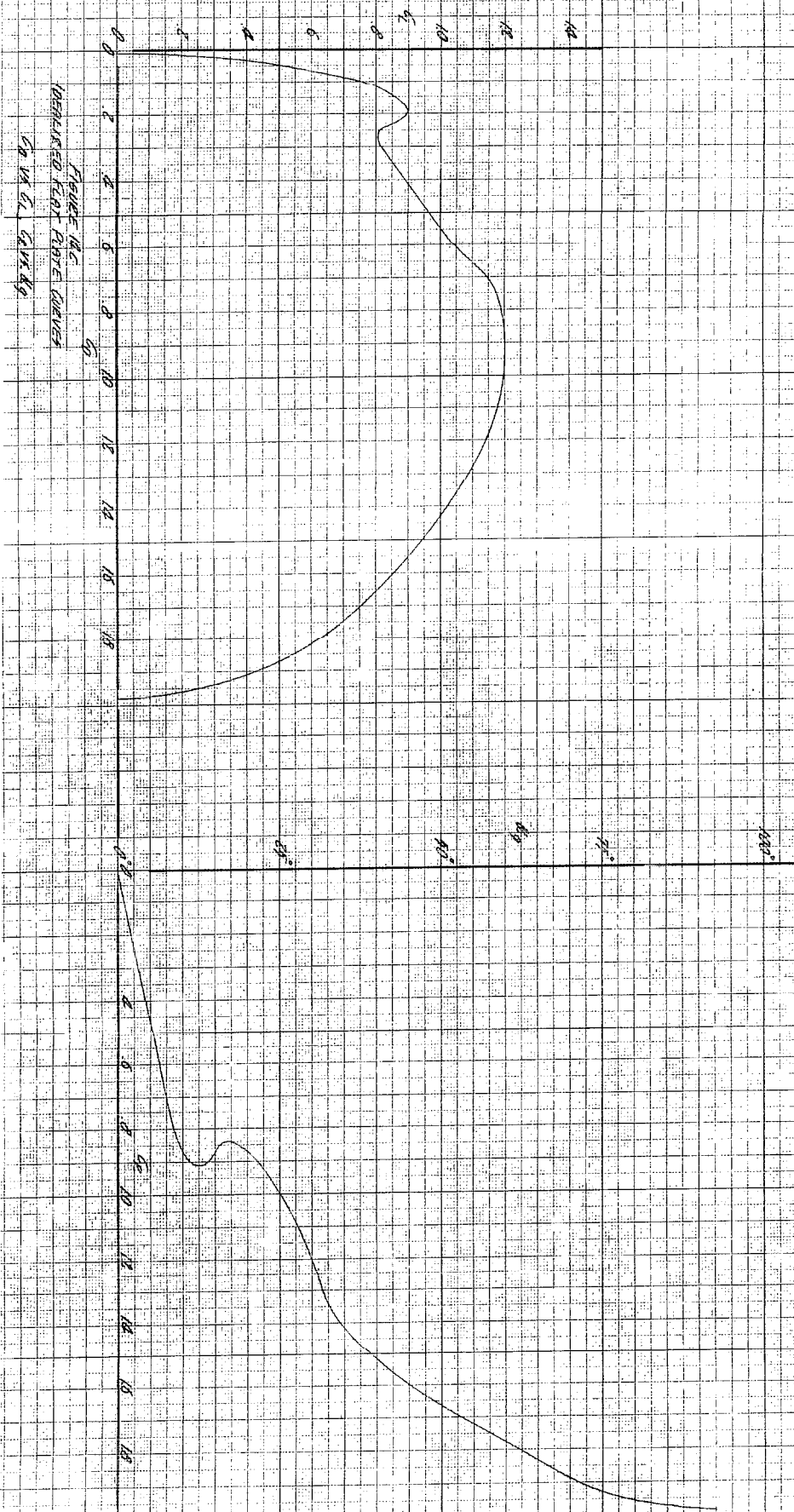


FIGURE 1A.C.
REMANENT FLAT PROTE. CURVES
CO IN G, GIVE KG

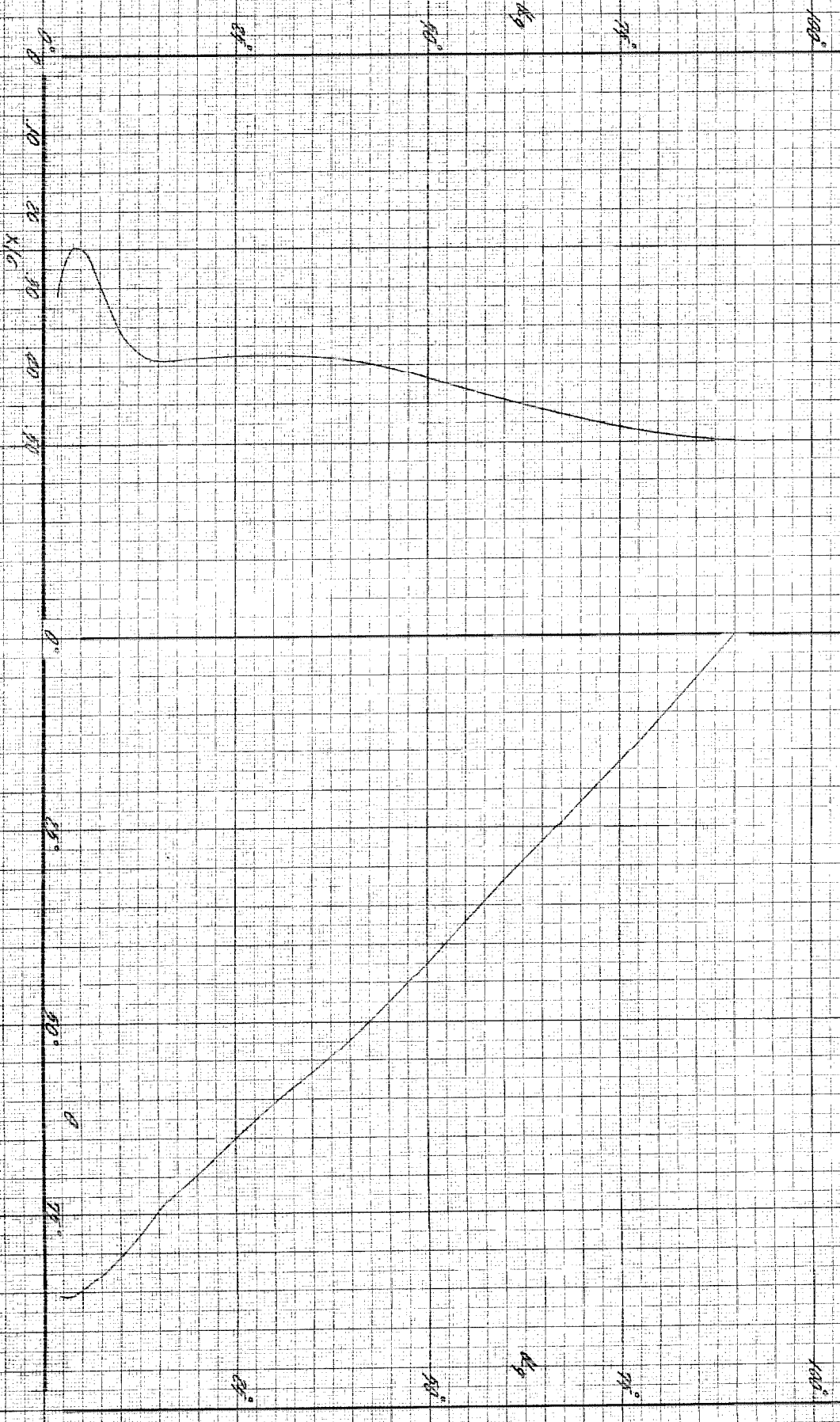
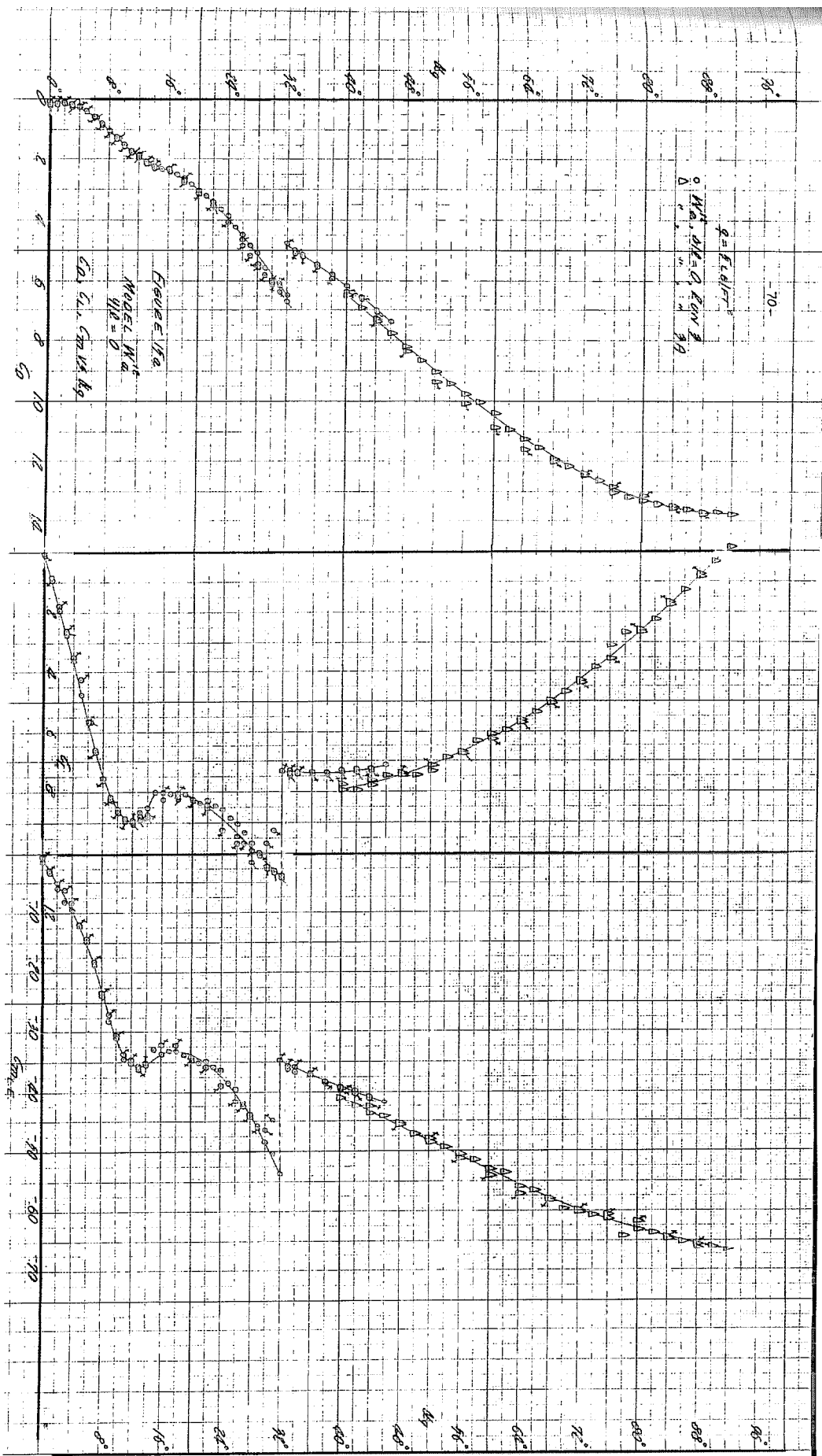


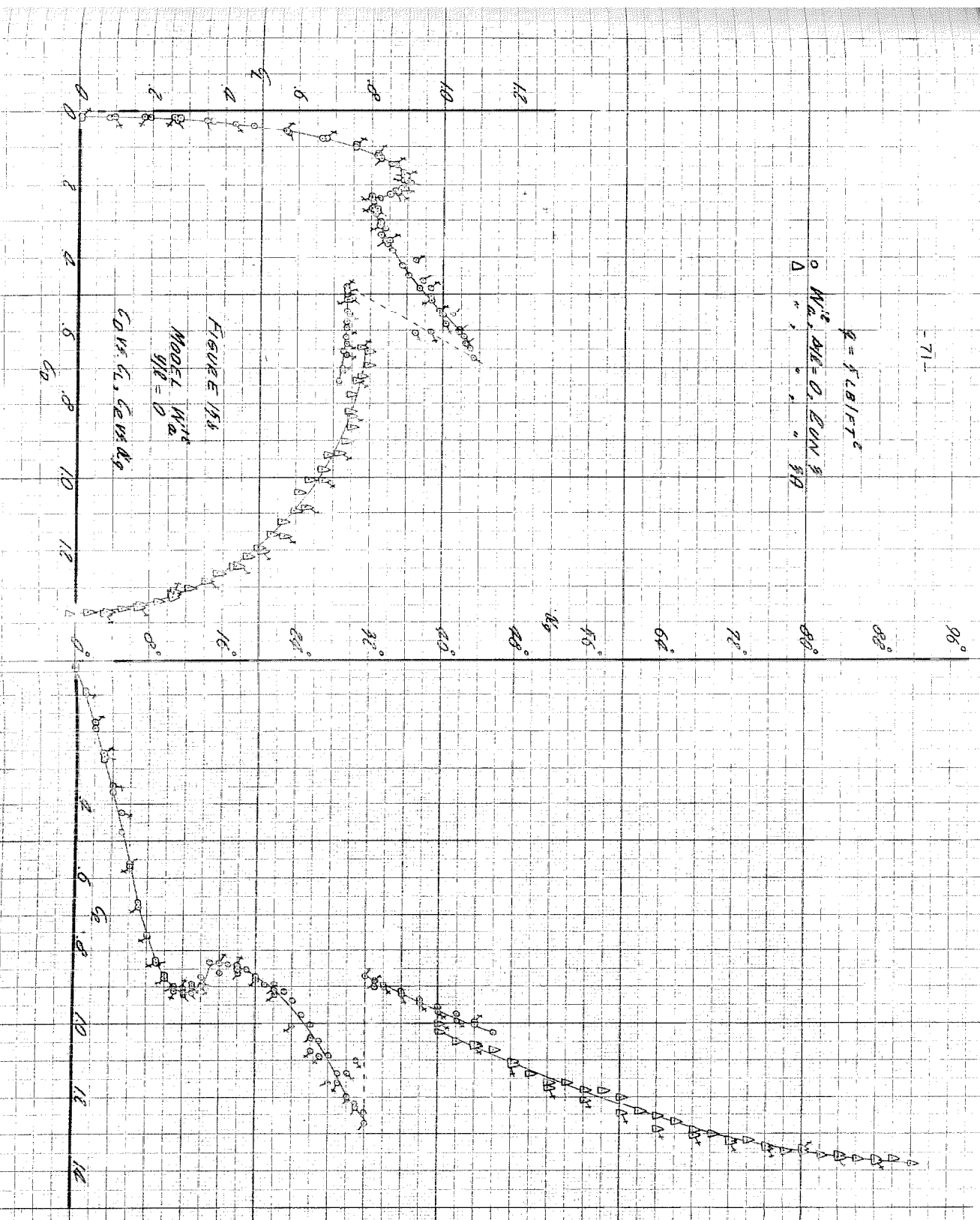
FIGURE 164
IDENTIFIED FLAT PLATE CURVES
X/G, θ vs. kg



-71-

$$\rho = f_{LB}/FT^2$$

\circ M_{α}^{12} , $M_{\alpha} = 0$, $E_{ON} = 3$
 Δ " " " " " "



-72-

$q = 1.81 \text{ ft}^3$
 $\Delta W_{\alpha}, W_{\alpha} = 0, \text{ CON } 1$

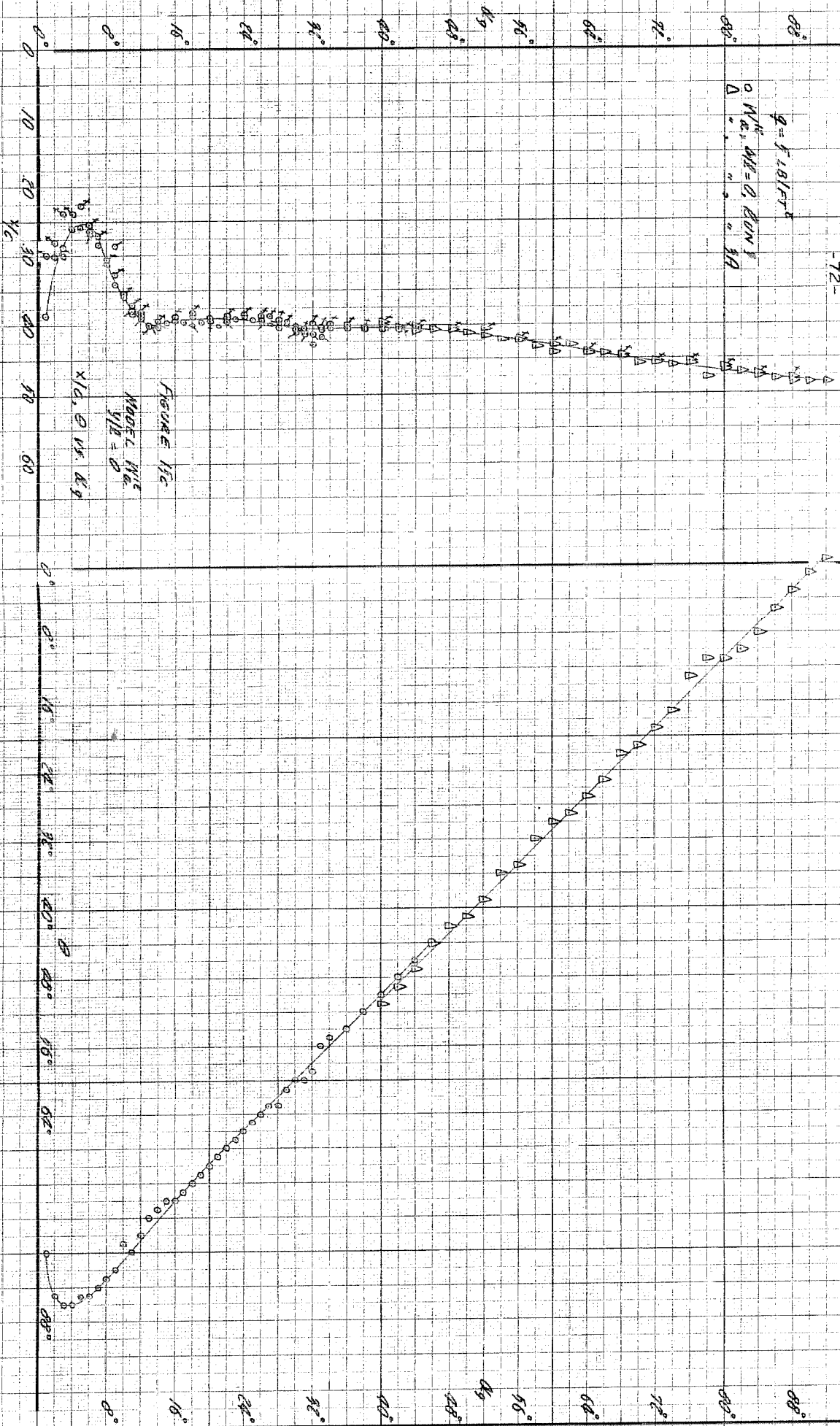
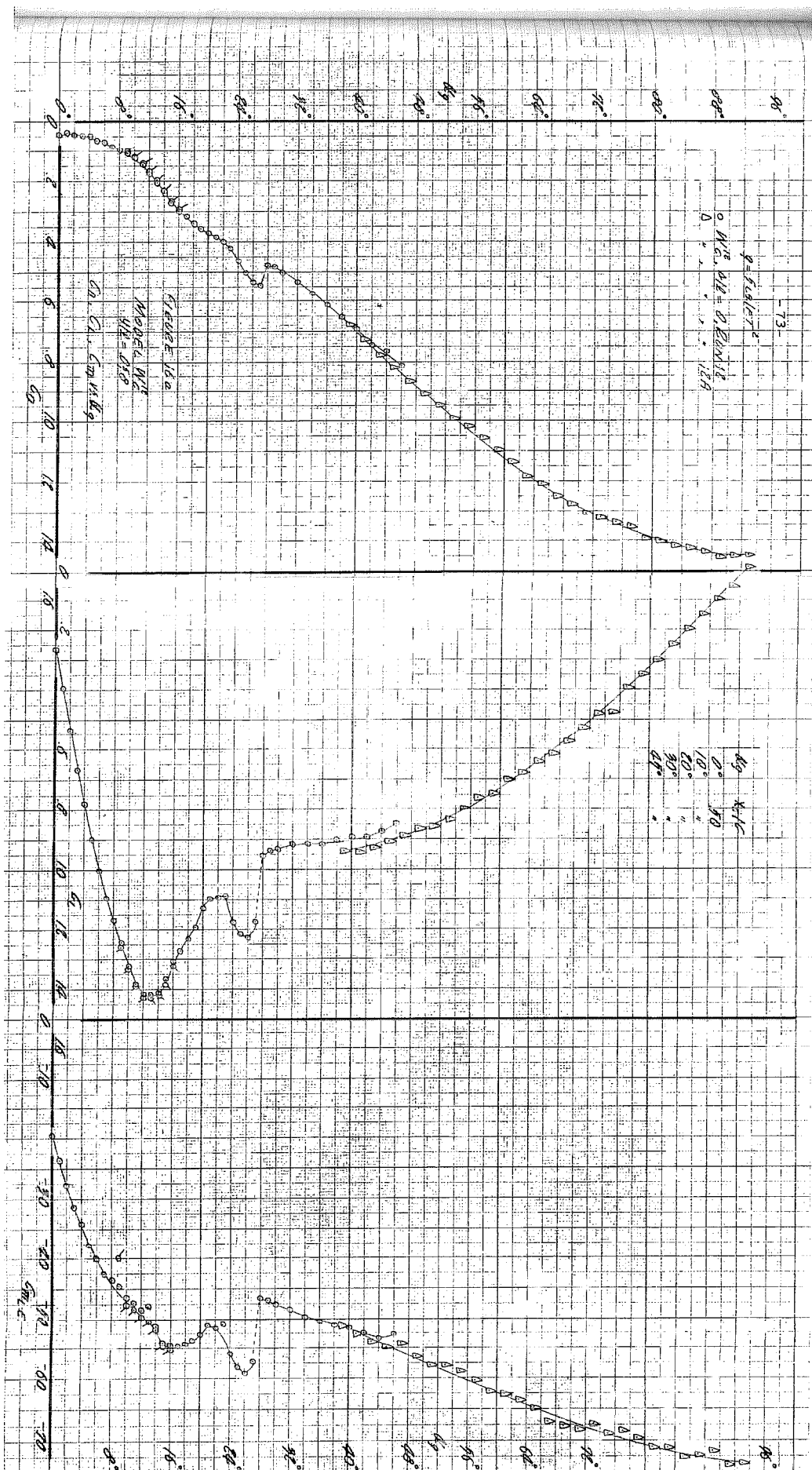


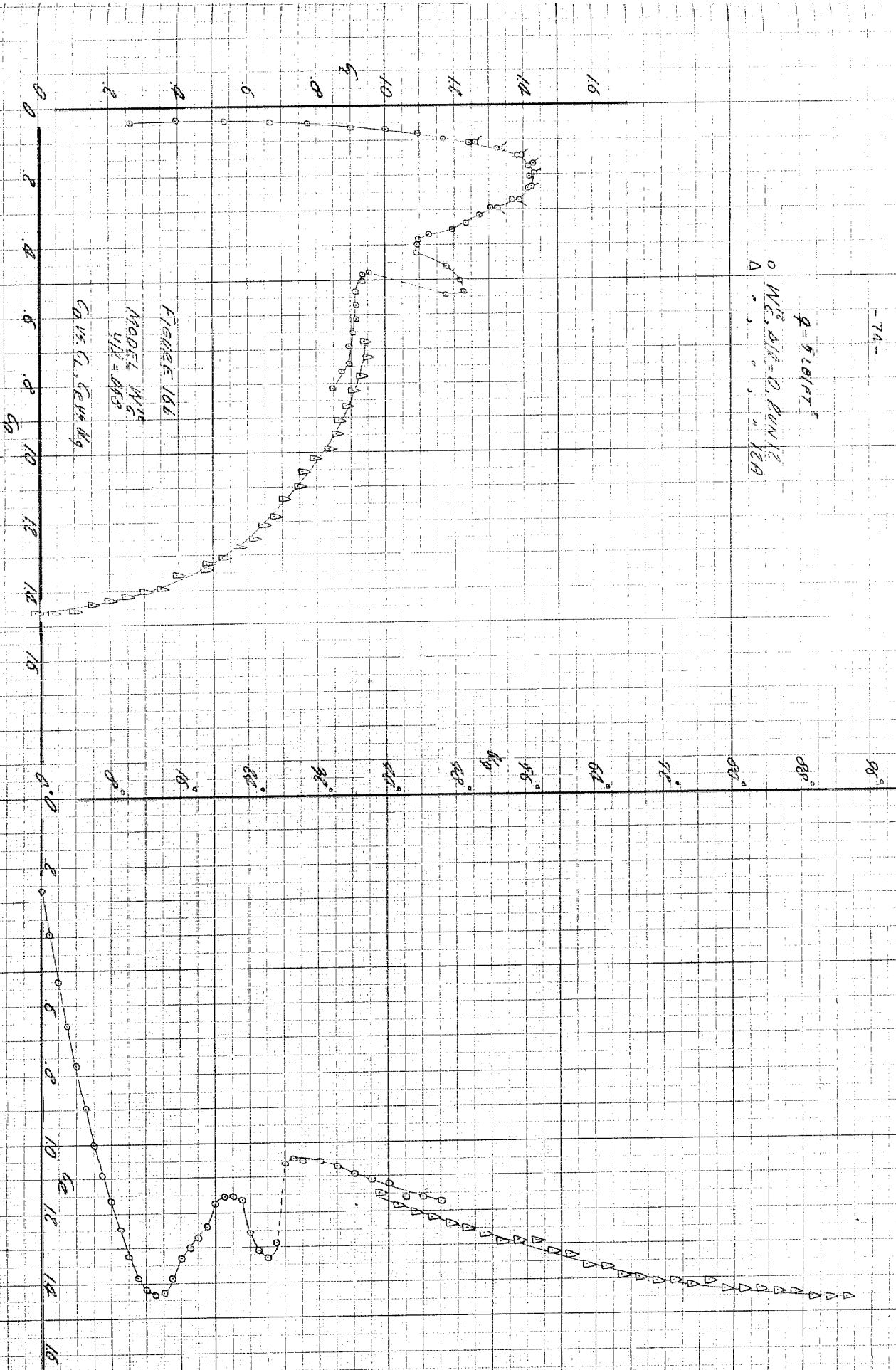
FIGURE 11c
MODEL M_{α}
 $W_{\alpha} = 0$
 $X/G, \Theta \text{ vs } K/g$

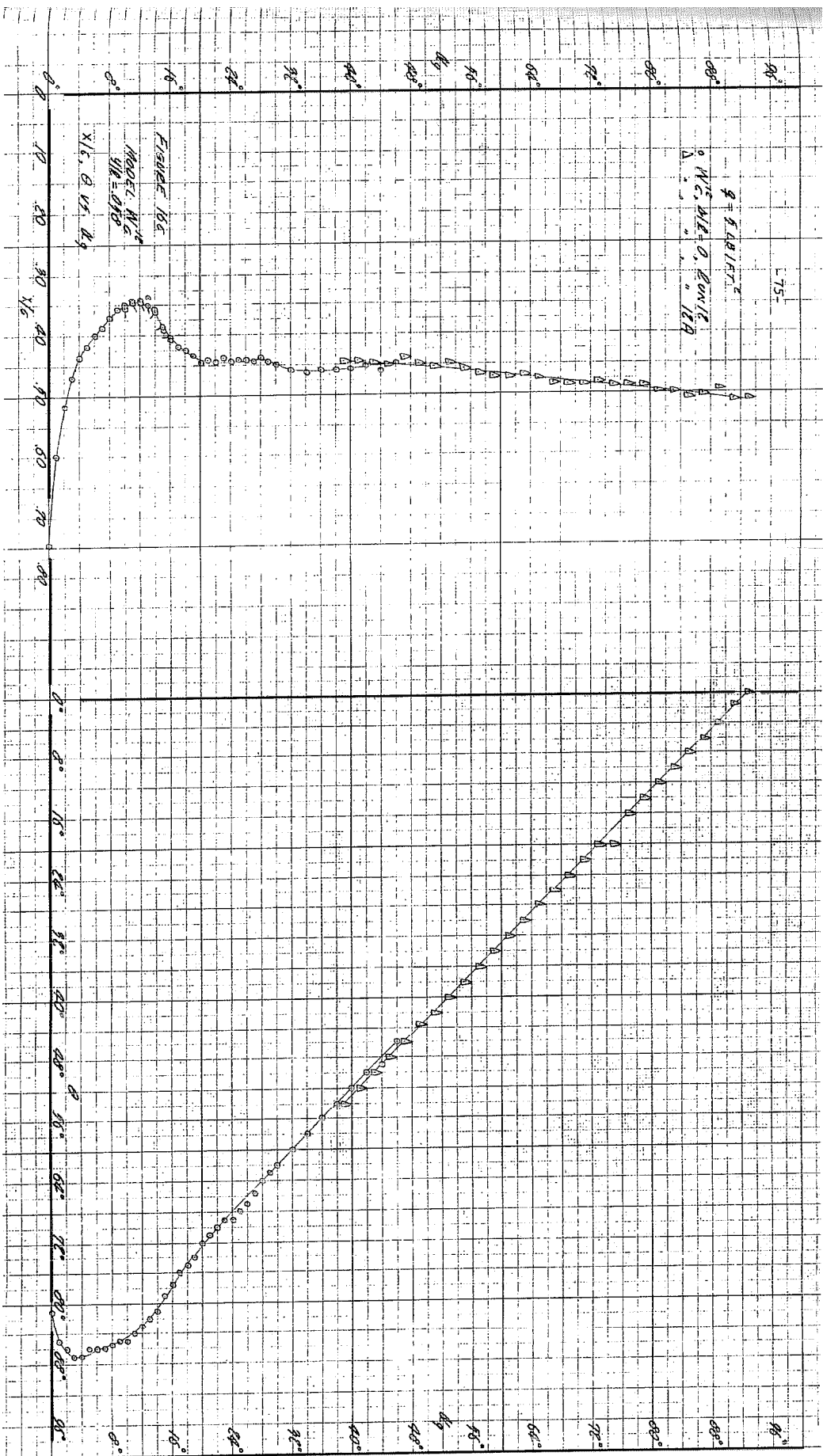


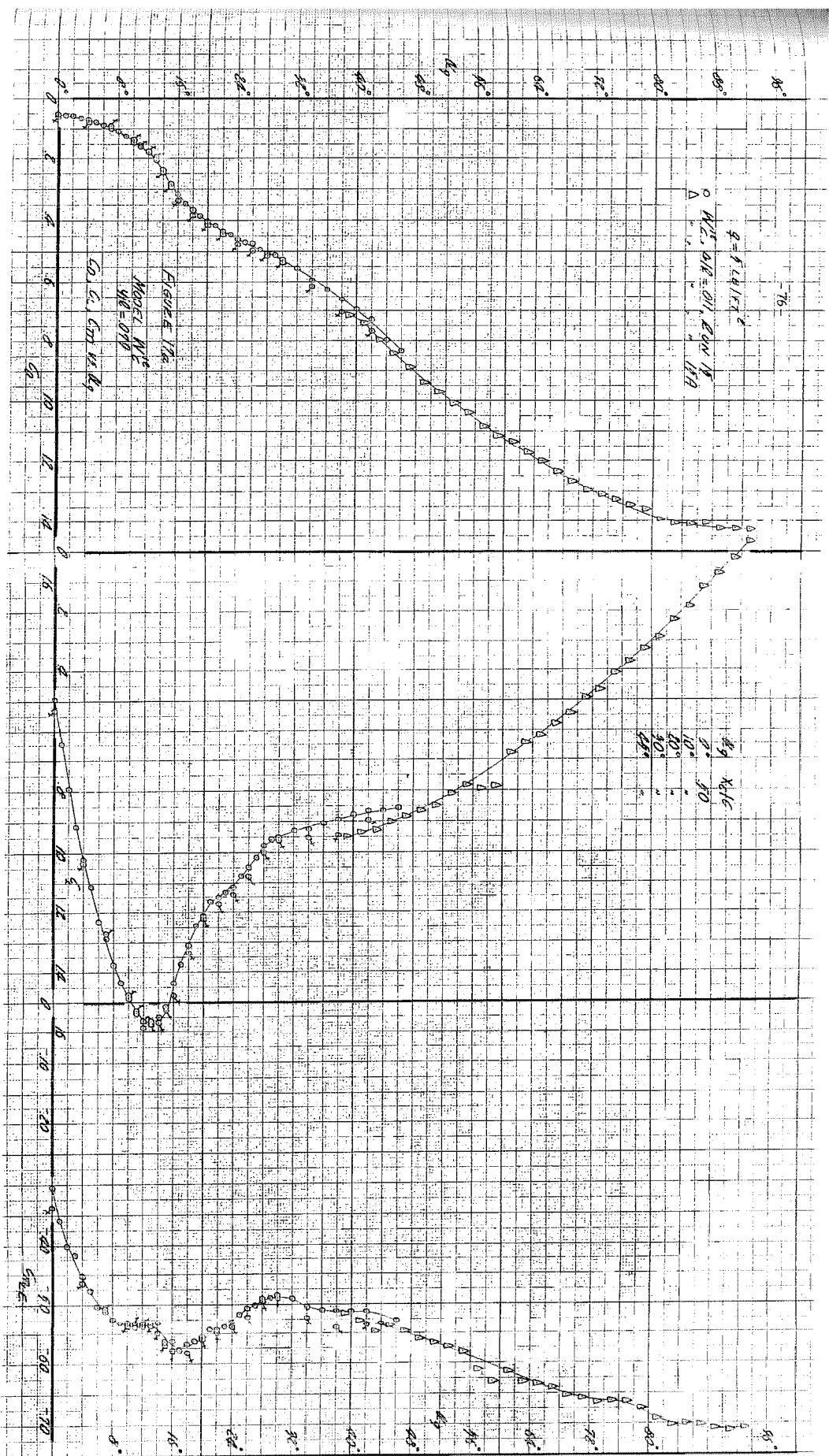
-74-

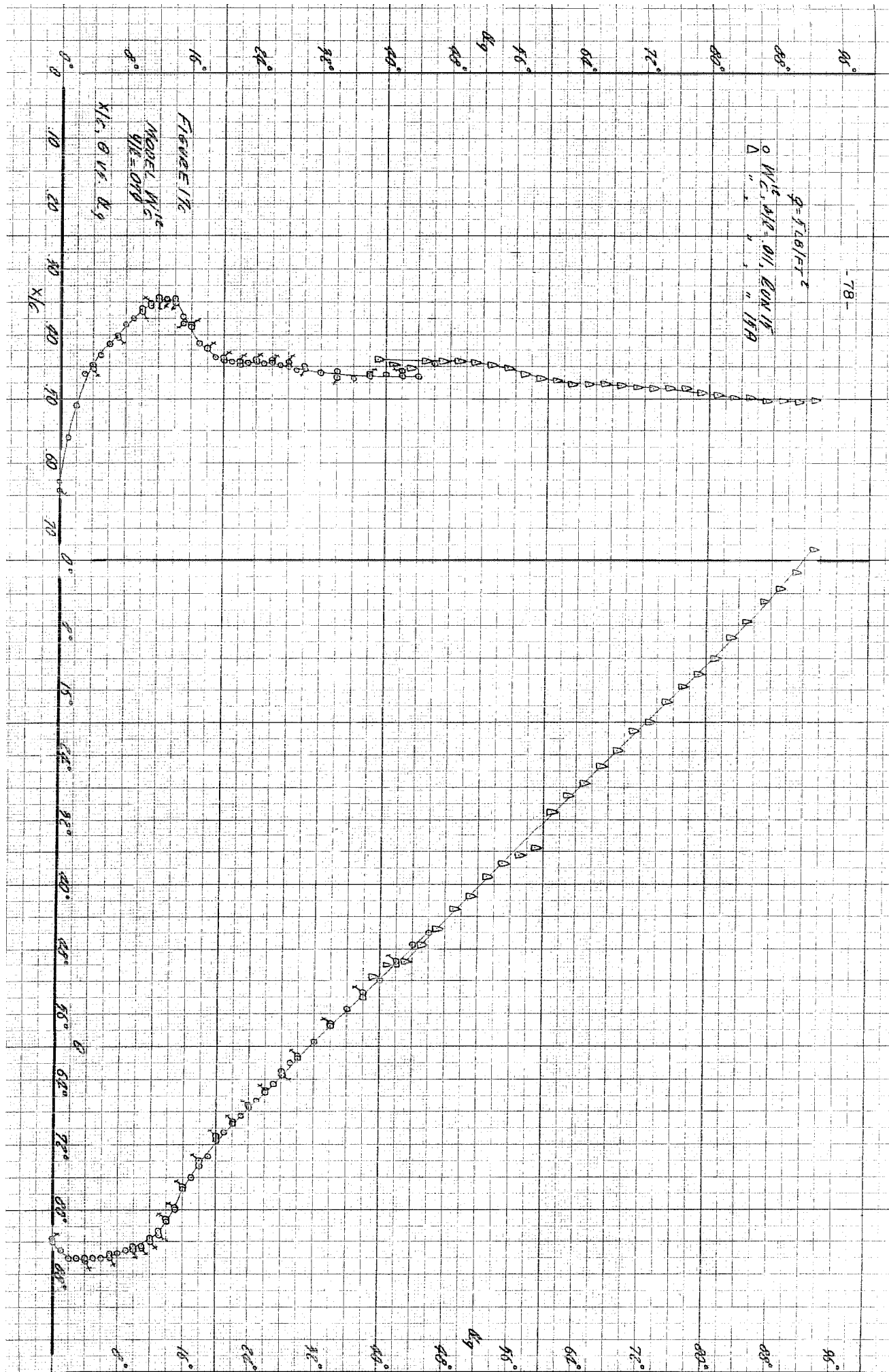
$$q = 5.18 / r^2$$

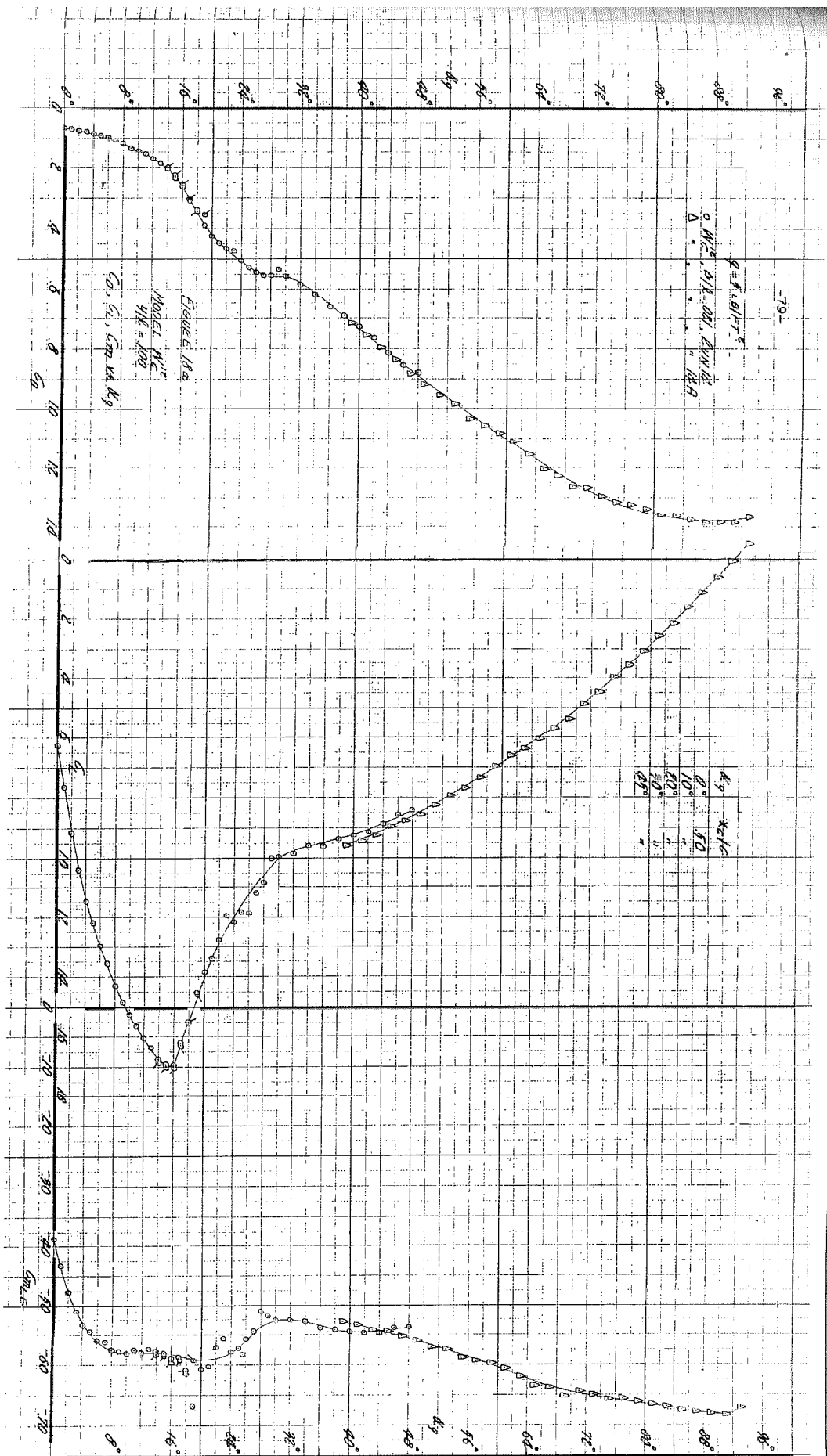
○ $W_C, \Delta W_C = 0, P_{CN} 10^6$
 Δ " " " " " " " " " " " "

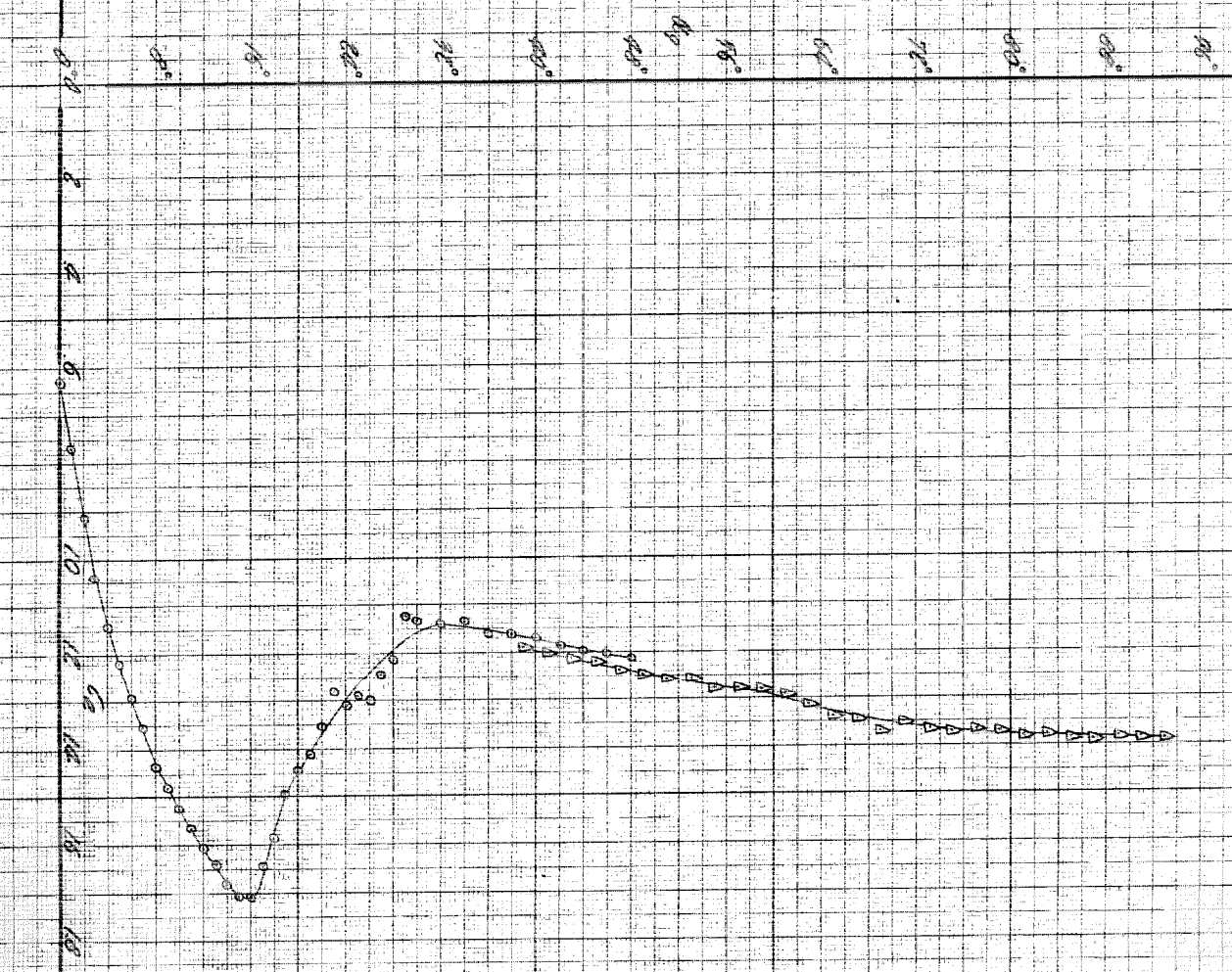


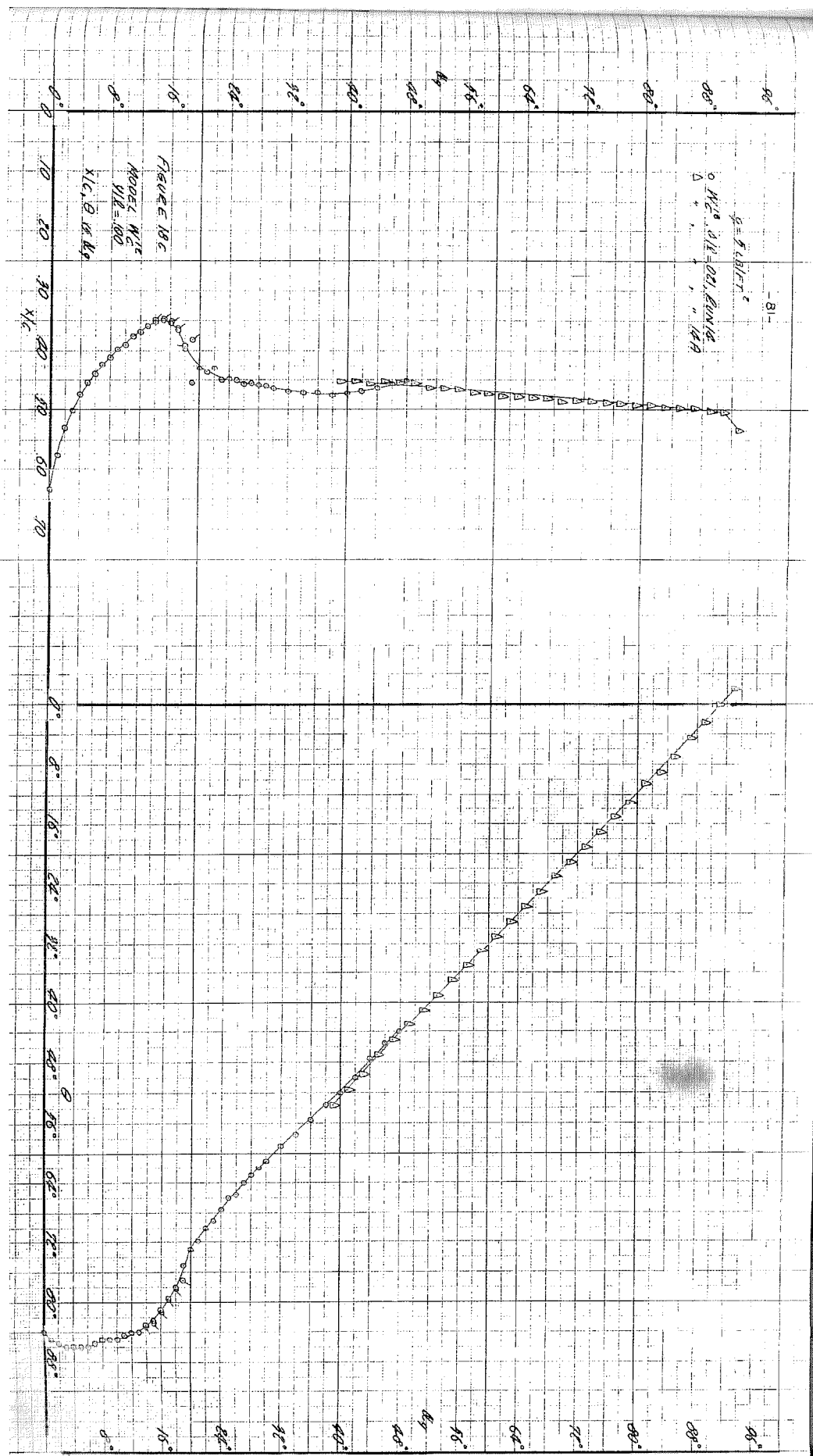


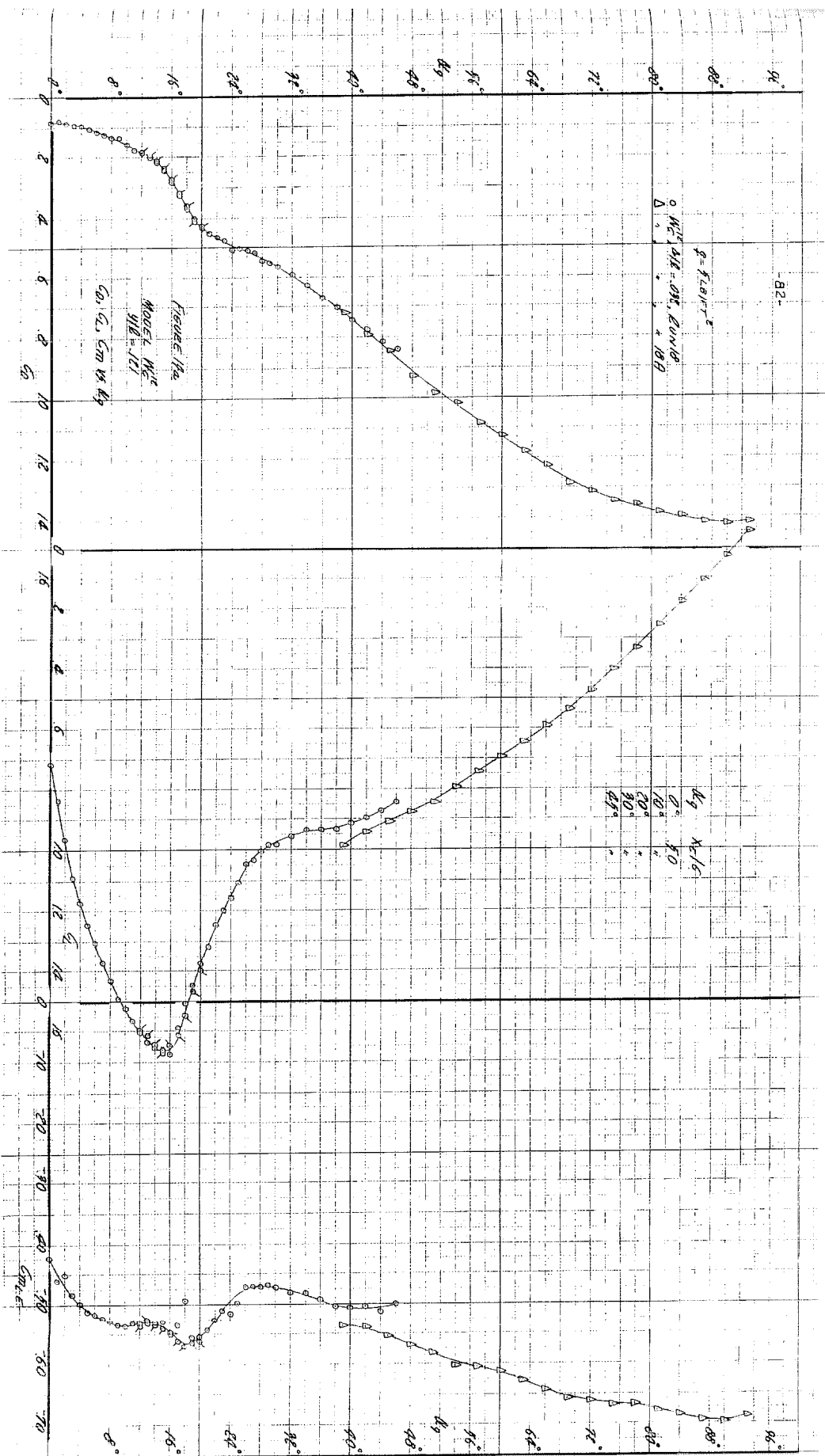






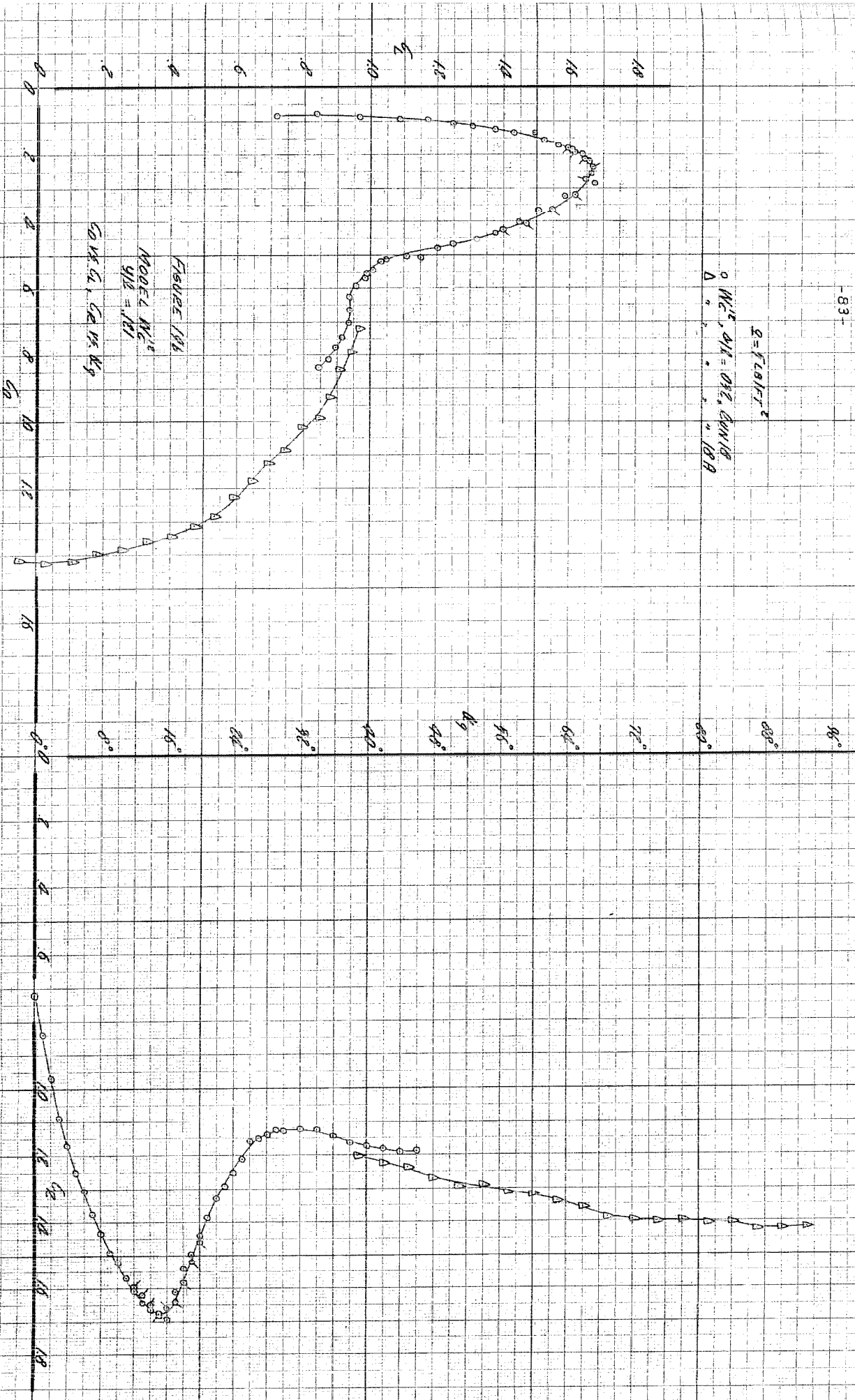
$$q = 6.4 \times 10^2$$


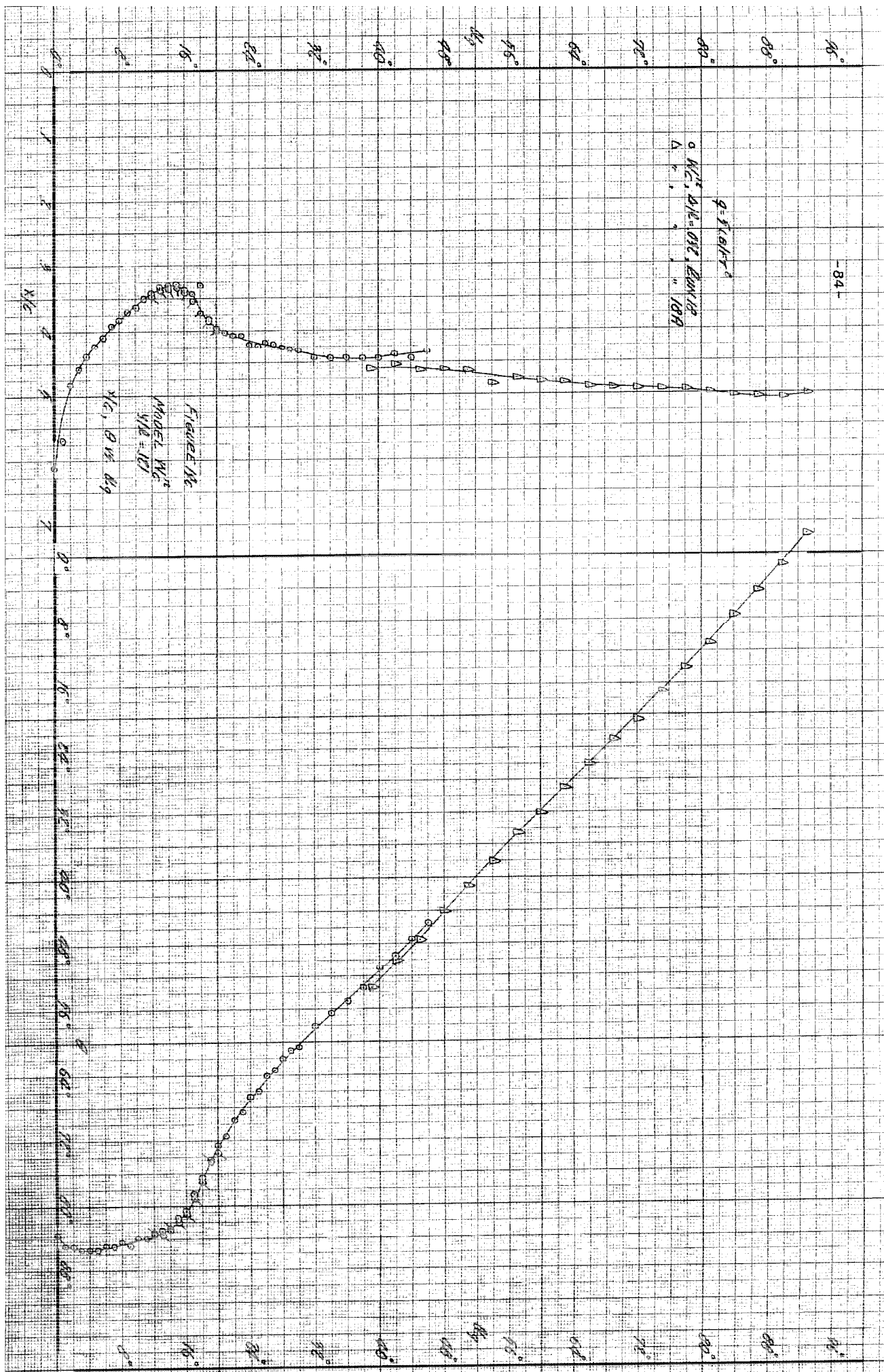


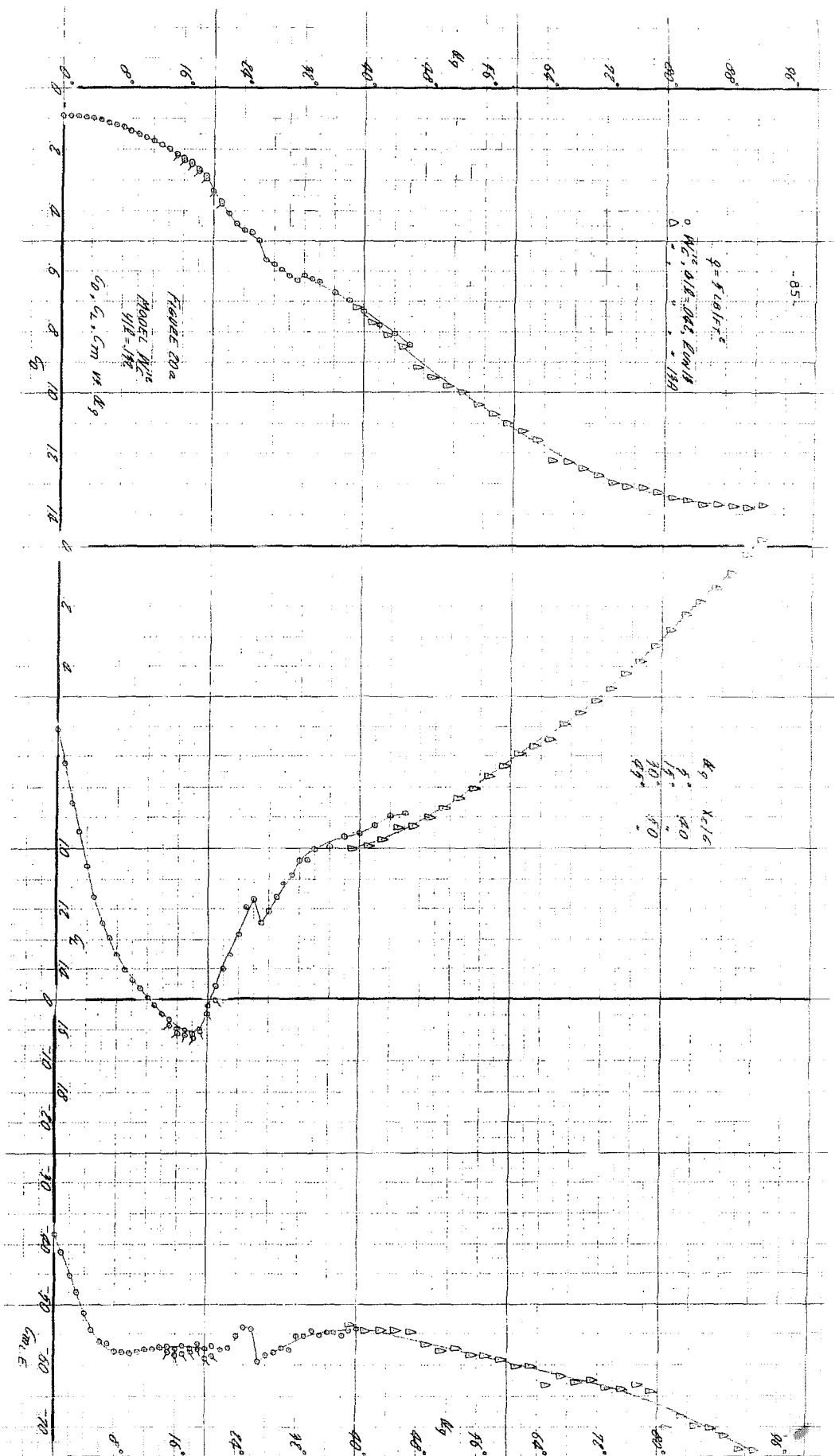


-83-

$\sigma = 1.08 \times 10^{-5}$
 $\Delta \theta = 0.1^\circ, \Delta \theta / \theta = 10.8$







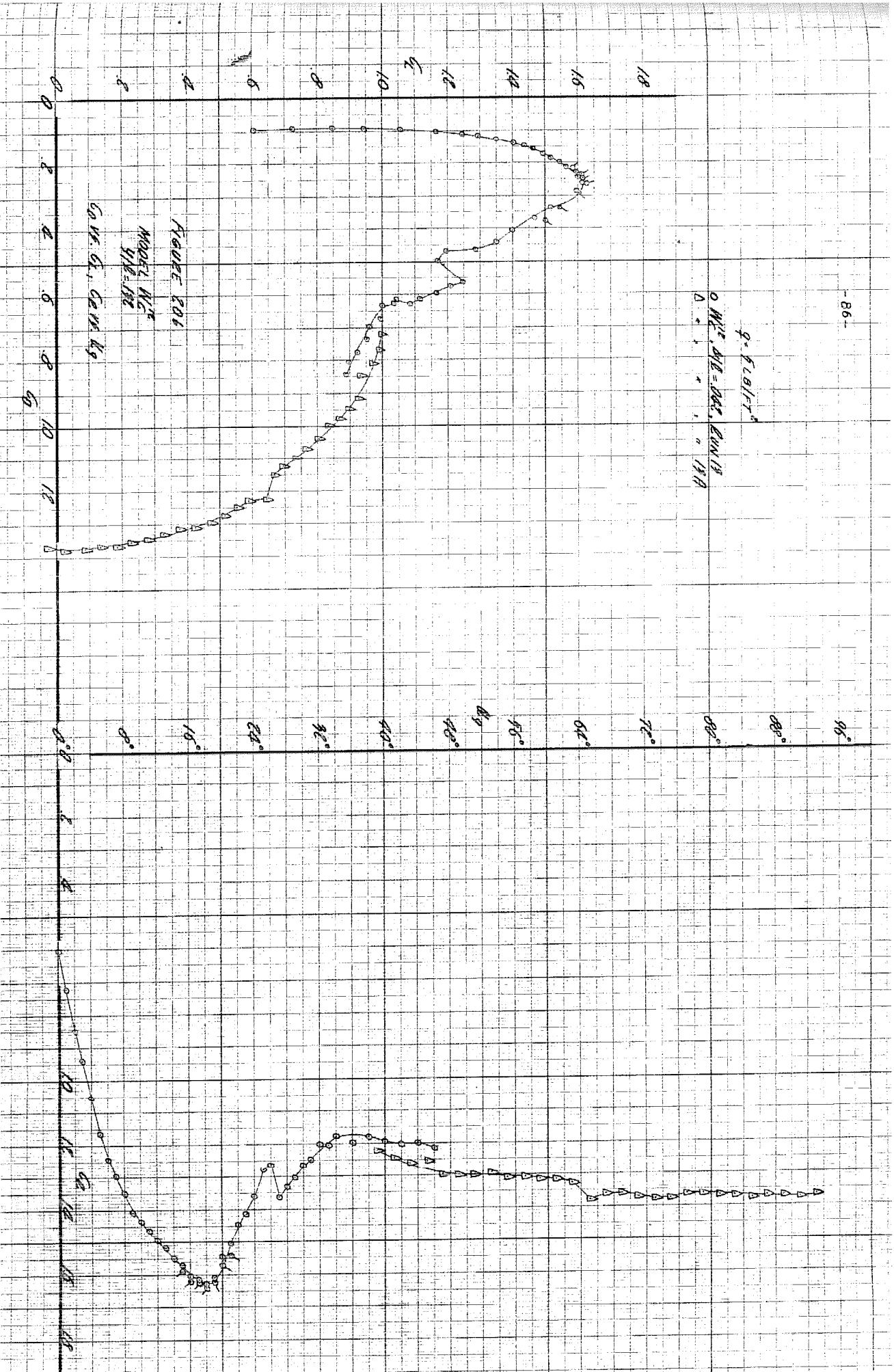
$$q = f(\theta/r^2)$$

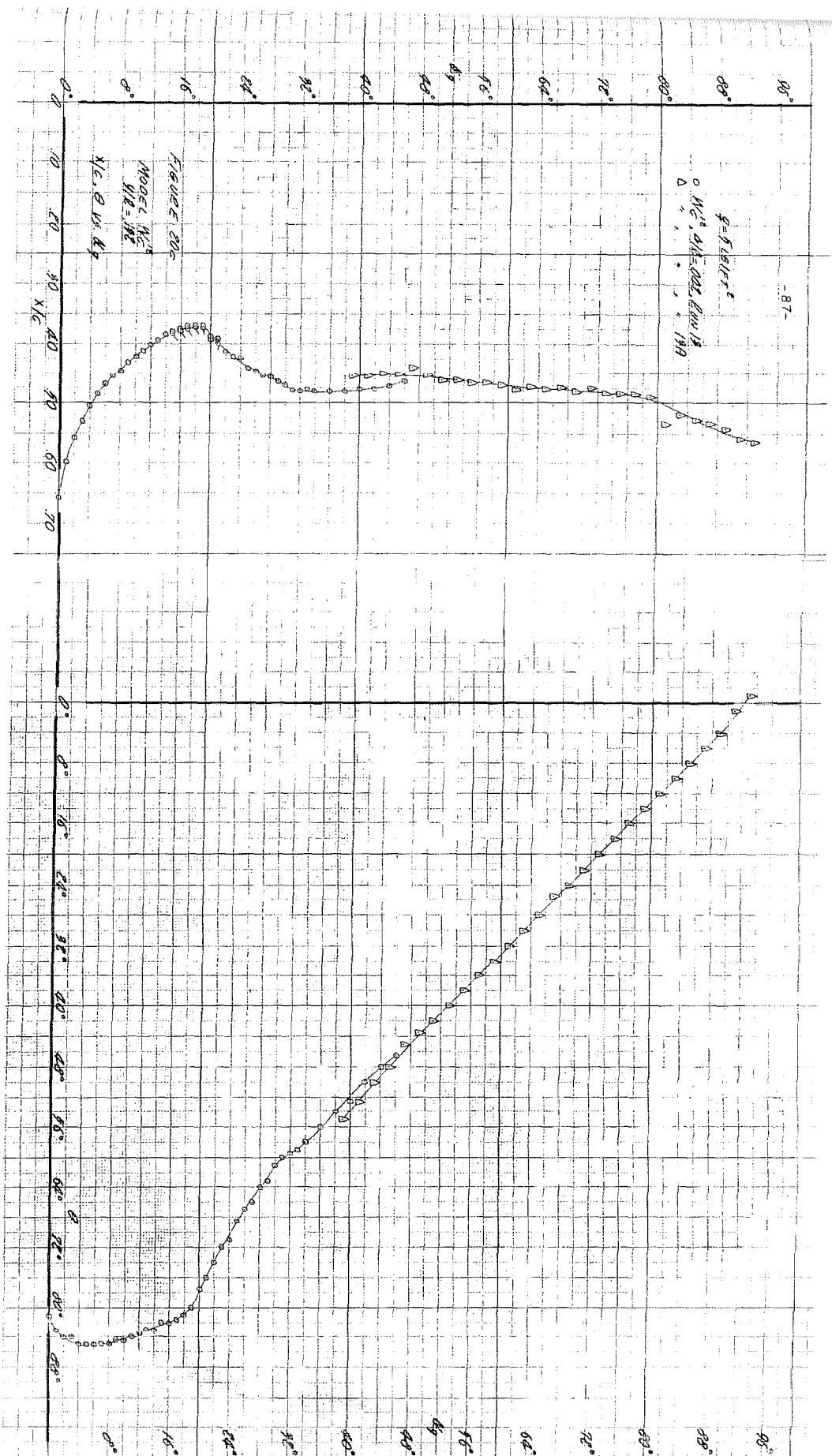
$$0.012 \cdot \frac{dV}{dt} = 0.012 \cdot \frac{dV}{dt}$$

$$\Delta = \dots$$

FLUID COB
MODEL H₂O
Y/B=182

CO W. G. GERM KG





$$q = \sqrt{c \cdot b} = r$$

0	MC	2	ONE	=	053	2	CON	19
Δ	"	"	"	"	"	"	"	17A

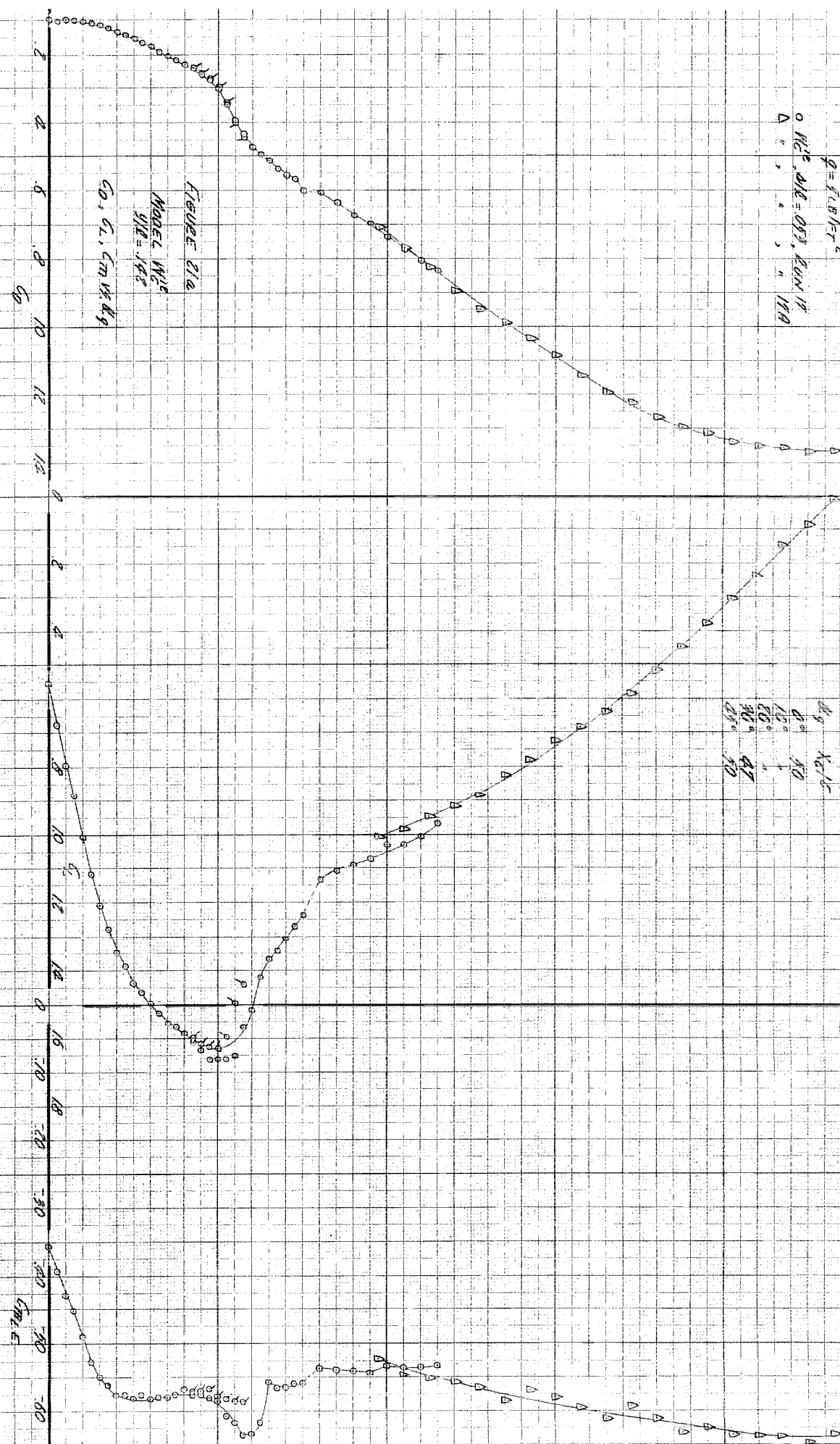
19.69

FIGURE 21a

MOE	142
$\frac{1}{2} = .5$	

$$241 = 215$$

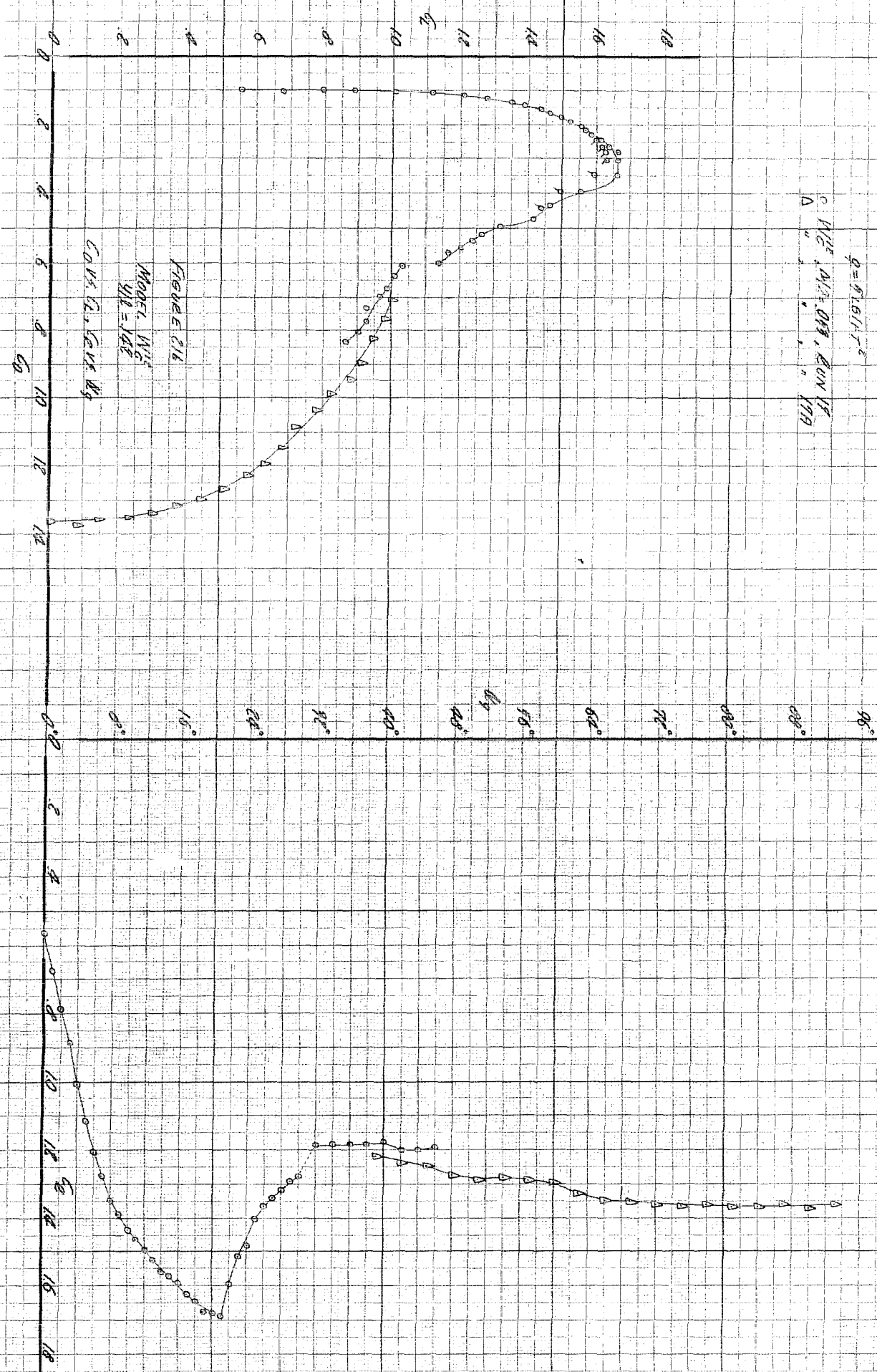
CO, CL, CM vs. dg

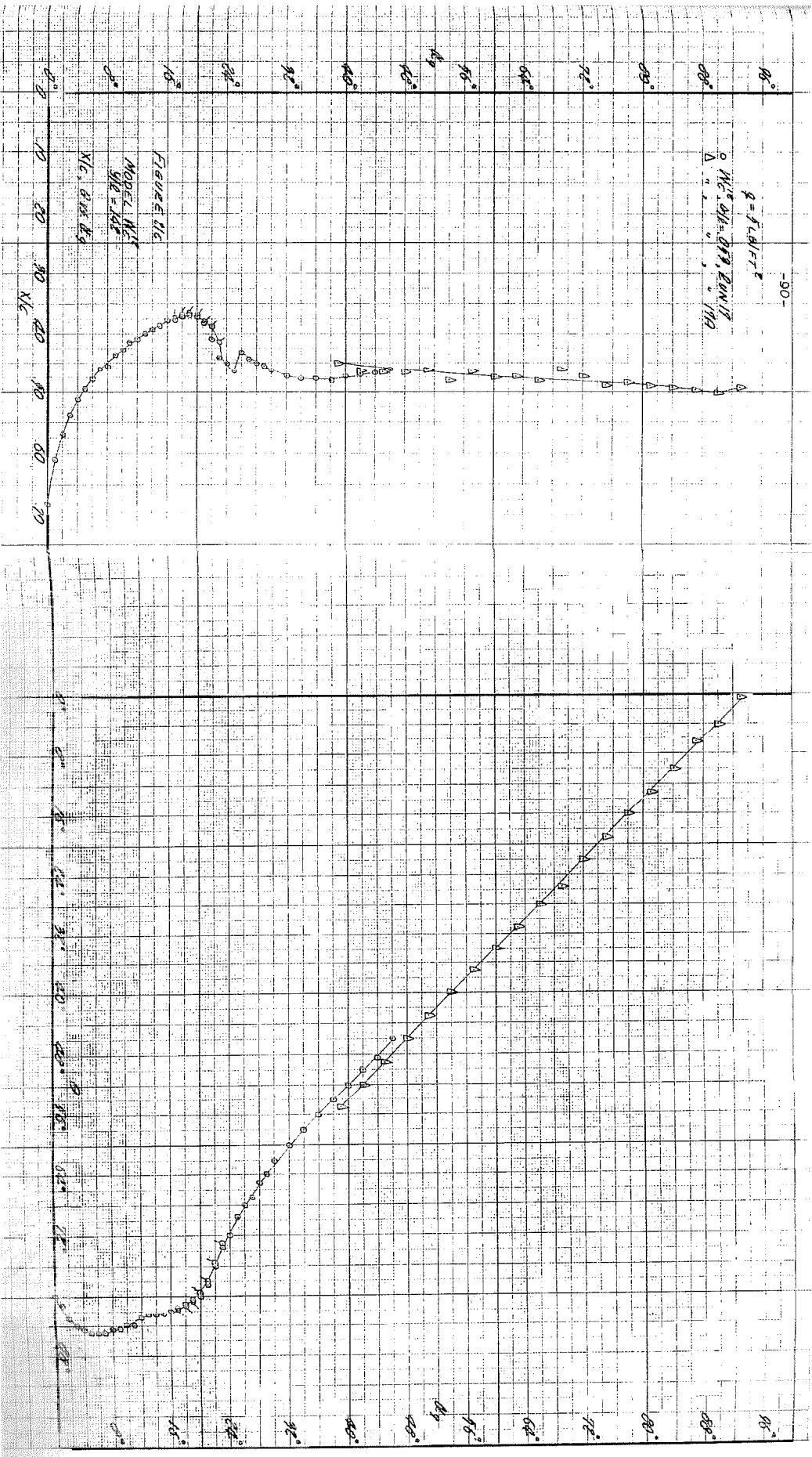


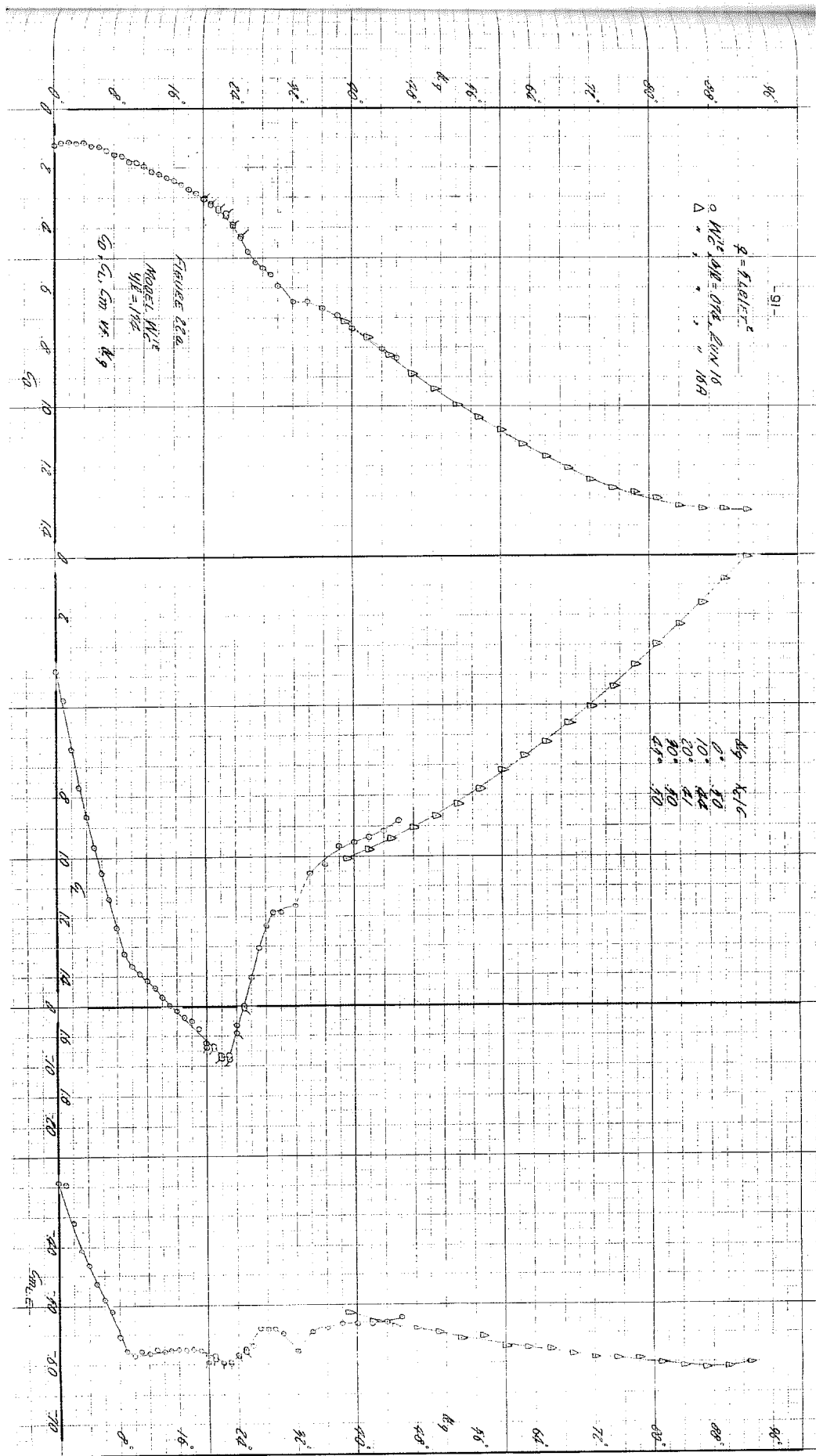
-89-

$$p = 21.611 T^2$$

$M_2^2, M_1 = 0.93, \text{GUN VI}$
 Δ " " " " " " " " " " " "







$$q = 4.18 \text{ J/g}^\circ\text{C}$$

$$M_{\text{C}}^{\text{H}} \cdot \frac{dN}{dV} = 0.04, \text{ 200 N 15}$$

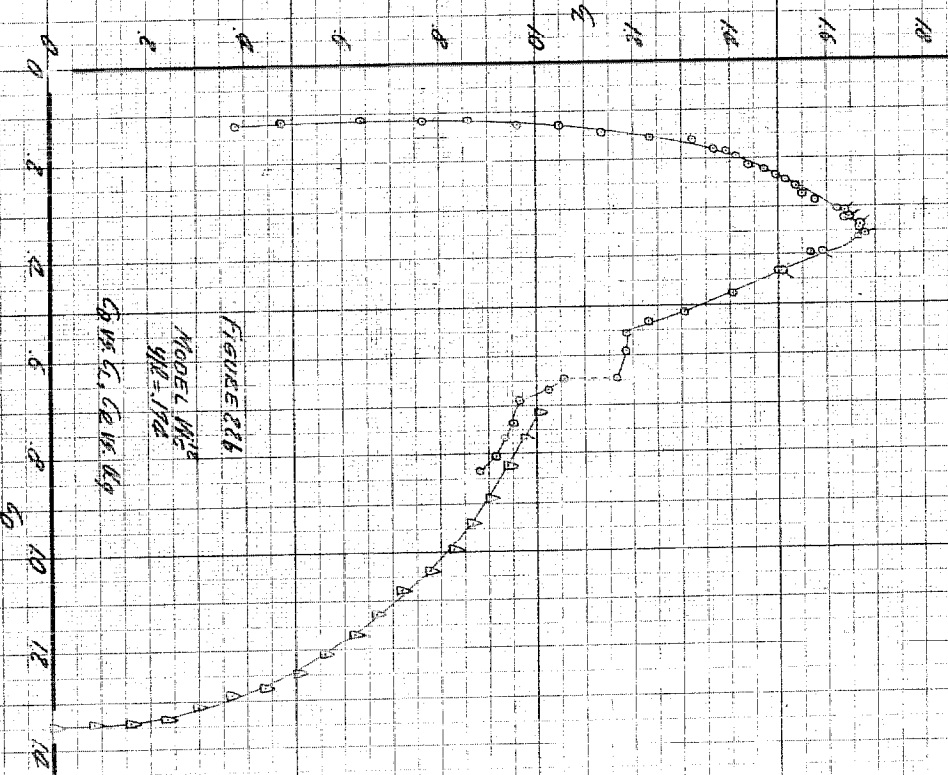
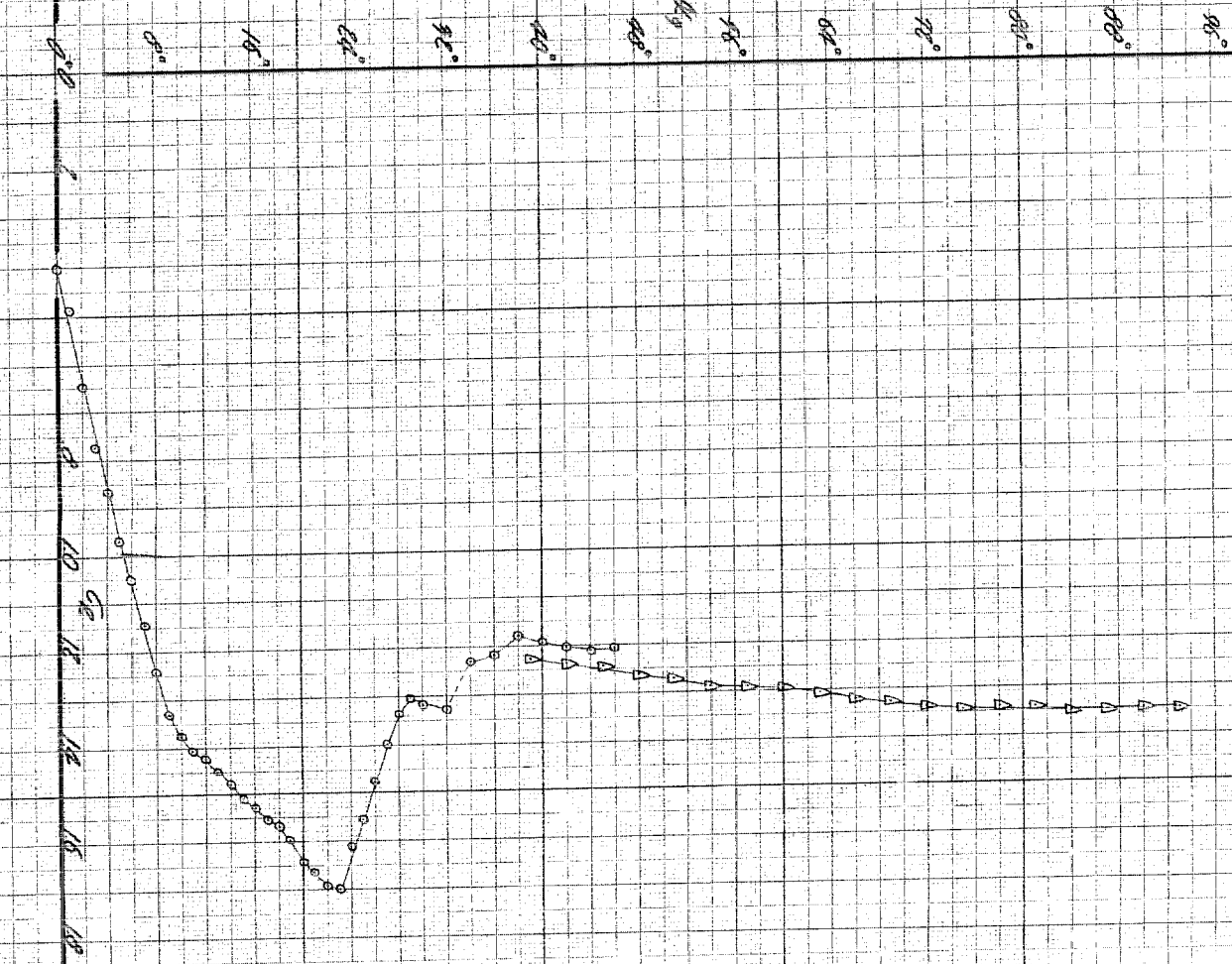
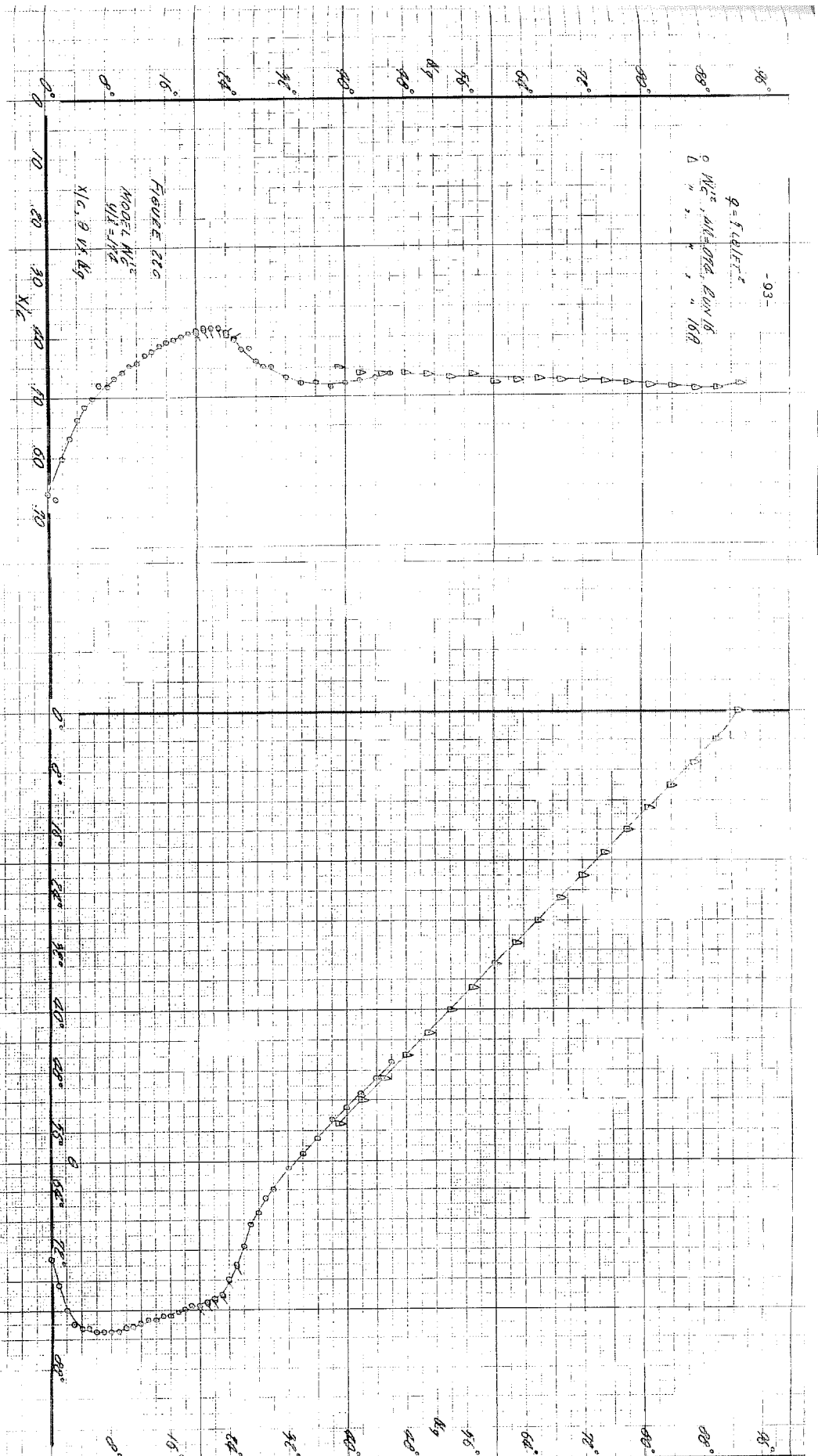
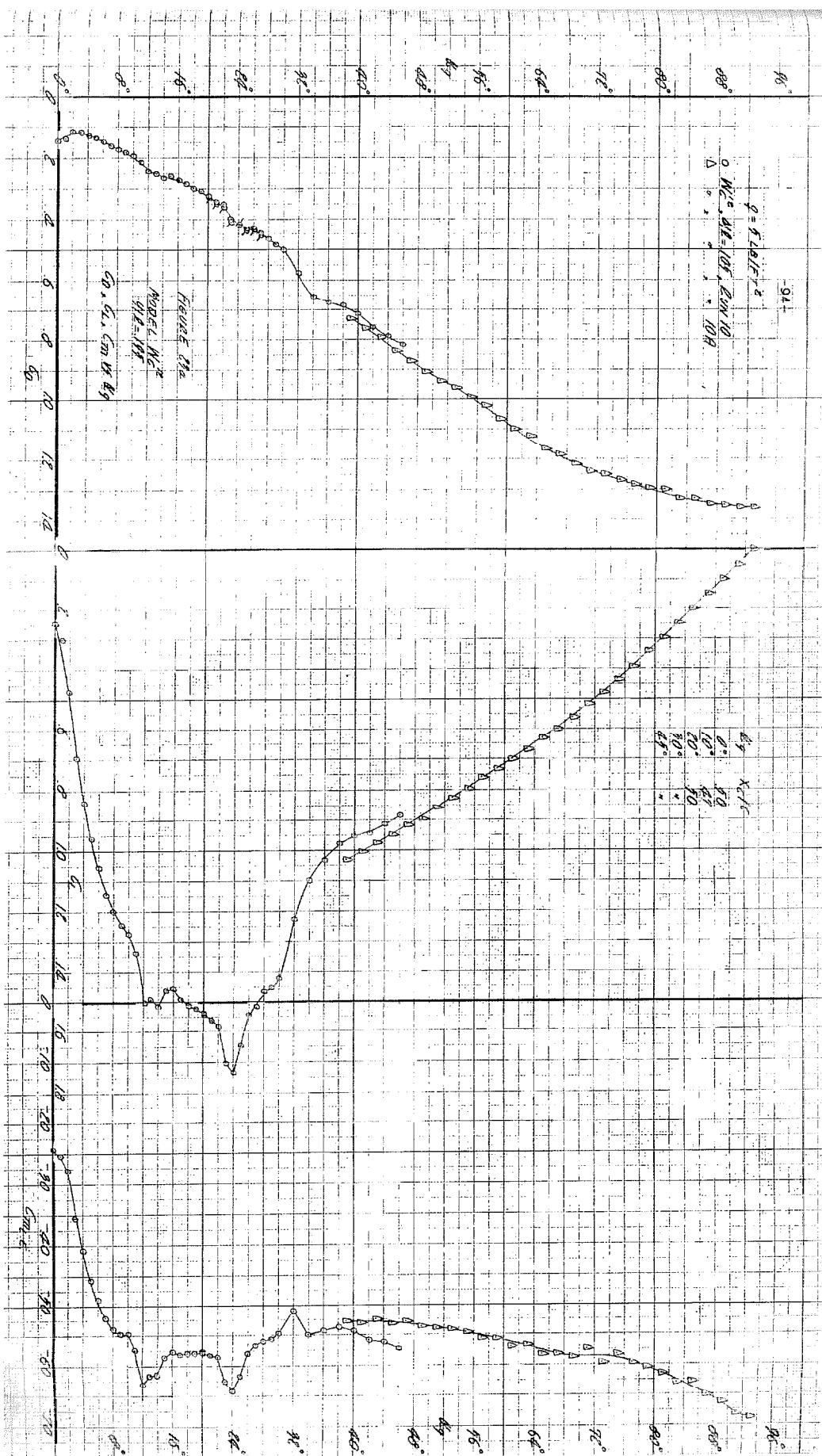


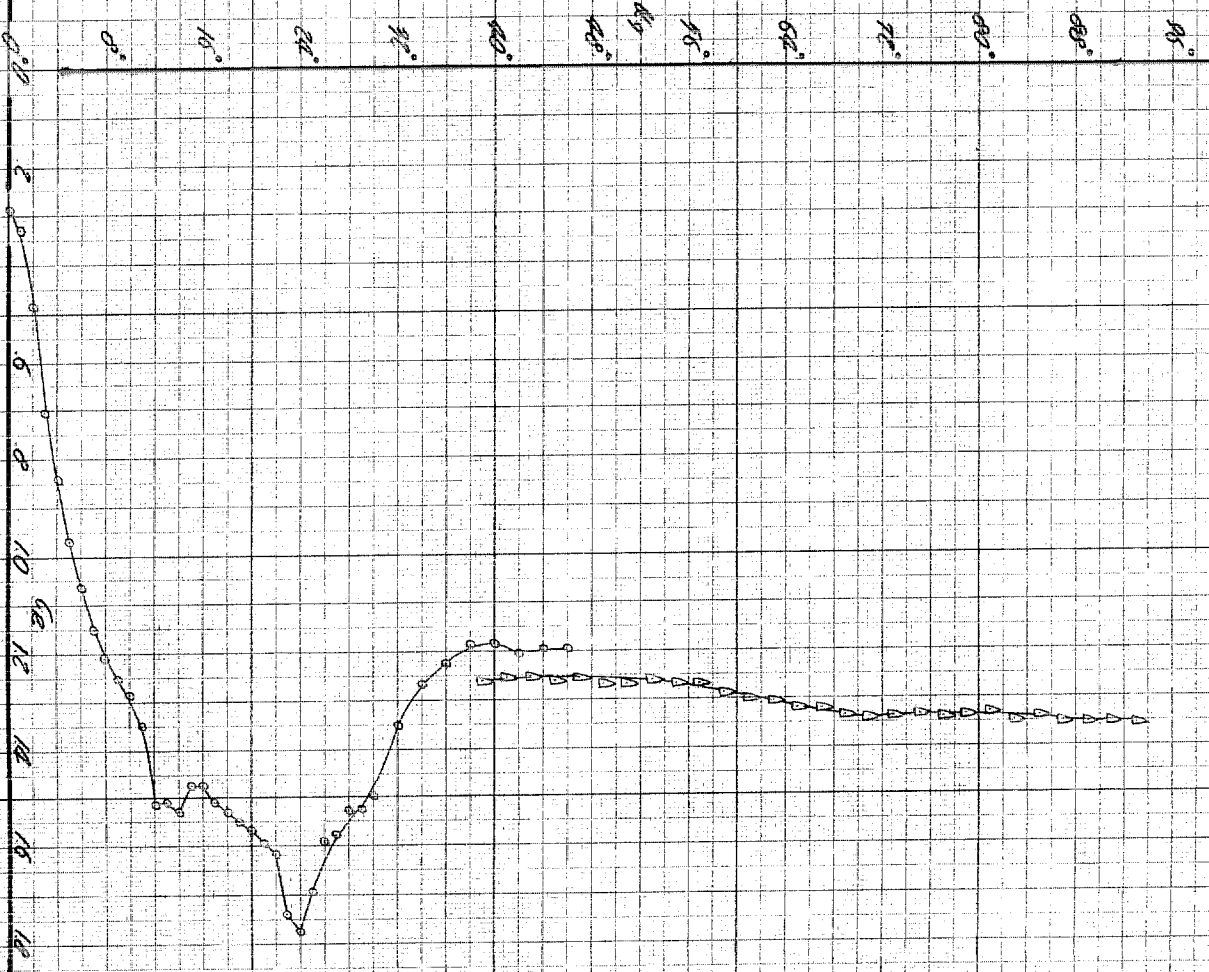
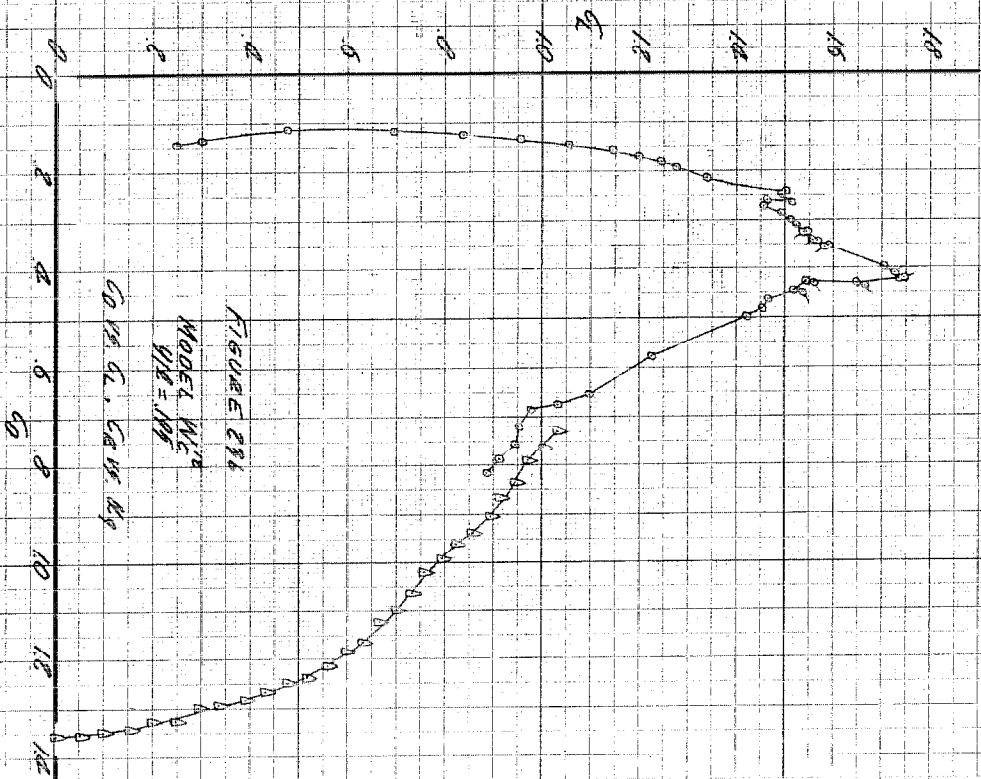
FIGURE 886
MODEL M_{C}^{H}
 $q_{\text{H}} = 1.74$
CE 18, CE 49, CE 149

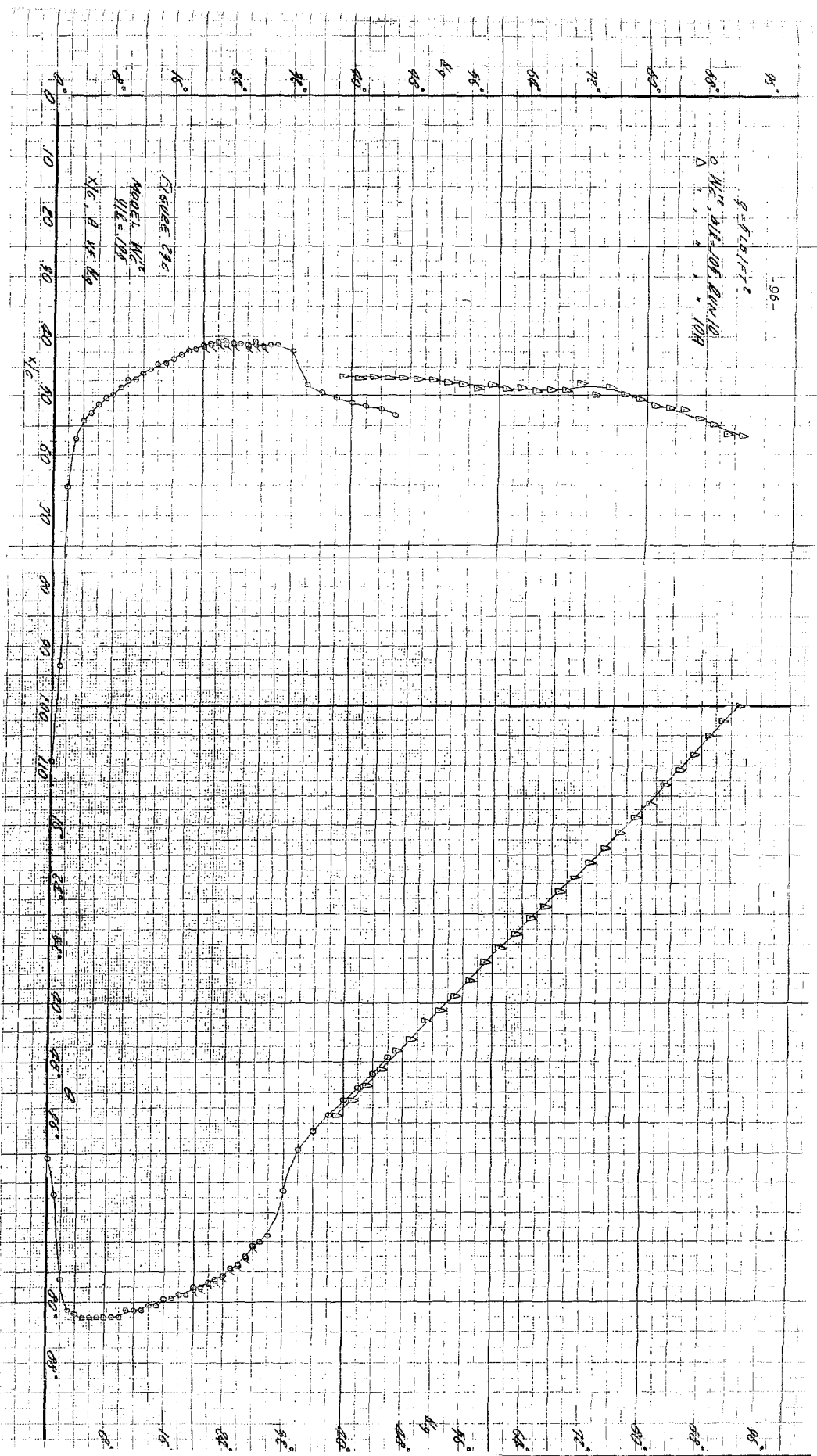


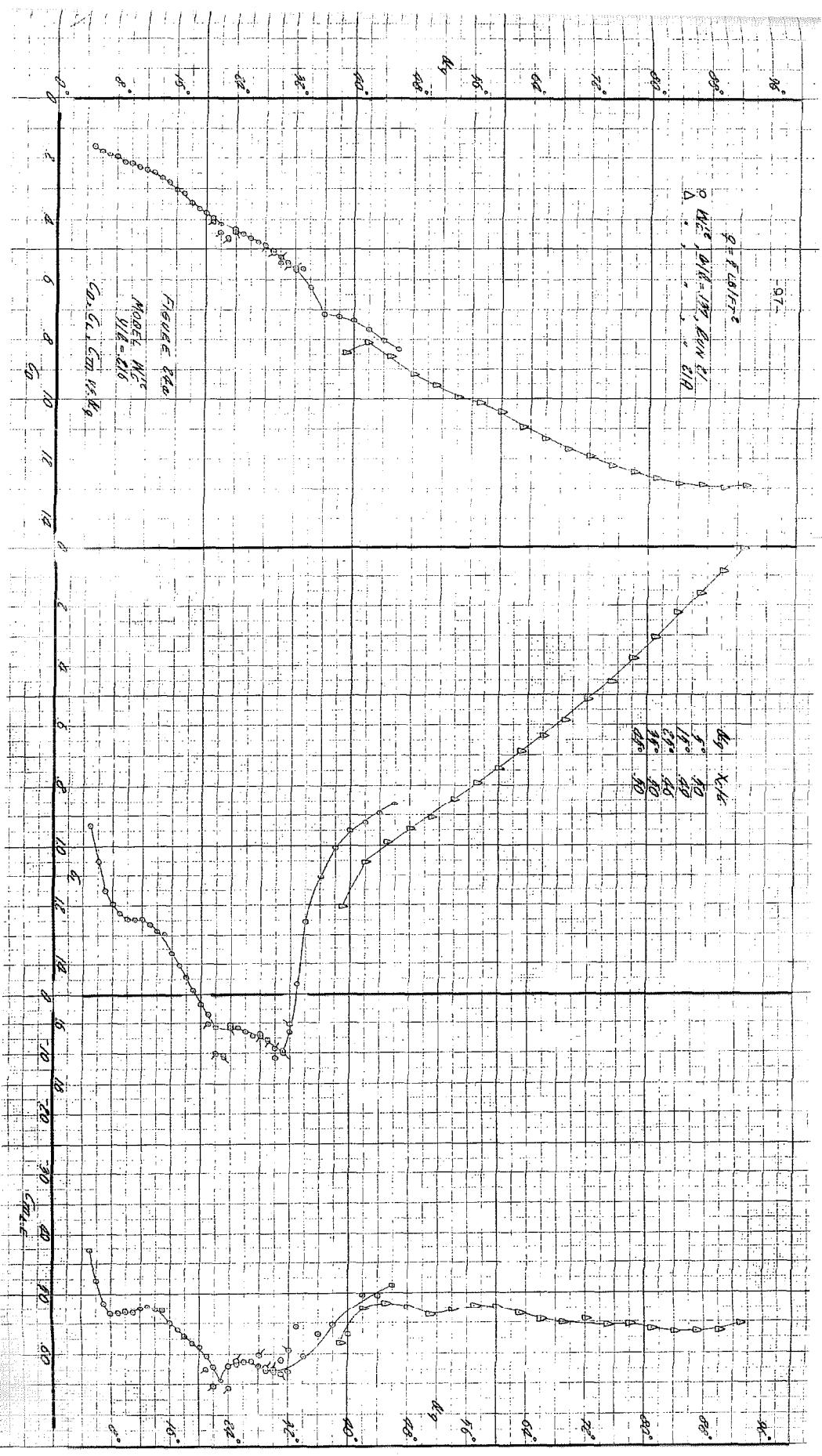




0 WC, $\Delta E = 105$, EUN NO
 Δ " " " " 109



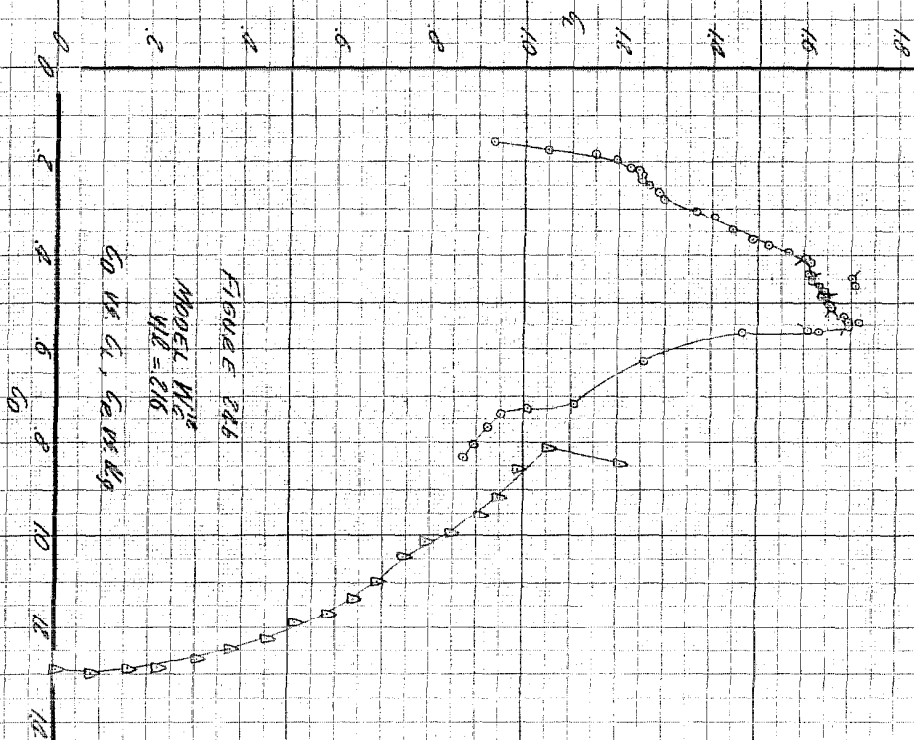




-98-

$q = 1.60 \text{ FT}^2$

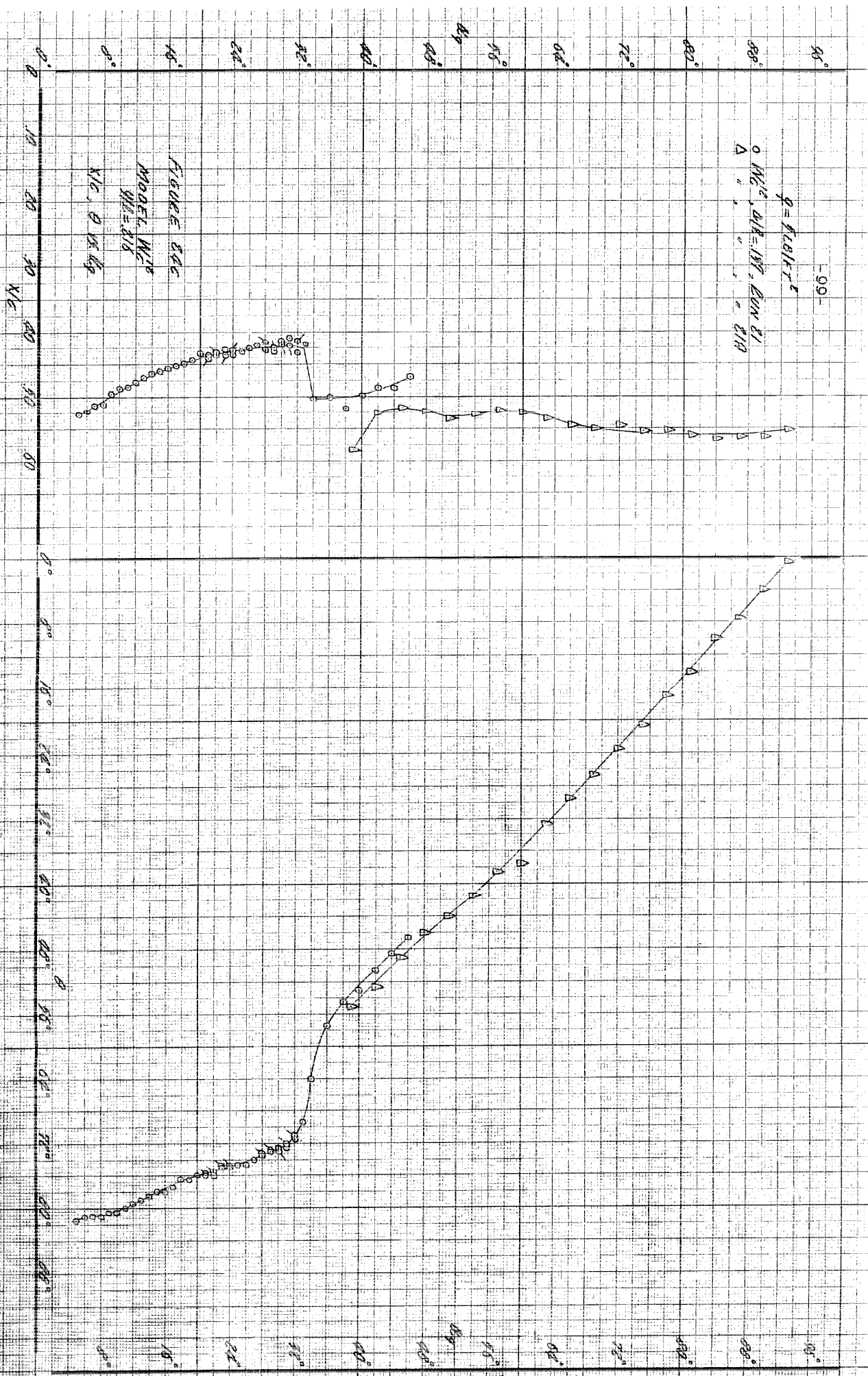
$\Delta W_{12}^2, \Delta W_{13}^2, \Delta W_{14}^2, \Delta W_{15}^2$
 $\Delta W_{16}^2, \Delta W_{17}^2, \Delta W_{18}^2, \Delta W_{19}^2$

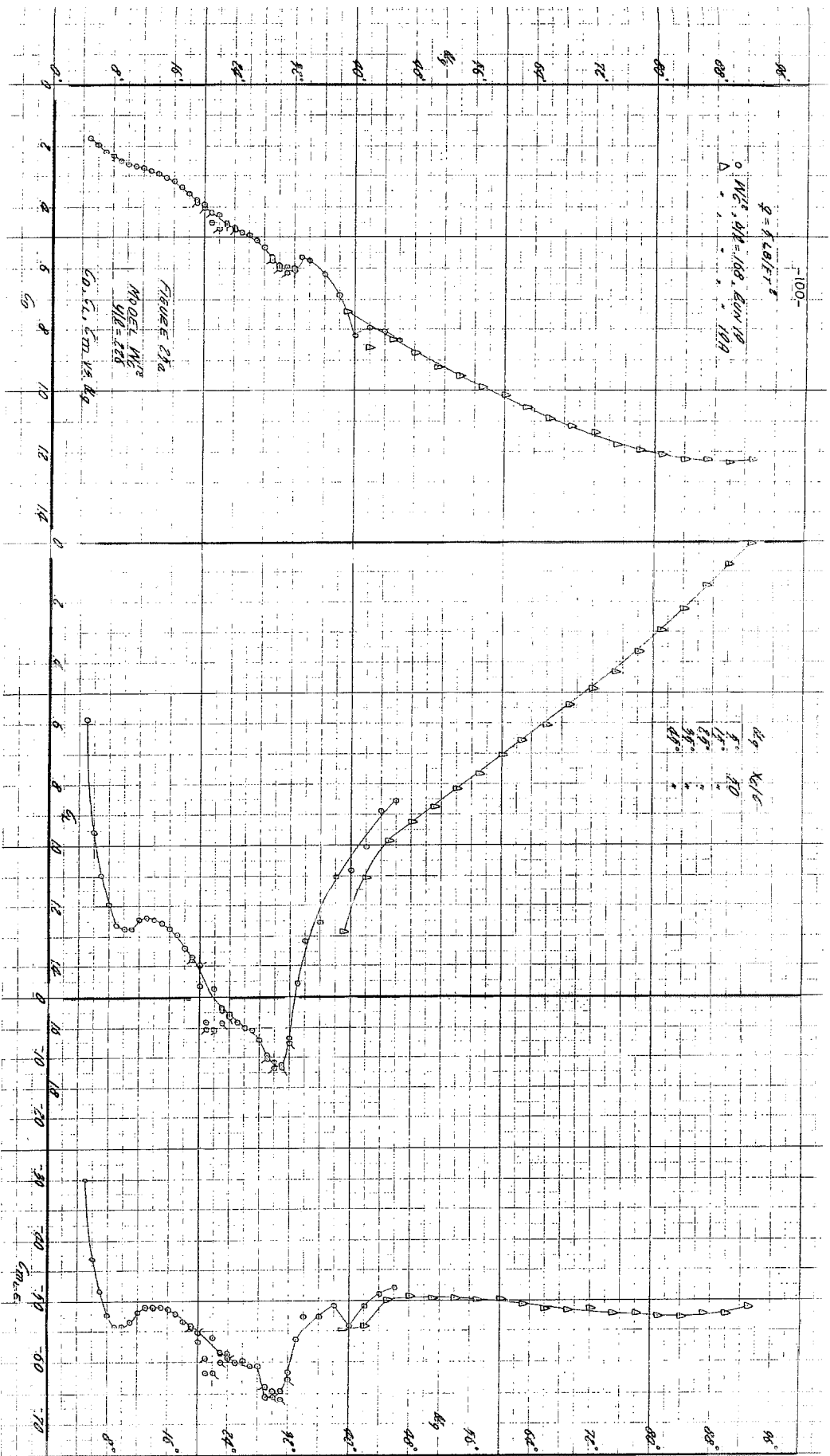


- 99 -

$\rho = 8.68 \times 10^{-8}$
 $\Delta M/E, \Delta/E = 1.87, \Delta/E = 2.1$
 Δ

FIGURE 84C
 MODEL M/C
 $\rho/E = 8.6$
 $\Delta/E, \Delta/E = 1.87$

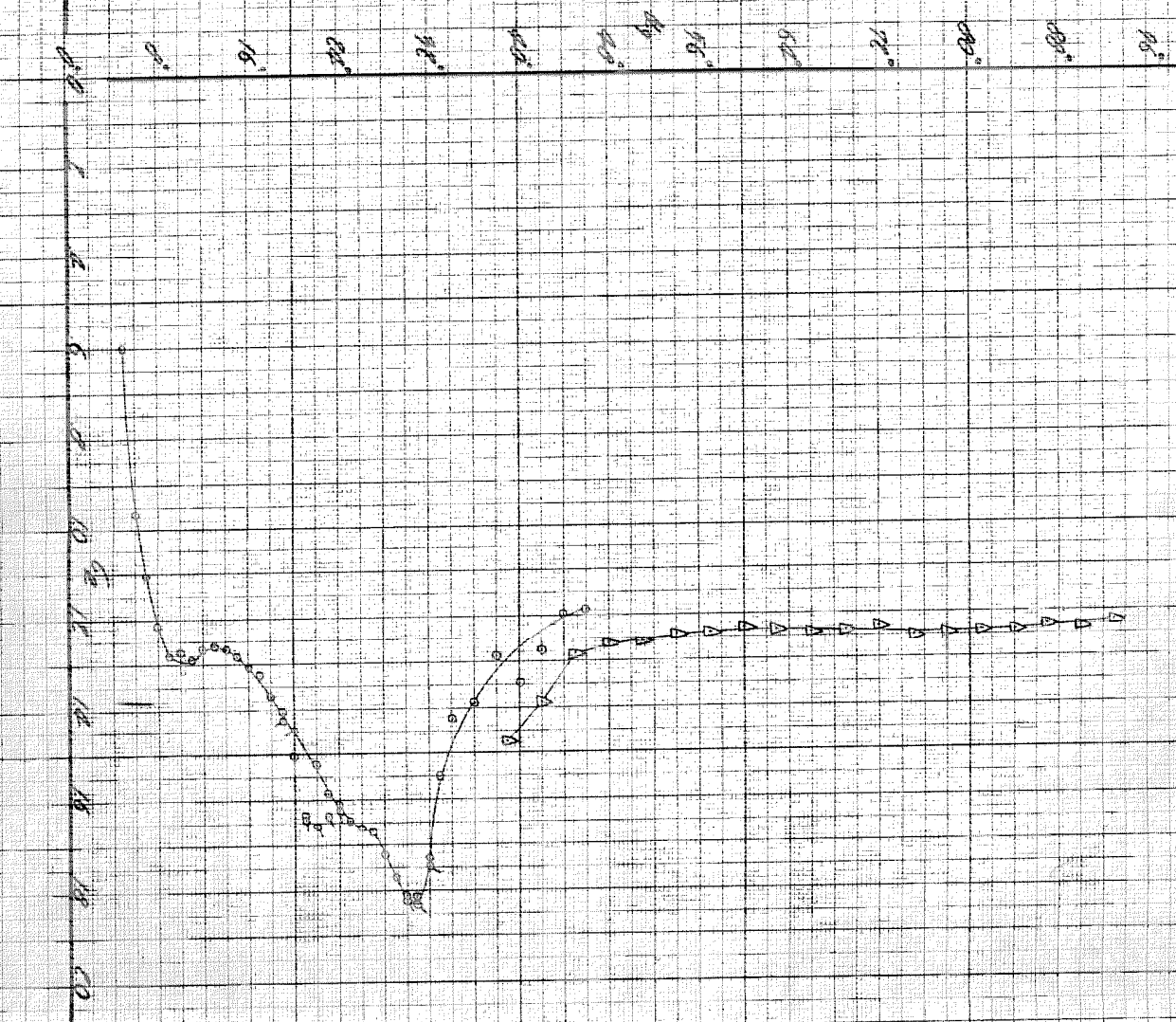
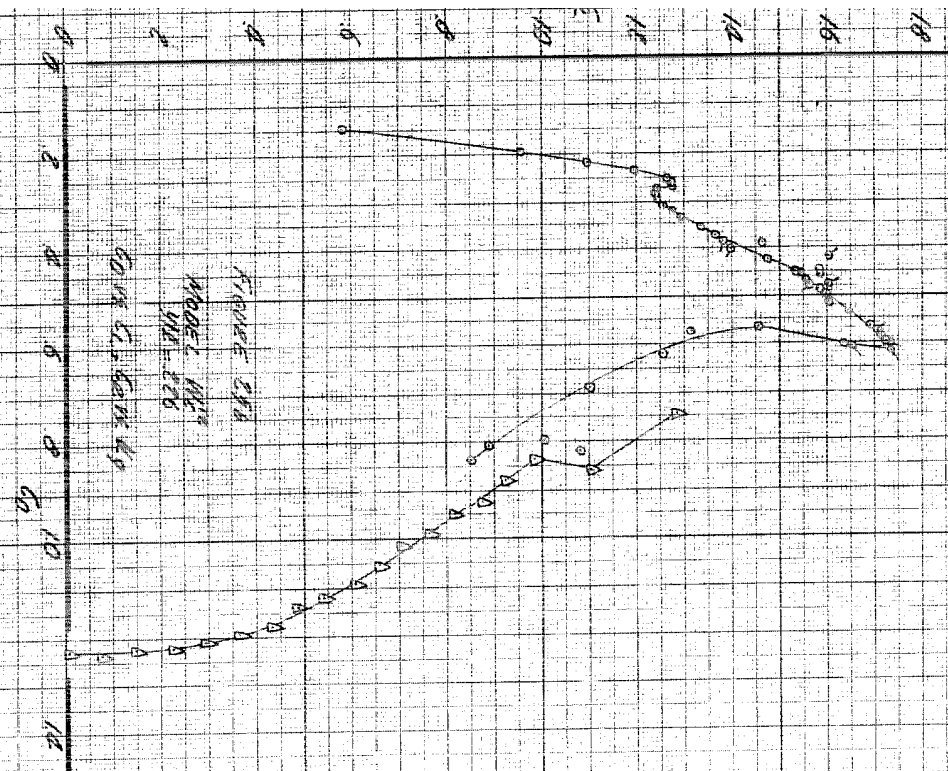


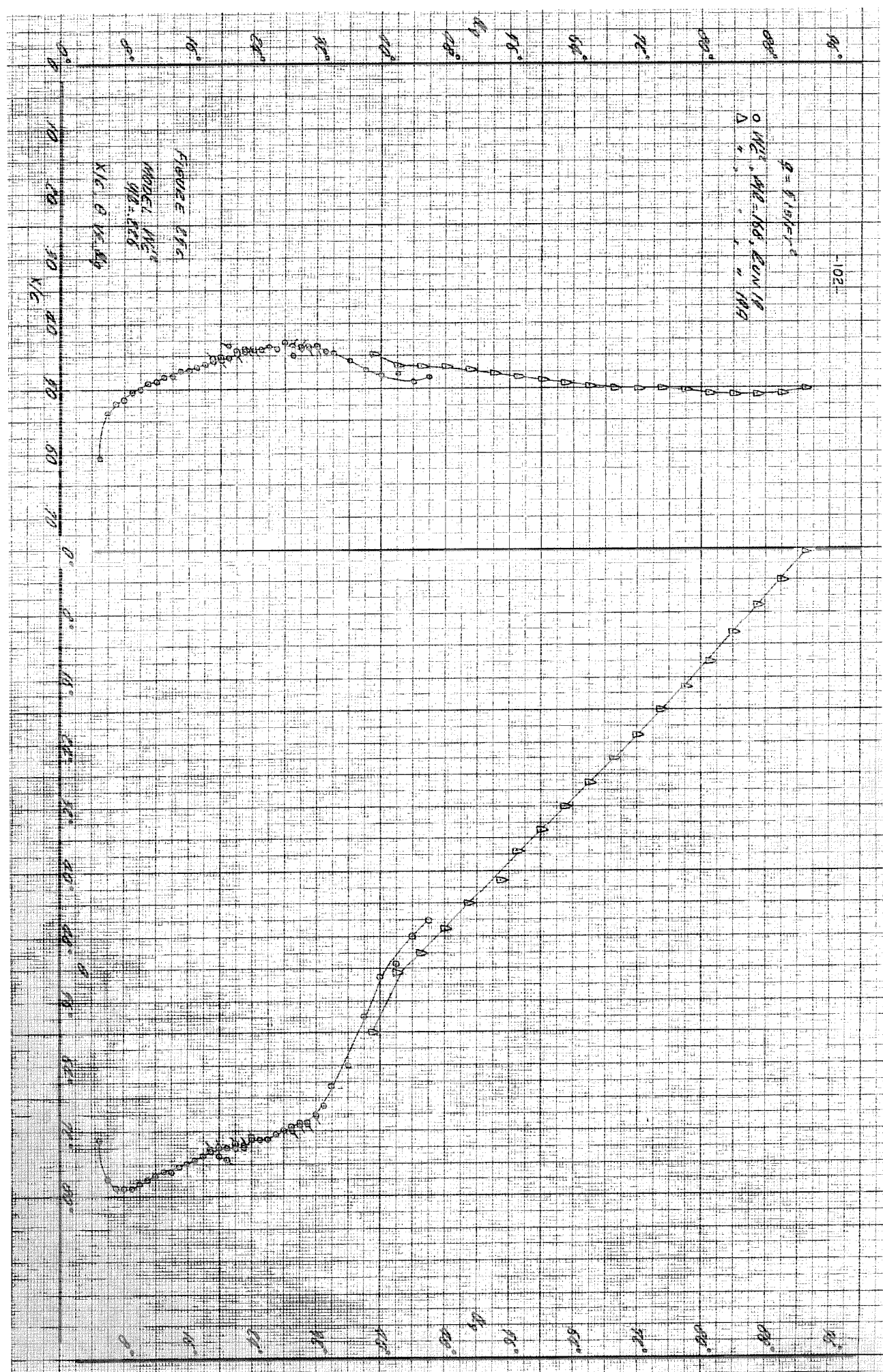


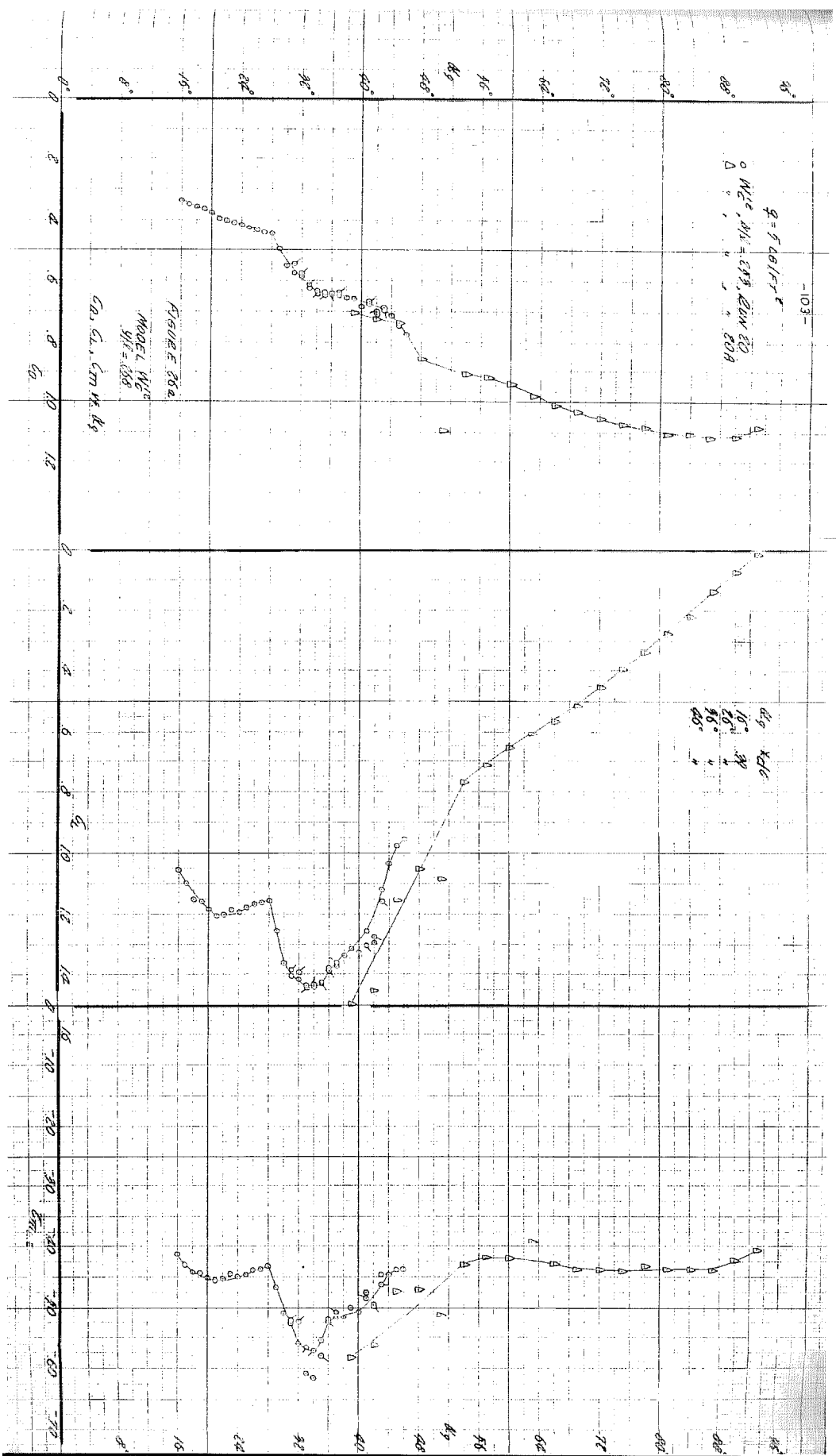
-101-

$$g = 8.015 \text{ cm}^2$$

\circ M_{25}^0 , $M_{10}^0 = 100$, $R_{25}/10$
 Δ M_{25}^0 , $M_{10}^0 = 100$, $R_{25}/10$

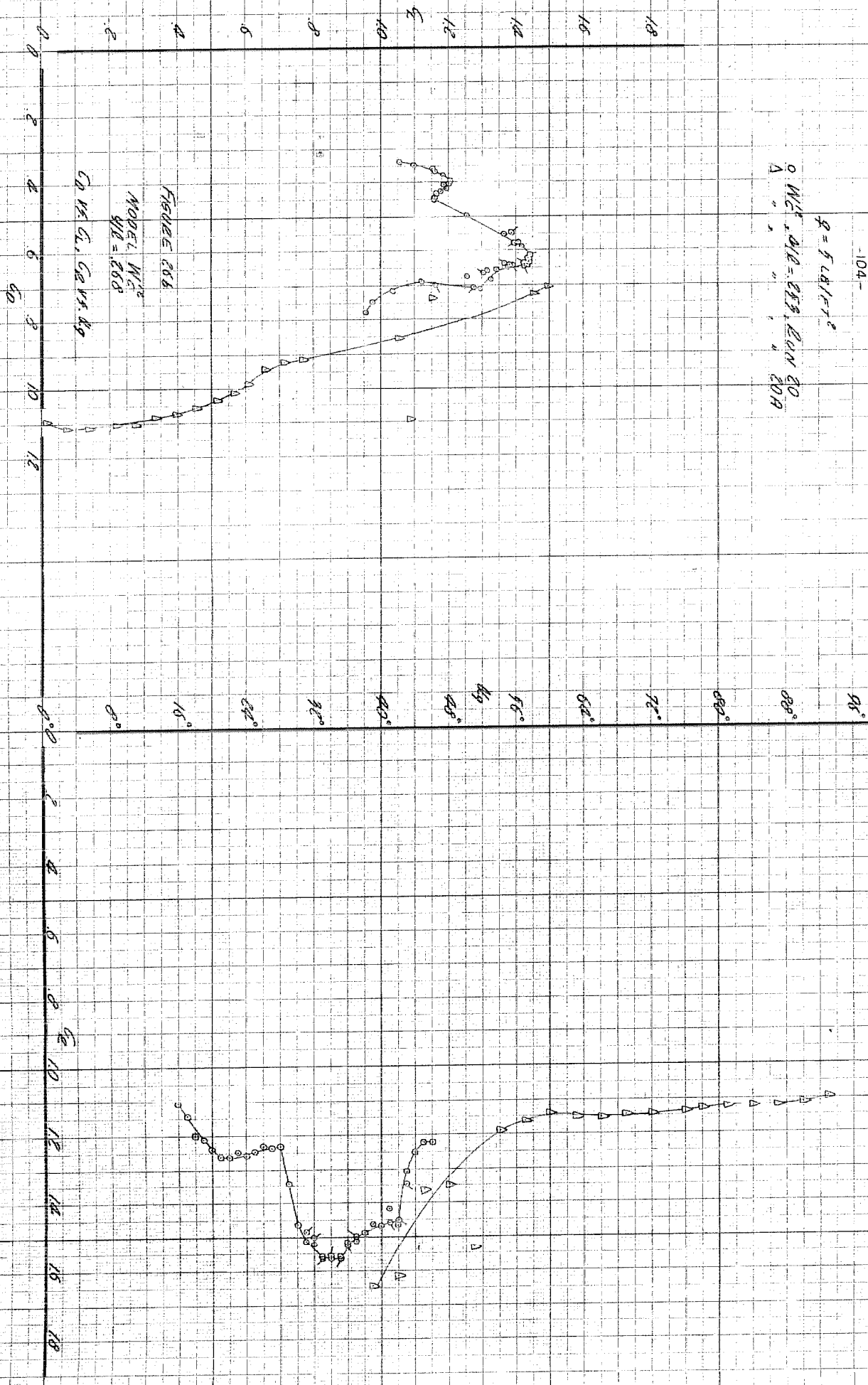


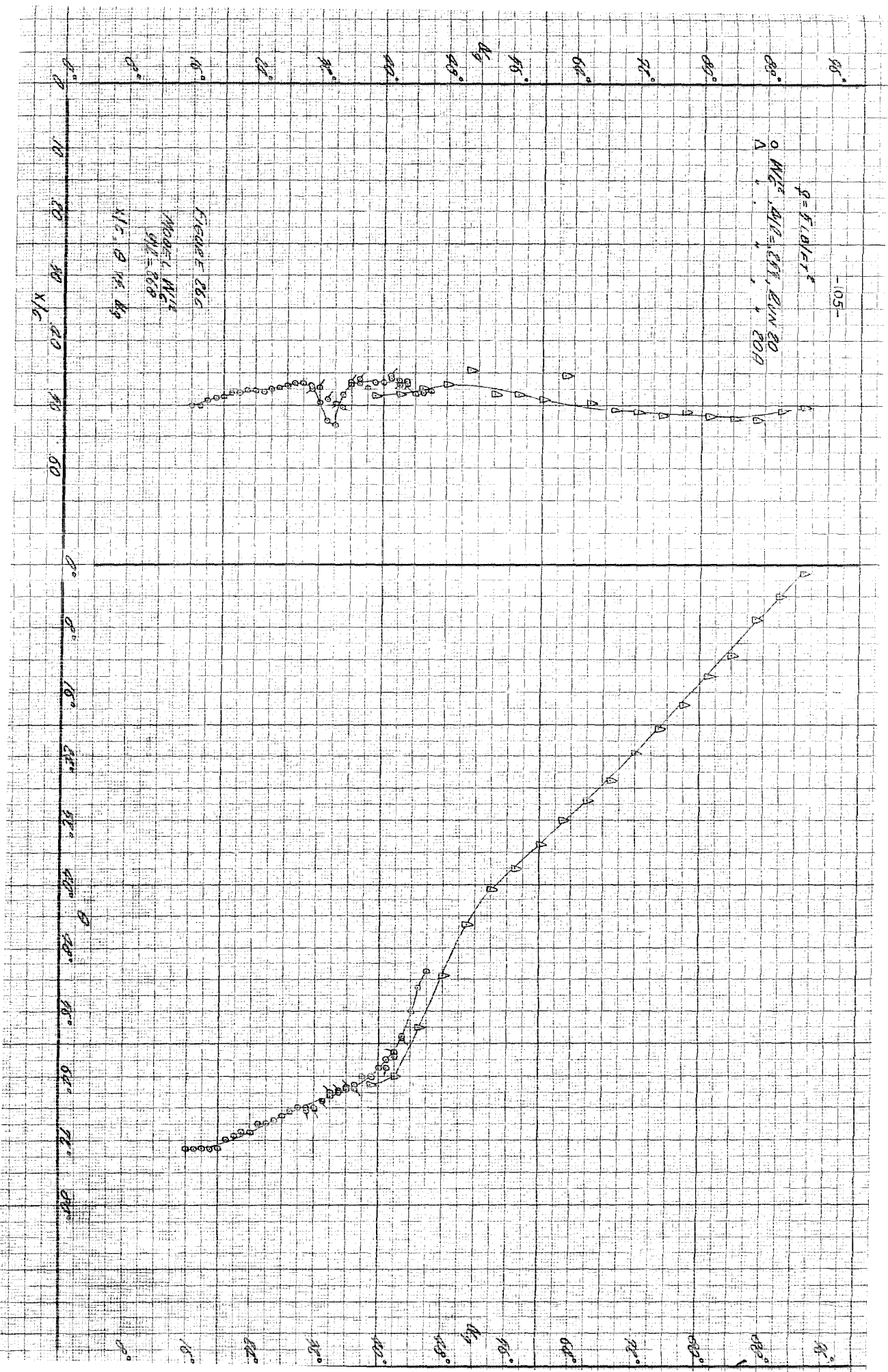




$$2.1 \times 10^7 \text{ g} = 21,000,000 \text{ g}$$

0 WC, d/E = 255, RAN 20
A " " " " 20A





-106-

$\rho = 10 \text{ lb/ft}^3$
 $0 \text{ W/C, } 0.1 \text{ OA, } 0.01 \text{ N } \theta$

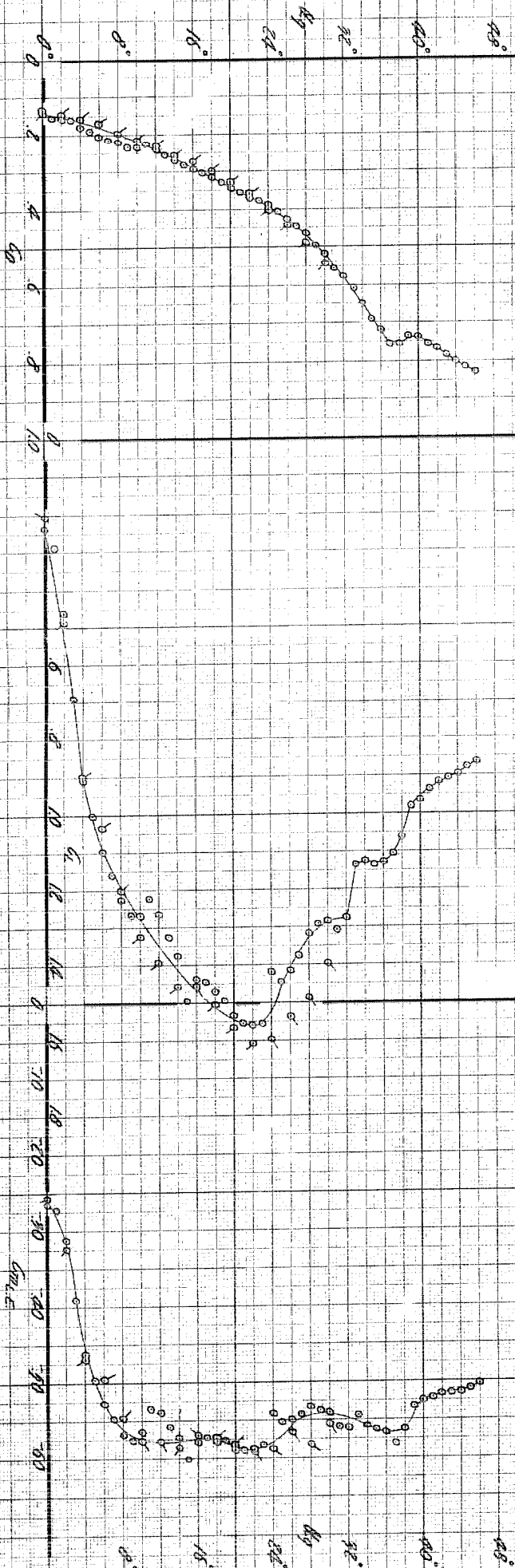


FIGURE
MODEL W/C
 $\rho/\theta = 0.01$
CA, CL, CM OF KG

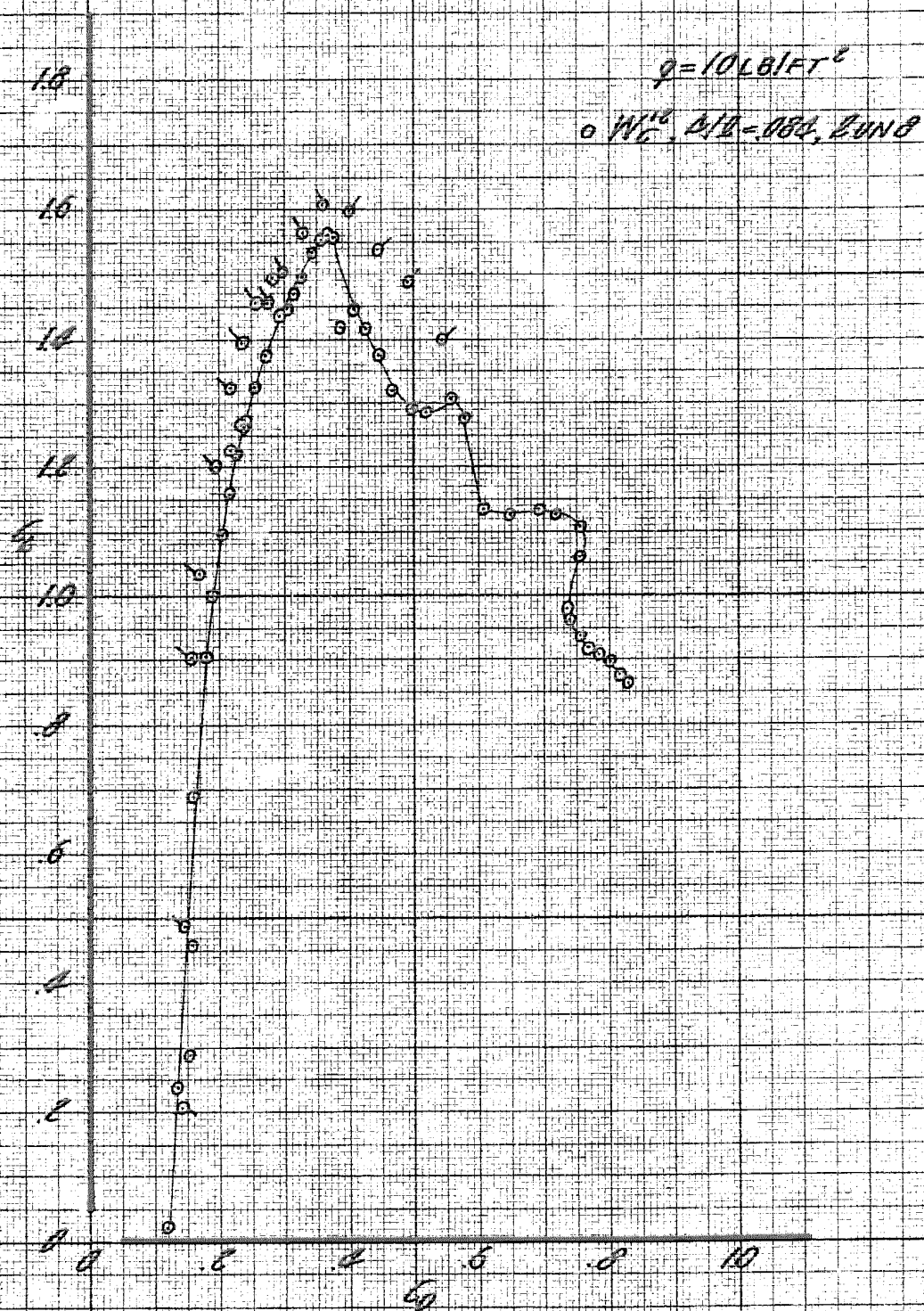


FIGURE 816

MODEL W/C
 $D/L = .004$

G_0 vs. G_1

90°

$$q = 8.681 \times 10^{-2}$$

$$\Delta \frac{W_0}{W_0}, \Delta W_0 = 0.1 \text{ e.u. } 1.0$$

-10E-

80°

72°

64°

56°

48°

32°

24°

16°

8°

0°

2

4

6

8

10

12

14

16

18

20

22

24

26

28

30

32

34

36

FIGURE 20a
MORSE W_0
 $W_0 = 0$
 C_0, C_1, W_0, K_0

2

4

6

8

10

12

14

16

18

20

22

24

26

28

30

32

34

36

38

40

42

44

46

48

50

52

54

56

58

60

62

64

66

68

70

72

74

76

78

80

82

84

86

88

90

92

94

96

98

100

102

104

106

108

110

112

114

116

118

120

122

124

126

128

130

132

134

136

138

140

142

144

146

148

150

152

154

156

158

160

162

164

166

168

170

172

174

176

178

180

182

184

186

188

190

192

194

196

198

200

202

204

206

208

210

212

214

216

218

220

222

224

226

228

230

232

234

236

238

240

242

244

246

248

250

252

254

256

258

260

262

264

266

268

270

272

274

276

278

280

282

284

286

288

290

292

294

296

298

300

302

304

306

308

310

312

314

316

318

320

322

324

326

328

330

332

334

336

338

340

342

344

346

348

350

352

354

356

358

360

362

364

366

368

370

372

374

376

378

380

382

384

386

388

390

392

394

396

398

400

402

404

406

408

410

412

414

416

418

420

422

424

426

428

430

432

434

436

438

440

442

444

446

448

450

452

454

456

458

460

462

464

466

468

470

472

474

476

478

480

482

484

486

488

490

492

494

496

498

500

502

504

506

508

510

512

514

516

518

520

$\rho = 1.2814 \text{ g/cm}^3$
 $\Delta W_B, \Delta W = 0, 20 \text{ mF}$
 $\Delta W = 0, 20 \text{ mF}$

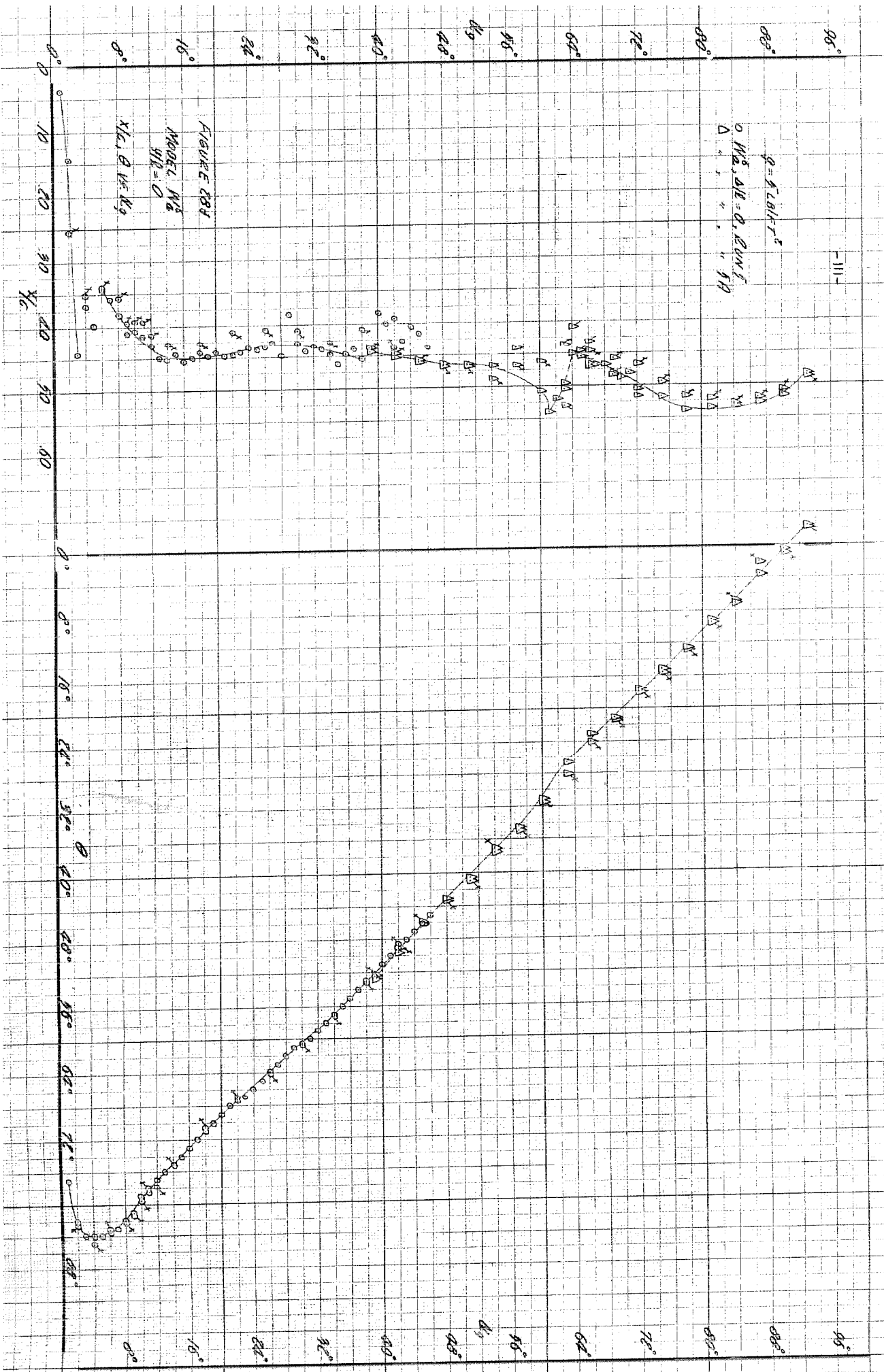
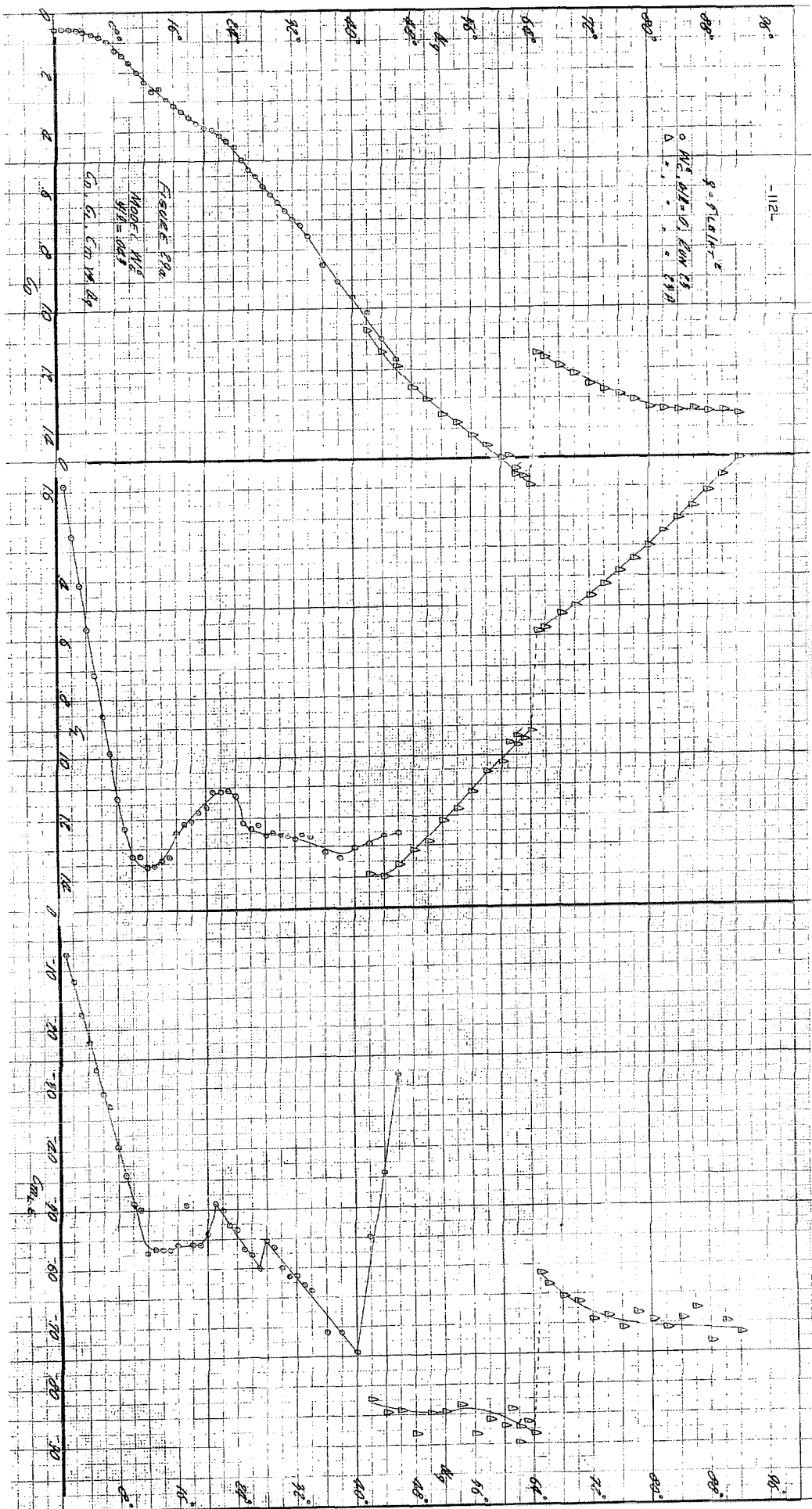


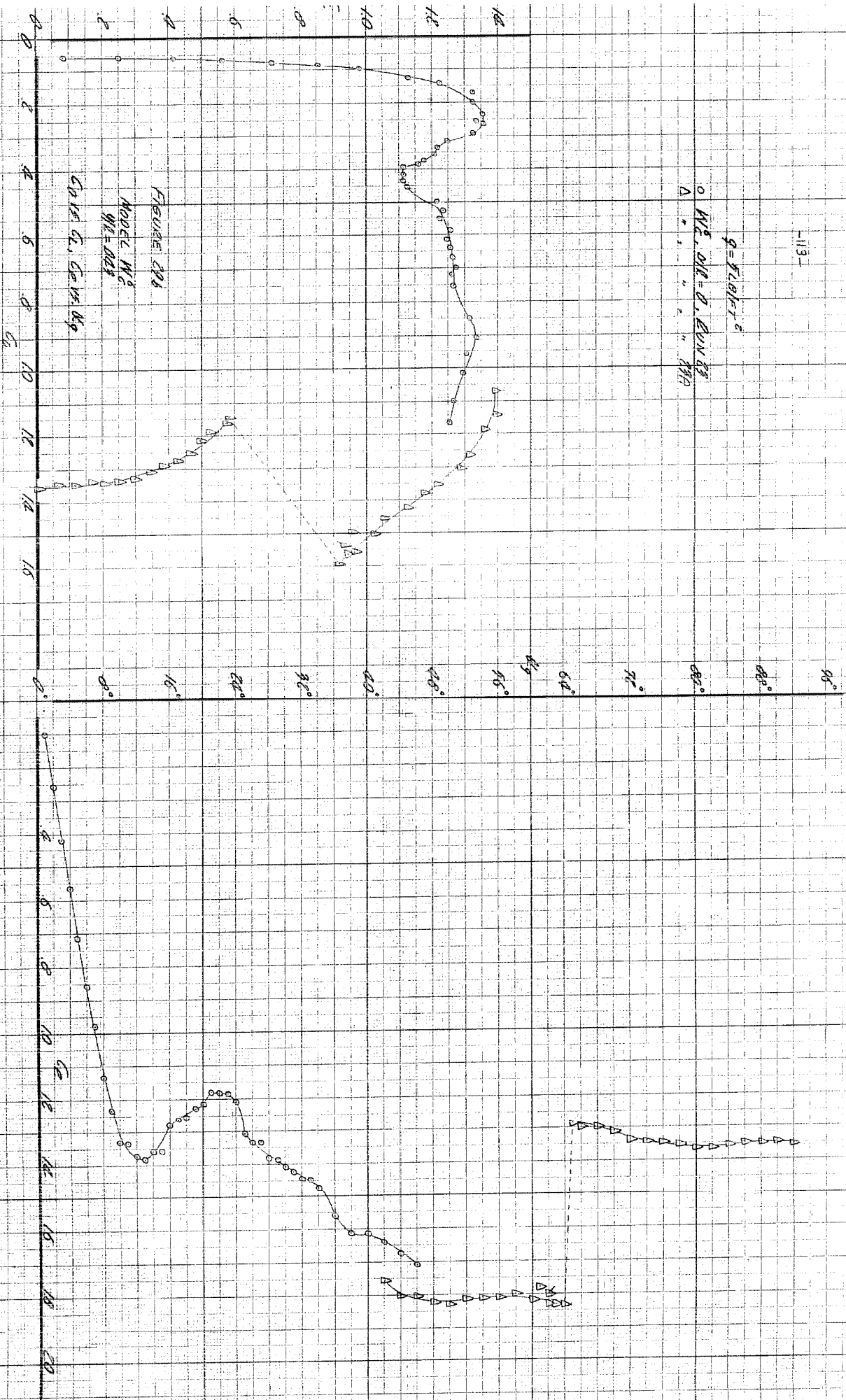
FIGURE 184
 MODEL N8
 $\eta R = 0$
 $x/c, \theta, W, W_B$

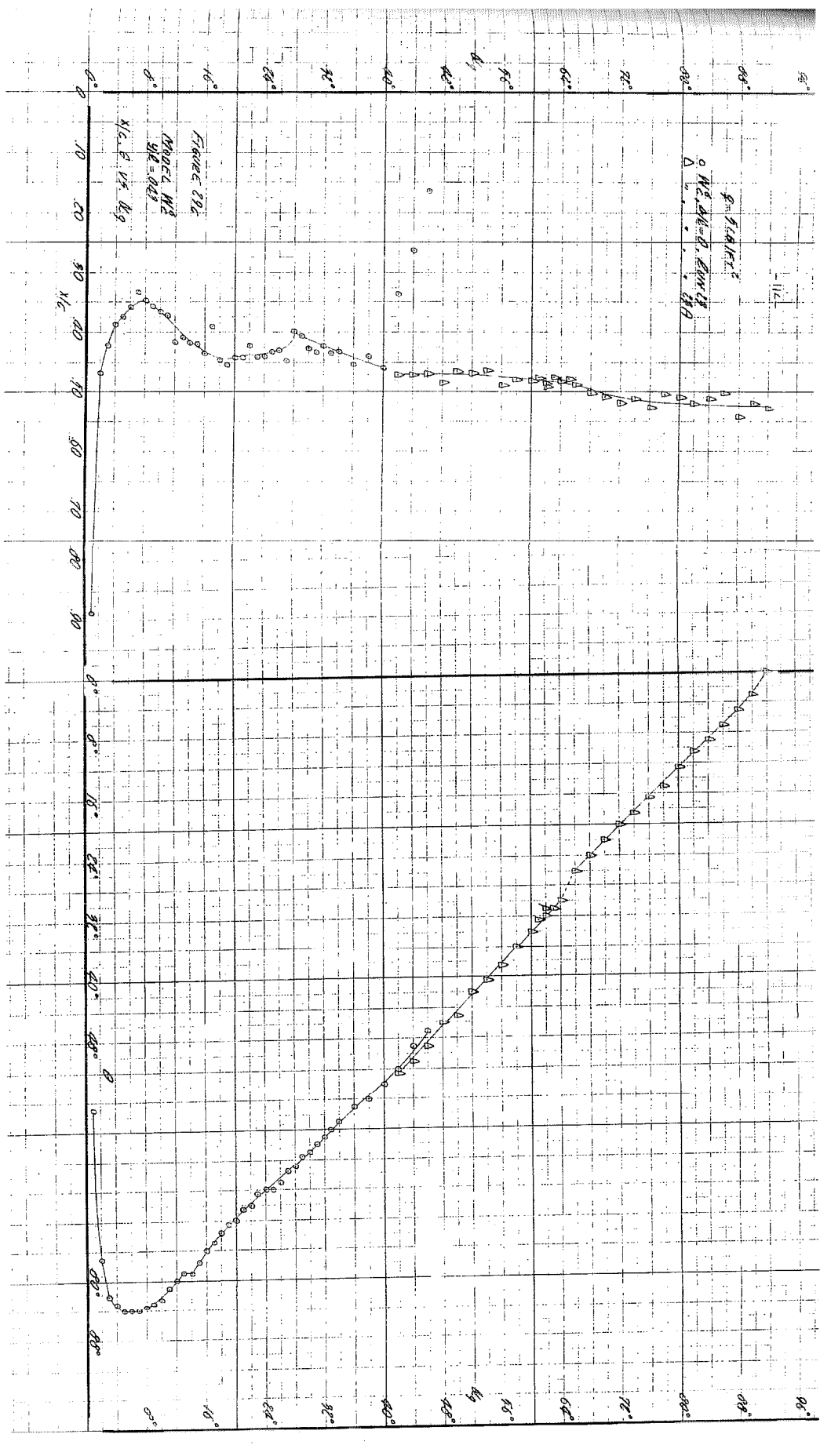


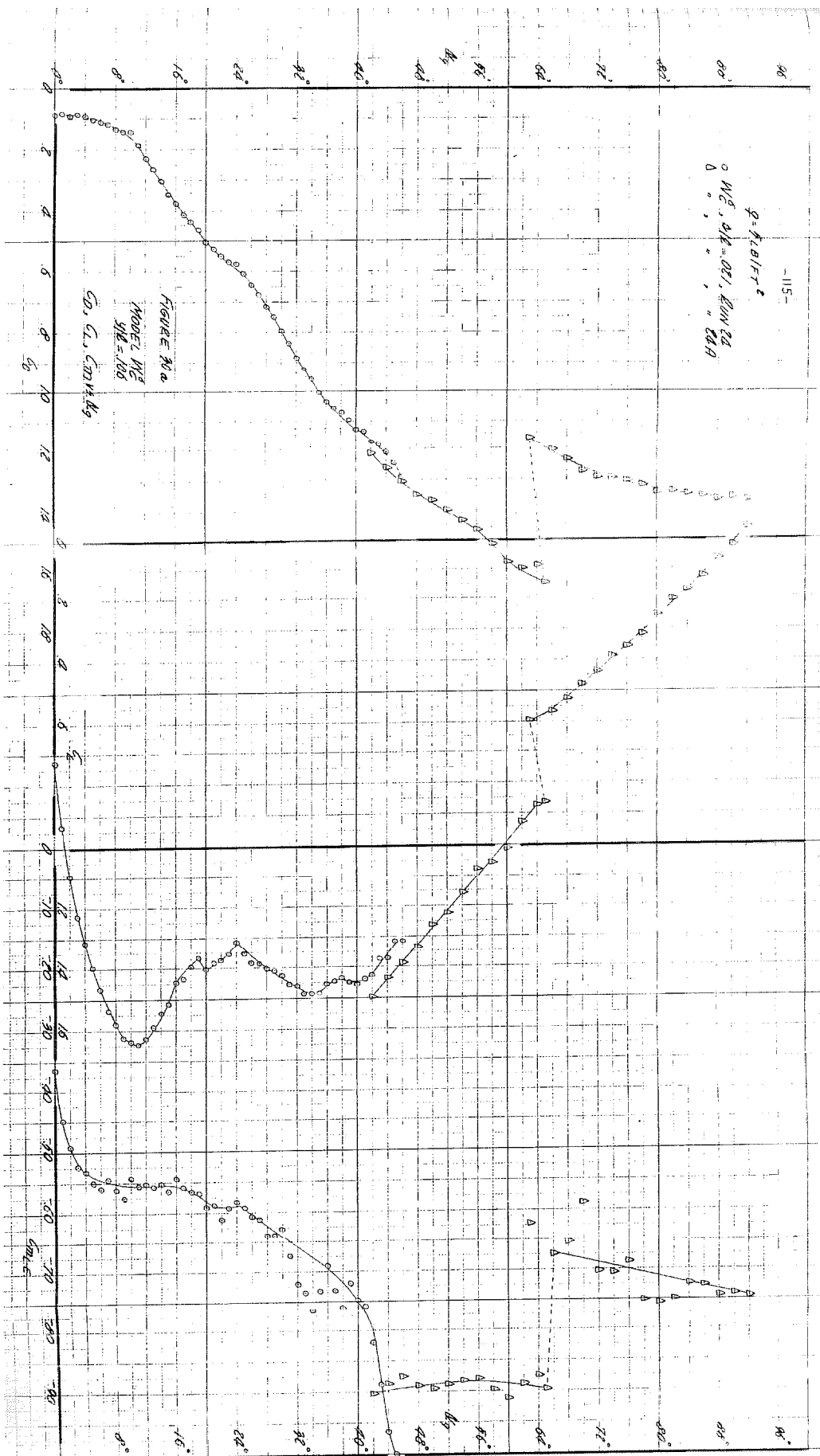
-113-

$$q = 5.0157^{\circ}$$

○ $W_2, \Delta W = 0, \text{EUN } 63$
△ " " " " " " " "

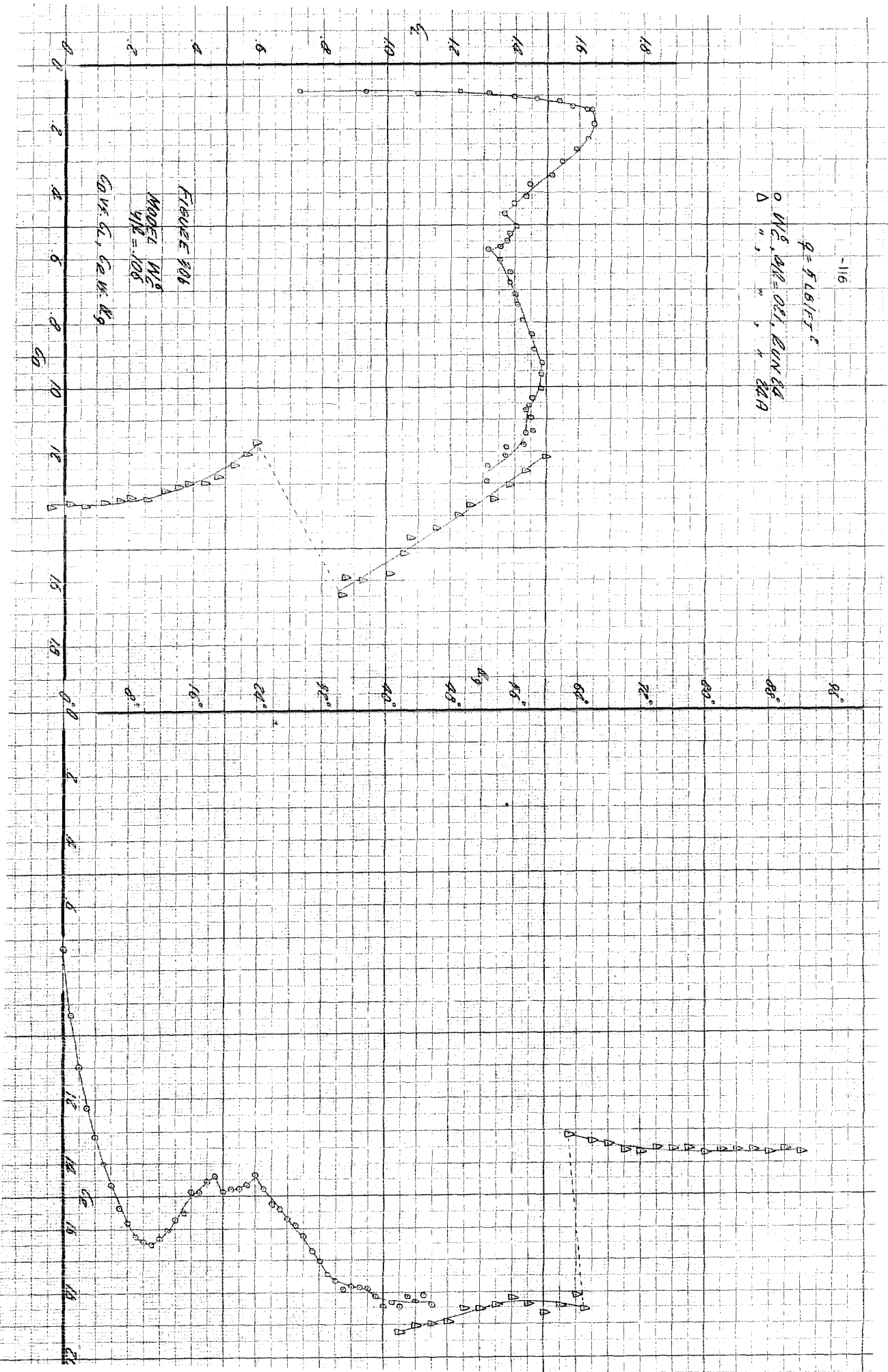






$$q = 561.5 \text{ J}^\circ$$

Δ " , " + AA
0 WC, AP = OCT, RUN ED



$$q = 8.281 \text{ FT}^2$$

○ $M/E = 0.11$, RUN 24
 △ " " " " " 24.9



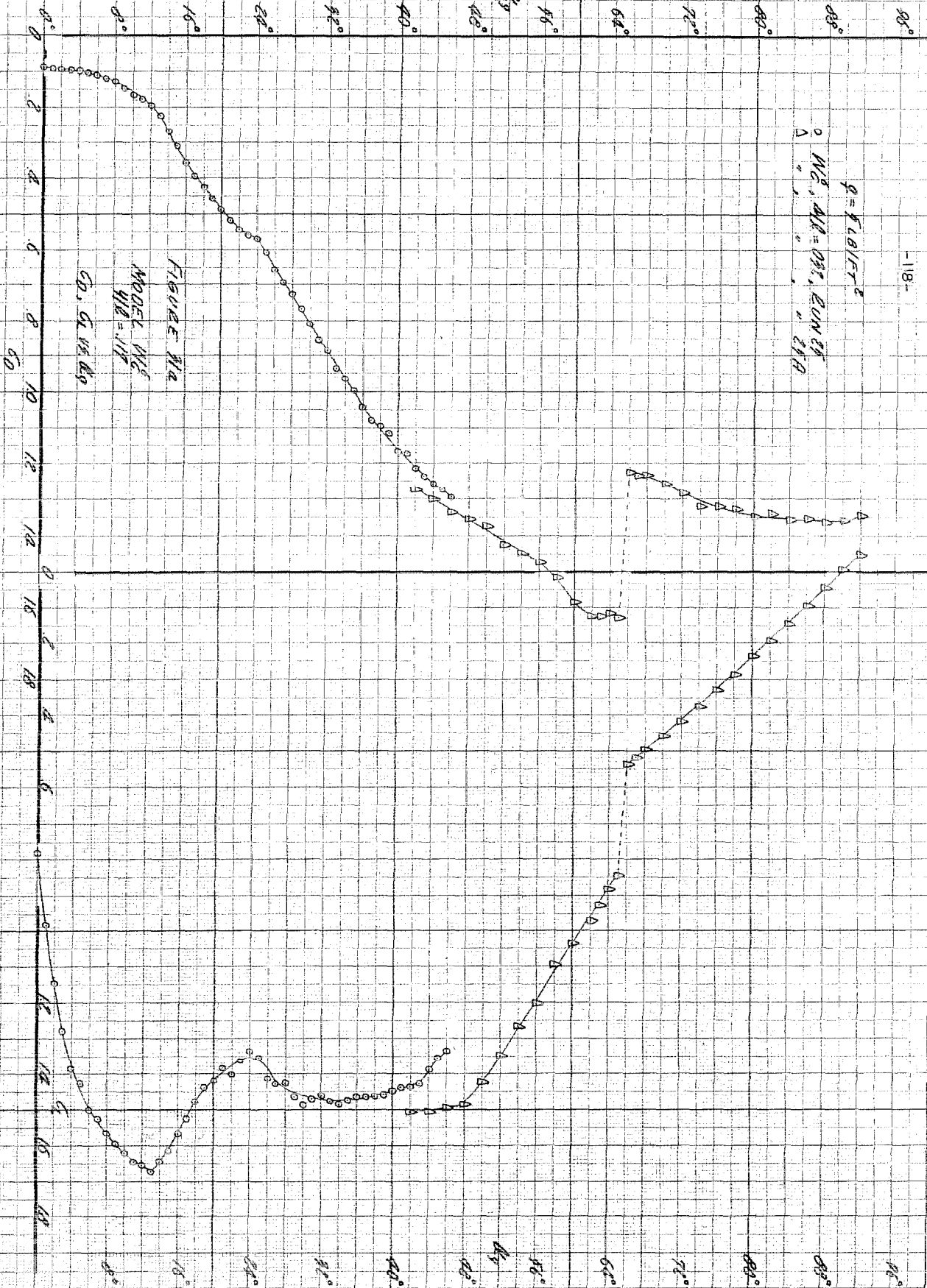
FIGURE 300

MOORE, W.C.

WHE = 100

XIC, 8 W. 40g

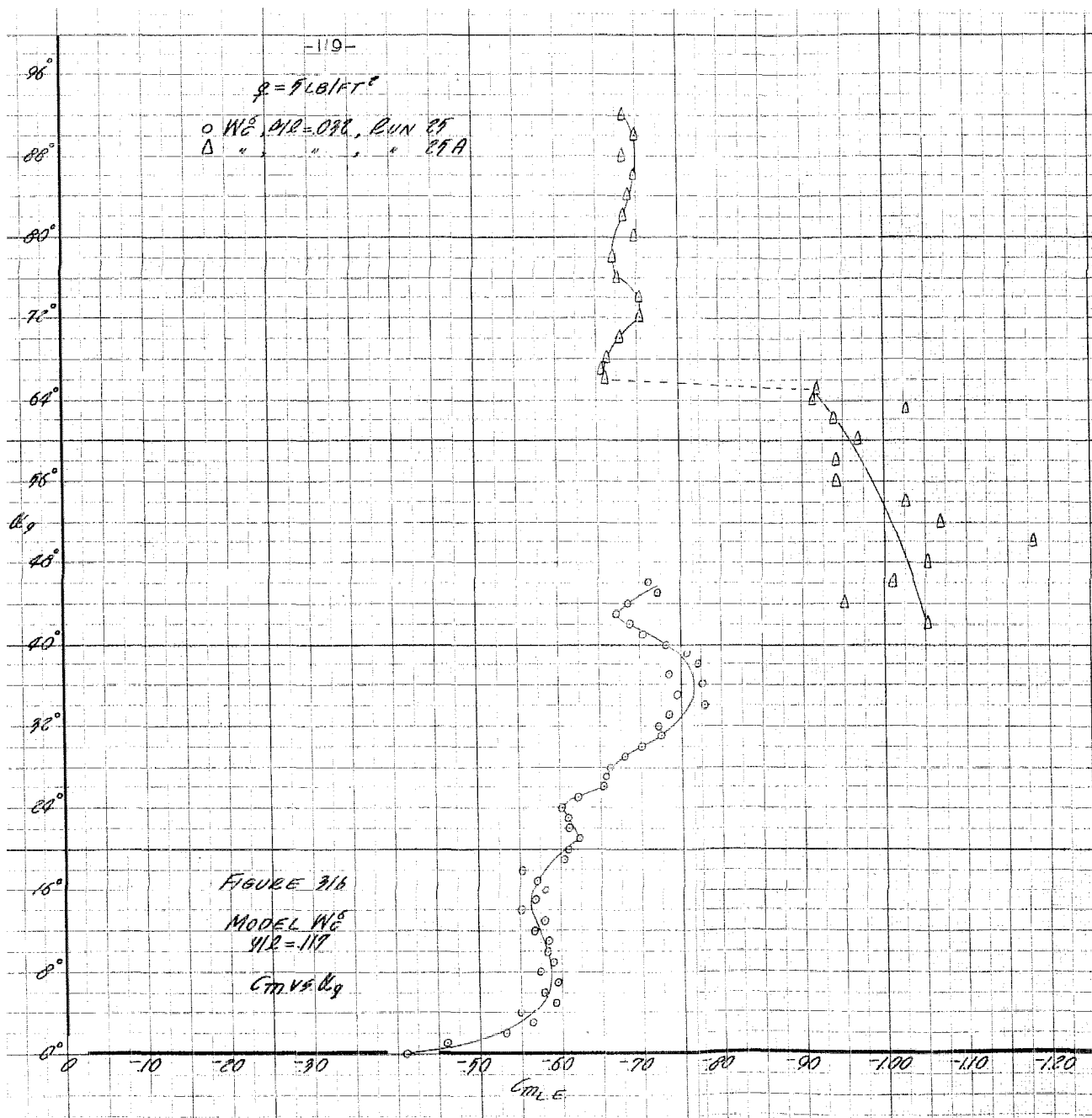
$\rho = 1.4015 \text{ g/cm}^3$
 $\Delta \text{ } M_C^0, A_C^0 = 0.31, 0.29 \text{ cm}^3$
 $\Delta \text{ } M_C^0, A_C^0 = 0.31, 0.29 \text{ cm}^3$



-119-

$$q = 9.18/ft^2$$

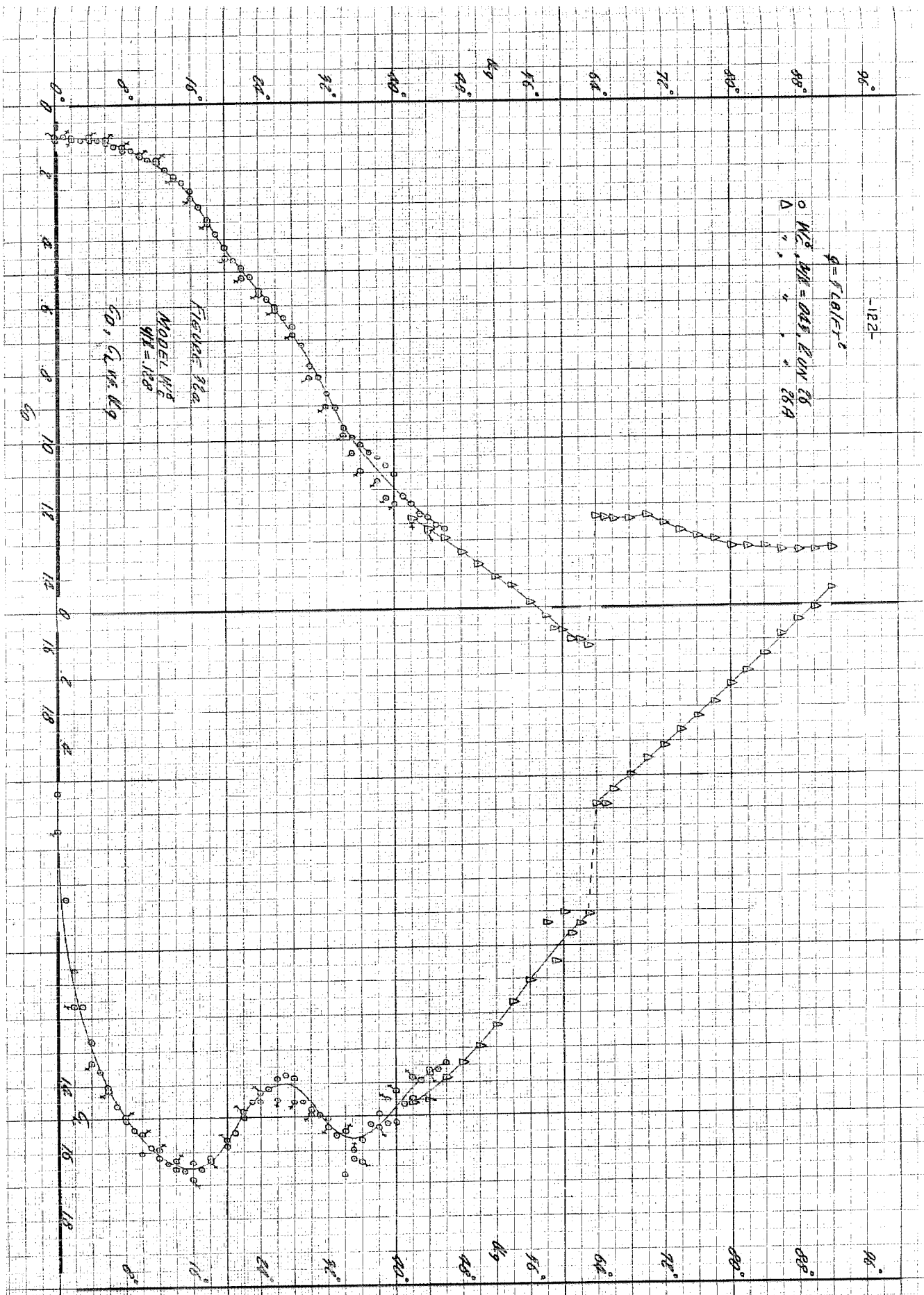
○ W_6^0 , $Y/R = 0.98$, RUN 25
△ " " " " " 27A

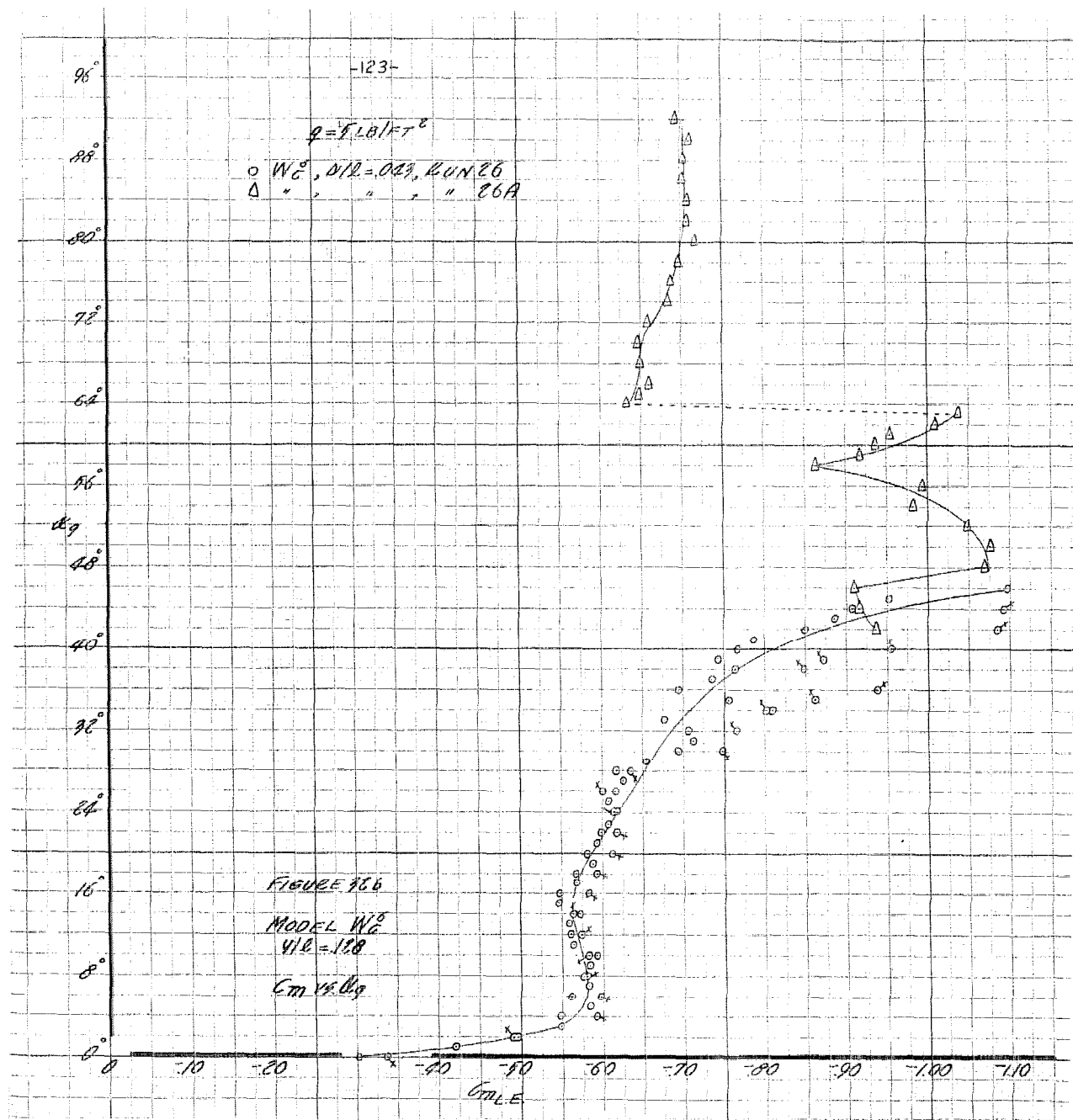


$\rho = 1.2815 \text{ g/cm}^3$
 $\Delta = 0.001, 0.002, 0.003, 0.004, 0.005$

FIGURE 11A
 MODEL, M_c
 $M_c = 117$
 $M_c, 0.15 \text{ kg}$



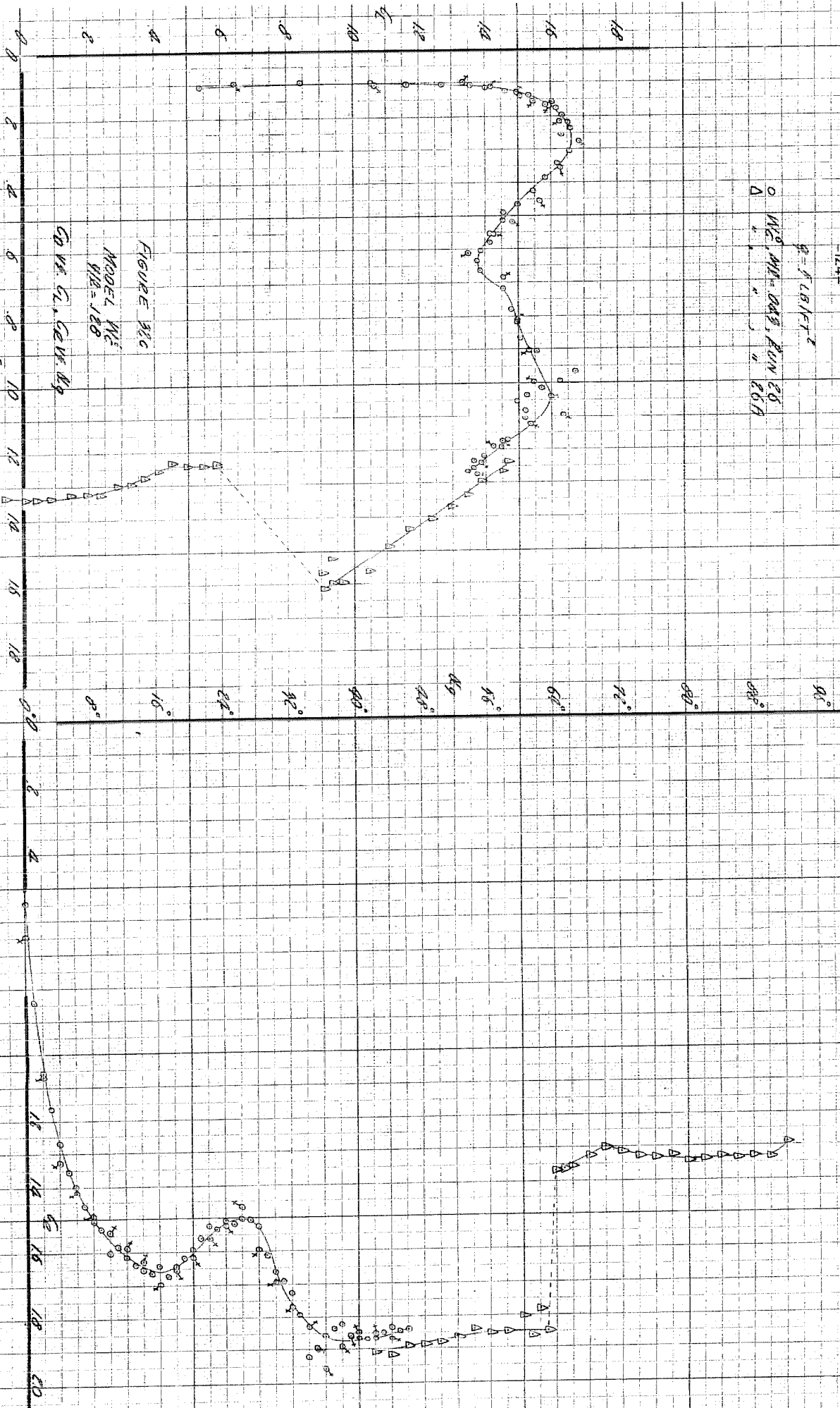


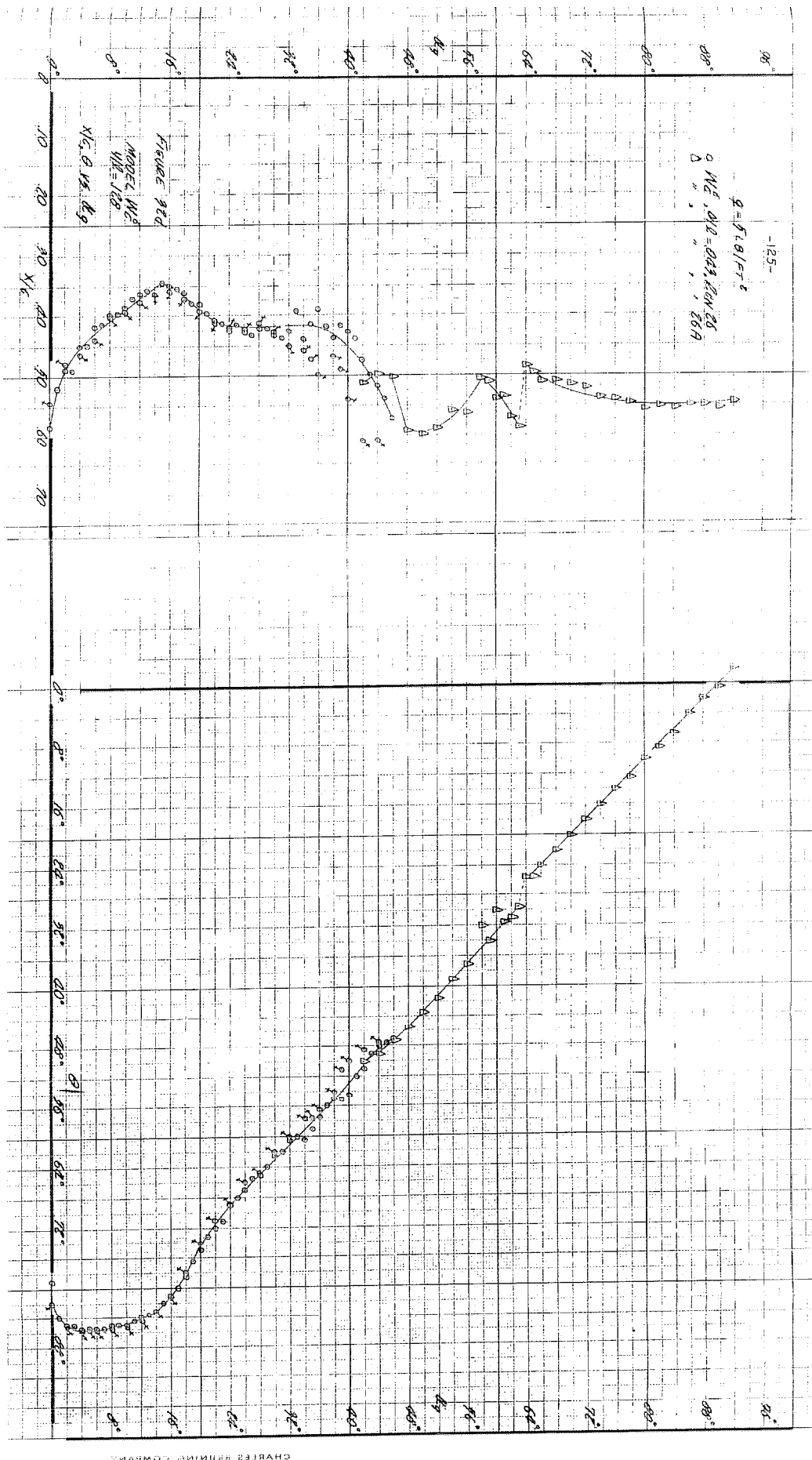


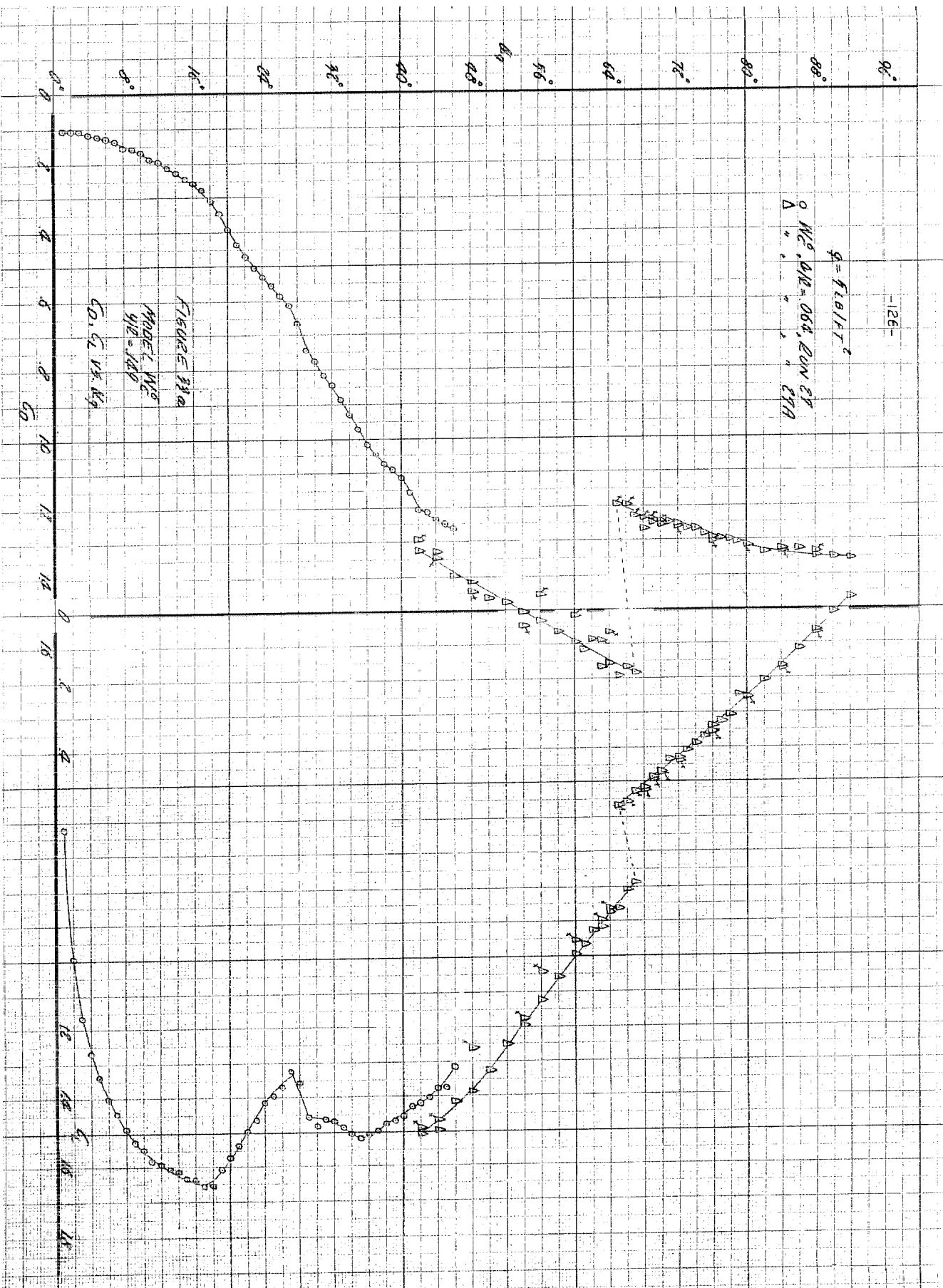
124

$$\phi = 1.681 \times 10^{-2}$$

\circ $M_0^0, M_1^0 = 0.45, \text{ RUN } 65$
 Δ " " " " " 60A







-127-

$\phi = \text{FLIGHT}$

○ W_C , $YR=864$, RUN 27
△ " " " " 27A

96°

88°

80°

72°

64°

56°

48°

40°

32°

24°

16°

8°

0°

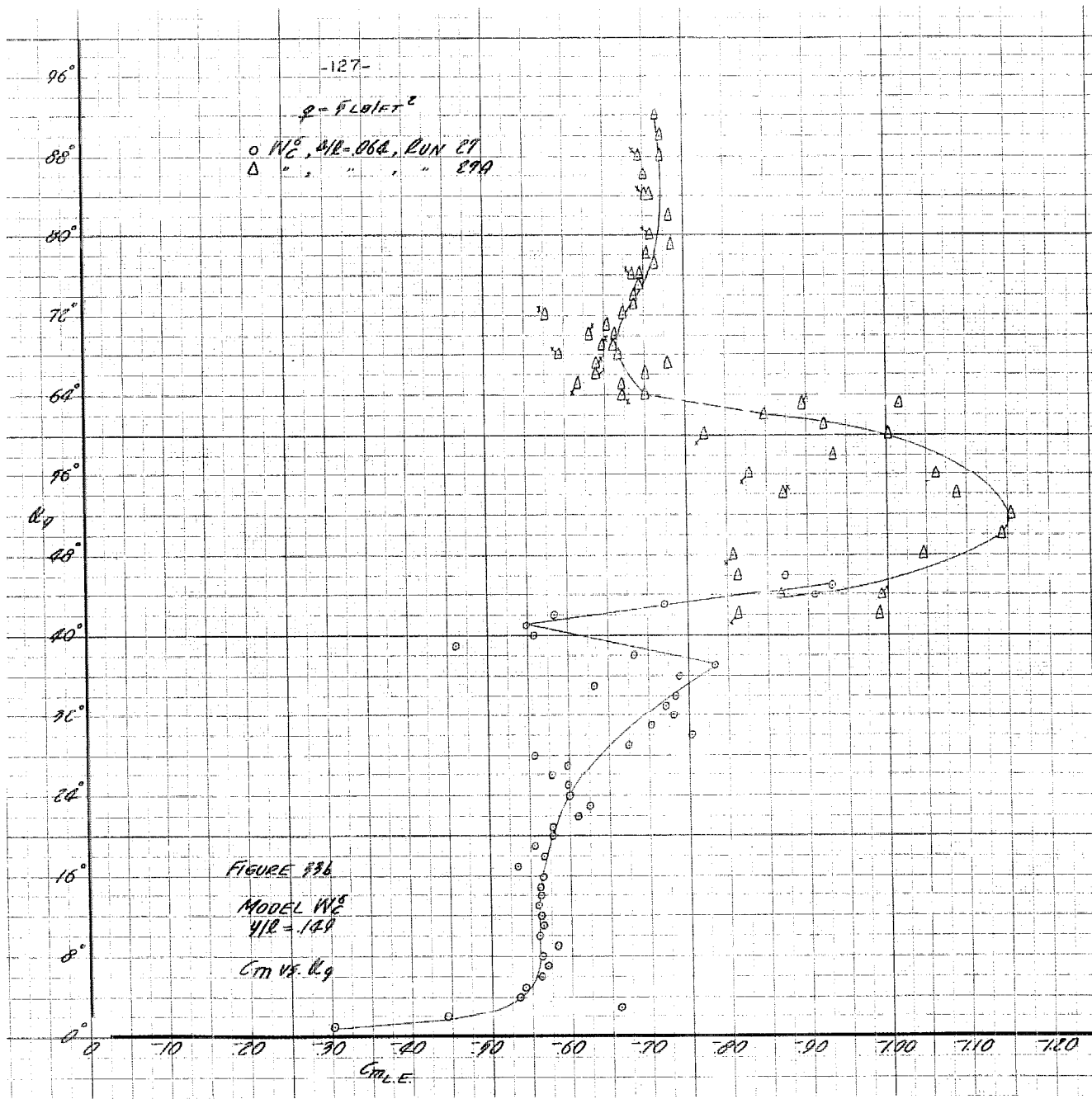
FIGURE 836

MODEL W_C

$YR=148$

C_M vs. C_{LE}

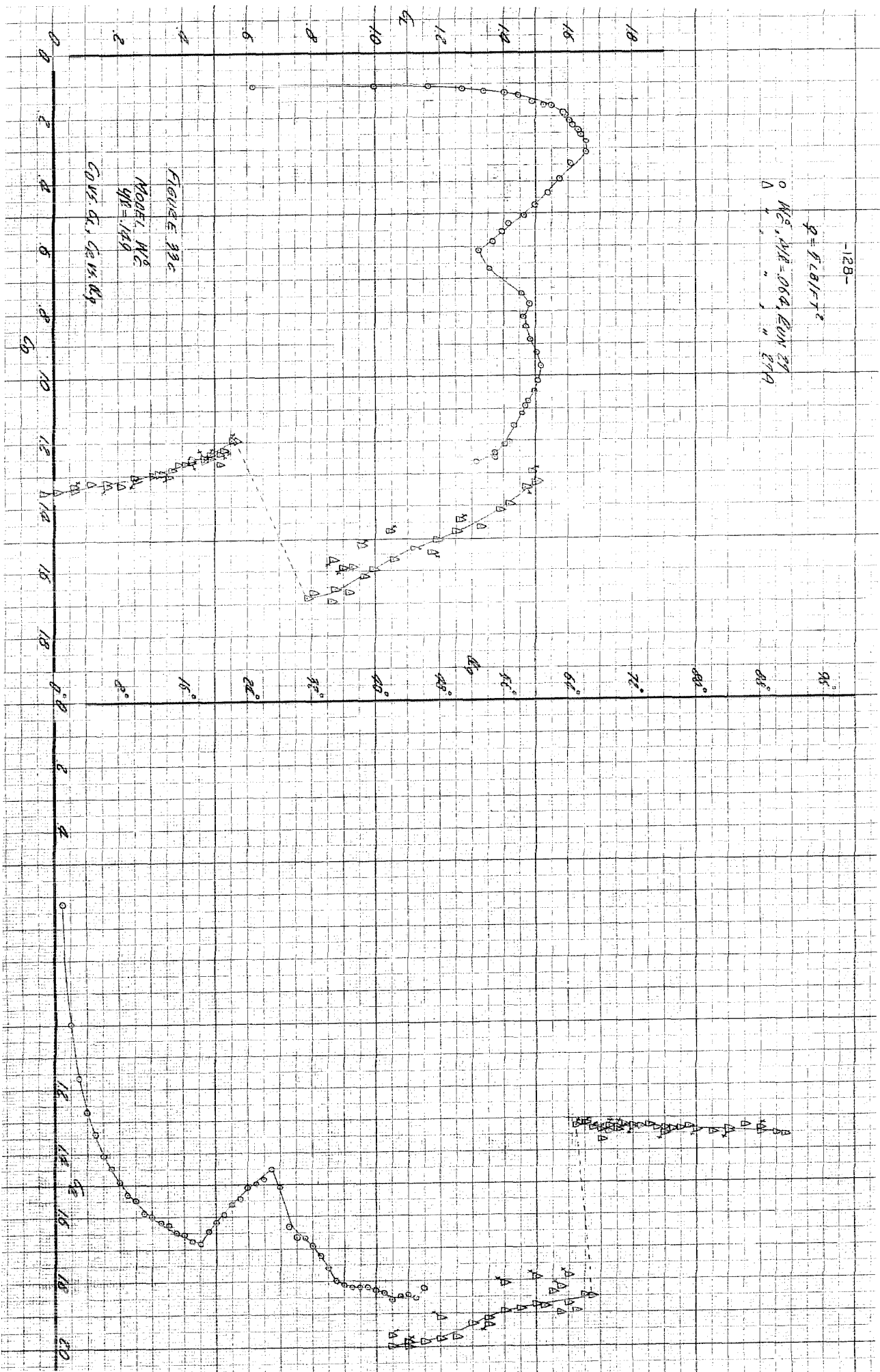
$C_{M,LE}$



-128-

$$\varphi = 0.015 \tau^2$$

Δ $M_0^2, \mu_{12} = 0.04, E_{111} 27$
 Δ $\mu_{12} = 0.04, E_{111} 27$



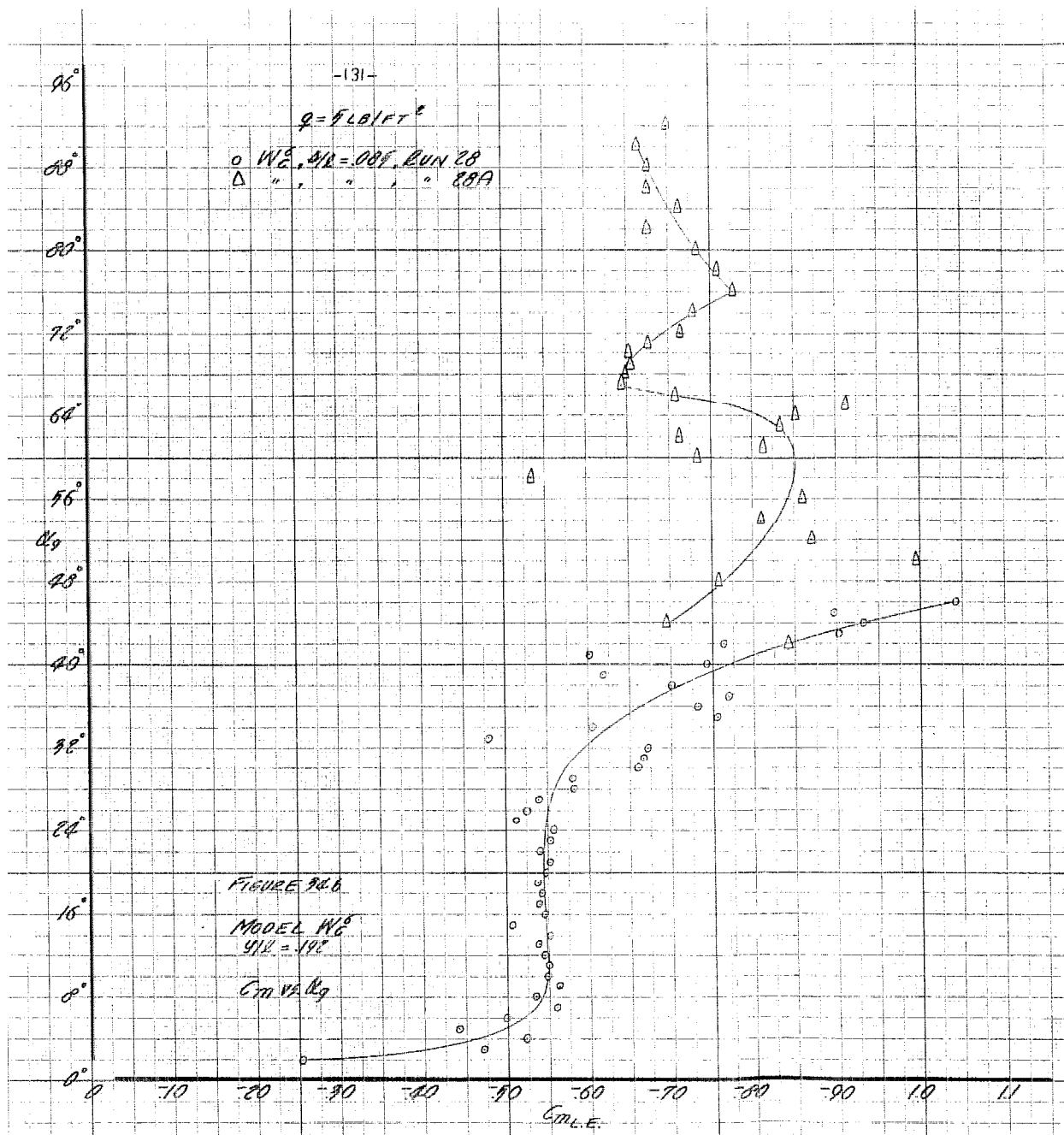
0 WE, $\Delta E = 0.66$, $E_{\text{ON}} = 1.1$
 Δ " " " " " " " "



$$q = \frac{1}{2} \frac{C_B}{A T^2}$$

0 We. DLE = .085, 100N 28
Δ " " " 28A

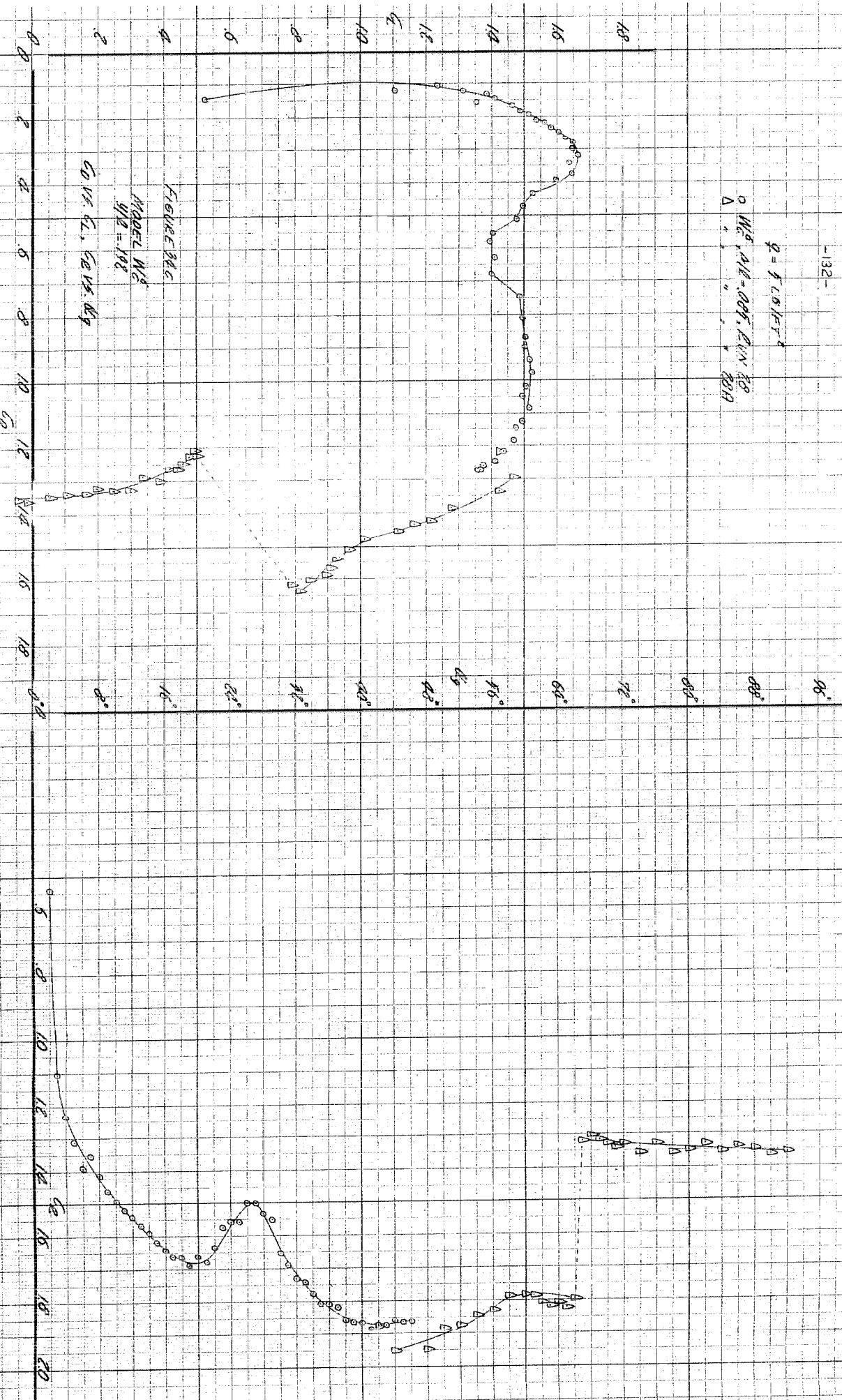


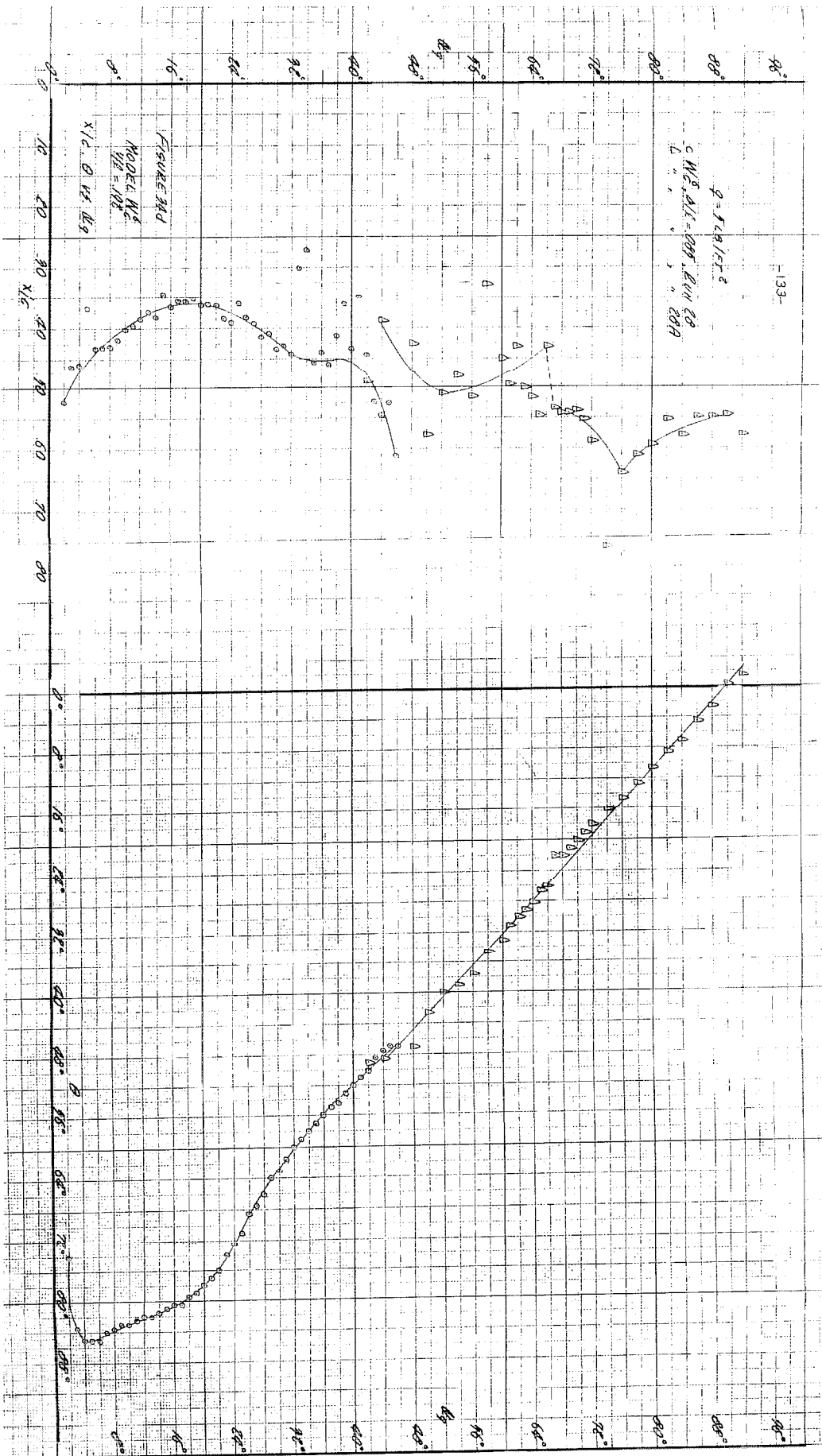


-132-

$$q = 5.0 \text{ lbf/ft}^2$$

$\Delta W_c, \Delta W_e = 0.05 \text{ lbf/in}^2$
 $\Delta W_c, \Delta W_e = 0.05 \text{ lbf/in}^2$





-134-

$\phi = 1.681/r^2$

0 W⁵, 412.009, 200 N. 37.

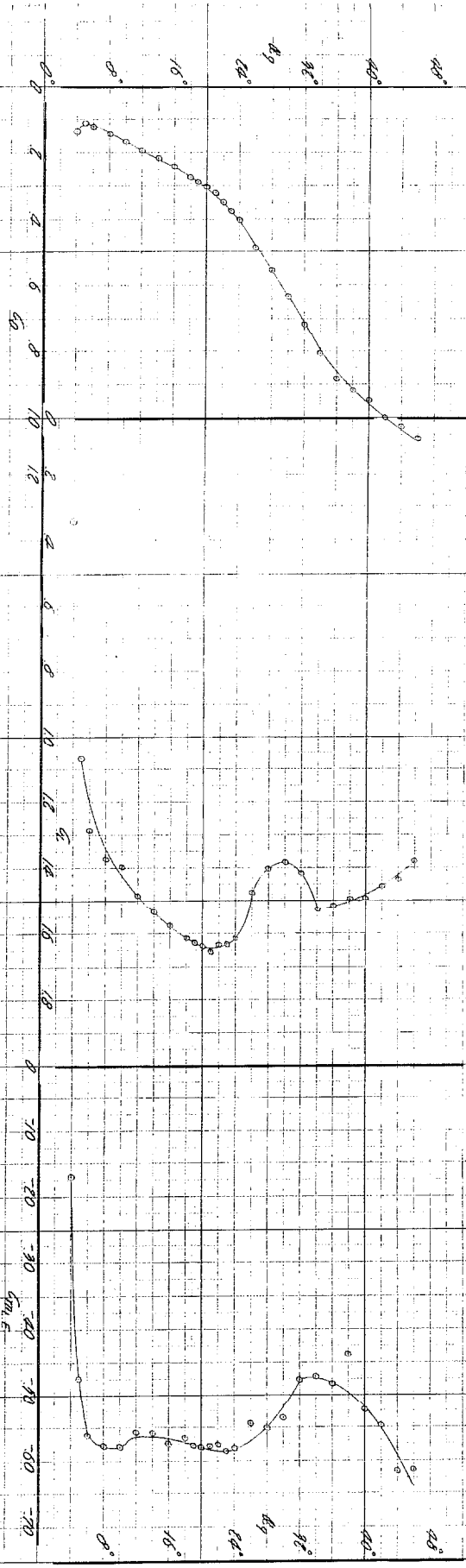


FIGURE 342

Model W⁵

$\eta_2 = 1.92$

C.O. C. 1 cm V. 49

- 35 -

$$q = \sqrt{L \theta / I}^2$$

$$0 \text{ } M_0^0, \Delta I^0 = 0.009, \text{EQUIN } 3.7$$

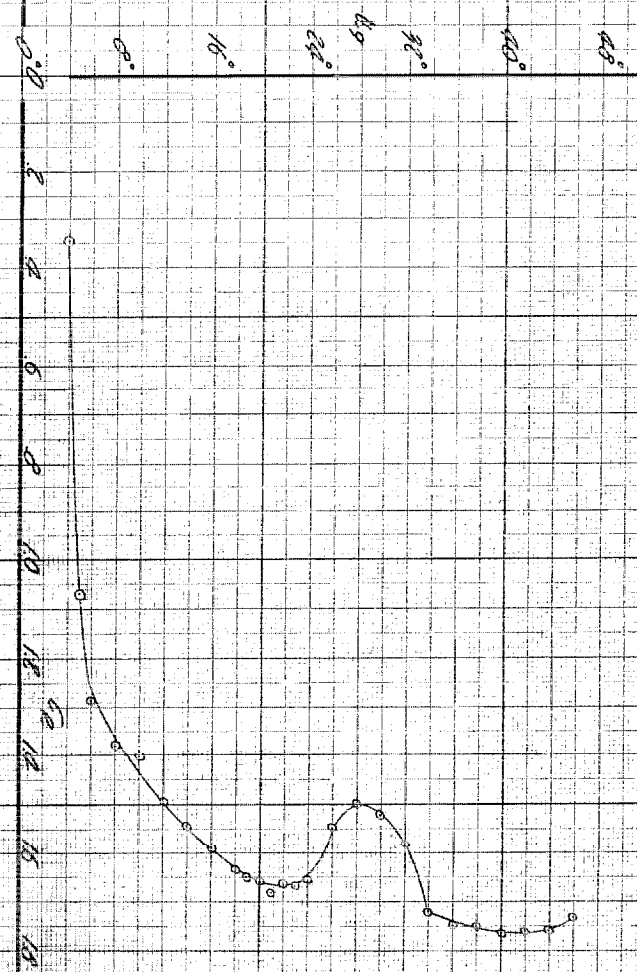
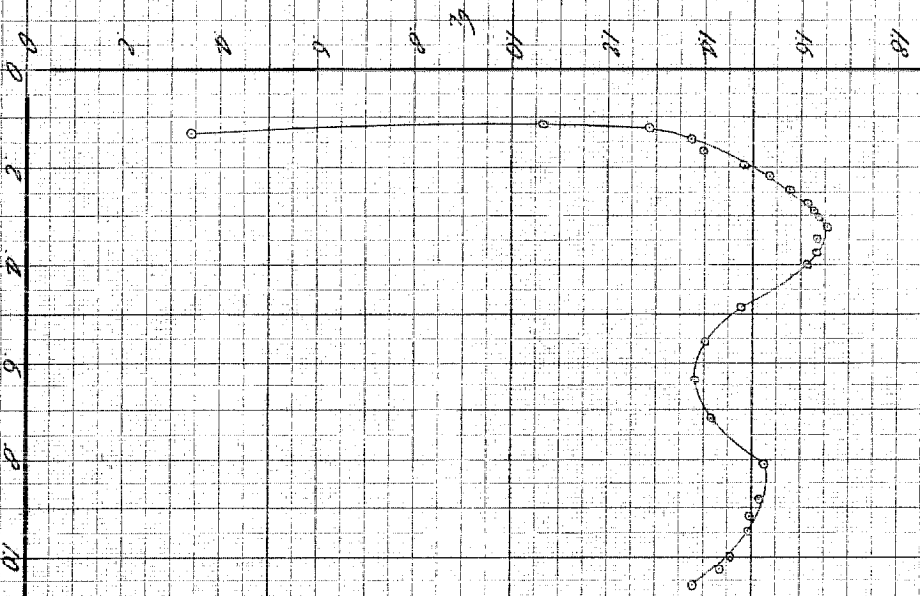


FIGURE 11.8

MODEL: M_0^0

$\Delta I^0 = 0.009$

CONV. G. 6.00000

$$q = \frac{1}{2} \rho V^2 C_d$$

$$M_C^2 \frac{dM_C}{dN/C} = 0.89, \text{ Run 97}$$

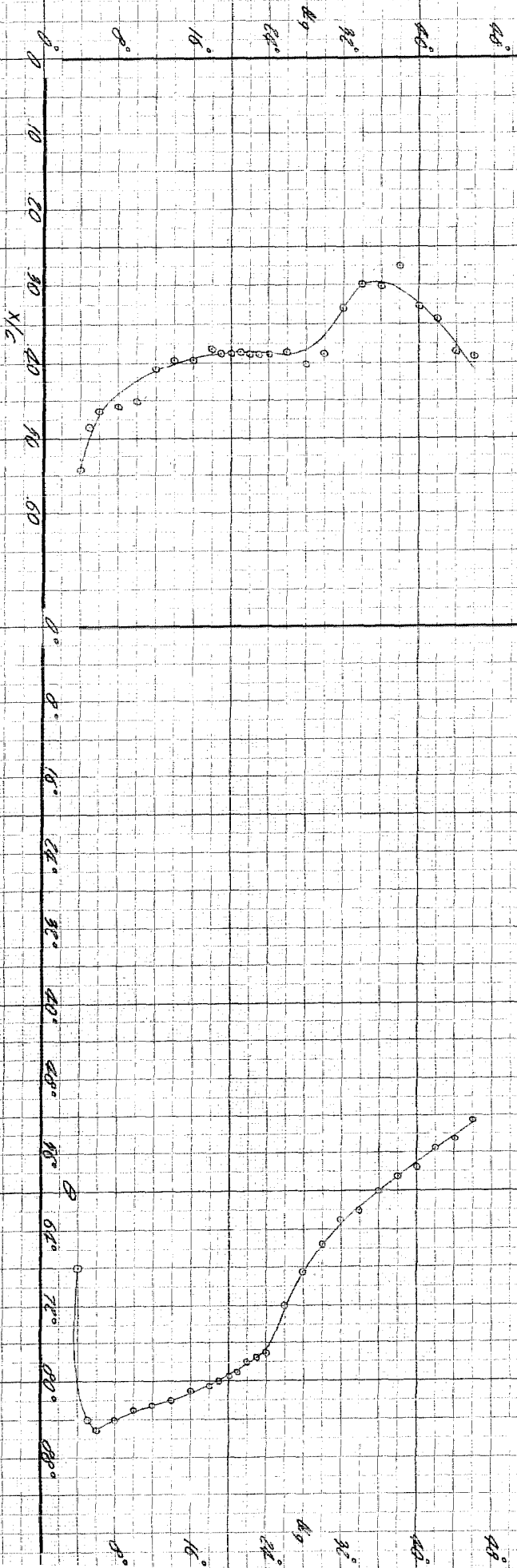
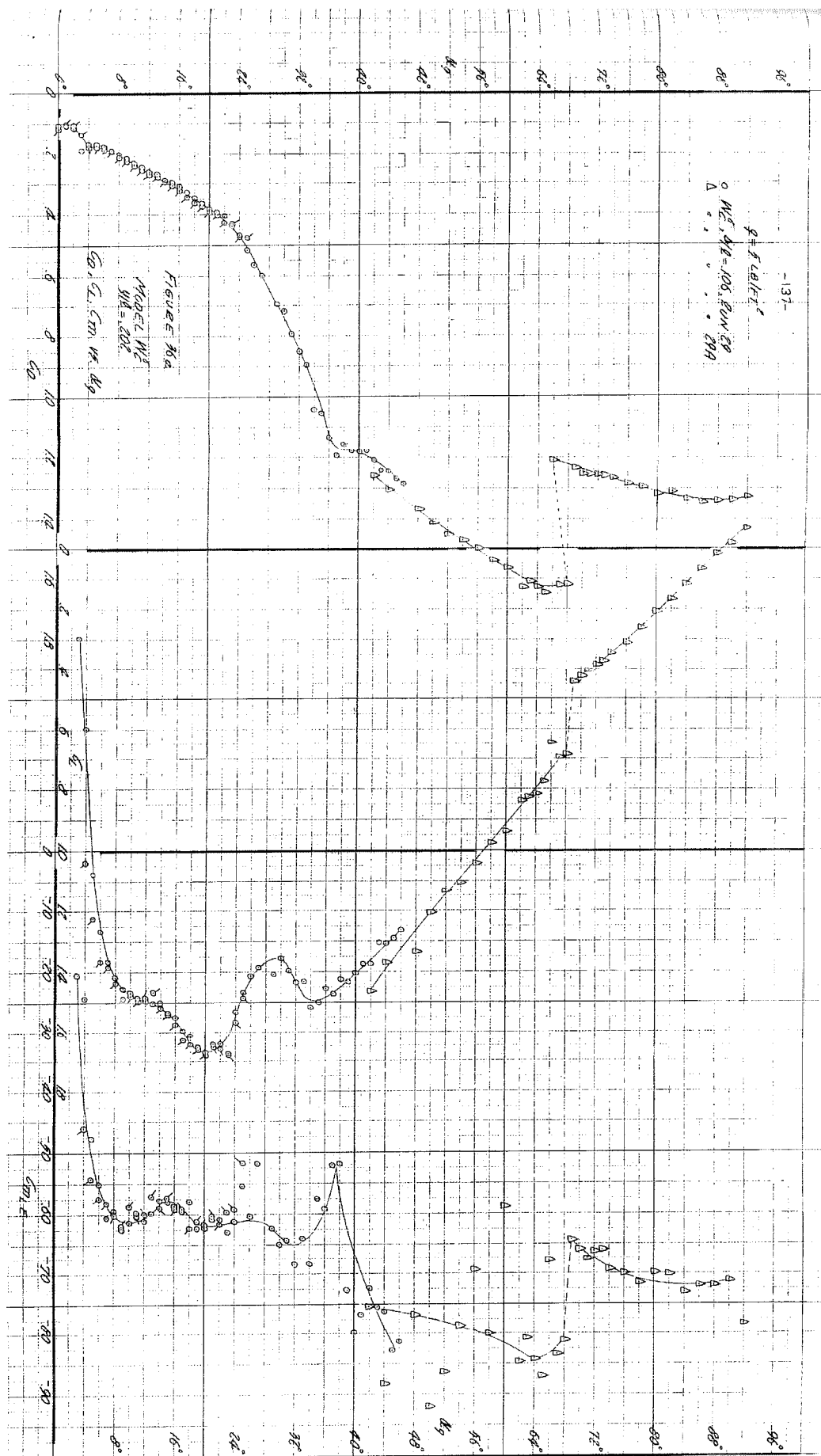


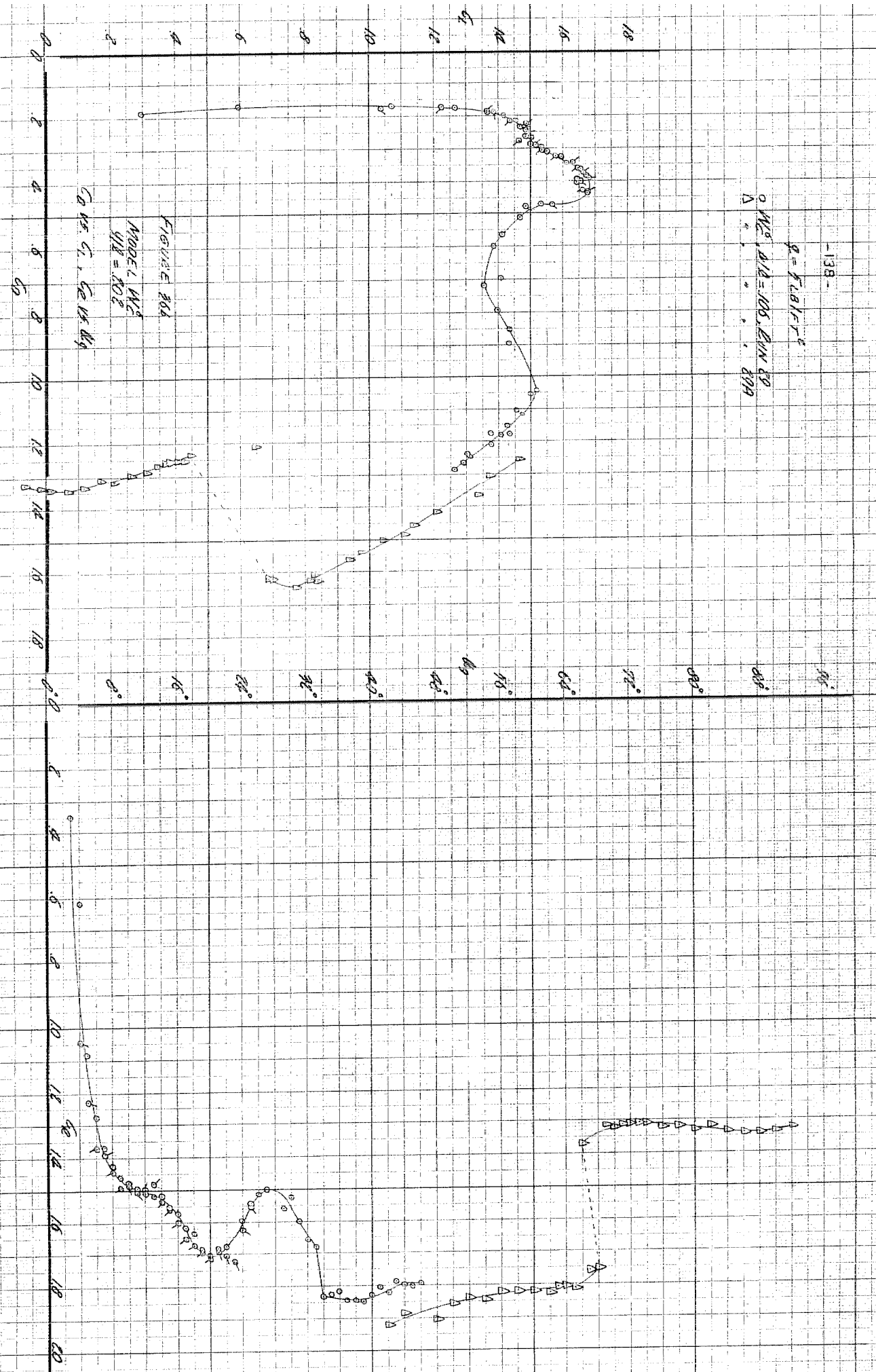
FIGURE 34C
MODEL M_C^2
 $M_C^2 = 1.92$
 $N/C, \theta$ vs. K_0

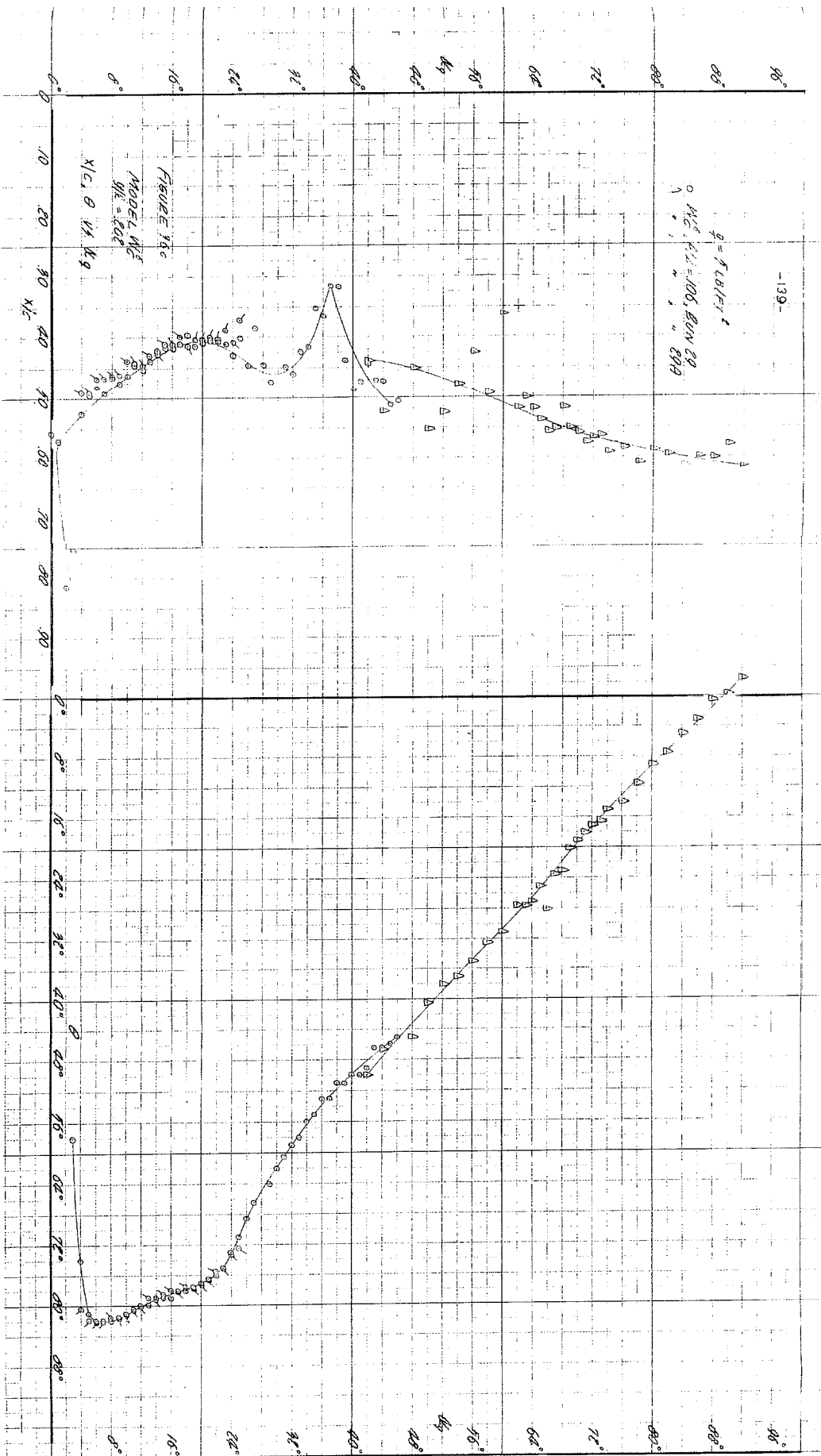


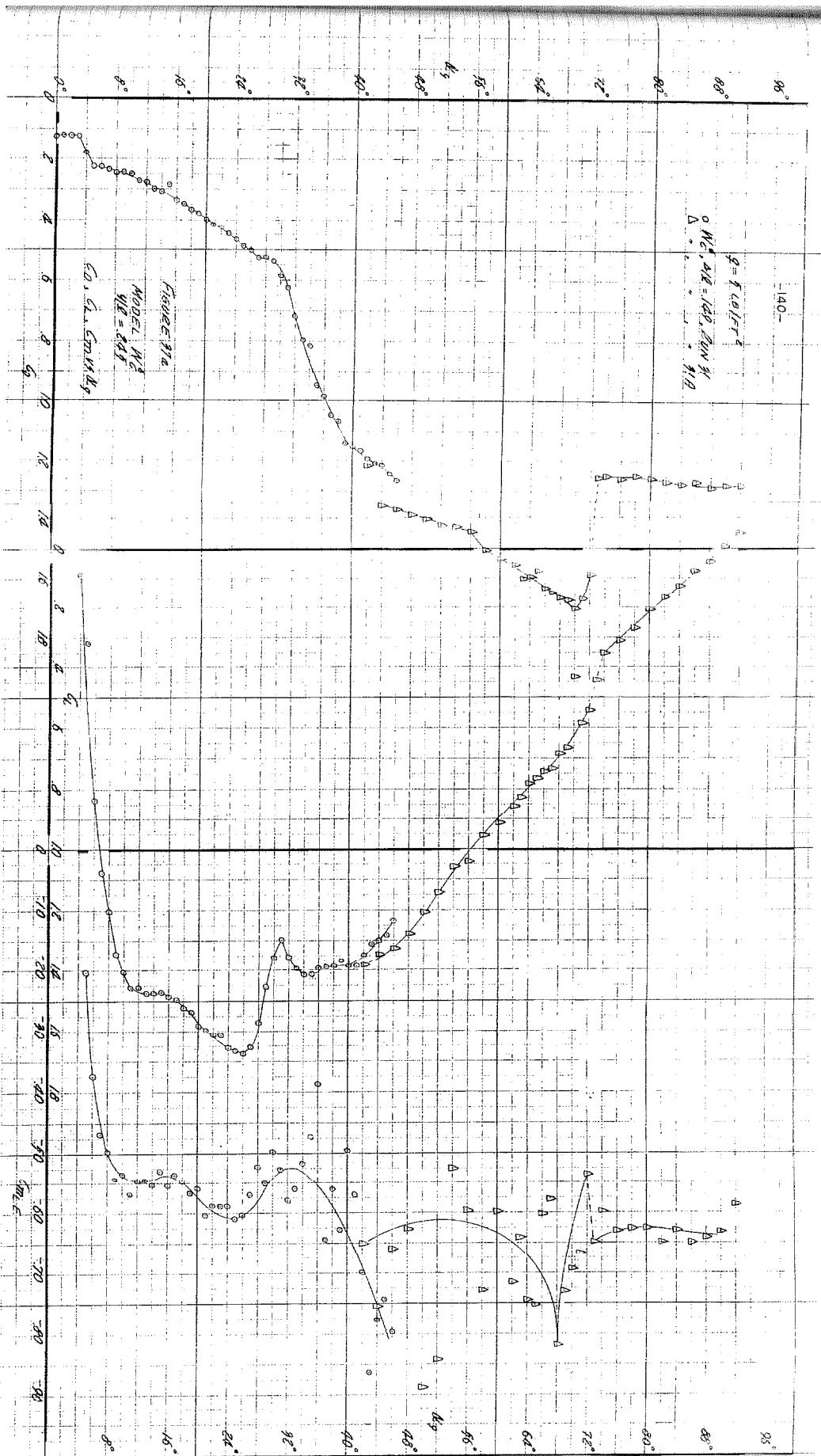
-138-

$$g = F_{LB}/r^2$$

$$M_0, \mu_0 = 105, 899$$

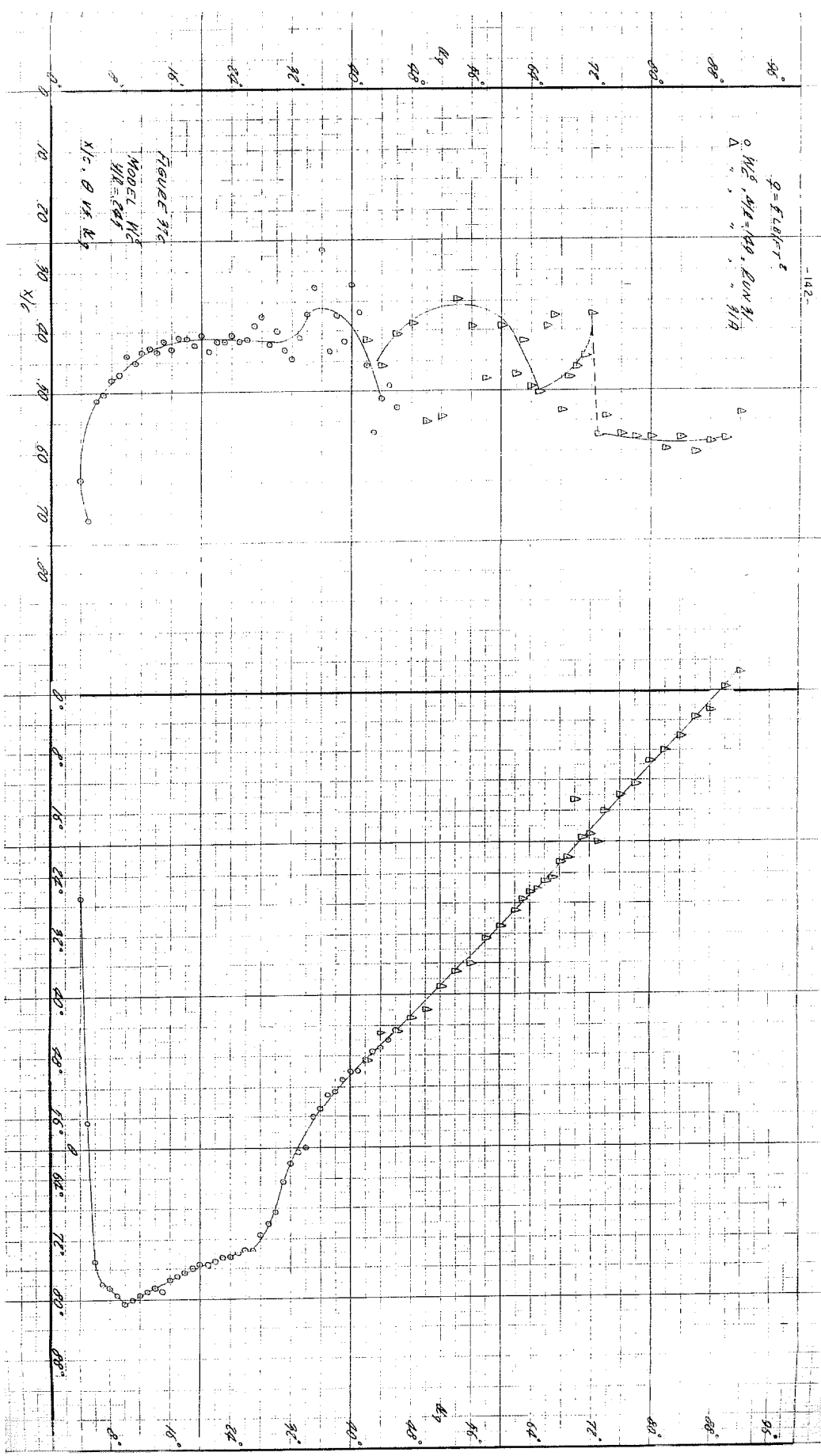






$\phi = 5.6 \times 10^{-7} T^2$
 $\Delta \mu_c, \Delta \mu_e = 140, 100 \text{ mV}$

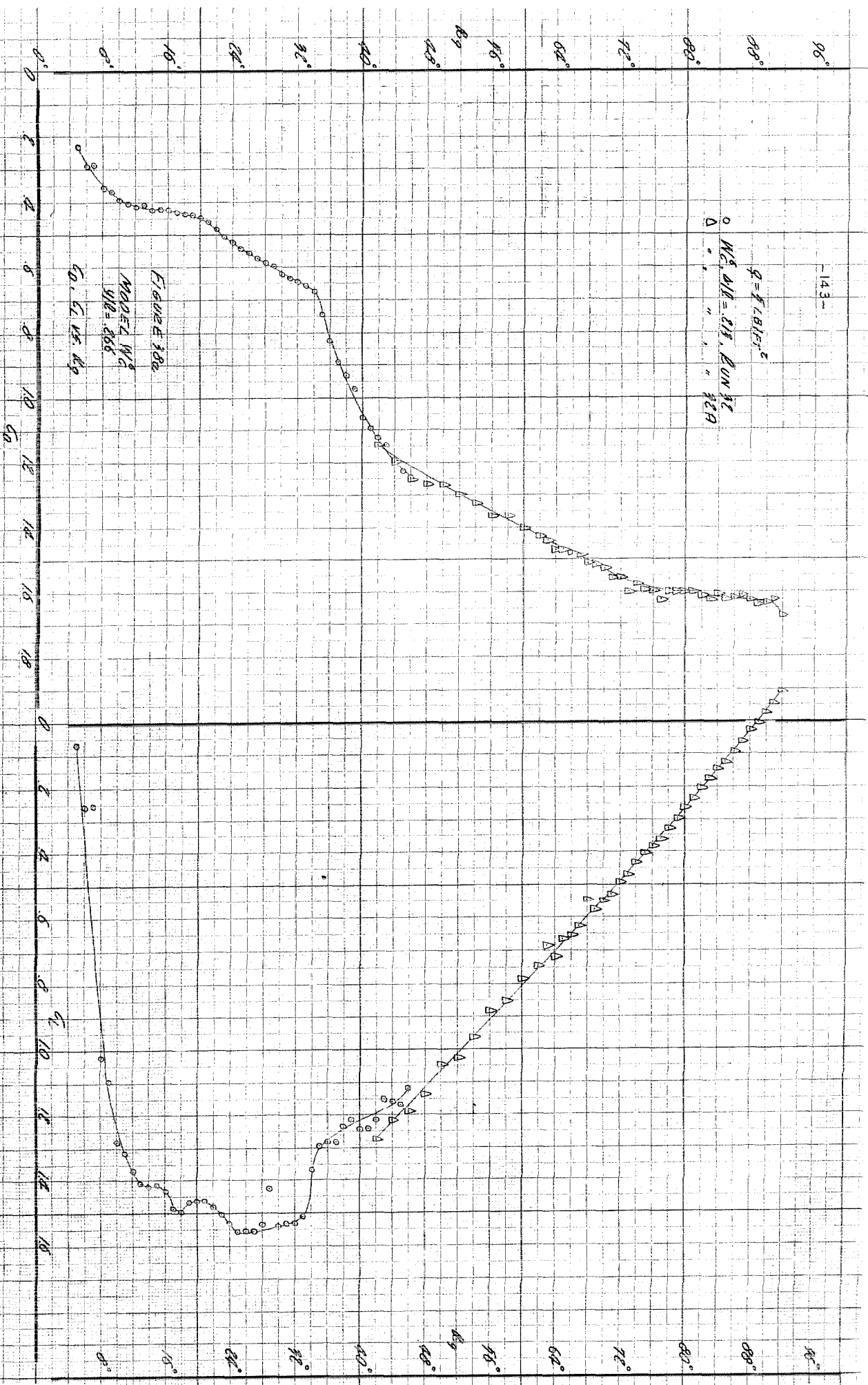
FIGURE 31C
 MODEL μ_c
 $\mu_e = 140 \text{ mV}$
 $\Delta \mu_c, \Delta \mu_e = 140, 100 \text{ mV}$



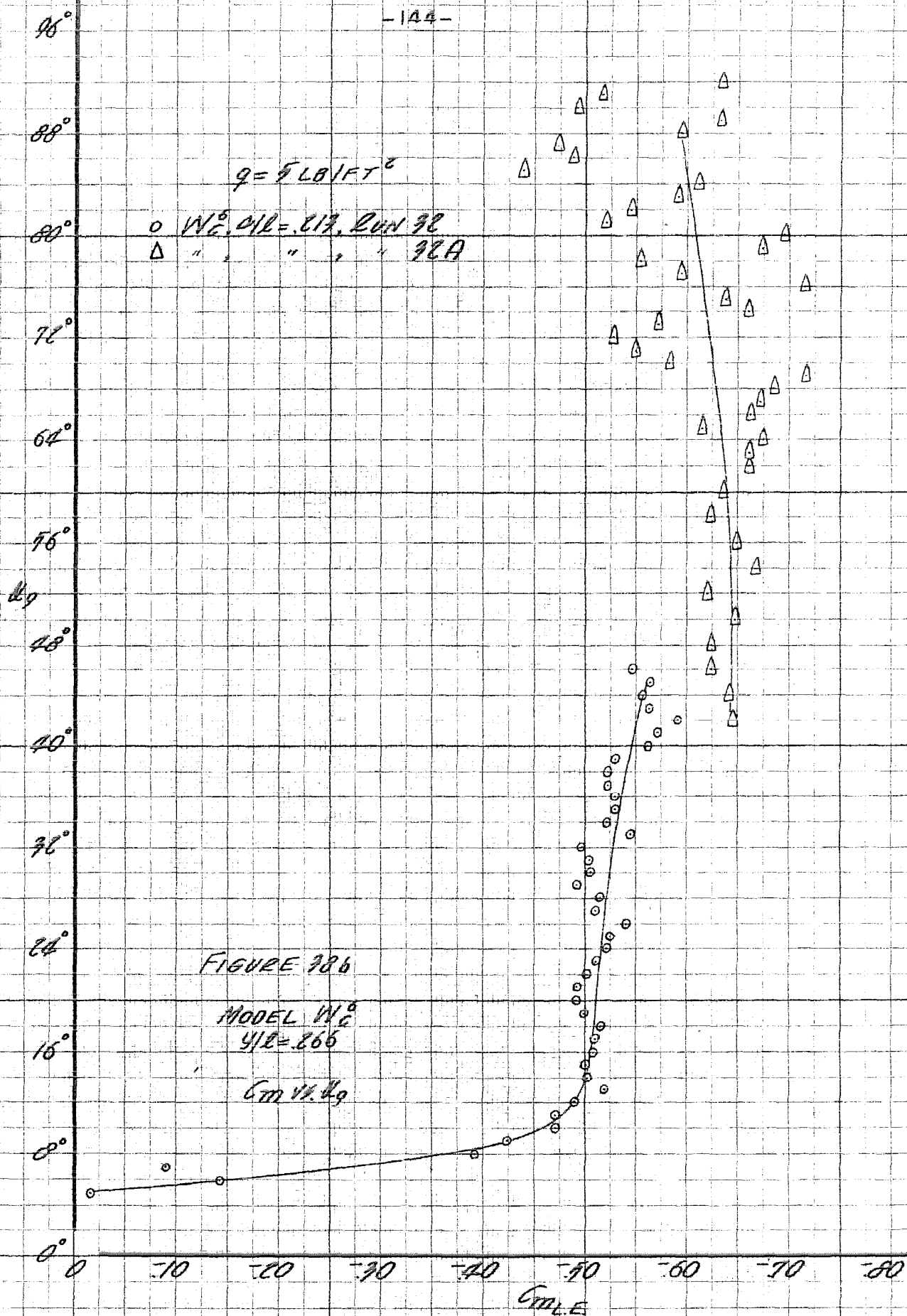
-143-

$$q = F \cdot L / E \cdot I$$

\circ $M_0, \Delta I_0 = 3.18, E \cdot I = 1.2$
 Δ " " " " " " " "



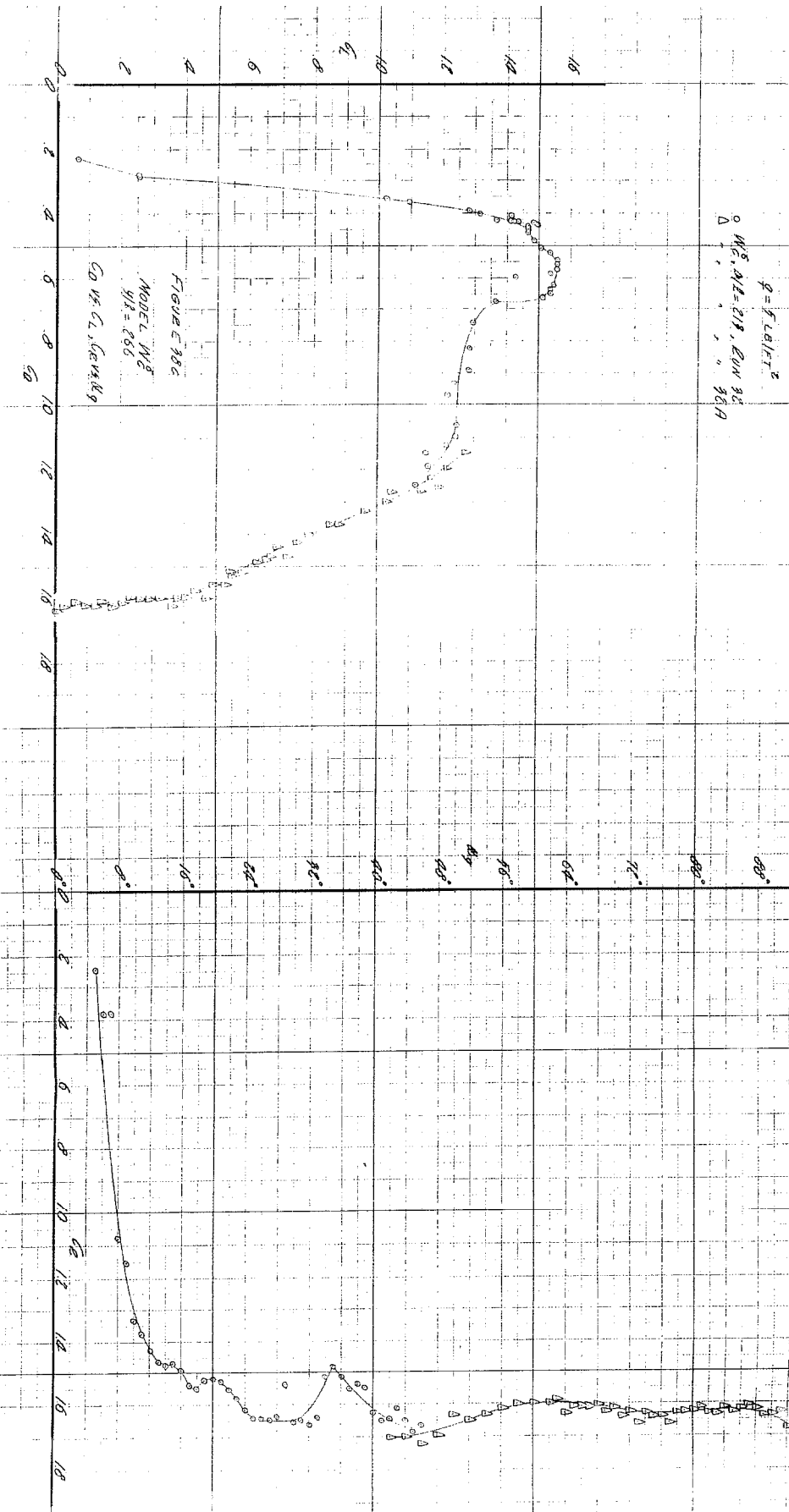
$E \cdot I = 1.2$
 $M_0 = 3.18$
 $\Delta I_0 = 3.18$

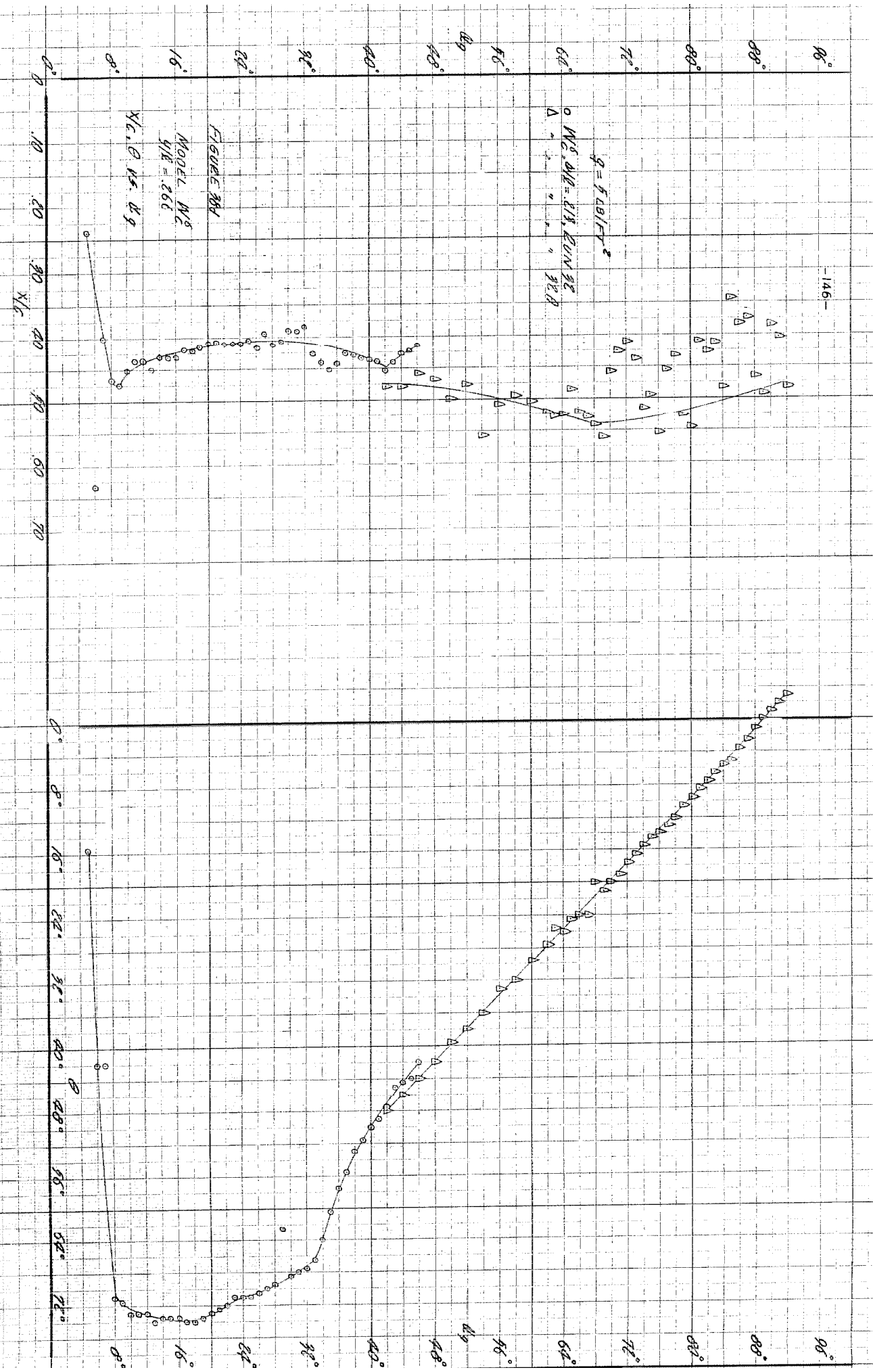


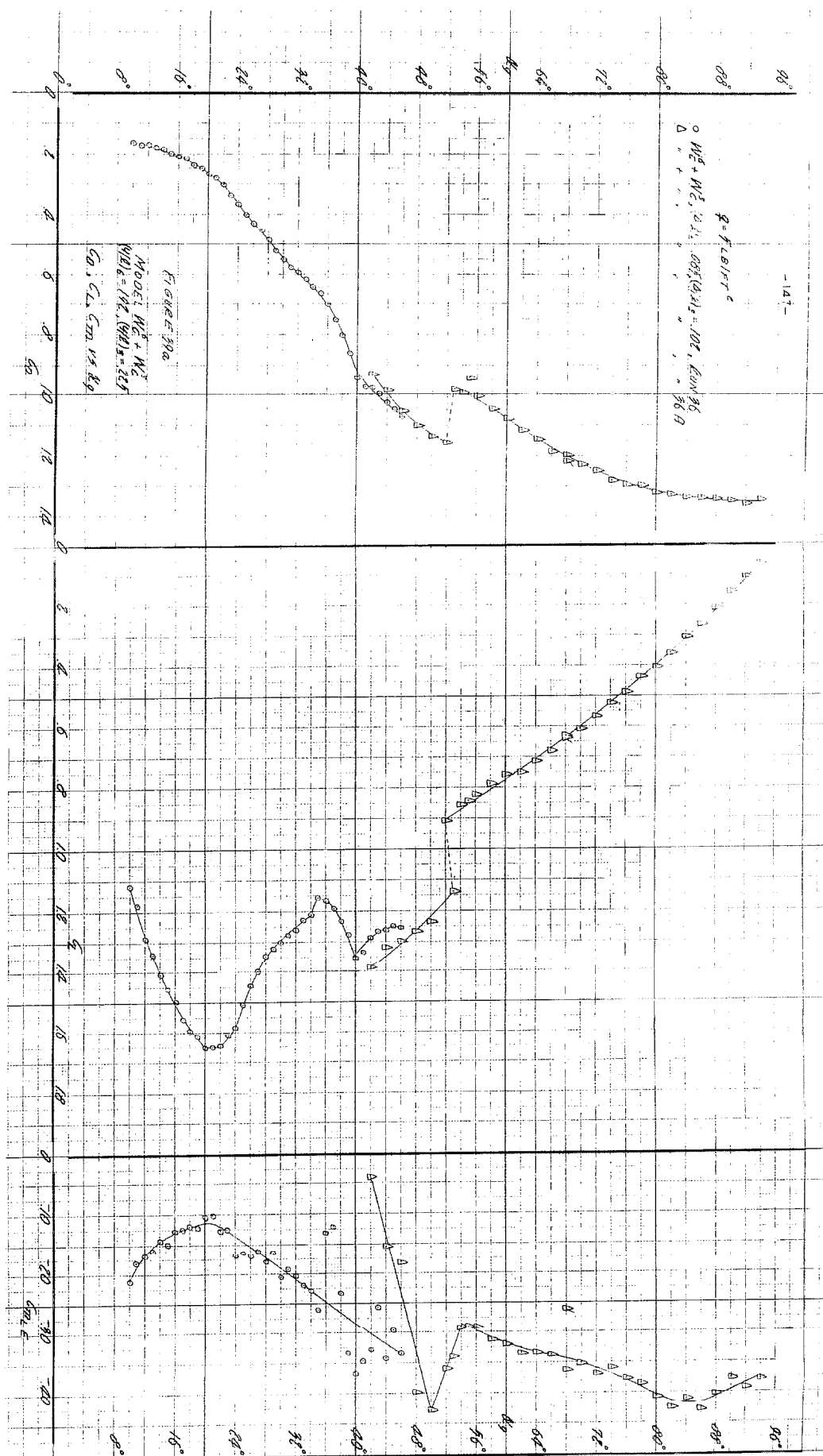
-145-

$$q = f \cdot \Delta T / T^2$$

○ $W_0, A = 0.19, R_{UN} 30^\circ$
△ " " " 30.9







-148-

$$q = 1.08 / \text{cm}^2$$

$$0.112 + 11.2 (0.112) = 0.04 (0.112) = 102, E_{\text{min}} 36A$$

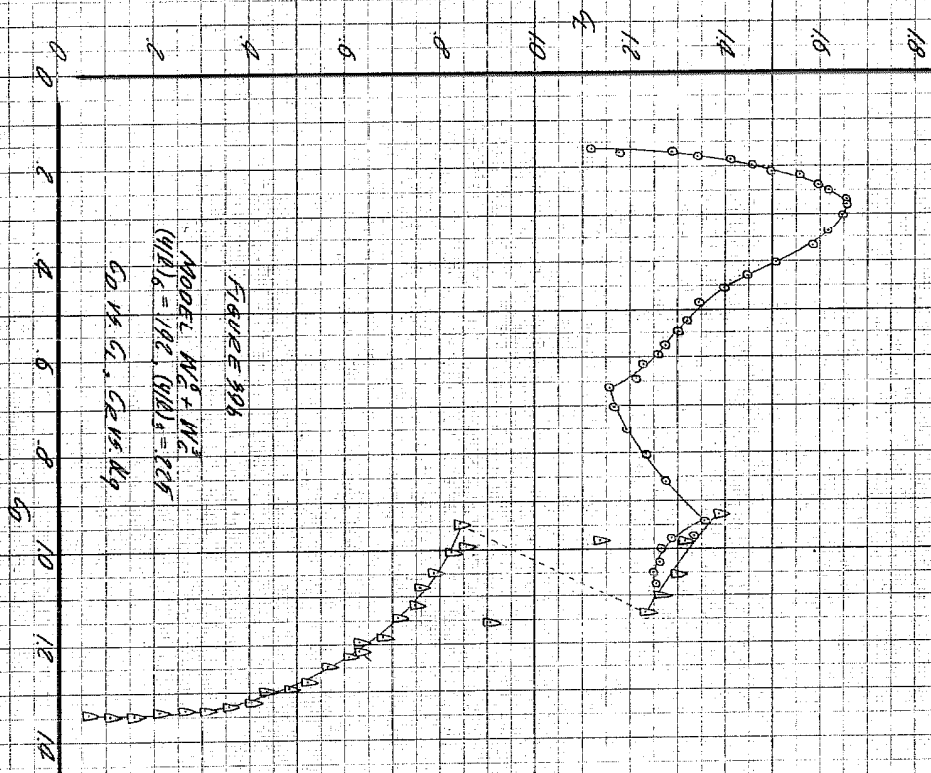
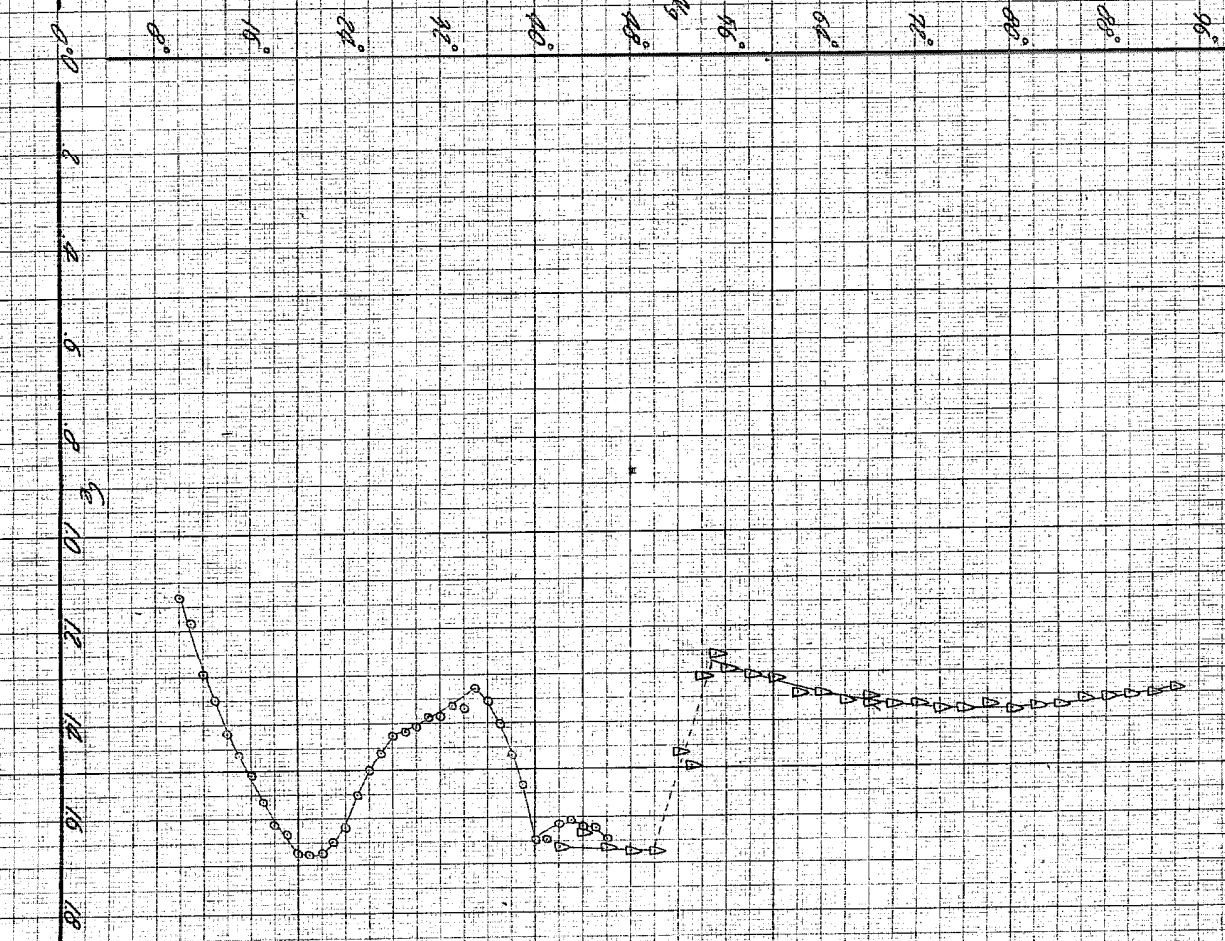
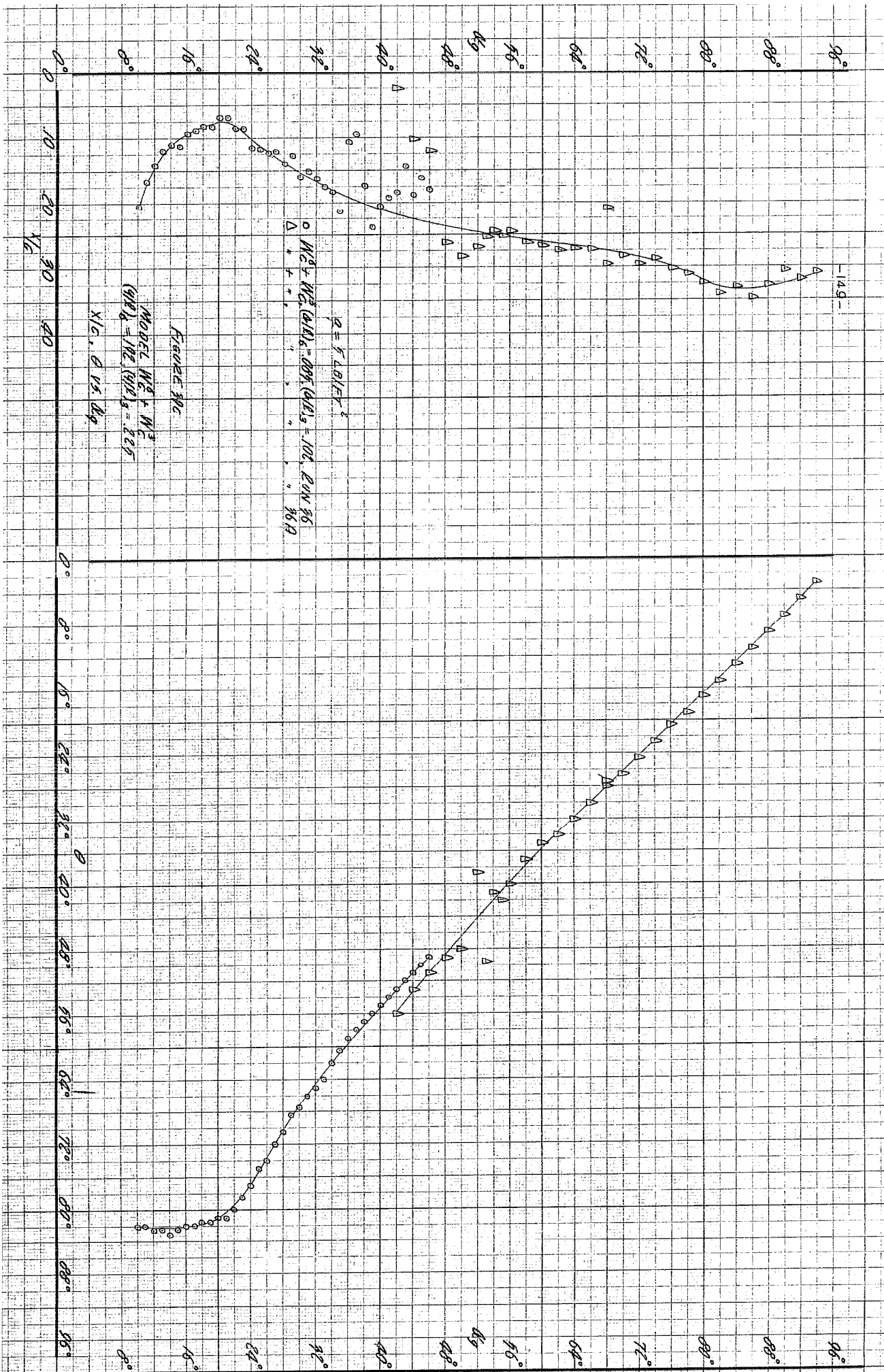


FIGURE 306

$$\text{MODEL: } N_2 + N_2$$

$$(11.2)_c = 192, (11.2)_s = 125$$





-150-

$$\rho = 5.68 \text{ g/cm}^3$$

$$W_C^S + W_C^F (4.0)_6 = 106, (4.0)_5 = 106, \text{ EUN } 32$$

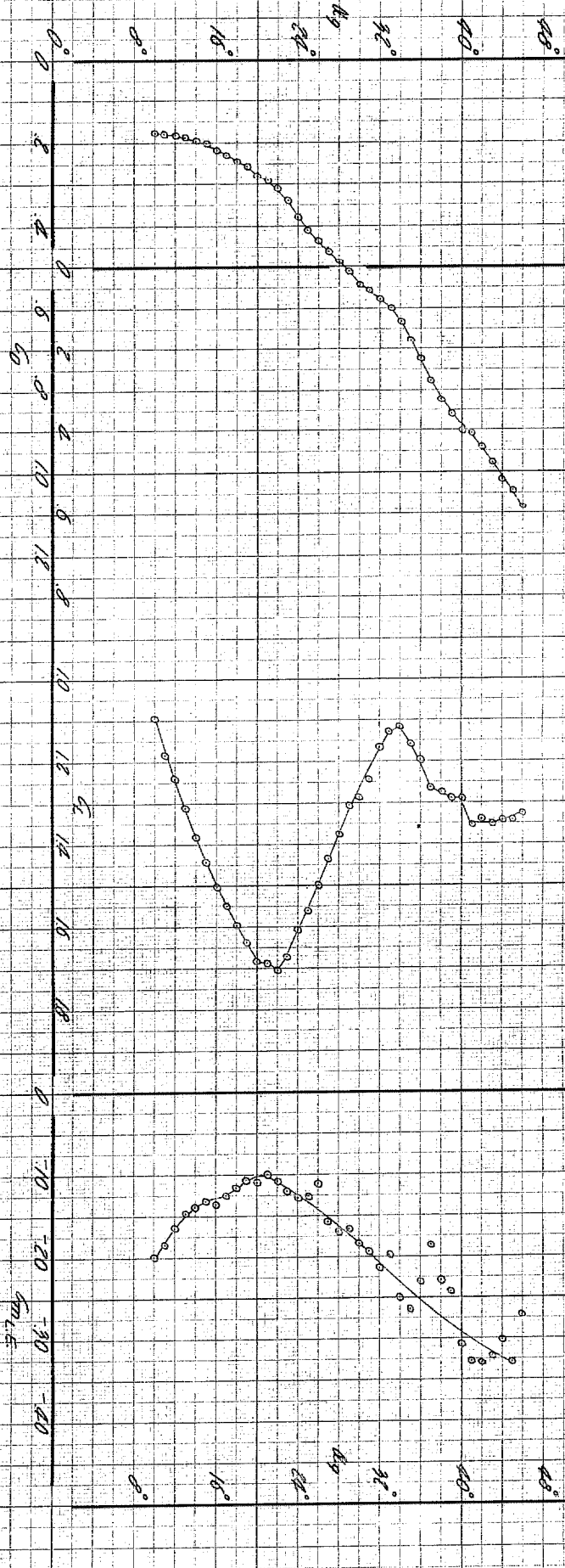


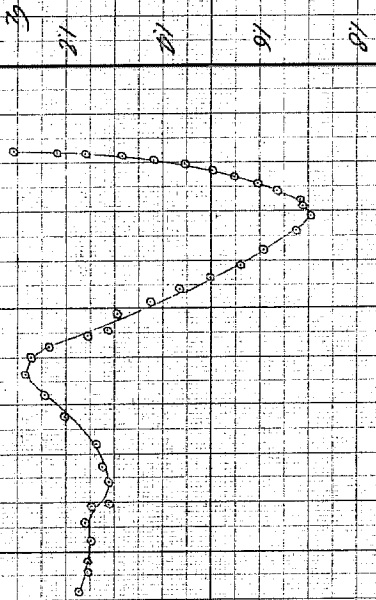
FIGURE 400

$$MODEL: W_C^S + W_C^F$$

$$CO, CL, CM, VC, WG$$

$$q = 5 \text{ LB/FT}^2$$

$$0 \text{ } M_C^0 + M_C^3, (2/E)_L = 100, (2/E)_L = 100, \text{ EUM 3.4}$$



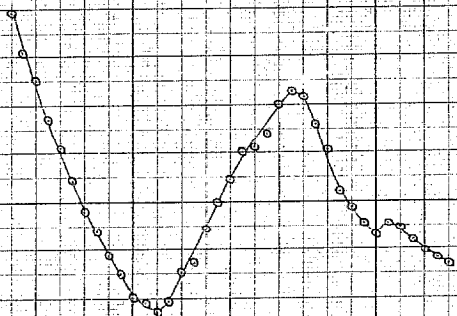
48°
40°
32°
24°
16°
8°

0 2 4 6 8 10 12 14 16 18

$$M_{ODE} \leq M_C^0 + M_C^3$$

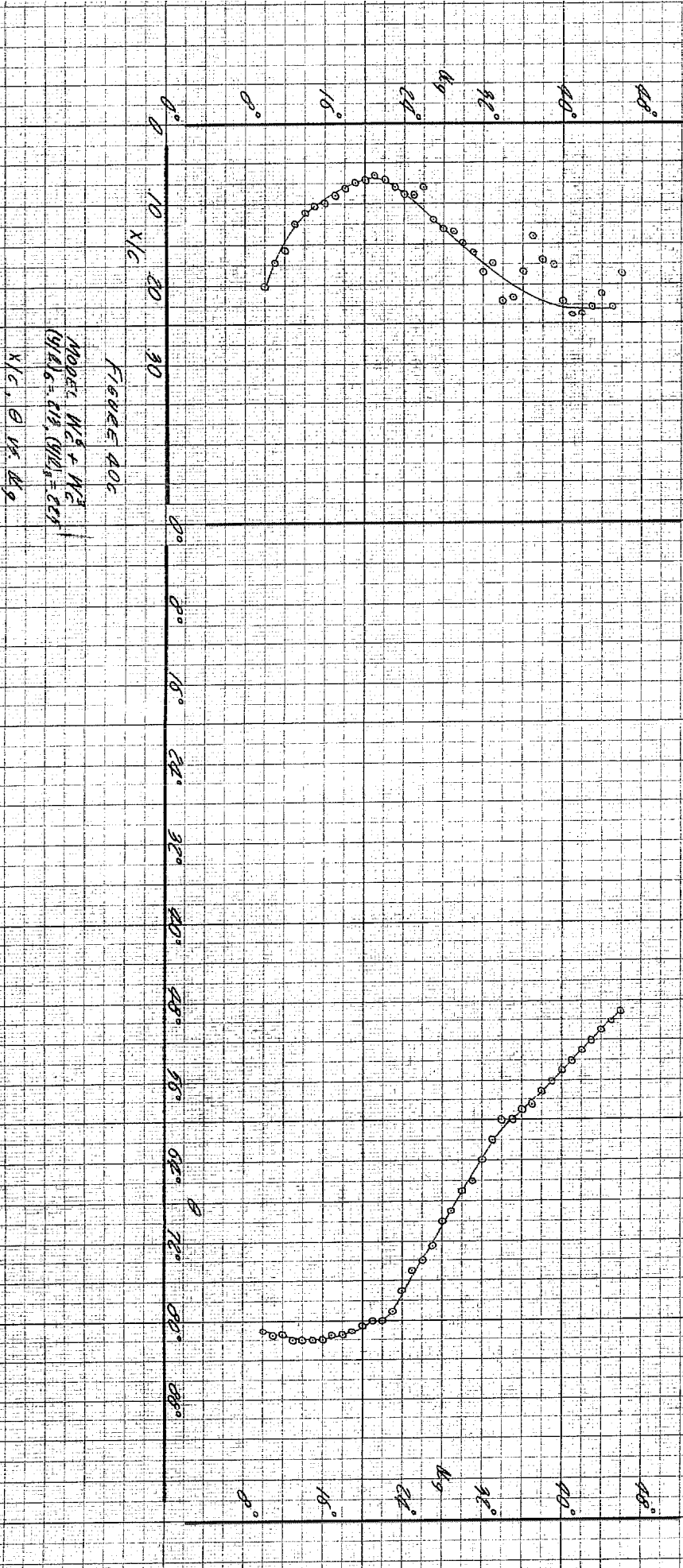
$$(M/E)_L = 0.13, (M/E)_L = 0.13$$

$$C_D, V_L, C_L, C_R, M, A, G$$



$$q = \gamma L B / E T^2$$

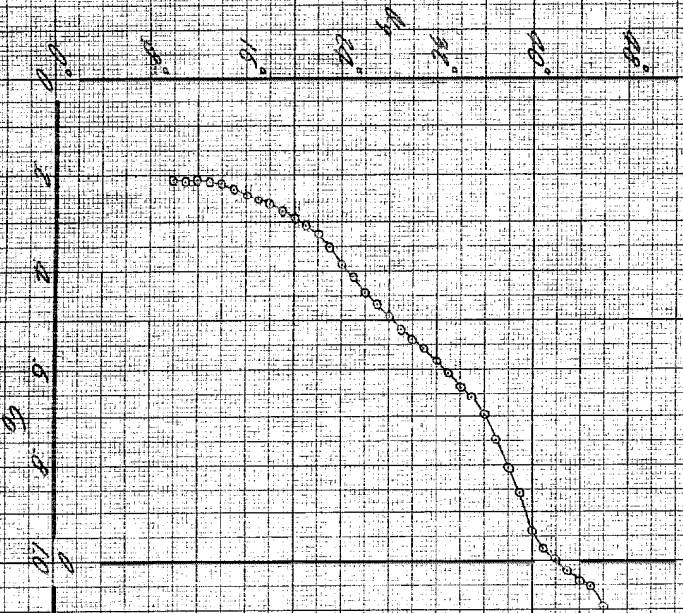
$$W_c^2 + W_c^3 (B/D)_c = 106, (B/D)_s = 106, E \text{ in } \text{lb/in}^2$$



-153-

$$q = 9.48 \text{ l/ft}^2$$

$$M_C^0 + M_C^1 (qH) = 148.14 \text{ ft} = \text{ft}, \text{ ft} \times 35$$

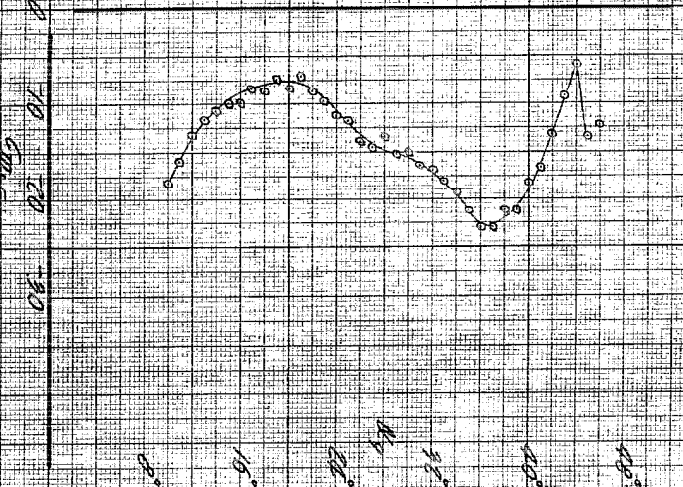
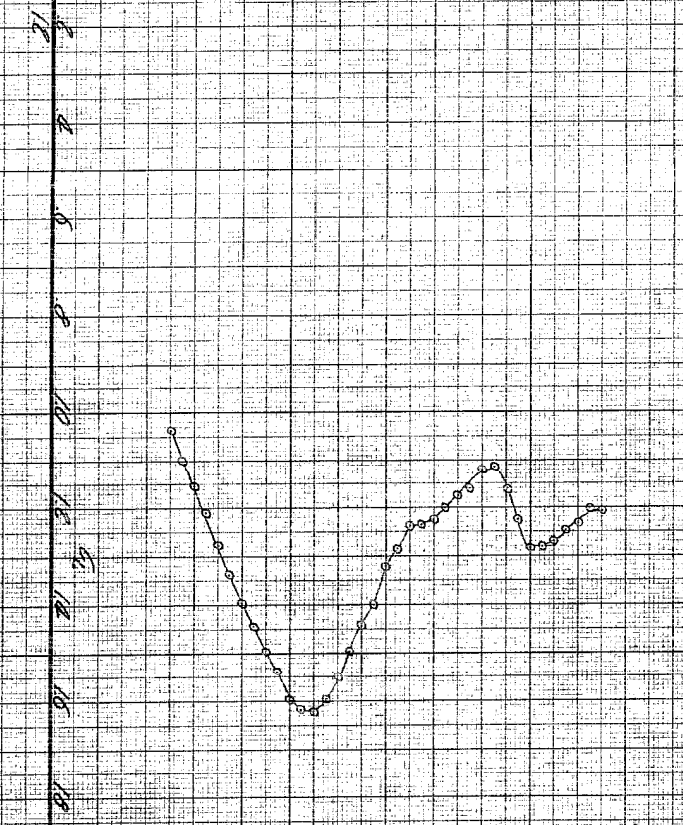


Force Dia

$$M_{max} = M_C^0 + M_C^1$$

$$(qH)_0 = 148.14, (qH)_1 = 148.14$$

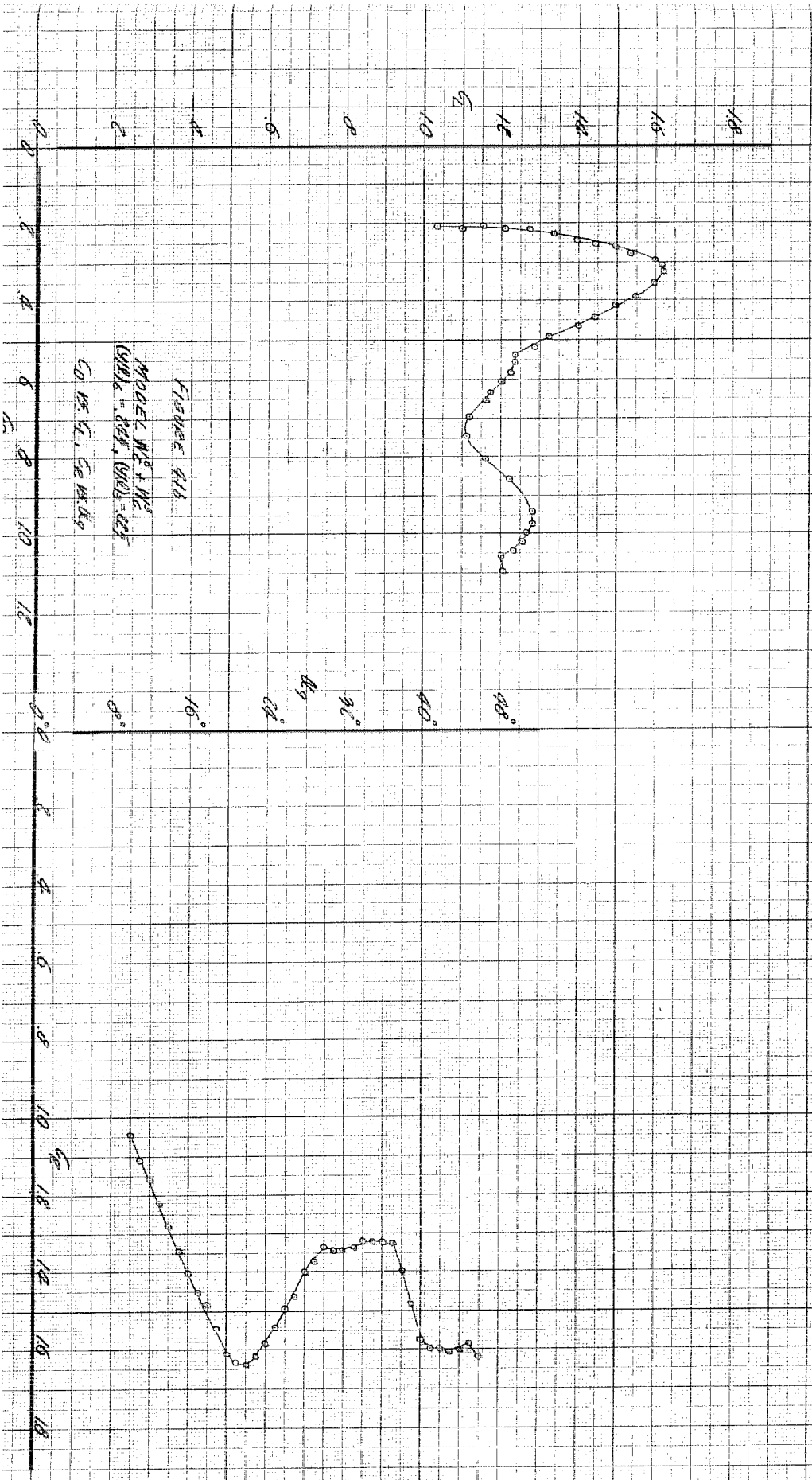
$$C_0 = 1.4, C_1 = 1.4$$



-154-

$$\rho = 1.5 / \text{cm}^3$$

$$M_C^2 + M_C^2 (210)_6 = 142, (210)_8 = 100, 120, 130, 140$$



$$M_C^2 + M_C^2 (210)_6 = 142, (210)_8 = 100, 120, 130, 140$$

$$M_C^2 + M_C^2 (210)_6 = 142, (210)_8 = 100, 120, 130, 140$$

$$M_C^2 + M_C^2 (210)_6 = 142, (210)_8 = 100, 120, 130, 140$$

$$g = 7.20 / s^2$$

$$M_1^2 + M_2^2 (4/11) g = 180, (4/11) g = 102, 4/11 \cdot 7.20$$

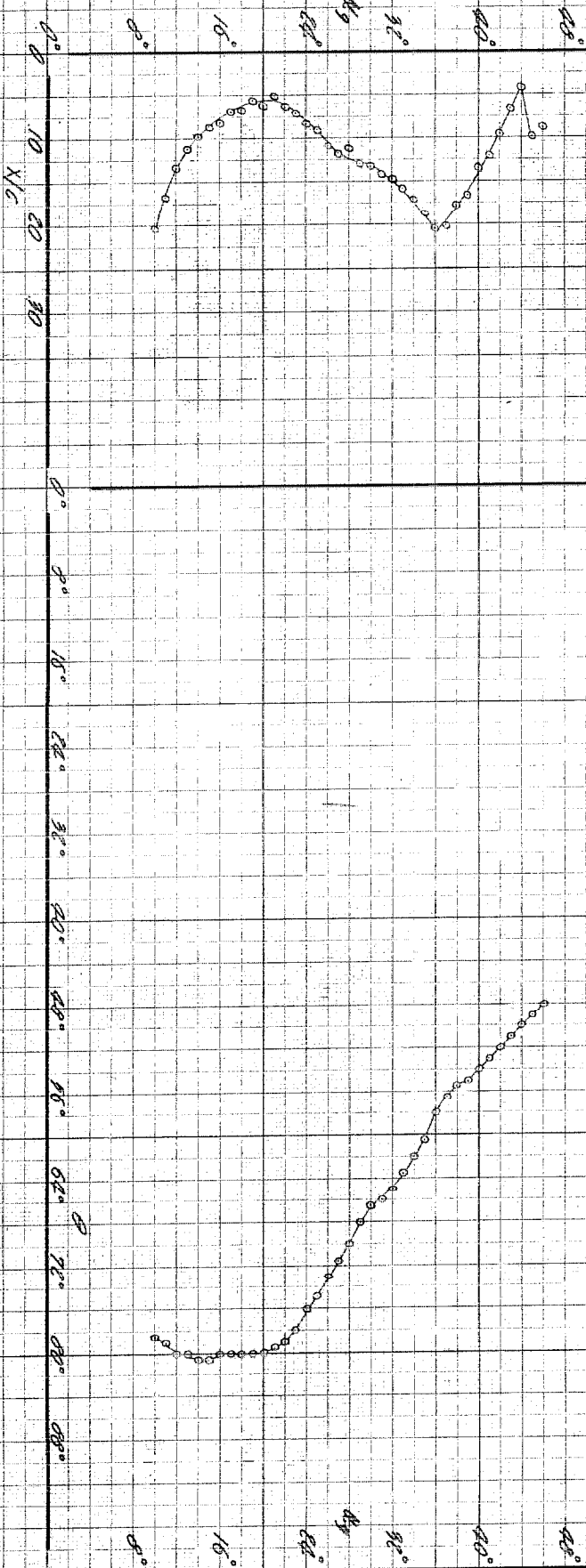
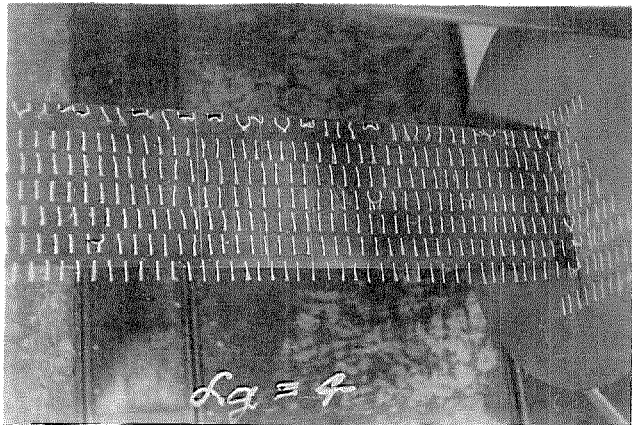


FIGURE 41c

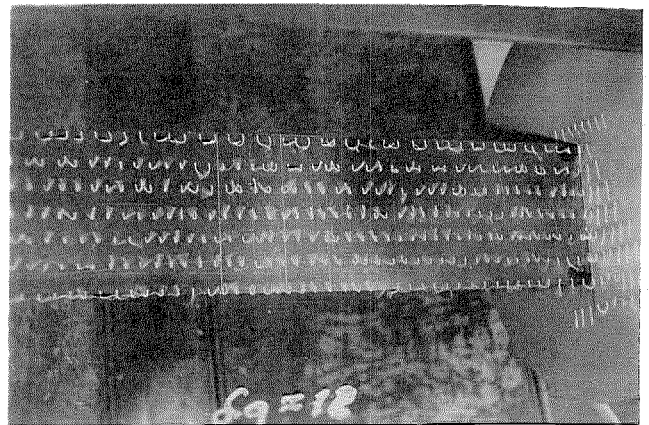
$$\text{MODEL } M_1^2 + M_2^2$$

$$(y_{11})_k = 245, (y_{11})_k = 227$$

Pictures of Tufts on Upper Surface of W_a^{12}
 $q=5 \text{ lb/ft}^2$, Runs 2 and 2A



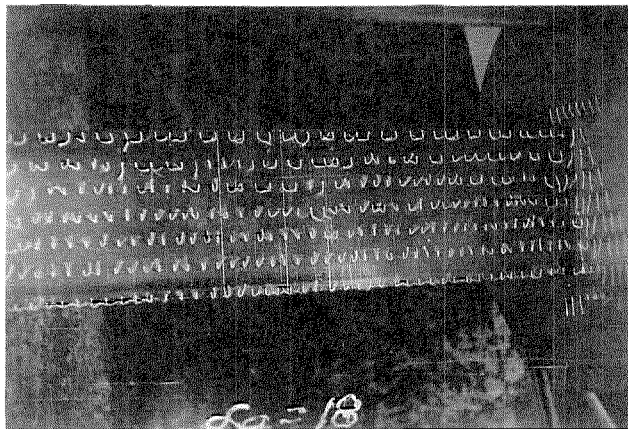
$\alpha_g = 4^\circ$



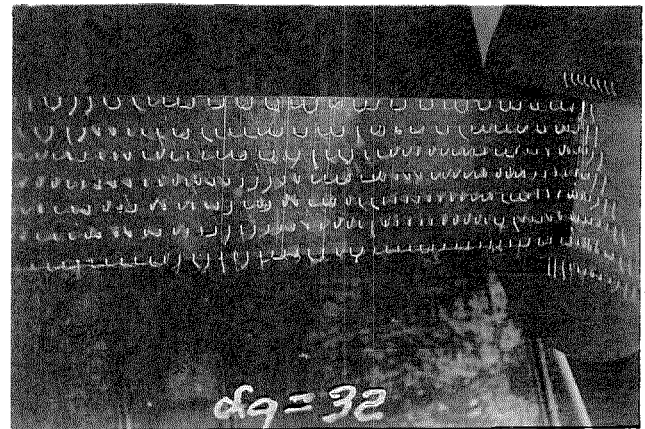
$\alpha_g = 12^\circ$

$\alpha_g = 4^\circ$

$\alpha_g = 12^\circ$



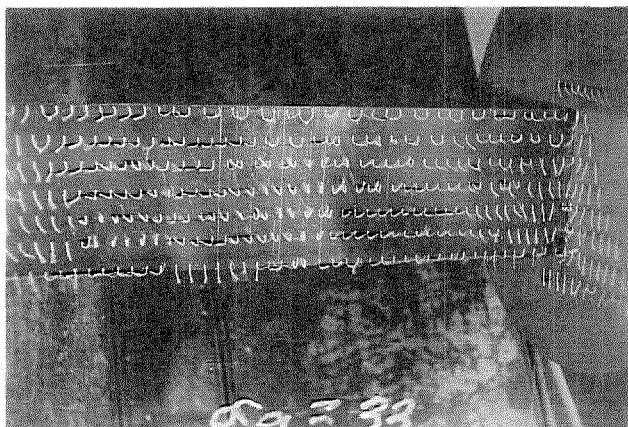
$\alpha_g = 18^\circ$



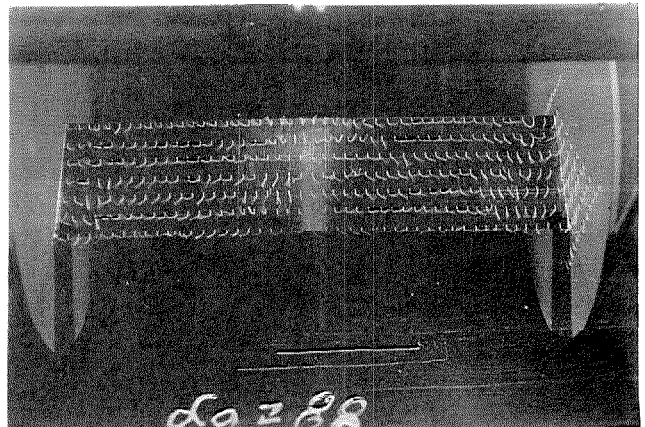
$\alpha_g = 32^\circ$

$\alpha_g = 18^\circ$

$\alpha_g = 32^\circ$



$\alpha_g = 33^\circ$



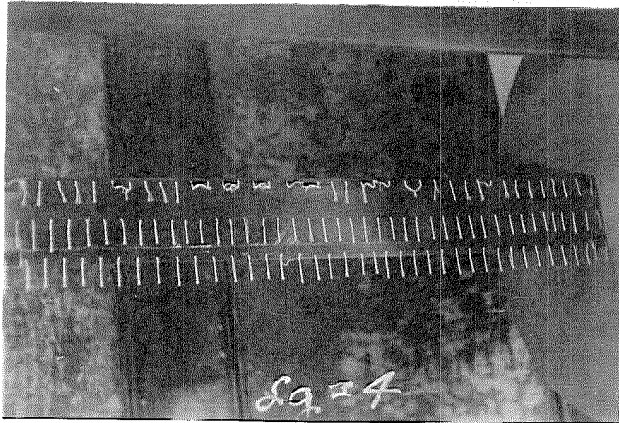
$\alpha_g = 88^\circ$

$\alpha_g = 33^\circ$

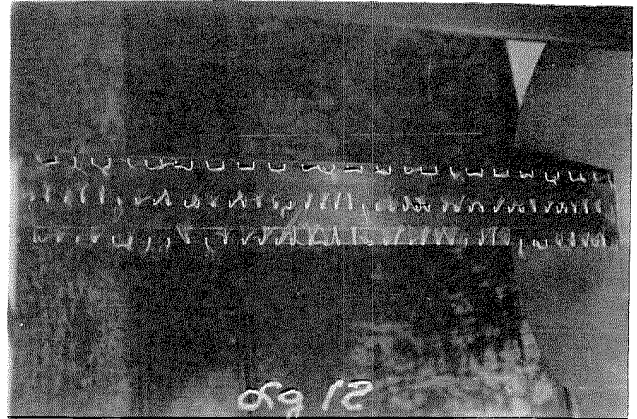
$\alpha_g = 88^\circ$

Figure 42

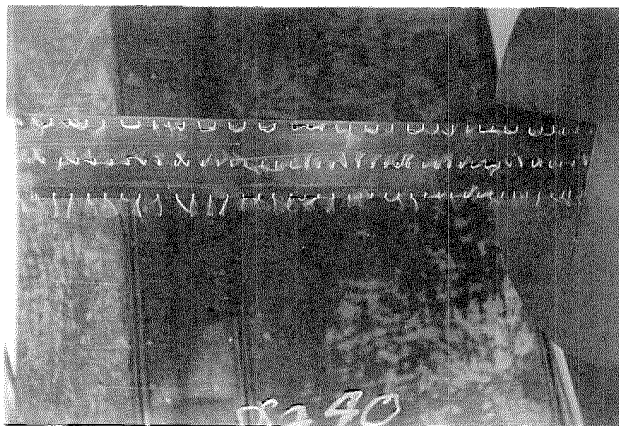
Pictures of Tufts on Upper Surface of W_2^e
 $q=5 \text{ lb/ft}^2$, Runs 5 and 5A



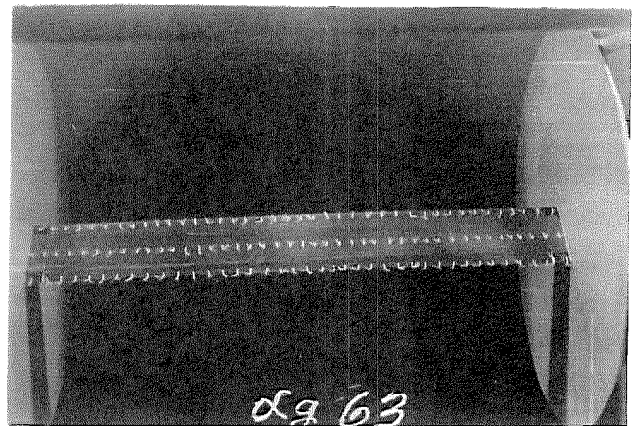
$\alpha_g = 4^\circ$



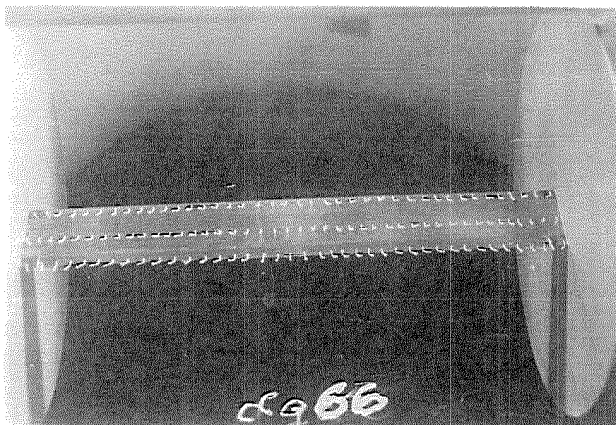
$\alpha_g = 12^\circ$



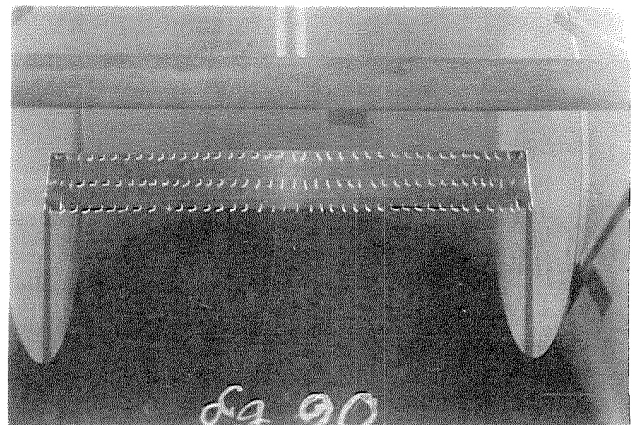
$\alpha_g = 40^\circ$



$\alpha_g = 63^\circ$



$\alpha_g = 66^\circ$



$\alpha_g = 90^\circ$

Figure 43

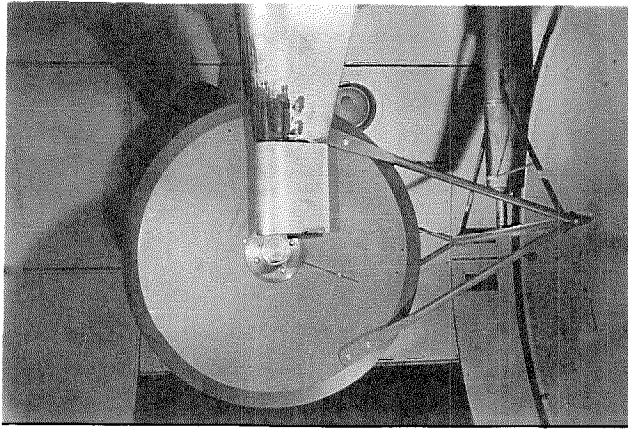


Photo 1. Side view of P_1

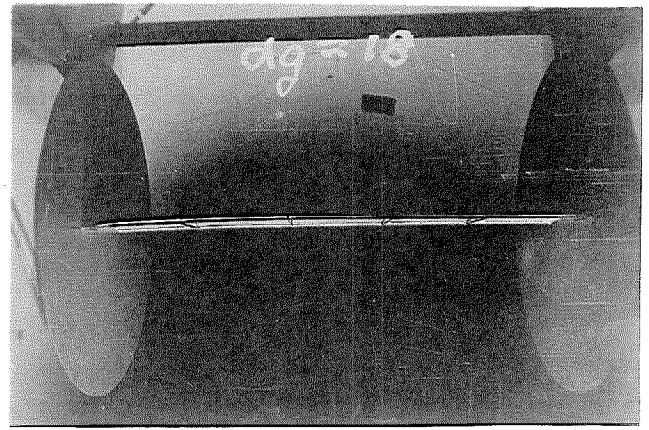


Photo 2. Rear view of $P_1 + W_p^{12}$
 $q \approx 5 \text{ lb/ft}^2$, $\alpha_p = 18^\circ$ (Run P_1)

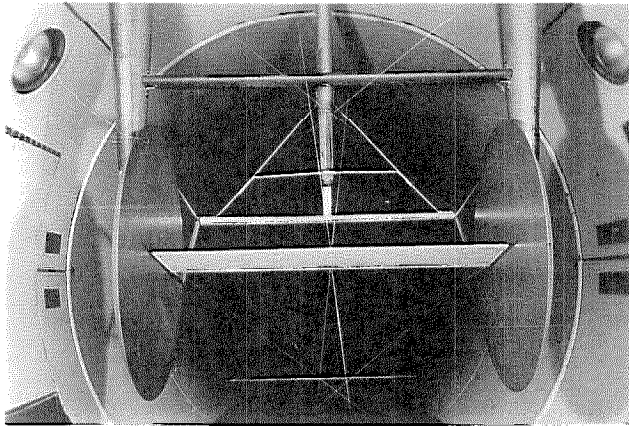


Photo 3. Front view of $P_1 + W_w^{12}$

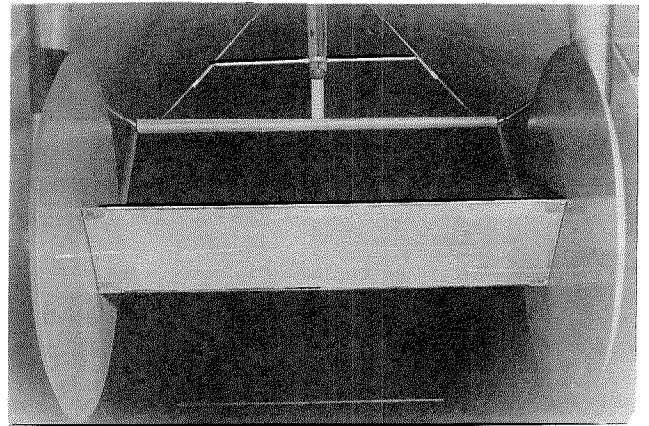


Photo 4. Front view of $P_2 + W_a^{12}$

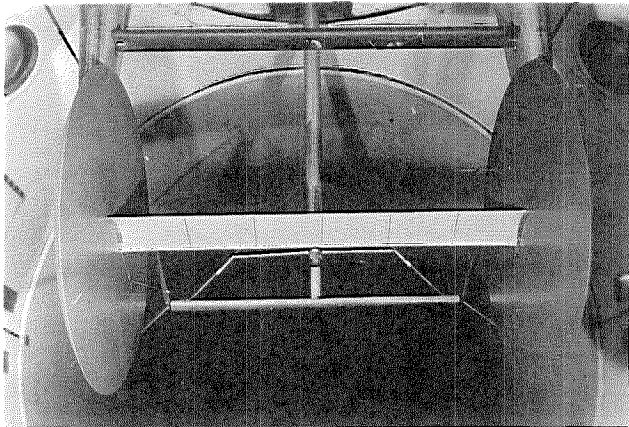


Photo 5. Front view of $P_1 + W_c^6$

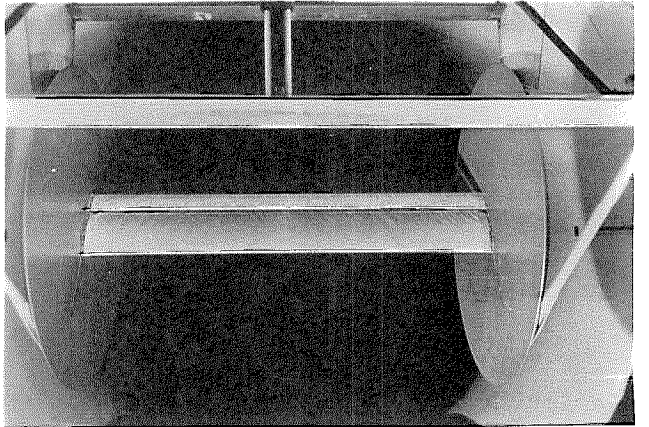


Photo 6. Rear view of $P_2 + W_c^6 + W_c^3$